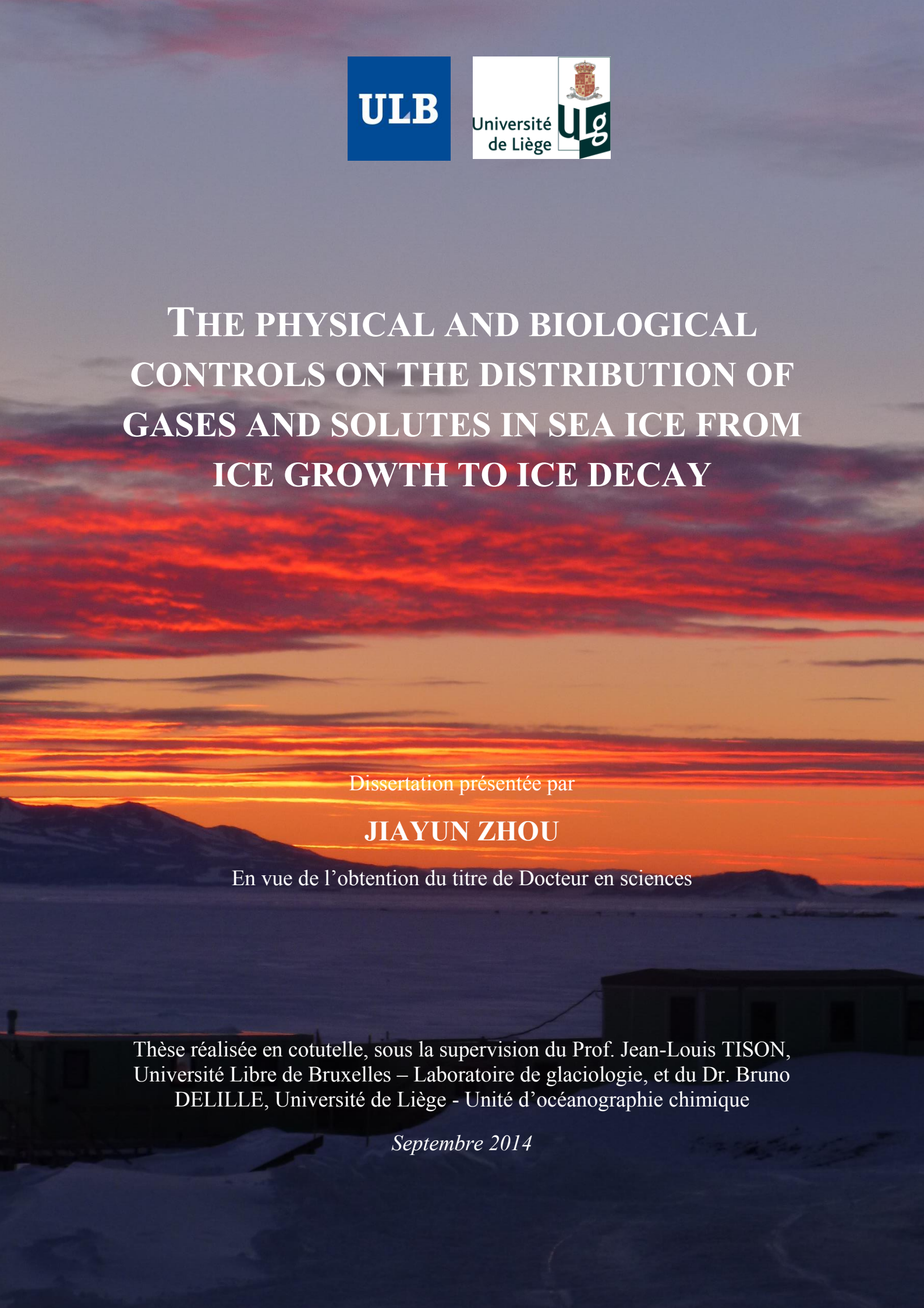

THE PHYSICAL AND BIOLOGICAL CONTROLS ON THE DISTRIBUTION OF GASES AND SOLUTES IN SEA ICE FROM ICE GROWTH TO ICE DECAY

Dissertation présentée par

JIAYUN ZHOU

En vue de l'obtention du titre de Docteur en sciences

Thèse réalisée en cotutelle, sous la supervision du Prof. Jean-Louis TISON, Université Libre de Bruxelles – Laboratoire de glaciologie, et du Dr. Bruno DELILLE, Université de Liège - Unité d'océanographie chimique

Septembre 2014

THE PHYSICAL AND BIOLOGICAL CONTROLS ON THE DISTRIBUTION OF GASES AND SOLUTES IN SEA ICE FROM ICE GROWTH TO ICE DECAY

Contrôles physiques et biologiques sur la répartition des gaz et solutés dans la glace de mer de la croissance à la fonte de la glace

Dissertation présentée par

JIAYUN ZHOU

En vue de l'obtention du titre de Docteur en sciences

Thèse réalisée en cotutelle, sous la supervision du Prof. Jean-Louis TISON, Université Libre de Bruxelles – Laboratoire de glaciologie, et du Dr. Bruno DELILLE, Université de Liège - Unité d'océanographie chimique

Thèse soumise le 6 septembre 2014

Défense privée le 6 octobre 2014 et défense publique le 30 octobre 2014

To my dad,

ABSTRACT

The ongoing changes in the extent and the properties of sea ice, associated with the warming climate, are affecting the polar ecosystem and the interactions between the atmosphere, sea ice and the underlying waters. How sea ice biogeochemistry will change in the foreseeable future is currently uncertain, but is a crucial problem to tackle.

To better understand how sea ice biogeochemistry could change, we investigated the factors regulating the distribution of some dissolved compounds (e.g., nutrients, dissolved organic matter (DOM)) and gaseous compounds (e.g., Ar, O_2, N_2, CH_4) in sea ice, from ice growth to ice decay. The results were obtained from a 19-day indoor experiment in Hamburg (Germany) and a five-month-long field survey in Barrow (Alaska). They were then compared to the physical properties of the ice (temperature, salinity, and other derived parameters such as brine volume fraction) and different biological parameters (bacterial activity, bacterial abundance, chlorophyll-a and phaeopigments).

Our work indicates that the physical properties of sea ice exert a strong influence on the distribution of the biogeochemical compounds in the ice, through their impact on brine dynamics, gas bubble formation and ice permeability. We have described 4 stages of brine dynamics, which affect the distribution of the dissolved compounds (e.g., silicate and DOM) in sea ice. However, inert gas (Ar) shows a different dynamic in comparison to the dissolved compounds, indicating a different transport pathway. We suggest that the formation of gas bubbles in sea ice is responsible for that different transport pathway, because gas bubbles should move upward owing to their buoyancy in comparison to brine, while dissolved compounds are drained downward due to gravity. Our observations further indicate that the critical permeability threshold for the upward gas bubble transport should range between 7.5 and 10 % of brine volume fraction, which is higher than the 5 % suggested for the downward brine transport. Increasing ice permeability and prolonged gas exchange tend to draw gas concentrations toward their solubility values, except when the under-ice water is supersaturated relative to the atmosphere (e.g., CH_4) or when in-situ production occurs in sea ice (e.g., O_2).

Because ammonium and O_2 obviously accumulate in the ice layers where convection is limited, we suggest that the changes of these biogeochemical compounds in sea ice depend on the competing effect between the physical transport and the biological activity; the biological impact on these biogeochemical compounds in sea ice is obvious when the biological production rate exceeds largely the physical transport rate. We further discussed on the potential of using Ar and N_2 as inert tracers to correct the physical controls on O_2 and to determine the net community production in sea ice.

In addition to the physical and biological controls, the chemical properties of some biogeochemical compounds (e.g., nitrate, ammonium, DOM) may further influence their distribution in sea ice; further investigations are however needed to confirm this.

Finally, based on our findings, we present an update of the processes regulating the distribution of gases in sea ice, with references to recent observations supporting each of the process. We also provide some insights on how sea ice biogeochemistry could change in the future and the research priorities for an accurate quantification of these changes.

RESUME

Les changements dans l'extension et les propriétés de la glace de la mer, liés au réchauffement climatique, affectent l'écosystème polaire, ainsi que les interactions entre l'atmosphère, la glace de mer et l'eau sous-jacente. Cependant, des incertitudes subsistent quant aux changements potentiels qui affecteront la biogéochimie de la glace de mer dans un futur proche.

Afin de mieux comprendre les changements potentiels qui affecteront la biogéochimie de la glace de mer, nous avons étudié les facteurs qui influencent la distribution de certains composés dissouts (e.g., nutriments, matière organique dissoute (DOM)) et gazeux (e.g., Ar, O_2, N_2, CH_4) au sein de la glace de mer, depuis la croissance de la glace, jusqu'à sa fonte. Les résultats ont été obtenus à partir d'une expérience de 19 jours dans un bassin expérimental à Hambourg (Allemagne) et une étude de terrain de 5 mois à Barrow (Alaska). Ils ont été ensuite comparés aux propriétés physiques de la glace (température, salinité et autres paramètres dérivés) et à des paramètres biologiques (activité bactérienne, abondance bactérienne, chlorophylle-a et phaeopigments).

Nos travaux ont montré que les propriétés physiques de la glace exercent une forte influence sur la répartition des composes biogéochimiques dans la glace de mer, à travers leur impact sur la dynamique des saumures, la formation de bulles de gaz et la perméabilité de la glace. Nous avons décrit 4 stades dans la dynamique des saumures qui influencent la distribution des composés dissouts (e.g., silice et DOM) dans la glace. Cependant, le gaz inerte étudié (Ar) montre une dynamique différente de celle des composés dissouts, indiquant un mécanisme de transport différent. Nous suggérons que la formation de bulles de gaz dans la glace de mer est le mécanisme responsable de cette différence, parce que les bulles de gaz devraient migrer vers le haut, à cause de leur différence de densité par rapport aux saumures, alors que les saumures sont drainées vers le bas à cause de la gravité. Nos observations montrent également que le seuil critique de perméabilité pour l'ascension des bulles de gaz devrait se trouver entre 7.5 et 10 % de volume relatif en saumure ; seuil qui est plus élevé que les 5 % suggérés pour le transport de saumure vers le bas. L'augmentation de la perméabilité de la glace et les échanges de gaz prolongés tendent à amener les concentrations de gaz vers leur valeur de solubilité, sauf lorsque l'eau sous-jacente présente une sursaturation par

rapport à l'atmosphère (e.g., CH_4), ou lorsque une production in-situ se produit au sein de la glace (e.g., O_2).

Etant donné que l'ammonium et O_2 s'accumulent clairement dans les couches de glace où la convection est limitée, nous suggérons que les variations de ces composés biogéochimiques dans la glace dépendent de la balance entre le transport physique et l'activité biologique ; l'impact de cette dernière sur les composés biogéochimiques est particulièrement visible lorsque le taux de production biologique du composé excède largement la vitesse d'élimination du composé par le transport physique. Nous avons ensuite discuté du potentiel d'utiliser Ar et N_2 comme traceurs inertes pour corriger l'impact des processus physiques sur les variations de O_2, afin de déterminer la production communautaire nette dans la glace de mer.

Les propriétés chimiques de certains composés biogéochimiques (e.g., nitrate, ammonium, DOM) pourraient également influencer leur répartition au sein de la glace de mer, en plus des processus physiques et biologiques. Cependant, il est nécessaire d'avoir plus d'études à ce sujet pour confirmer cela.

Enfin, sur base de nos résultats, nous présentons une mise à jour des processus qui régulent la répartition des gaz dans la glace de mer, avec des références à des observations récentes qui illustrent chacun des processus. Nous donnons également un aperçu des changements qui pourraient affecter la biogéochimie de la glace de mer à l'avenir, et des pistes de recherches pour une quantification précise de ces changements.

ACKNOWLEGMENTS

Mes remerciements vont d'abord à mes promoteurs, Jean-Louis Tison et Bruno Delille. Jean-Louis, un tout grand merci à toi pour m'avoir transmis ta passion sur la glace à travers les cours de Master, et puis de m'avoir donné l'opportunité de faire cette thèse chez toi. Merci aussi pour tes relectures détaillées de chacun de mes documents et tes impulsions d'énergie. Bruno, un tout grand merci à toi, surtout pour ta patience, ton attention et ton soutien durant les deux mois d'hiver à Scott Base. Merci également pour ta confiance en cette fin de thèse. Encore un tout grand merci à tous les deux pour avoir veillé sur moi durant ces 4 années de thèse ; merci pour votre écoute et conseils tant sur le plan professionnel que personnel. Vous êtes comme mon papa et ma maman de la vie professionnelle (je vous laisse choisir qui veut être le papa et qui veut être la maman)… Bien sûr, comme tout enfant qui détient des marques de ses parents, je constate que moi aussi, je commence à mettre des points de suspension dans mes mails, et que je traine un peu longtemps au téléphone… Vraiment, je me sens chanceuse de vous avoir tous les deux comme promoteurs : déjà, avoir un promoteur exceptionnel, qui est rigolo et humain, est une grande chance, mais avoir un deuxième, tout aussi gentil et humain, c'est quand même le jackpot !

I would like then to thank my thesis committee members, Lei Chou, Bernard Heinesch, David Thomas and Martin Vancoppenolle for their comments on my thesis. Lei, thank you for your kindness and attention. Bernard, thanks for teaching me the fundamentals of eddy covariance and for coming to my committee presentations from Gembloux. Martin, thanks for initiating me into the mysteries of modeling and for inviting me to give a talk at the LOCEAN. David, thank you for my mobile phone! (I HAVE to place that first, as it was so unbelievable); thank you also for your support during the Interice V experiment and your trust for the general paper afterwards.

I would like to extend my gratitude to my other collaborators: Hajo Eicken and Tim Papakyriakou, who have considerably improved my scientific writing skills; Gerhard Dieckmann, for his warm welcome at the AWI and his help during the Interice V experiment; Gerhard Kattner, Colin Stedmon, Harry Kuosa, and Hermanni Kaartokallio, for filling my gaps in river biogeochemistry and bacterial metabolism; one more "like" for Harry, for the guided tour and boat tour in Tvärminne! Thanks also to Linda Jørgensen, Riitta Autio, Anne-

Mari Luhtanen and Marie Kotovitch for the great time we had in Finland (especially, in the sauna☺); Karl-Ulrich Evers and the rest of the ice tank crew of the Hamburg Ship Model Basin (HSVA) for their support throughout the Interice V experiment, and Sébastien Moreau for his tolerance towards my mistakes (no no, I will not touch the remote anymore) and his patience during all the long meetings between modellers and experimentalists.

A special thanks to the New Zealanders: Tim Haskell, Simon Trotter, Peter McCarthy, Paul Woodgate and the others staffs of Antarctica New Zealand, for their help in organizing our stay in Scott Base and field survey in Cape Evans. Special thanks plus a big big hug to the winter-over team 2011-2012: Caro and Cliff for their efficient help on the field; Bobby for the yummy food supply; Tank and Jody, (the AHT's) Martin, Jena for their great company; and of course!!! … *jingles*… Brian Staite! Brian, you are an amazing guy, my super-hero and secretly adopted grandpa☺. Despite the cold and harsh conditions during our winter-over, your cleverness made all the fieldworks much more easy-going than what they could have been without you. Your attention, kindness and positive attitude also make you the best-ever field-partner.

Ensuite, je voudrais remercier mes collègues de bureau de l'ULB. Merci à Gauthier Carnat, mon grand frère en sciences, que j'admire et envie secrètement pour sa connaissance encyclopédique. Merci pour ta compagnie à Scott Base, ton écoute, tes conseils et nos discussions philosophiques sur les choix d'un doctorant. Merci à Morgane, ma collègue de bureau talentueuse. Merci de ta compagnie durant le magnifique voyage que nous avions entrepris en Tasmanie ; merci de m'avoir soutenu dans mes délires annuels de réaménagement de bureau et d'avoir accepté de prendre la place de la secrétaire ; merci aussi pour tous les spectacles et fêtes auxquels tu m'as invité et qui m'ont permis de découvrir tes talents de danse, de chants, de cuisine, d'élevage … (euh… j'arrête ici parce que je suis limitée en nombre de pages :p). Merci au duo de choc, Saïda El Amri et Claire Lelouchier pour votre aide en laboratoire et pour ce qui est de l'administratif. Merci au chef, Frank Pattyn, pour tous les pizza break-outs et le partage des tes goûts artistiques. Ta sélection de jazz et tes cartes postales de peintures contrastent avec le bruit des machines du laboratoire et le couloir qui ne demande qu'à être rénové. Cela donne un petit côté surréaliste et inattendu, comme ton personnage. Merci à Véronique Schoemann, ma roommate à Scott Base, qui a bien veillé sur moi, surtout le jour de notre retour ;). Merci à Célia de m'avoir accueilli à Utrecht et de m'avoir appris plein de choses sur les isotopes et le méthane. Merci aux

modélisateurs et/ou matlab-users, Denis Callens, Brice Van Liefferinge, David Docquier, Reinhard Drews, Lionel Favier, qui m'ont certainement aidé à un moment ou un autre pour mes routines matlab. Merci aussi aux derniers arrivés, Thomas Goossens, Ceri Middelton, Sophie Berger et Mathieu Depoorter. Un nouvel arrivé = un anniversaire et d'autres évènements à fêter en plus = plein de drinks et de goûters ! Yeaaaah ! ☺ Encore un grand merci à Ceri, Morgane, Véro, Gauthier et Lionel, pour avoir relu des parties de ma thèse, et merci à tous pour la bonne ambiance au labo. Vous allez me manquer l'année prochaine ☹

Merci à mes ex-collègues de bureau, aînés et coachs, Marie Dierckx, Charlotte Delcourt, Lt. Dr. Ir. Frédéric Brabant, Thierry Boerenboom, Nicolas-Xavier Geilfus, et François Fripiat, pour vos conseils, en matière de gestion de la thèse et des papiers administratifs… même si, j'arrive quand même à me retrouver dans une situation administrative hyper compliquée... Merci d'ailleurs à l'administration de l'ULB, pour les petits coups d'adrénaline de dernières minutes.

Merci aussi à mes collègues à l'ULg : Alberto Borges, François Darchambeau, Willy Champenois, Jérôme Harlay, Marc-Vincent Commarieu, Aurore Beulen, Fleur Roland, Gaëlle Speeckaert, Sandro Petrovic et Thibault Lambert. Merci pour votre accueil et pour le partage de vos passions sur les estuaires belges et les lacs africains. Un grand merci à Willy aussi pour les superbes photos durant la mission Yrosiae, et le partage de ton bureau (que tu ne savais peut-être pas) quand je suis à l'ULg.

Of course, I would like to thank the F.R.S.-FNRS for all the financial supports. These were crucial for my attendance to diverse conferences, summer school, etc., where I had to opportunity to share my findings and where I met several super-friendly scientists. Thanks to Alice Pestiaux, François Massonnet, and Daniel Price for the funny and unforgettable games in Svalbard; Philipp Griewank for the great time we had in Svalbard and in Hamburg; Cecilia Peralta Ferriz, for the great time in Ventura, and for hosting me in Seattle; Paul Cziko for the ice fishing near Scott Base; Denis Poëhler, for the tour in New Zealand; Inka Koch, Inga Smith, Greg Leonard and Pat Langhorne for their warm welcome when I was in Dunedin, and thanks to Inga and Greg for hosting me in their amazing house. Merci aussi à Julie pour ton hospitalité à Hobart, tes conseils sur les endroits à visiter en Tasmanie et tes tuyaux pour repérer la présence des wombats hihihi.

Je remercie bien évidemment Isabelle Jacobs et Benoît Collet, pour m'avoir fait découvrir tous des styles de musiques différentes, sans oublier les deux autres flûte2, Sophie Verschuren et Philippine Stalins, et le reste de l'ensemble Anacruz, pour les super concerts (oui, c'est peut-être bien un euphémisme) et surtout la dernière soirée de barbecue chez Anne-Laure qui a été agréablement surréaliste. C'était vraiment chouette d'avoir pu travailler avec vous. Et promis, je continuerai à m'entraîner aux states pour notre rendez-vous en Argentine ;)

Merci aussi à ceux et celles qui ont veillé sur ma vie sociale : Stéphane Vranckx, Aurore Woller, Mathieu Caby et Guillaume Jumet, pour les après-midis sushis et rédaction ; mais également, Nathalie Meganck, Cindy Wilvers, Laurie Massaad, Laura Marcus, Thomas Still, Deborah Manderlier, David Mathieu, Emilie La, Alex Chen, Manu Chiambretto, Lucien Culot (Le Maître du monde pour les intimes), Thibault De Laet, Olivier Vossen, Gregory De Greef, Sophie Schools, Thomas Hofer, Caroline Veiders, pour les nombreux voyages ; les soirées toujours bien arrosées avec les PAF ; les discussions délirantes, surtout avec Lucien ; les concours de celui-qui-mange-le-plus-de-bidoche chez Greg, etc. etc.

謝謝我教會裡的弟兄姊妹，尤其是青少年團契的張潔，唐嘉鴻，林芳儀和應懷媛。和你們一起帶領敬拜和青少年團契真的是讓我學習和領受到很多。

最後我要謝謝我的爸爸，媽媽和妹妹。爸爸，雖然你已經回天家了，但跟你在一起的點點滴滴我都沒有忘記。記得從小你就教導我要好好讀書，將來要做一個有用的人。。。我不知道我現在算不算是個有用的人，但最起碼，我有好好讀書，用心工作；我希望你會為今天的我而自豪。媽媽，謝謝你。謝謝你的愛心湯水，謝謝你的照顧，謝謝你為我禱告。雖然你愛我的方法有點與眾不同，有時候會讓我不知所措，但我知道那是因為你太過愛護我。

我也謝謝嘉慧。謝謝傻乎乎的你令嚴肅的我多了笑容。

CONTENT

Chapter I – Motivation

Sea ice forms from the freezing of seawater [*WMO*, 1970]. It covers about 7 % of the Earth's ocean surface [*Vaughan et al.*, 2013] and plays an important role in the climate system, the ocean circulation and the global biogeochemical cycles. Indeed, sea ice formation increases the albedo of the ocean surface and reduces the exchange of heat, moisture and momentum between the ocean and the atmosphere. Sea ice formation further leads to the rejection of brine in the upper layers of the ocean, inducing thereby deep-water formation, while sea ice melt induces water mass stratification. Finally, sea ice affects the global biogeochemical cycles either directly, through the biogeochemical processes within the ice, or indirectly, through the exchanges of gases and fluid at the air-ice and ice-ocean interfaces [*Vancoppenolle et al.*, 2013b, for a review]. The significance of that last role of sea ice is the less well quantified at large scales, because the involved processes are not precisely understood or quantified [*Vancoppenolle et al.*, 2013b]. The most relevant processes are given here below.

First, sea ice biogeochemistry affects the primary production in the polar oceans. Sea ice hosts microorganisms, which produce organic matter depending on the light and nutrient availability. Therefore, by hosting microorganisms, sea ice extents the duration of the primary production in the polar oceans and provides food source for the higher trophic-level species in winter and early spring. The thickness of sea ice and the snow cover further alter the light available for the phytoplankton production in the under-ice water. In addition, when sea ice melts, it stratifies the surface water, releases organic matter and nutrients, and in particular trace metals like iron, which affect phytoplankton growth in the iron-limited Southern Ocean. However, one main uncertainty is the partitioning of the released materials: how much is in-situ remineralized, and how much is exported to the seafloor?

Second, sea ice affects the exchanges of gases between the atmosphere and the ocean, and in particular, the exchanges of climate-active gases, like carbon dioxide CO_2, dimethylsulfide DMS and methane CH_4. Although sea ice has long been assumed to be an inert and impermeable ice layers that impede all gas exchanges between the atmosphere and the ocean, recent measurements of CO_2 [*Delille et al.*, 2007; *Geilfus et al.*, 2012; *Nomura et al.*, 2010; *Papakyriakou and Miller*, 2011], DMS [*Nomura et al.*, 2012; *Zemmelink et al.*, 2008] and CH_4 fluxes [*He et al.*, 2013] at the ice-air interface indicates that sea ice is permeable.

Theoretical considerations [*Golden et al.*, 1998] and laboratory experiments [*Gosink et al.*, 1976; *Pringle et al.*, 2009] further support that sea ice may be permeable under specific conditions of temperature and salinity. Therefore, by assuming that sea ice is impermeable, we underestimate the duration of gas exchange between the ocean and the atmosphere. In addition, brine rejection associated with sea ice formation may also drain gases to the surface ocean [*Rysgaard et al.*, 2007]. The issue of gas exchange through sea ice is further complicated by the biogeochemical processes that occur within the ice: carbonate precipitation [*Geilfus et al.*, 2013; *Rysgaard et al.*, 2011] and microbial activity within the ice change the amount of CO_2 in transit through sea ice [*Geilfus et al.*, 2012], and in-situ biological production affects oxygen O_2 and DMS [*Delille et al.*, 2007]. Thus, sea ice is not simply a physical barrier across which a certain amount of gases transits, it is also a platform where the production and consumption of some biogases occur.

CO_2 is one of the most studied gases in sea ice. The concentrations of CO_2 in the ice not only depends on the air-ice exchange of CO_2, but also the export of inorganic carbon transport with brine rejection, calcium carbonate precipitation and biological activity in sea ice. Although the mechanisms responsible for the changes in CO_2 concentrations in sea ice are identified, their significance has been rarely quantified [*Vancoppenolle et al.*, 2013b]. As a result, the overall contribution of sea ice in terms of air-ocean gas exchange is still debated. Some claim that Antarctic sea ice may accounts for 58 % of the annual uptake of CO_2 in the Southern Ocean [*Delille et al.*, 2014], while others claim that sea ice from the Bering Sea accounts for less than 2 % of the annual CO_2 fluxes [*Cross et al.*, 2014].

DMS has drawn considerable interest, because the oxidation of DMS may produce sulphate aerosols, which affect the radiative properties of the atmosphere, with a potential cooling effect on the planet [*Charlson et al.*, 1987]. Sea ice has been suggested to be a potentially important source of DMS in the polar oceans, because the microorganisms in sea ice produce large amounts of dimethylsulfoniopropionate DMSP, the precursor of DMS. Sea ice melt is indeed associated with an increase of the DMS concentration in the surface water, which may contribute to the regional oceanic DMS emission [*Levasseur et al.*, 1994; *Tison et al.*, 2010; *Trevena and Jones*, 2012]. DMS fluxes through sea ice before ice melt may represent an additional source of DMS, but very few measurements have been done [*Nomura et al.*, 2012; *Zemmelink et al.*, 2008]. Therefore, a general picture of DMS emission over the whole Arctic and Antarctic sea ice is missing, and the contribution of sea ice to the global DMS emission is currently unknown.

CH_4 is an important greenhouse gas which accounts for 20 % of the global radiative forcing of well-mixed greenhouse gases [*Myhre et al.*, 2013]. Its emission from the destabilized permafrost and hydrates in the Arctic shelf regions, associated with the ongoing climate warming may have positive feedback on the climate, as it occurred in the past [*O'Connor et al.*, 2010]. The role of sea ice in that scenario is uncertain. To date, CH_4 measurements in sea ice are scarce [*Lorenson and Kvenvolden*, 1995; *Shakhova et al.*, 2010b], but some suggest that sea ice impedes air-ice CH_4 exchange [*He et al.*, 2013; *Kitidis et al.*, 2010; *Kort et al.*, 2012; *Shakhova et al.*, 2010b], and that CH_4 oxidation could occur in the ice [*He et al.*, 2013] and in the under-ice water [*Kitidis et al.*, 2010], based on CH_4 measurements in air and seawater. It has also been suggested that the degradation of DMSP could produce CH_4 in seawater [*E. Damm et al.*, 2010], but whether the same pathway could occur in sea ice where large DMSP concentrations are found is currently uncertain.

In the Arctic, sea ice extent has drastically decreased over the last thirty years (decrease of 13.5 % and 4.1% per decade for multi-year ice and first-year ice respectively) [*Vaughan et al.*, 2013]. In Antarctica, despite the overall increase of sea ice extent (1.8 % per decade), regional variability is large [*Vaughan et al.*, 2013], and model simulations project significant decrease of the Antarctic sea ice extent by the end of this century [*Arzel et al.*, 2006]. In that context, we may wonder how the sea ice related biogeochemical cycles will change; in particular, how the exchanges of the climate-active gases will be affected, and would it have feedbacks on the climate. Earth system models could help to answer these questions, but since they currently represent sea ice as a biogeochemically inert blanket, a first step would be to identify the most relevant processes to implement in the models.

The overarching objective the thesis is thus **to identify the most relevant processes regulating the dynamics of solutes and gases in sea ice**. The work is based on observations made on experimental ice and Arctic first-year sea ice. The focus on first-year ice is motivated by its proportion to the total amount of ice; it accounts for 60 and 80 % of the maximum sea ice extent in the Arctic and Antarctica, respectively [*Vaughan et al.*, 2013]. That percentage is increasing in the Arctic, because the loss of multi-year ice was more drastic than the loss of first-year ice (Figure 3a on http://nsidc.org/arcticseaicenews/2014/09/). Focusing on Arctic first-year ice is also relevant for studying the interactions between sea ice and the emission of CH_4 from the Arctic shelf regions as described earlier.

Chapter II – State of the art

Before identifying the most relevant processes affecting the dynamics of solutes and gases in sea ice, we will first review **the state of the art on the biogeochemical compounds in sea ice**, with a focus on the differences compared to seawater. The most important concepts are synthesized here below, with references to the more detailed explanations in the next sections.

1. **Sea ice is a heterogeneous material**

Although sea ice is formed from the seawater, the biogeochemical compounds are not homogeneously distributed as they were in seawater (section 1). Most of the solutes and gases are concentrated in the brine inclusions within the pure ice matrix. Therefore, the physical transport of solutes and gases (section 4) are mainly exchanges between the atmosphere, the brine inclusions and the ocean; not with the pure ice matrix.

The brine volume fraction, which is the percentage of the total ice volume occupied by brine, is a function of the ice temperature and ice salinity (section 3). Assuming that all the solutes and gases are in brine inclusions, dividing the measured concentrations in bulk ice by the brine volume fraction (section 3) allow to assess the concentration in brine.

The heterogeneous structure has also implications on the measurement techniques. Ice melting may induce biases in the estimate of the biological activity, due to the realted osmotic shock on the microorganisms. It may also dissolve some mineral precipitates, which change the concentrations of some dissolved compounds. Other examples are given and further described in section 6.

2. **The concentrations of solutes in sea ice**

Both physico-chemical and biological processes may affect the concentrations of solutes in sea ice (section 5). To assess the significance of the concentration of a solute in sea ice, we need to compare it with a reference value; that reference value could be determined by the dilution curve. A solute is said conservative against salinity, i.e., it was incorporated (section 2) and transported (section 4.1) in the same way as salts, if its concentration in the ice increases linearly with the ice salinity, along the dilution curve. Deviation of the solute concentration from the dilution curve is generally attributed to biological processes (section 5.2).

3. The concentrations of gases in sea ice

Similarly to the solutes, physico-chemical and biological processes also affect the concentrations of gases in sea ice (section 5). However, the transport of gases through sea ice may be different to that of the solutes for two reasons. First, gas exchange could occur at the air-ice interfaces (section 4.2); while most of the solutes are drained out of the ice, at the ice-ocean interfaces, through brine drainage (section 4.1). Second, gases may be present in the form of gas bubbles, which should tend to move upward – if the ice is permeable – while the dissolved gases tend to move downward, as the other solutes, due to brine drainage (section 4.1).

The saturation level of a gas is a crucial parameter determining the gas fluxes at the ice-air interfaces, and affects gas bubble formation (section 5.1.2). Gas supersaturation, i.e., gas concentration that is higher than its solubility, could easily occur during ice growth, because of the brine concentration effect and the decrease of gas solubility. First, decreasing ice temperature decreases the brine volume fractions, which increases the concentration of the dissolved gases in brine; this is the so-called brine concentration effect (section 3). Second, decreasing ice temperature tends to increase gas solubility, but its associated increase of brine salinity (section 3.2) over-compensates the effect of cooling on the solubility, and induces a net decrease of gas solubility. In addition to these physical processes, biological activity and mineral precipitation could also affect gas saturation. Gas supersaturation could lead to ice-air gas fluxes if the ice is permeable, and the formation of gas bubbles, if the sum of the partial pressures of all the dissolved gases is higher than the local hydrostatic pressure.

The detailed section of the state of the art starts from here. It first describes the crystal structure (section 1) and the different textures of sea ice (section 2), which play an important role in the distribution of the biogeochemical compounds (e.g., gases, nutrients) in sea ice during sea ice formation. Section 3 describes the physical parameters of sea ice which have been proven to affect the transport of the biogeochemical compounds (section 4) and the biogeochemical processes in sea ice (section 5). Section 6 further highlights the observational constraints related to the sampling and the measurements of the biogeochemical compounds.

1 The crystal structure of sea ice

At the Earth's surface, water crystallises in the Ih structure, with the « h » indicating the hexagonal crystal system, as described in Figure 1 [*Weeks*, 2010]. The water molecules (H_2O) are arranged tetrahedrally around each other, and the so-formed crystal system is characterized by four axes: three equivalent a-axes, which lie in a basal plane separated by angles of 120°, and the c-axis, which is oriented perpendicular to the basal plane [*Weeks*, 2010]. The c-axis is the principal crystallographic axis, because it is the axis of maximum (six-fold) rotational symmetry; it is also referred to as the optic axis of the crystal, i.e., the direction along which a ray of transmitted light can go through the crystal without undergoing double refraction, and perpendicular to which the ray cannot pass [*Hobbs*, 1974, p. 200-205]. It is based on the optical properties of the c-axis that the universal stage system determines the exact orientation of each crystal in a thin section [*Langway*, 1958].

Because of the tetrahedral arrangement of the water molecules, the ice Ih has a lower density than liquid water; this allows sea ice to float [*Weeks*, 2010]. However, despite the low density of the ice Ih, only few species of ions and molecules, with specific size and/or electric charge, may be incorporated in the ice crystal lattice (e.g., F^-, HF, NH_4^+, NH_3 and to a minor extent, HCl, HBr and HI) [*Hobbs*, 1974, p. 112-119 and references therein]. In contrast, most of the impurities that were present in seawater (e.g., Na^+, Cl^-, K^+, Ca^{2+}, Mg^{2+}, SO_4^{2-}, CO_3^{2-}) are not incorporated into the ice crystal lattice, and are rejected ahead the advancing ice-water interface during ice growth [*Petrich and Eicken*, 2010]. Therefore, although sea ice is formed from seawater, the biogeochemical compounds that were initially present in seawater are no longer homogeneously distributed in sea ice. Instead, the water molecules form a matrix of pure ice, whereas most of the biogeochemical compounds are concentrated in the brine inclusions.

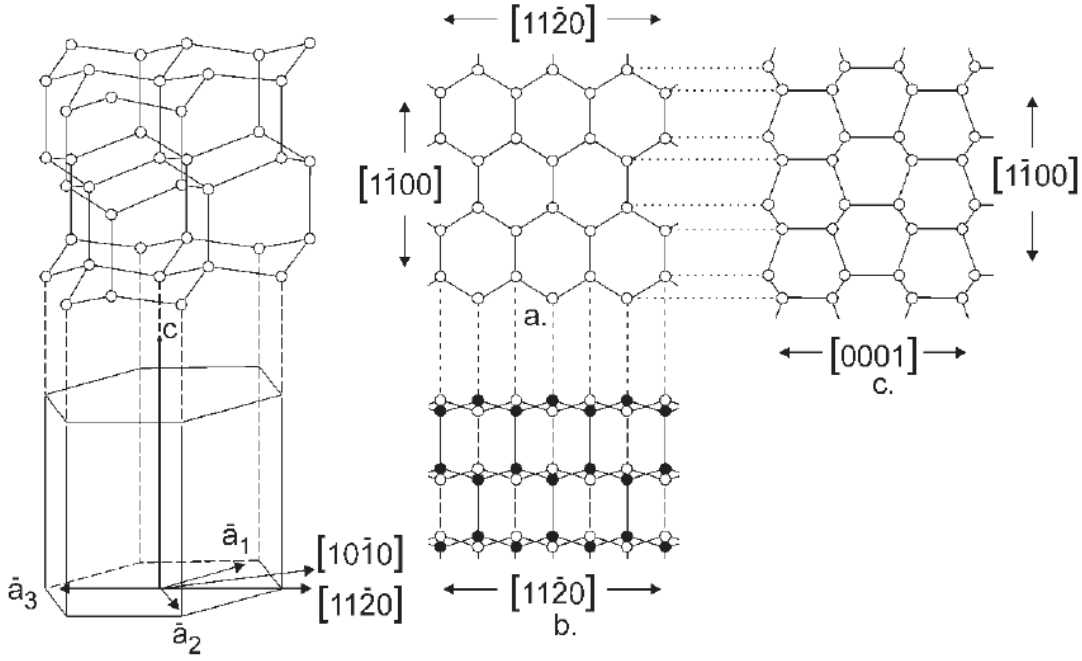

Figure 1 Crystal structure of sea ice (from *Weeks and Ackley* [1986]) on the left. The central panel presents the arrangement of oxygen atoms along (top) and perpendicular (bottom) to the c-axis (symmetry axis of order-6). The 3 a-axes (symmetry of order-2) are lying within the basal plane (left panel).

2 Sea ice formation and the incorporation of impurities in sea ice

Macroscopically, the matrix of pure ice presents different types of ice textures depending on the conditions of sea ice formation. There are three main types of ice textures associated with ice growth (frazil ice, columnar ice and platelet ice) and two others associated with the presence of snow on the top of the ice and ice melt (snow ice and superimposed ice); these are summarized by *Petrich and Eicken* [2010] in Figure 2. At larger scale, sea ice cover presents different morphologies which are classified according to their genetic processes (ice growth, melt or deformation), their ice age and their thickness [*Petrich and Eicken*, 2010] (Figure 3) (see also aspect.antarctica.gov.au for a glossary based on *WMO* [1970] and an image library of the most commonly encountered ice types).

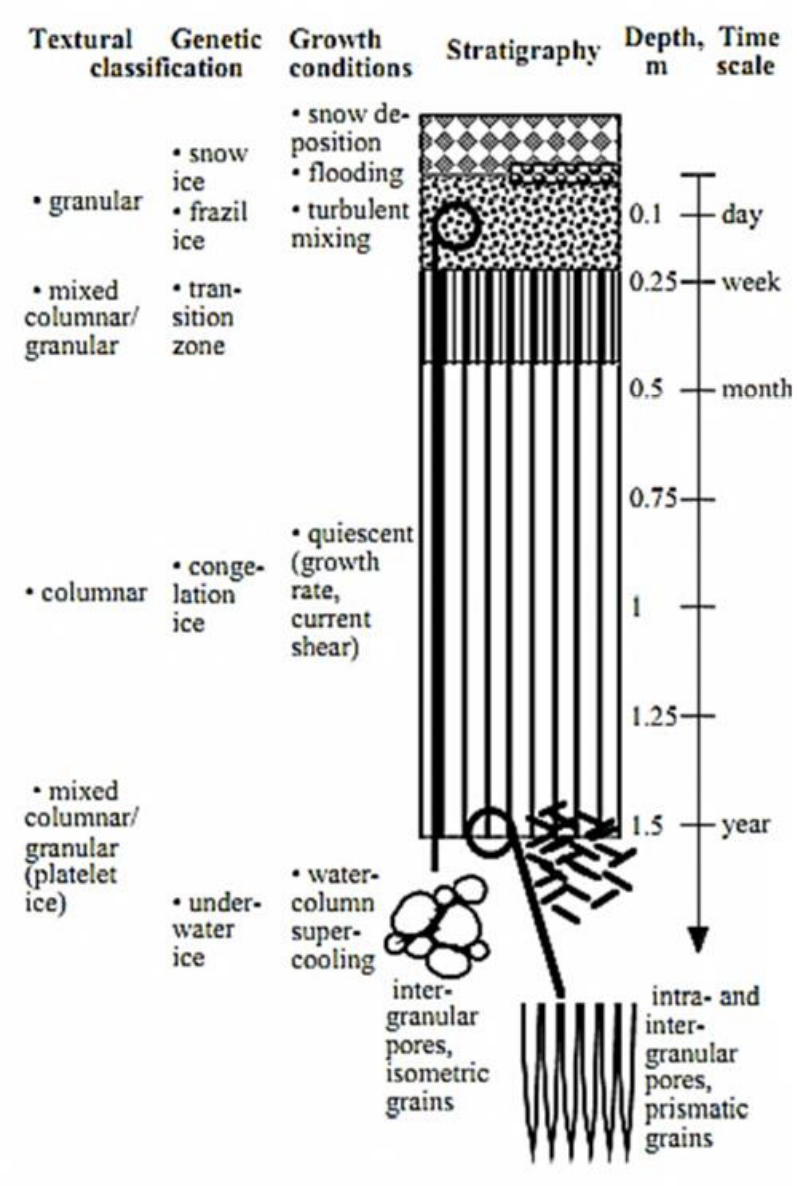

Figure 2 Scheme summarizing the main ice textures encountered in different ice growth conditions and at time scales for first-year ice [*Petrich and Eicken*, 2010]

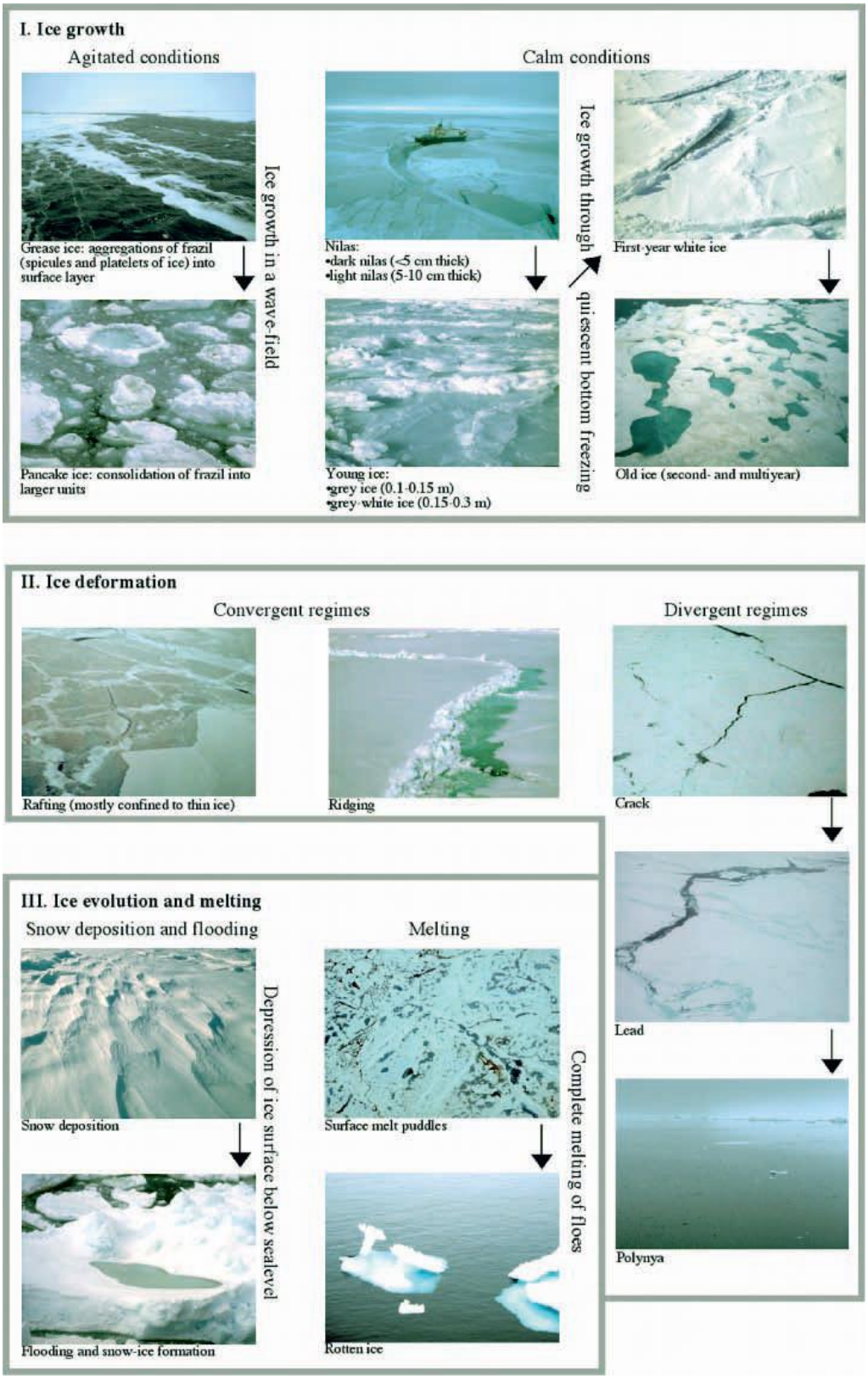

Figure 3 Large-scale morphologies of sea ice cover associated with ice growth, melt and deformation processes [*Petrich and Eicken*, 2010]

2.1 Frazil ice

The top of sea ice cores generally consists of frazil ice, because they are the first ice crystals to form in the open ocean, under agitated conditions (wind and waves). They have granular texture, with rounded millimetre-sized crystals, but could take the shape of needles, spicules or platelet, and are often intertwined with aggregates [*Weeks and Ackley*, 1986].

According to *Weeks and Ackley* [1986], the frazil ice found at the surface of sea ice forms as following. In winter, when seawater cools down, it becomes denser than the underlying (relatively warmer) seawater. This is because the temperature of the maximal density of seawater is below its freezing point (Figure 4). As a result, the relatively cooler and denser body of seawater sinks, while the relatively warmer and less dense water at depth rises, causing a mixing process [e.g., *Foster*, 1968] termed "convection" or "convective overturning" [*Petrich and Eicken*, 2010]. Theoretically, that convection will continue until the entire mixed layer is at the freezing point. In practice, however, frazil ice crystals may form before that the entire mixed layer has reached the freezing point, because the aggregates in seawater may serve as nucleation site for ice crystals [*Petrich and Eicken*, 2010]. Frazil ice has a granular texture, because the convective overturning is usually supported by wind and waves, which break the new protrudes of the growing ice crystals; it is often intertwined with aggregates, which are entrained with the ice crystals in suspension during the convective overturning [*Weeks and Ackley*, 1986]. That process of entrainment is also referred to as harvesting or scavenging [*Garrison et al.*, 1983; *Weissenberger and Grossmann*, 1998].

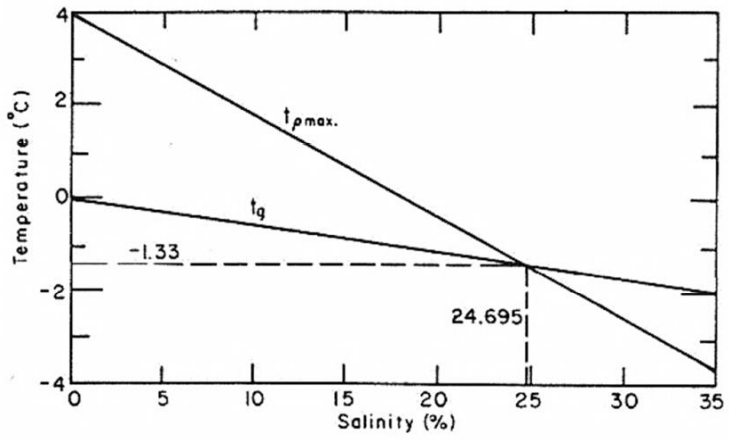

Figure 4 Temperature of the maximum of density $t_{\rho max}$ and the freezing point t_g of seawater for different temperatures and salinities [*Weeks and Ackley,* 1986]

While the layer of frazil ice is millimetre-thick in the Arctic, it is generally much thicker in the Southern Ocean, because the higher wind speeds and the open-configuration of the Southern Ocean allow a larger number of openings in the ice (i.e., leads and polynyas – see ice deformation, divergent regimes in Figure 3), which favour the formation of frazil ice [*Weeks and Ackley*, 1986]. Frazil ice growing in these turbulent waters may also aggregate into larger floes of crystals than in the Arctic (e.g., pancake ice, Figure 3) [*Lange et al.*, 1989].

2.2 Columnar ice

Following the consolidation of a surface ice layer composed of frazil ice, which reduces the wind- and wave-driven turbulence, a relatively quiet ice growth condition develops; the formation of columnar ice may then take place through downward congelation. The process leading to congelation ice formation is well described in *Petrich and Eicken* [2010] and is summarized here below.

As described in section 1, growing sea ice rejects most of the impurities in brine (including salt), because they are not incorporated in the ice crystal lattice. The rejected salt thus increases the salinity of a thin layer, which is a few millimetres to a few centimetres thick, ahead of the advancing interface; this results in a transport of salt from the more saline ice/water interface toward the less saline seawater (see section 4 for a detailed description of the transport process). At the same time, assuming thermodynamic equilibrium, the increase of salinity at the ice-water interface goes along with a decrease of the freezing point and a decrease of the temperature (Figure 4). As a result, there is a heat flux in the opposite direction (i.e., from the seawater towards the ice-water interface). Because heat transport occurs faster than the transport of salt, the thin layer ahead of the ice-water interface is said constitutionally supercooled; in other words, the temperature of the layer is below the salinity-dependent freezing point (Figure 5).

Any ice crystal that protrudes into the constitutionally supercooled zone will have an advantaged ice growth, because the heat released from the formation of the protrusion is conducted away from the ice-water interface (either upward through the ice, or downward, into the heat sink of the supercooled water layer). In addition, that ice crystal will grow faster than adjacent crystals, because it will reject the salt, which reduces the freezing point of the brine along its boundaries, making ice growth more difficult just next to it. Further, because ice grows faster in the basal plane, crystals with horizontal c-axes will outgrow those with c-axes off the horizontal (this is the so-called “geometric selection”). As a result of the previous

processes, the ice/water interface generally consists of submillimetre-thick vertical lamellar blades of ice crystals (termed "**columnar ice" texture**), separated by narrow films of brine (termed "brine layers") (Figure 5), and the layer where the ice volume fraction varies from 0 to 30 % is referred to as the skeletal layer.

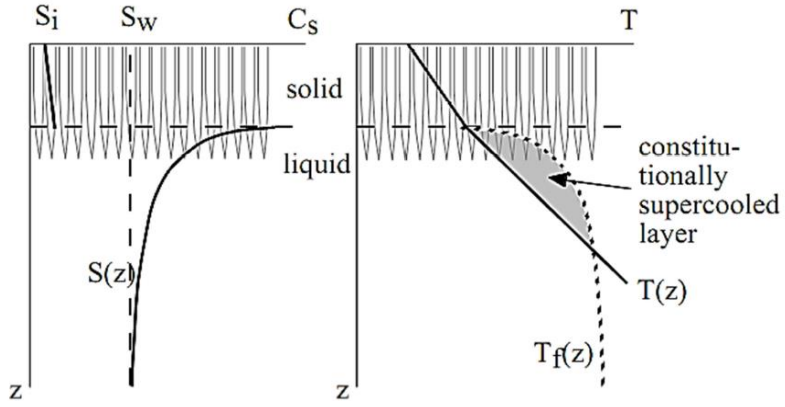

Figure 5 Drawing of the lamellar ice crystals and representation of the changes of salinity (left) and temperature (right) below the ice/water interface (dashed horizontal line). $T_f(z)$ is the freezing temperature for the actual salinity (S(z)). The shaded area where (T(z)) is below the $T_f(z)$ is the constitutionally supercooled layer [*Petrich and Eicken,* 2010]

.

As the skeletal layer further grows (i.e., addition of ice underneath), the ice temperature will decrease in the upper part of the skeletal layer; the water molecules in brine will freeze, adding ice to the existing ice blades, and resulting in a decrease of brine volume fraction. Eventually, the ice lamellae join up to form the so-called pure ice matrix, with isolated brine inclusions which concentrate almost all the impurities of the ice.

2.3 Platelet ice

Although platelet ice may have resulted from the processes described for granular frazil ice or columnar ice, it has neither the granular or columnar texture. Platelet texture is made of elongated (needle-like) grains, both in the vertical and horizontal thin sections [*Lange*, 1988] and could present a mixed platelet/congelation facies [*Jeffries et al.*, 1993] (see [*Tison et al.*, 1998] for a detailed description and illustrations of the different types of platelet textures). The highly disorganized texture of platelet ice (i.e., with crystals extending in all directions) results from a repetitive cycle of in-situ ice growth and freezing of voids in between the randomly orientated platelets [*Dempsey and Langhorne*, 2012]. The process of platelet formation is still discussed, but appears that to be associated with the presence of supercooled

water [*Crocker and Wadhams*, 1989; *Eicken and Lange*, 1989; *Jeffries et al.*, 1993; *Lewis and Perkin*, 1983].

In the vicinity of Antarctic ice shelves, platelet ice may form at deep water-depths [*Dieckmann et al.*, 1986], in supercooled ice shelf waters (ISW) which formation is associated with the deep thermohaline convection (DTC). Sea ice growth and the associated salt rejection contribute to the formation of the cold and saline high salinity shelf water (HSSW), which adiabatically descends to the ice shelf grounding line and melts the continental glacial ice (as it is warmer than the local freezing point at depth). The mixing between the meltwater and the HSSW forms the ISW, which rises adiabatically under its buoyancy and becomes supercooled (due to the changes of freezing point with depth) [*Crocker and Wadhams*, 1989; *Eicken and Lange*, 1989; *Foldvik and Kvinge*, 1974; *Jacobs et al.*, 1992]. Frazil ice crystals that unrestrainedly nucleate and grow from that supercooled ISW form platelet ice crystals [*Jeffries et al.*, 1993], which may then float or be dragged by the ISW to the front of the ice shelf, where they accrete at the bottom of sea ice [*Tison et al.*, 1998].

Direct nucleation and growth of platelet ice at the bottom of an existing ice cover from a supercooled water mass is also possible [*Gow et al.*, 1998]. The formation mechanism is thus similar to that of columnar ice, but since platelet ice directly grows into the supercooled water, while columnar forms its own pool of supercooled water through salt rejection (section 2.2), in-situ grown platelet ice presents a more disorientated texture than columnar ice, although less random than the "buoyant" platelet ice (described here above) [*Gow et al.*, 1998].

In Arctic, where large ice shelves are absent, platelet ice is scarce and supercooling is more usually associated with under-ice melt ponds [*Eicken*, 1994; *Jeffries et al.*, 1995] where double diffusion occurs (i.e, supercooling induced by the more rapid transfer of heat than salt between the under-ice meltwater and the surrounding water mass) [*Martin and Kauffman*, 1974].

2.4 Snow ice

Snow ice is frequently observed in the Southern ocean, where the snow is sufficiently thick, in comparison to the ice thickness, to depress the ice under the sea level (i.e., negative freeboard). Seawater may thus infiltrate laterally and vertically, floods the ice surface and subsequently refreezes with the water-saturated snow to form snow ice [*Fritsen et al.*, 1998]. Because snow ice has also a granular texture as for frazil ice, stable water isotope measurements are useful to discriminate the two ice types [*Eicken*, 1998; *Lange et al.*, 1990] (section 3.3).

2.5 Superimposed ice

In late summer, surface snow melt may percolate into the underlying snow. Depending on the snow permeability and the thermal regime of the ice, the meltwater can refreeze as a distinct bubble-free layer of pure ice within the snow or at the snow/ice interface, forming the superimposed ice [*Haas et al.*, 2001; *Nicolaus et al.*, 2003].

2.6 Large-scale deformation of sea ice covers

Depending on the intensity and the direction of winds and depending on the ocean circulation, sea ice cover may experience a convergent or divergent regime over a large extent (Figure 3). Divergent regimes may results in the formation of opening in the pack of ice: (with increasing width) cracks or fractures, leads or polynyas. Cracks and fractures do not allow the navigation of surface vessels, in contrast to leads and polynyas [*WMO*, 1970]; the latter may extend over tens to tens of thousands of square kilometres [*Brandon and Wadhams*, 1999]. Convergent dynamics result in the overlap of ice layers on the top of each other [e.g., *Eicken and Lange*, 1989]. Thin ice layers (e.g., frequently new ice) that slide on the top of each other are referred to as “rafting”, while thicker ice layers that fracture and pile on the top of themselves are referred to as “ridging” [*WMO*, 1970].

2.7 Implications of sea ice texture and morphologies on the distribution of biogeochemical compounds

The identification of sea ice texture not only provides information on the history of the sea ice cover, but also on the development of the different biological communities in it. It has been suggested [*Garrison et al.*, 1983] and verified experimentally [*Garrison et al.*, 1989] that the scavenging associated with the formation of frazil crystals leads to the incorporation of microorganisms at the beginning of the ice growth, forming thereby the surface

community. As sea ice further grows, it may serve as a substrate for the development of the internal-, the bottom-, and the sub-ice communities [*Horner et al.*, 1992]. For the surface- and the internal communities, where nutrient availability is often restricted [*Arrigo et al.*, 2010], the infiltration of seawater associated with snow ice formation, rafting or ridging, appears crucial for the nutrient supply of the surface and internal communities [*Ackley and Sullivan*, 1994; *Kattner et al.*, 2004]. For the bottom communities, where nutrient supply is less restricted because of the proximity to seawater, the formation of platelet ice, which is more porous than the columnar ice and any other ice types, is known to be associated with a much larger concentrations of microorganisms [*Arrigo et al.*, 2010].

The influence of sea ice texture on gases has been little studied. Theoretical considerations suggest that the formation of the "primary ice layer" (i.e., frazil ice) and "infiltration ice" (i.e., snow ice and superimposed ice) should induce the incorporation of gases from both seawater and the atmosphere [*Tsurikov*, 1979]. Observations show that turbulent conditions enhance gas incorporation in sea ice [*Tison et al.*, 2002], and there are both evidence indicating that superimposed ice affects gas exchanges through sea ice [*Tison et al.*, 2008] and the contrary [*Nomura et al.*, 2010].

3 Characterization of the physical properties of sea ice

For the interpretation of biogeochemical dynamics in sea ice, it is recommended to provide data about the physical framework [*Miller et al.*, under revision]. These data – namely temperature, salinity, brine volume fraction, brine salinity, ice texture and water stable isotopes – are often referred to as the physical properties of sea ice, although the term "physical properties" may have a wider meaning, including properties like thermal conductivity, albedo, dielectric properties and ice strength [*Petrich and Eicken*, 2010].

Ice temperature and bulk salinity (i.e., the salinity of a melted ice sample) are arguably the two most important physical variables for understanding the physical constraints on biogeochemical processes on non-deformed sea ice [*Hunke et al.*, 2011]. Indeed, using temperature and salinity, and assuming thermodynamic equilibrium between ice and brine, we may calculate the brine volume fraction and the brine salinity of sea ice, which determine the permeability of the ice [*Golden et al.*, 1998] (section 3.1), and whether mineral precipitation [*Assur*, 1958] (section 5.1.1) or brine convection could occur [*Notz and Worster*, 2009] (section 4.1.1).

3.1 Brine volume fraction

Based on the data compiled by *Assur* [1958] for the phase relations and based on the continuity equations for a multiphase sea ice mixture, *Cox and Weeks* [1983] derived a set of equations describing the brine volume fraction (φ) as a function of ice temperature (T) and salinity (S):

$$\varphi = \left(1 - \frac{Va}{V}\right) \frac{(\rho_i/1000)S}{F_1(T) - (\rho_i/1000)S \quad F_2(T)} \qquad \text{(Eq. 1)}$$

The density of pure ice is given as:

$$\rho_i = 917 - 0.1403\,T \qquad \text{(Eq. 2)}$$

with ρi in kg m^{-3} and T in °C. F_1 (T) and F_2 (T) are empirical polynomial functions $F_i(T) = a_i + b_iT + c_iT^2 + d_iT^3$, based on the phase relations. The coefficients for different temperature intervals are listed in Table 1. V_a/V is generally neglected in the calculation of brine volume fraction in eq.1, because it is typically much smaller than φ in first-year ice. However, in multiyear or deteriorated ice [*Timco and Frederking*, 1996], where V_a/V may be significant, it is important to either measure the density of a sea ice sample or its total gas content, in order to subtract the air volume fraction (V_a/V) for accurate estimate of φ.

Table 1 *Petrich and Eicken* [2010]'s compilation of the coefficients for $F_1(T)$ and $F_2(T)$ for different temperature intervals, based on *Cox and Weeks* [1983] and *Leppäranta and Manninen* [1988].

T, °C	a_1	b_1	c_1	d_1
$0 \geq T > -2$	−0.041221	−18.407	0.58402	0.21454
$-2 \geq T \geq -22.9$	−4.732	−22.45	−0.6397	−0.01074
$-22.9 > T \geq -30$	9899	1309	55.27	0.7160
T, °C	a_2	b_2	c_2	d_2
$0 \geq T > -2$	0.090312	−0.016111	1.2291×10^{-4}	1.3603×10^{-4}
$-2 \geq T \geq -22.9$	0.08903	−0.01763	-5.330×10^{-4}	-8.801×10^{-6}
$-22.9 > T \geq -30$	8.547	1.089	0.04518	5.819×10^{-4}

With the introduction of the mushy layer theory to sea ice, describing sea ice as a mixture of solid ice and liquid brine (i.e. assuming an ideal gas-free sample) [*Wettlaufer et al.*, 1997], bulk salinity S is given by the salinity of brine S_{br} multiplied by the brine volume fraction (φ), and the salinity of the pure ice (S_{ice}) multiplied by the fraction of solid ice (1- φ) (eq. 3).

$$S = \varphi * S_{br} + (1- \varphi) * S_{ice} \quad \text{(Eq. 3)}$$

Rearranging eq. 3 and assuming that S_{ice} equals to 0:

$$\varphi = S / S_{br} \quad \text{(Eq. 4)}$$

In comparison to the previous equations from *Cox and Weeks* [1983] (eq. 1), this mushy-layer formulation only considers two phases (ice and brine), and thus is only valid for ideal gas-free samples. However, the main advantage is that eq. 3 is much easier to grasp (i.e, to represent physically) than the eq. 1.

φ fraction is often used as a proxy of sea ice permeability, following *Golden et al.* [1998], who suggested that the permeability for fluid in sea ice increases drastically when the φ fraction exceeds 5 %. Since this corresponds to an ice temperature of 5 °C for a typical ice salinity of 5, that theory is also referred to as "the law of fives". However, as discussed later, this is probably not fully accurate (section 4.1.4).

3.2 Brine salinity

Phase equilibrium between the brine and its surrounded pure ice matrix implies that changes in ice temperature result in changes in φ and S_{br} [*Hunke et al.*, 2011]. Indeed, when cooling a sea ice sample, some of the liquid water of the brine freezes, reducing the volume of the brine inclusion (i.e., φ) and increasing S_{br}. In contrast, when warming a sea ice sample, some of the freshwater ice dissolves in brine, increasing the φ and decreasing the S_{br} [*Hunke et al.*, 2011].

Notz et al. [2005] determined an empirical function for BrS as a function of the ice temperature (T) based on the data of [*Assur*, 1958]:

$$S_{br} = -1.2 - 21.8T - 0.919T^2 - 0.0178T^3. \quad \text{(Eq. 5)}$$

Vancoppenolle et al. [2013a] noted that a simpler, linear relationship between S_{br} and T is sometimes used [e.g., *Bitz and Lipscomb*, 1999; *Schwerdtfeger*, 1963] (eq. 6). That relationship is based on a linear extrapolation of the dependence of the freezing point to seawater salinity (seen in Figure 4) and gives quite different results in comparison to eq. 5 (about a difference of 100 in S_{br} at -15 °C). As S_{br} strongly affects the calculation of φ (eq. 4) and Ra (eq. 8), it is recommended to use eq. 5 rather than eq. 6 [*Vancoppenolle et al.*, 2013a].

$$S_{br} = - T / 0.054 \quad \text{(Eq. 6)}$$

3.3 Water stable isotopes in sea ice ($\delta^{18}O$, δD)

The measurement of water stable isotopes ($\delta^{18}O$ and δD) has been shown useful for distinguishing snow ice and superimposed ice from naturally frozen sea ice (which all have a granular texture; section 2.1), and for highlighting the changes in water masses and sea ice growth rate (section 4.1.2) [*Eicken*, 1998].

$\delta^{18}O$ of a sample describes the relative abundance of the $^{18}O/^{16}O$ ratio of the sample in comparison to that of the standard VSMO (Vienna Standard Mean Ocean Water), as in the following equation where ^{18}O and ^{16}O are two isotopes of oxygen:

$$\delta^{18}O\ (‰) = \frac{\left(\frac{^{18}O}{^{16}O}\right)sample - \left(\frac{^{18}O}{^{16}O}\right)standard}{\left(\frac{^{18}O}{^{16}O}\right)standard} x\ 1000 \qquad \text{(Eq. 7)}$$

δD of a sample can be expressed with the same equation, but with $^{2}H/^{1}H$ instead of $^{18}O/^{16}O$, and where ^{2}H and ^{1}H are two isotopes of hydrogen.

The interest in measuring $\delta^{18}O$ and δD is based on the isotope fractionation (i.e. changes in the abundance of $^{18}O/^{16}O$ and $^{2}H/^{1}H$ respectively) that occurs during a phase transition. When a water mass evaporates, the vapour phase is enriched in light isotopes (^{16}O and ^{1}H), leaving the parent water mass with a higher abundance of heavy isotopes (^{18}O and ^{2}H). When precipitation occurs, the rain droplets or snow are enriched in heavy isotopes in comparison to the clouds, but as they are derived from the vapour phase, they are still more depleted in heavy isotopes than the parent water mass. Now, as seawater freezes, the solid phase (ice) is enriched in heavy isotopes in comparison to the parent seawater. As a result of the isotope fractionation described here above, the $\delta^{18}O$ and δD of snow are more negative than those of seawater, which are more negative than those of sea ice (from the same location).

Because $\delta^{18}O$ and δD have a conservative property (i.e. they do not change due to chemical or biological processes), knowing the distinct $\delta^{18}O$ or δD of snow, ice and seawater (e.g., $\delta^{18}O$ of -21, 2.1 and 0.3 ‰ respectively in Fram Strait [*Meredith et al.*, 2001]), it is possible to highlight the influence of snow meltwater in superimposed ice and the influence of seawater in snow ice [*Eicken*, 1998; *Eicken et al.*, 2002].

In addition, since the $\delta^{18}O$ and δD of sea ice depend on those of the parent water, and the fractionation efficiency (i.e., the difference of $\delta^{18}O$ and δD between sea ice and the parent

water) partly depends on sea ice growth rate, $\delta^{18}O$ and δD of sea ice have been used for the study of under-ice water circulation and mixing in estuaries [*Macdonald et al.*, 1999; *Macdonald et al.*, 1995], and for deducing ice growth rate [*Eicken*, 1998; *I J Smith et al.*, 2012; *Souchez et al.*, 1987].

4 Initial incorporation and transport processes in sea ice

Among all the transport processes, those related to the transport of brine have been the most extensively discussed. As some concepts for describing the transport of gases directly derive from those established for the transport of brine [*Tsurikov*, 1979], this section begins with a state-of-art on the transport of brine, in non-deformed ice.

4.1 The transport of brine

4.1.1 Processes regulating the vertical distribution of salinity in sea ice

It is well known that the bulk salinity of sea ice is lower than that of the seawater from which it has formed, and that the bulk salinity profile changes across seasons [e.g., *Malmgren*, 1927; *Nakawo and Sinha*, 1981]. Nine processes have been suggested to explain these observations; five of which are associated with the ice growth (the initial rejection of salt at the ice-ocean interface during ice growth, the diffusion of salt, brine expulsion, gravity drainage and flushing), two others, with snow load (flooding and flushing), one, with tidal effect, and the last one, with EPS (extracellular polymeric substances) secretion. Each of these processes will be described here below, and their significance discussed in the next section (see *Weeks* [2010, p.156-170] for a more detailed discussion).

- **Initial entrapment or initial rejection**

The initial rejection of salt has been described using the "Burton-Prim Slichter" model [*Cox and Weeks*, 1975; *Cox and Weeks*, 1988], also referred to as the stagnant boundary-layer diffusion model [*Eicken*, 1998]. This model is based on the concept of *Burton et al.* [1953], where the solidification of a multi-component melt (e.g., a mixture of two metal melts) leads to a fractionation, so that the mixing ratio of the two components in the solid is different from that in the initial liquid. Applied to sea ice, the BPS model suggests that the mixing ratio of salt and water in sea ice is different from that in seawater, due to the salt rejection during ice growth. That fractionation is described by the effective distribution coefficient k_{eff} ($=S_i/S_w$), which is derived from empirical functions of ice growth velocity and the thickness of the

boundary layer (see equations in *Weeks* [2010, p.156-170] and *Eicken* [1998, p.101-102]). Note that k_{eff} varies largely in the literature, ranging from 0.12 [*Nakawo and Sinha*, 1981] to 0.95 (for frazil ice) [*Smedsrud et al.*, 2003].

- **Brine diffusion**

Initially proposed by *Whitman* [1926], brine diffusion describes the migration of brine inclusions due to decreasing ice temperature. In winter, if the ice temperature increases downward, the colder upper end of a brine pocket is more saline than the warmer lower end (due to phase equilibrium), and salt will diffuse from the upper end to the lower end. Because of that salt diffusion, ice would form in the now-less-saline upper end but dissolve in the now-more-saline bottom. The repetition of that migration process in cooling sea ice results in a downward migration of brine pockets, which eventually leave the ice.

- **Brine expulsion**

Brine expulsion describes the transport of salt due to the increasing pure ice volume during ice growth. When a sea ice sample is cooled, part of the liquid water in brine freezes, forming a pure ice structure, which is less dense than brine and which thus, occupies a larger volume than brine (section 1). That increase of pure volume may fracture the ice, resulting in an upward or downward redistribution of brine [*Bennington*, 1963].

- **Gravity drainage**

When the ice temperature increases downwards, brine salinity decreases downwards (section 3.2). This salinity gradient drives an unstable density gradient that promotes brine convection in permeable ice layers. That convection of brine and its replacement with the less dense underlying seawater is referred to as gravity drainage, brine convection, or mushy-layer mode convection [*Notz and Worster*, 2009; *Worster and Wettlaufer*, 1997] (section 4.1.3).

The potential of gravity drainage at an ice depth z using the Rayleigh number, formulated as following:

$$Ra = \frac{g\ h\ \Delta\rho\ \Pi(\varphi_{min})}{\kappa\mu} \qquad \text{(Eq. 8)}$$

where g is the gravity coefficient, $\Delta\rho$ and h, the density gradient and the thickness between the ice depth z and the bottom of the ice respectively. κ is the thermal diffusion coefficient, μ the viscosity of the ice, and Π the permeability of the ice, which is a function of φ.

The Rayleigh number can be interpreted in two ways: it could be the ratio of the potential energy $g\Delta\rho h$ available for convection and the energy $\kappa\mu/\Pi$ that is dissipated during convection through thermal diffusion and internal friction due to the viscosity of brine [*Notz and Worster*, 2009], or, it could be the ratio between a conductive time scale z^2/k and a convective time scale $z\mu/g\Delta r\Pi$ as determined from Darcy's law [*Vancoppenolle et al.*, 2013a]. If the conductive time scale is shorter than the convective time scale, i.e., heat conduction occurs faster than the brine convection, then, the convecting brine will quickly adopt the temperature of the surrounding pure ice, with an adjustment of the brine salinity (due to phase equilibrium), and convection will stop as there is no longer density gradient [*Vancoppenolle et al.*, 2013a].

- **Flushing**

Flushing describes the downward movement of brine under the pressure of the overhead snow meltwater [*Eicken et al.*, 2002; *Eicken et al.*, 2004]. It can further cause a smaller scale downward displacement of brine afterwards, if the ice is still permeable and if the meltwater refreezes at the bottom of the ice, which results in an elevation of the freeboard and a hydrostatic readjustment [*Eicken et al.*, 2002; *Eicken et al.*, 2004].

- **Flooding**

In locations where the snow load is sufficient to press the ice surface below the sea level, the brine may displace upward due to hydrostatic readjustment until it causes flooding. That process has been investigated in details in *Hudier et al.* [1995] (although it was termed "upward flushing") and in *Maksym and Jeffries* [2000]. But as highlighted in *Maksym and Jeffries* [2000], there are other ways by which surface flooding can occur: infiltration from the edges of an ice floe, and migration through poorly consolidated ice (e.g., ridged ice and cracks).

- **Forced-convection**

Forced-convection occurs at the bottom of the ice and is driven by a shear flow (above 5.8 cm s^{-1}) under the ice (i.e. ocean current or tides) [*Neufeld and Wettlaufer*, 2008a; b]. The shear flow is thought to create pressure perturbations at the ice/water interface, which drive brine convections (i.e., gravity drainage) [*Feltham et al.*, 2002; *Neufeld and Wettlaufer*, 2008b]. This process supports the previous hypotheses of tide-driven nutrient supply for ice algae [*Cota and Horne*, 1989; *Cota et al.*, 1987].

Forced-convection is also found to be associated with the formation of aligned ice lamellae [*Neufeld and Wettlaufer*, 2008a], because the under-ice current that drives forced-convection also causes an alignment of ice lamellae perpendicular (c-axes parallel) to the direction of the flow [e.g., *Langhorne and Robinson*, 1986; *Stander and Michel*, 1989; *Weeks and Gow*, 1978]. Some have suggested that the alignment is due to the mechanic strains exerted by the current on the ice crystals [*Stander and Michel*, 1989], while others claim that the alignment is due to the formation of forced-convection rolls [*Neufeld and Wettlaufer*, 2008a] or turbulent eddies [*Weeks and Gow*, 1978]. In the latter theory, ice lamellae orientated perpendicularly to the current flow have a advantaged ice growth and will quickly outgrow the other ice crystals, because they promote the formation of rolls and eddies that favour salt transport away from their ice/water interface [*Neufeld and Wettlaufer*, 2008a; *Weeks and Gow*, 1978]. Although there is no consensus on how the current affects the alignment of ice crystals, it is however certain that under-ice current significantly modifies the texture (i.e., the arrangement, size and shape) and the porosity of the ice [*Petrich and Eicken*, 2010], and thereby influences the incorporation of salts [*Petrich and Eicken*, 2010] and gases [*Tison et al.*, 2002] in the ice.

- **EPS production**

It has been suggested that the microbial production of EPS (extracellular polymeric substance) (section 5.2.2) alters the microstructure of the brine channels, reducing the pore spaces, and thus the permeability of the ice [*Krembs and Deming*, 2008]. As a result, salt expulsion from the ice is less efficient and salts are better retained in ice than if EPS was absent [*Krembs et al.*, 2011].

4.1.2 Significance of each process regulating the vertical distribution of salinity in sea ice

To determine the significance of each process of desalination during ice growth, *Notz and Worster* [2009] simulated the changes of bulk salinity with depth and over time, assuming that sea ice is a mushy layer (section 3.1), and assuming a conservation of heat, mass and solutes, and phase equilibrium between brine and the pure ice matrix, but without gravity drainage. Their results show that brine diffusion and brine expulsion are relevant for the redistribution of salt within sea ice, but not for large-scale loss of salt from it. The velocity of salt advection due to brine diffusion is only a few centimetres per year, whereas the velocity due to brine expulsion is always lower than the growth rate of the ice. Further, their simulations result in a continuum of brine salinity between the bottom of the ice and the underlying seawater, which are consistent with observations in the laboratory [*Notz et al.*, 2005]; hence, there is apparently no segregation of salt at the ice/water interface, and thus, no initial rejection of salt (section 4.1.1)), in the absence of gravity drainage. Therefore, *Notz and Worster* [2009] conclude that gravity drainage (or brine convection) should be the main process of desalination during ice growth.

Although the initial rejection of salt does not contribute to large-scale loss of salt from sea ice [*Notz and Worster*, 2009], it is useful for describing the fractionation of ^{16}O and ^{18}O between seawater and ice during sea ice formation [*Eicken*, 1998]. This is expected since the formulation was expressly developed for describing the solidification (e.g., seawater – sea ice) rather than the concentration (e.g., seawater - brine) (section 4.1.1). When describing the fractionation of ^{16}O and ^{18}O, the use of the fractionation factor α or coefficient ε replaces that of the effective distribution coefficient k_{eff} (section 4.1.2) [*Eicken*, 1998].

Flushing is commonly recognized to be the main desalination process during ice decay, and flooding may also significantly affect the salinity profiles in locations with heavy snow loading. However, their large-scale impacts remain difficult to assess, because these are three-dimensional processes [*Eicken et al.*, 2002; *Eicken et al.*, 2004]; assessing flushing and flooding requires a good estimate of both the horizontal and the vertical permeability, which is currently missing. The impact of forced-convection on bulk ice salinity has not been investigated yet, but EPS production may apparently increase bulk ice salinity by 11 to 59 %, according to the experiment of *Krembs et al.* [2011].

4.1.3 The mushy-layer theory and its implications

The observations of the continuum of salinity at the ice/water interface in experiments [*Notz et al.*, 2005] and in mushy-layer-based simulations [*Notz and Worster*, 2009] have marked a significant transition in our understanding of the incorporation of impurities in sea ice during ice growth.

- **Boundary-layer theory versus mushy-layer theory**

Figure 6 presents the differences between the boundary-layer theory (i.e., the traditional view on how impurities get incorporated in sea ice) and the mushy-layer theory (i.e., the relatively more modern view).

The boundary-layer theory suggests that a fractionation (with a coefficient k_{eff}) occurs during sea ice formation, leading to a difference of salinity, between the ice and seawater (section 4.1.1). It was initially suggested that salts diffuse in the boundary-layer, from the ice/water interface that is enriched in salt (due to the rejection of salt from sea ice ahead of the growing freezing front) to the underlying seawater [e.g., *Cox and Weeks*, 1988; *Nakawo and Sinha*, 1981]. However, since it was then verified that the transport of solutes rarely occurs through molecular transport alone, but is enhanced by convecto-diffusive fluxes and turbulent mixing [e.g., *Garandet et al.*, 2000], the concept of convecto-diffusion is then used for describing the transport of solutes in the boundary layer [*Eicken*, 1998].

In contrast to the boundary-layer theory, the mushy-layer theory suggests a continuum of salinity at the ice/water interface. Because bulk ice is a mixture between pure ice and brine, at the ice/water interface where the solid fraction approaches 0 % and the liquid fraction 100 %, bulk ice salinity approaches the brine- and seawater salinity. The proponents of the mushy-layer theory agree on the rejection of salt by the growing ice crystals, with enrichment of the interstices of the mushy layer and the boundary-layer (green and orange dashed lines respectively in Figure 6). However, they suggest that convection occurs when the conditions become sufficiently unstable, i.e., with increasing Rayleigh numbers. The convection is referred to as a "boundary-layer mode convection", when it is limited to the boundary-layer or as a "mushy-layer mode convection" (i.e., gravity drainage or brine convection (section 4.1.1)) when it develops within the ice and beyond the lower-bond of the boundary-layer. As a result, the salinity of bulk ice approaches brine- and seawater salinity [*Worster*, 2000; *Worster and Wettlaufer*, 1997].

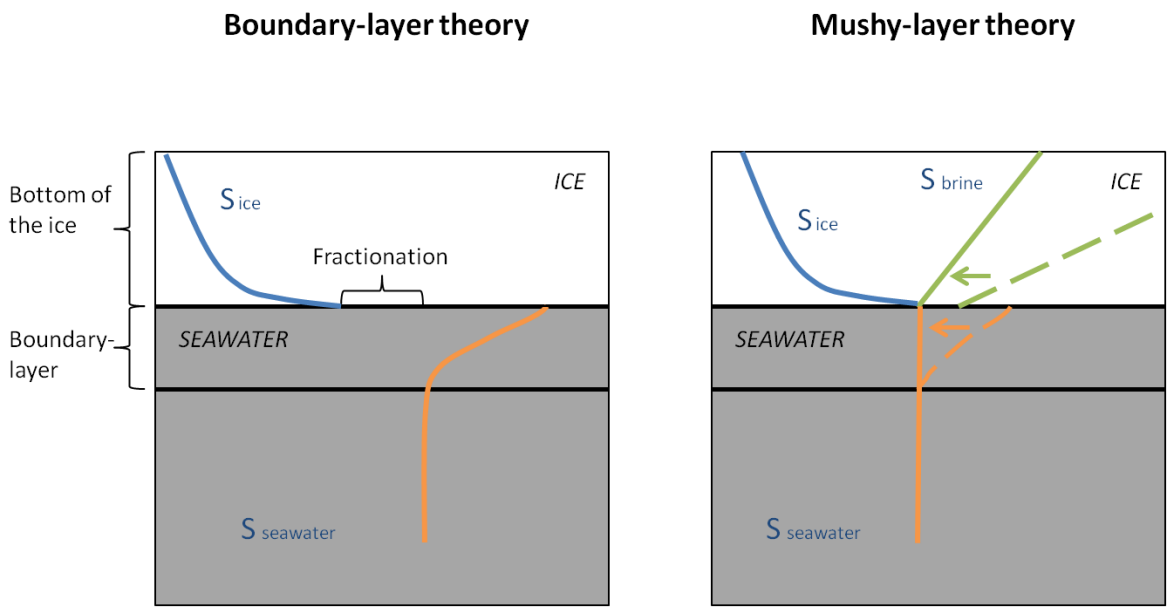

Figure 6 Schematic diagrams showing the differences in the perception of the salinity profiles at the ice/water interfaces between the boundary-layer theory and the mushy-layer theory. Dashed-lines in the right hand figure are temporary profiles of brine salinity and seawater salinity, before a convection event (see details in the text).

- **Percolation theory versus mushy-layer theory**

The introduction of the mushy-layer theory has also brought a new point of view in our understanding on the transport of impurities in sea ice during ice growth, initially focused on the percolation theory.

The percolation theory suggests that sea ice, like other porous materials (e.g., soils, rocks), has a critical porosity threshold below which the permeability decrease drastically (i.e., the pores are too disconnected to allow a downward fluid percolation through the pore network) [e.g., *Hunt et al.*, 2014]. That threshold is estimated to be at a φ of 5 %, based on the similar microstructural properties between compressed powder and columnar ice [*Golden et al.*, 1998]; on the percolation model of *Golden et al.* [2007]where sea ice is described as a lattice network with randomly placed open and closed bonds; and on the measurements made on natural ice cores (Figure 7). Since φ of 5 % corresponds to an ice temperature of 5 °C for a typical ice salinity of 5, that theory is also referred to as “the law of fives” [*Golden et al.*, 1998].

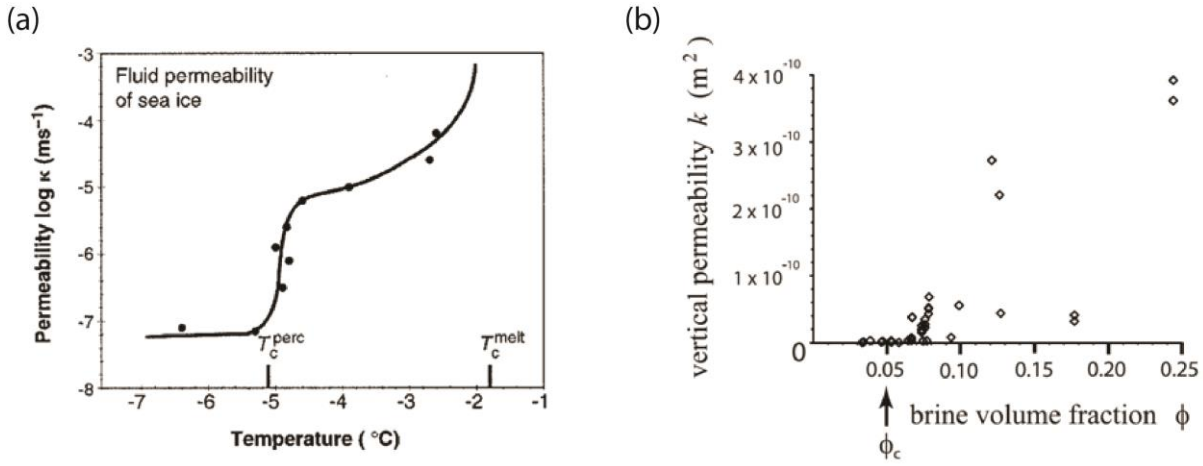

Figure 7 (a) Changes in permeability as a function of the ice temperature from *Golden et al.* [1998], based on *Ono and Kasai* [1985], and (b) changes in vertical permeability as a function of the brine volume fraction from *Golden et al.* [2007]. Φ_c is the critical percolation threshold, φ = 5 %. The SI unit for permeability is m² (as in b). What *Golden et al.* [1998] and *Ono and Kasai* [1985] have described as permeability and expressed in ms^{-1} was likely the hydraulic conductivity, according to the description of their measurement method. Permeability is the property of the porous media, while the hydraulic conductivity integrates both the permeability and the property of the fluid (i.e., its viscosity and density) that passes through the media [*ASCE*, 1996, p.263-264].

Although a φ of 5 % is generally used as a criterion for distinguishing the permeable and the impermeable ice layers, one needs to be aware of some important assumptions underlying that critical percolation threshold. First, sea ice permeability strongly depends on the distribution of brine inclusions. *Golden et al.* [1998] have thus suggested that the percolation threshold that was established for columnar ice could be higher for granular ice, which is more randomly distributed. In addition, *Zhu et al.* [2006] and *Golden et al.* [2007] used a percolation model and a hierarchical model respectively, but with a different representation of the distribution of the brine inclusions than *Golden et al.* [1998], and found no critical threshold. *Pringle et al.* [2009], in contrast, found critical vertical percolation thresholds ranging from 3.9 to 6.9 % of φ, using finite size scaling analyses. Second, the percolation threshold is lowered if the pore network contains excluded volumes, i.e., non-brine inclusions that are accounted in the brine volume fraction. The so-called excluded volumes include precipitated crystals and microorganisms, as well as gas bubbles, while air volume is assumed to be negligible in eq. 1 – section 3.1).

While the percolation theory is solely based on φ for describing the propensity for a fluid to transit from the top to the bottom of sea ice – either naturally or forced –, the mushy-layer Rayleigh number (Ra) describes the propensity for – natural – gravity drainage based on the

competing effect of the energy available for convection and the energy that is dissipated during convection through thermal diffusion and internal friction due to the viscosity of brine [*Notz and Worster*, 2009]. Therefore, φ is only one parameter among many others in the calculation of Ra (section 4.1.1), in contrast to the percolation theory. As a result, an ice layer could have a φ above 5 % (i.e., being permeable according to *Golden et al.* [1998]), but with a Ra below the critical threshold [*Jardon et al.*, 2013]; this indicates that natural convection does not occur, but does not mean that forced convection or diffusion could not occur through the permeable ice layer [*Neufeld and Wettlaufer*, 2008b; *Worster and Wettlaufer*, 1997].

Similar to the controversy on the critical threshold in the percolation theory discussed above, there is currently no consensus on the critical Ra values for convection: theoretically 1 [Notz, personal communication], but 3.2-7.1 in *Griewank and Notz* [2013], 5 in *Vancoppenolle et al.* [2010], 7 in *Notz and Worster* [2008] and 10 in *Worster and Wettlaufer* [1997]. These diverse critical Ra values result from the differences in their assessment method and parameterization [*Vancoppenolle et al.*, 2013a]. For instance, using the linear relationship between the temperature and brine salinity instead of the formulation of *Notz et al.* [2005] leads to a difference of S_{br} of 100 g/kg at -15 °C (section 3.2), which inevitably results in different values for the critical Ra. In addition, different formulations also exist for the thermal diffusivity [*Notz and Worster*, 2008; *Pringle et al.*, 2007] and the ice permeability [*Eicken et al.*, 2004; *Freitag*, 1999, p. 48; *Petrich et al.*, 2006] (section 4.1.4). The issue of parameterization is further complicated if the Ra number is derived from temperature and salinity that are measured on extracted ice cores. Indeed, brine drainage due to gravity during the sampling may lead to an underestimation of the salinity. An average salt loss of about 0.3 induces an underestimation of Ra by 0.5, and an salt loss of 5 at the ice base, an underestimation of Ra by 2.7 [*Vancoppenolle et al.*, 2013a].

4.1.4 The relationship between the brine volume fraction and sea ice permeability

Sea ice permeability is a crucial parameter for quantifying the fluid flow through sea ice, regardless of whether we consider the percolation- or the mushy-layer theory (section 4.1.3) [*Pringle and Ingham*, 2009].

Vertical ice permeability has been shown to depend on the total porosity of the ice, thus φ, although the scarcity of the data does not help to establish one obvious empirical relationship between vertical permeability and φ (Figure 8); instead, diverse relationships between these parameters have been proposed [*Eicken et al.*, 2004; *Freitag*, 1999; *Petrich et al.*, 2006].

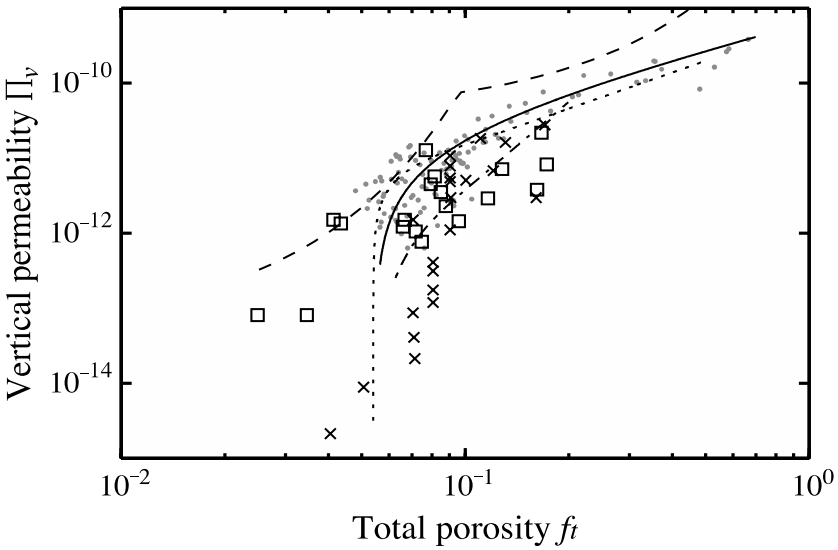

Figure 8 Vertical permeability as a function of total porosity from *Petrich et al.* [2006]. Relationships are from *Petrich et al.* [2006] (solid), *Eicken et al.* [2004] (dashed) and *Freitag* [1999] for young and old ice (dash-dot and dotted lines respectively). The data points are from *Saeki et al.* [1986] (squares), *Maksym and Jeffries* [2000] (crosses) based on *Ono and Kasai* [1985] and *Saito and Ono* [1978], and *Cox and Weeks* [1975] (grey dots).

φ represents the total porosity f_t of sea ice, whereas the volume fraction of brine that is effectively connected for fluid transport is the effective porosity f_e. Therefore, it is more accurate to calculate sea ice vertical permeability as a function of f_e, rather than φ, as in *Freitag* [1999, p. 48, eq. 2.18]. In spite of that, different authors provide equations for calculating the vertical permeability as a function of φ rather than f_e [*Eicken et al.*, 2004; *Freitag*, 1999, p. 48, eq. 2.19; *Petrich et al.*, 2006]; this is understandable, because φ can be easily obtained from temperature and salinity measurements (section 3.1), and because the difference between f_e and φ is only significant for φ between 5 and 9 %. Indeed, f_e approaches 0 for φ below 5 % (following the percolation theory of *Golden et al.* [1998]) and approaches φ for φ exceeding 9 % (see *Petrich et al.* [2006] for a detailed discussion).

Sea ice permeability further depends on the morphology of the brine inclusions, in addition to the pore space connectivity (determined by the φ) [*Pringle et al.*, 2009]. The early experiment of *Ono and Kasai* [1985] has already shown that sea ice permeability is different for upward and downward brine movement, but *Pringle et al.* [2009] provide a far more

comprehensive study on the anisotropy of sea ice permeability: they found vertical critical porosities ranging from 3.9 to 6.9 % of φ, and horizontal critical porosities of 9 and 14 % for fluid motion parallel and normal to the ice lamellae.

4.1.5 A synthesis on the relationship between the brine volume fraction, sea ice permeability, and brine transport

Sections 4.1.3 and 4.1.4 have highlighted how the relationship between φ, sea ice permeability and brine transport is not straightforward. The most certain and relevant observation is that brine transport halts (or near halts) at low φ, but the exact critical φ and Ra below which brine transport and natural brine convection halt are still matter of debate. This calls for caution when assessing sea ice permeability and brine convection based on φ and Ra respectively. A solution is to interpret the data qualitatively and relatively (e.g., "*in winter, the ice is more prone to convection at the base than at the top"*, from [*Vancoppenolle et al.*, 2013a]), another one is to combine different approaches (or measurements) to strengthen the indication of φ and Ra on sea ice permeability and brine convection [e.g., *Jardon et al.*, 2013; *Zhou et al.*, 2013].

4.2 Transport of gaseous compounds

4.2.1 Comparison with the transport of sea salt

Because gases may be present in the dissolved and gaseous states in sea ice, the temperature-driven processes causing salt loss from sea ice should be relevant for dissolved gases, but not for gas bubbles. However, most of the proposed processes for describing gas transport, reviewed in *Tsurikov* [1979], are primarily theoretical, i.e., unsubstantiated. *Tsurikov* [1979] boldly wrote that he has *"imagined some processes which result (or would result) in the formation of gas inclusions"*.

Similarly to initial rejection, *Matsuo and Miyake* [1966] have also proposed that gas diffuses from sea ice before its consolidation (processes 1a in *Tsurikov* [1979]). Moreover, similarly to brine diffusion, gas inclusions are also believed to move downward under the effect of the temperature gradient in the ice (process 3b in *Tsurikov* [1979]). The increase of pure ice volume, which has been suggested to cause brine pocket migration, has not been discussed in *Tsurikov* [1979], but intuitively, dissolved gas should be redistributed in sea ice as does salt. The reverse process (i.e., the decrease of pure ice volume during ice melt) has been proposed to cause the formation of "*water-vapour-filled pores*" in sea ice (process 2b in *Tsurikov*

[1979]). Because the pure ice is less dense than brine, pure ice melt inevitably causes the formation of void that will rapidly be filled with water vapour [*Tsurikov*, 1979]. Observations showing that gas inclusions increase in size during ice melt [*Light et al.*, 2003] tends to support that suggestion, but it is doubtful that the gas inclusions are exclusively filled with water vapour, because gas equilibrium between the gas inclusions and brine would change the composition of the gas inclusions [*Perovich and Gow*, 1996].

Brine drainage should also cause the loss of dissolved gas. However, although that process has been suggested as the main cause of desalination during ice growth, its impact on gases still need to be assessed. Indeed, the impact of brine drainage on the gas content in sea ice depends on the partitioning of gases between the gas inclusions (or gas bubbles) and brine. The transport pathway for gas bubbles has not yet been described, but it would differ from that of dissolved gases which are subject to brine drainage, if one assumes that gas bubbles migrate upward due to their buoyancy (as the gas bubbles in a champagne flute) [*Liger-Belair*, 2005]. Therefore, if gases are mainly present in sea ice as gas bubbles, then brine drainage will not be effective for removing gases from sea ice. In contrast, if gases are mainly present in sea ice as dissolved gases, then brine drainage would be more effective. The partitioning of gases between gas bubbles and brine still has to be verified experimentally for the temperature and salinity conditions of sea ice (section 5.1.2), but gas bubbles likely contribute a significant part to the total gas content in sea ice during ice growth, because gas concentrations that are 2000 % larger than their solubility in seawater have been observed in sea ice [*Killawee et al.*, 1998]. Therefore, the effect of brine drainage in changing the total gas content could be minor during ice growth.

The formation of snow ice and superimposed ice may also change the gas composition of the ice (process 3a in *Tsurikov* [1979]) in addition to the ice salinity (section 2.7), but the impact of rifted/rafted ice, forced-convection and EPS production on gas composition has not yet been investigated.

4.2.2 Gas exchange at the air/ice interface, the specific particularity of the transport of gases in comparison to salts

The main particularity for the transport of gases is the air-ice exchange, which is much less relevant for the transport of salts. Direct injection of atmospheric air into sea ice is possible, during the formation of frazil ice (process 1a in *Tsurikov* [1979]), and during the whole ice

growth, as long as part of the sea ice remains above the sea-level (i.e., positive freeboard) (process 2a in *Tsurikov* [1979]), and provided that sea ice is permeable.

Based on our knowledge from open seawater studies, air-ice gas exchange should at least depend on the difference of partial pressure between brine and the atmosphere, wind speed and the diffusion coefficient [*Wanninkhof*, 1992]. However, in contrast to air-sea exchange, the diffusion coefficient in sea ice is only known for a few species (CO_2, SF_6, O_2, Ar and N_2) at specific temperatures (Table 2). The parameterization of air-ice gas exchange is further complicated by the fact that gas exchange does not occur through a free-surface of seawater, but rather through the pores of a perforated surface, that is possibly covered with snow; therefore air-ice gas exchange also depends on the permeability of the ice and the snow. As described in section 4.1.4, ice permeability is related to the φ and the morphology of the brine inclusions; in particular, the formation of superimposed ice may impede air-ice gas exchange [*Tison et al.*, 2010]. Snow permeability depends on the grain radius and the density of the snow [e.g., *Zermatten et al.*, 2014]. Although snow is generally more permeable than ice (ca. 10^{-10} to 10^{-8} m² for snow [*Zermatten et al.*, 2014] in comparison to 10^{-14} to 10^{-10} m² for sea ice [*Petrich et al.*, 2006]), snow cover may still act as an intermediate reservoir (or buffer) for gases until wind speed exceeds a critical threshold [*Heinesch et al.*, 2009; *Papakyriakou and Miller*, 2011].

Table 2 Diffusion coefficients in sea ice

References	Ice Temperature (°C)	Diffusion coefficients (10^{-5} cm^2 s^{-1})				
		CO_2	SF_6	O_2	Ar	N_2
Gosink et al. [1976]	-15 to -7	2	0.01			
Loose et al. [2010]	-12 to -2	24	13	3.9		
Crabeck et al. [submitted]	-3.8 to - 0.8			1.5-1.8	1.5-1.8	2.5

4.3 Transport of particulate compounds

Particulate compounds in sea ice are either inorganic (solid precipitates) or organic (particulate organic matter and microorganisms). Although some processes for their transport have been identified, they are not yet well constrained [*Vancoppenolle et al.*, 2013b]. For instance, it is still a matter of debate as to whether inorganic and organic particles are

transported passively as brine or whether they are retained by the sticky EPS (extracellular polymeric substance) [e.g., *Juhl et al.*, 2011; *Krembs et al.*, 2000], as for salts [*Krembs et al.*, 2011] (section 4.1.1). Further, some of the microorganisms (e.g., flagellates) are known to move actively (i.e., independently of the brine movement) within the brine channels [*Ackley and Sullivan*, 1994]; this makes the parameterisation of the particulate compounds in sea ice even more difficult [*Vancoppenolle et al.*, 2013b].

5 Biogeochemical processes in sea ice

In addition to the transport processes (section 4), biogeochemical processes within sea ice also change the concentrations of the biogeochemical compounds. Some of them are abiotic (section 5.1), while others are biotic (section 5.2).

5.1 Abiotic processes

5.1.1 Mineral precipitation

Decreasing ice temperature increases the ions concentrations in sea ice (section 3.2) and decreases the equilibrium constant K_{sp}, which both may result in mineral precipitation in sea ice. The simultaneous changes in brine concentration and K_{sp} theoretically result in the precipitation of different minerals [*Assur*, 1958]: for instance, calcite ($CaCO_3$) at -2.2 °C, mirabilite (Na_2SO_4 . $10H_2O$) at -6.3 °C, gypsum ($CaSO_4$. $2H_2O$) and hydrohalite (NaCl . $2H_2O$) at -22.9 °C, sylvite (KCl) at -33.0 °C, and hydrates of magnesium chloride ($MgCl_2$. $12H_2O$) at -36.2 °C, following the thermodynamic models of *Marion and Farren* [1999].

It has been suggested that mineral precipitation changes the ion composition of the brine in comparison to seawater, because the ions that are part of the minerals are less subject to diffusion and gravity drainage than those dissolved in brine [*Reeburgh and Springer-Young*, 1983]. For instance, because sylvite precipitates at lower temperature than mirabilite, gravity drainage and diffusion may reduce the concentration of Cl^- in comparison to SO_4^{2-}; as a result, SO_4^{2-} is more enriched with respect to Cl^- in brine, in comparison to their respective concentration in seawater [*Reeburgh and Springer-Young*, 1983]. However, more recent results of *Maus et al.* [2011], which combine both ion measurements and a description of the physical framework (including ice temperature and salinity), suggest that the differential diffusion of ions from fine lateral pore networks, coupled with intermittent brine convection

in the large vertical brine channels, may also induce ion fractionation in sea ice in comparison to seawater.

5.1.2 Gas bubble formation

In comparison to mineral precipitation (section 5.1.1), gas bubble formation also depends on the temperature, salinity and pressure constraints, but the equilibrium constant and solubility values are more poorly constrained.

The equilibrium between the gaseous phase and the aqueous phase in sea ice pores is described by Henry's law:

$$p_i = C_i / K_H \qquad \text{(Eq. 9)}$$

were p_i is the partial pressure of a given gas i just above the solution (in the gaseous phase), Ci, the concentration of the gas dissolved in the solution (the aqueous phase), and K_H, the Henry's law constant, which is a function of the temperature, salinity and pressure, as does K_{sp} (section 5.1.1). However, while K_{sp} is known for the temperature and salinity conditions in sea ice, it is not the case for K_H.

The levels of saturation (ΔC_i) compare the concentration of the gas in brine (Ci) with respect to an equilibrium state (C_{eq}), the solubility of the gas i in brine at equilibrium with the atmosphere:

$$\Delta C_i = \frac{C_i}{C_{eq}} - 1 \qquad \text{(Eq. 10)}$$

where ΔC_i higher than, equals to or lower than 1 indicates that the gas is supersaturated, at saturation or undersaturated respectively [*Craig and Hayward*, 1987].

Gas supersaturation could easily occur during ice growth, because of two synergetic effects related to decreasing ice temperature. First, decreasing ice temperature decreases the brine volume fraction, which increases dissolved gas concentration in brine C_i. Second, decreasing ice temperature decreases gas solubility (C_{eq}). Actually, C_{eq} has not been established yet for the range of temperatures and salinities in brine. However, if we assumed that the relationships established for seawater (i.e., generally, for temperatures between 0 and 30 °C and salinities between 0 and 35) still hold for brine – although sea ice temperature may be as low as -30 °C [*Miller et al.*, 2011], which corresponds to a brine salinity of 306 (Eq. 5) – then,

C_{eq} in brine should increase with decreasing temperature and decrease with increasing salinity (Figure 9a,b), but with a stronger dependency to salinity rather than temperature. In other words, C_{eq} in brine should decrease during ice growth, due to increasing brine salinity that is coupled with the decreasing ice temperature (Figure 9c). Above saturation, if the sum of the partial pressures of all the dissolved gases is higher than the local hydrostatic pressure, gas bubbles can nucleate and accumulate in the direct vicinity of the brine inclusions (see *Lubetkin* [2003] for a review on the conditions required for gas bubble formation).

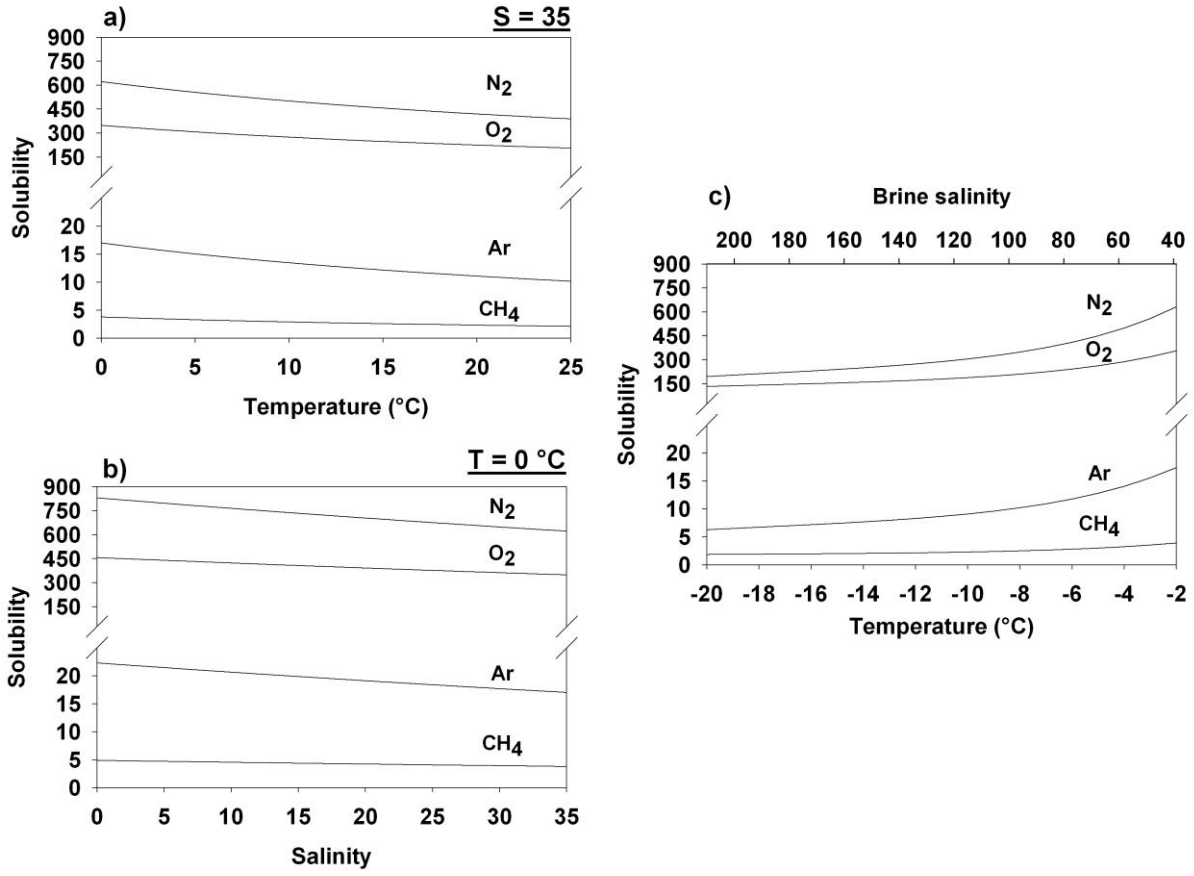

Figure 9 The solubility of gases in seawater for different temperature and fixed 35 of salinity (a), for different salinity and fixed temperature of 0 °C (b), and the solubility of gases in brine (c). The solubility of N_2, O_2 and Ar are in µmol L^{-1}, the solubility for CH4 is in nmol L^{-1}.

5.1.3 The particular case of calcium carbonate precipitation

The precipitation of calcium carbonate ($CaCO_3$) is particular in the way that it combines the processes related to mineral precipitation (section 5.1.1) and gas equilibrium (section 5.1.2). Indeed, it produces CO_2 (gas) and $CaCO_3$ (solid) according to the equation:

$$Ca^{2+} + 2HCO_3^- <-> CaCO_3 + CO_2 + H_2O \qquad \text{(Eq. 11)}$$

The parameterization of $CaCO_3$ precipitation is complicated because of the equilibrium between the carbonate species ($CO_{2(aq)}$ or H_2CO_3, HCO_3^- and CO_3^{2-}). The respective abundance of the carbonate species in brine depend on the following equilibrium:

$$CO_{2(aq)} + H_2O \Leftrightarrow H_2CO_3 \overset{K_1}{\Leftrightarrow} HCO_3^- + H^+ \overset{K_2}{\Leftrightarrow} CO_3^{2-} + 2H^+ \quad \text{(Eq. 12)}$$

where K_1 and K_2 are respectively the first and second dissociation constants of the carbonate system, which depend on temperature, salinity and the pH (see *Zeebe and Wolf-Gladrow* [2001] for a review).

To date, observations of $CaCO_3$ are scarce in natural sea ice [*Dieckmann et al.*, 2010; *Dieckmann et al.*, 2008; *Geilfus et al.*, 2013], but they already feed speculation on the amount of $CaCO_3$ that can precipitate in sea ice and the related climate impacts [*Moreau et al.*, submitted; *Rysgaard et al.*, 2013]. In addition, conjectures on the subsequent transport pathways of $CaCO_3$ and CO_2 [*Delille*, 2006] lead *Rysgaard et al.* [2011] to suggest that the formation of ikaite (a form of $CaCO_3$) in sea ice may favour the export of atmospheric CO_2 to the deep ocean. Their proposed scenario is as follows: when ikaite precipitates in sea ice, if the minerals are trapped in the tortuosity of the pore network while the produced CO_2 is expelled from the ice due to gravity drainage and then sinks due to the dense water formation, then sea ice would contribute to the export of CO_2 to the deep water. In addition, when the dissolution of ikaite occurs, it would further pump CO_2 from the atmosphere if sea ice is permeable. However, that proposed scenario is still debated, because of current uncertainty of the transport pathway of CO_2. Indeed, if the produced CO_2 remains in sea ice, or if it is expelled to the atmosphere (as suggested in *Geilfus et al.* [2013]) rather than the underlying water, then the impact of $CaCO_3$ precipitation on the annual budget of CO_2 in the atmosphere is nil (see *Delille et al.* [2014] for a recent and detailed review).

5.2 Biotic processes

In addition to the previously described abiotic (geochemical) processes, microorganisms that are able to survive at high salinity and low temperature in sea ice also modify the chemical composition of sea ice through their activity. This section aims to provide an overview of the impact of the biological activity on the changes in the biogeochemical compounds, with a focus on the impact of these changes on the underlying seawater and the atmosphere, and vice-versa.

A simplified metabolism pathway in sea ice would be as follows: providing that light is not limiting, ice-algae utilize inorganic macro- and micro-nutrients (section 5.2.1) and CO_2 for their metabolisms, transferring therefore part of the dissolved inorganic compounds from brine within their cells, and producing particulate organic matter (POM). That organic matter (section 5.2.2) could be released to brine (forming dissolved organic matter, DOM) after algal exudation due to physiological stress, cell-lysis or grazing, and then be broken down due to the activity of grazers and decomposers. In that process, termed remineralization, the organic matters that can easily be broken down are said "labile", and the others, "refractory". The metabolic cycle of the microorganisms in sea ice may also be accompanied by the production and consumption of biogases (section 5.2.3).

5.2.1 Inorganic nutrient dynamics

- **Macro-nutrients**

All macro-nutrients in sea ice (nitrate, nitrite, phosphate, silicic acid) are dissolved in brine, with the exception of ammonium that can be incorporated within the lattice of the pure ice matrix (section 1). Therefore, except for ammonium, it is assumed that macro-nutrients are subject to brine drainage as for salt (section 4.1) and that they are thus conservative against salinity in abiotic conditions. Thus, their concentrations increase linearly with increasing bulk ice salinity, following the so-called dilution curve, as it has been observed for the major ions (e.g., sodium, potassium, magnesium, calcium), which are much less involved in biological processes than the macro-nutrients [*Meese*, 1989] (Figure 10). In biotic conditions however, because of the uptake or the release of the macro-nutrients due to the metabolic cycle of the microorganisms living in sea ice (and possibly, complexation processes), macro-nutrients become non-conservative against salinity [e.g., *Becquevort et al.*, 2009; *Meese*, 1989; *Papadimitriou et al.*, 2007; *Thomas et al.*, 2010].

Following the initial incorporation of nutrient during sea ice formation (entrapment of the brine inclusions or frazil accumulation) (section 2.1), nutrient exchange through brine convection, lateral infiltration of seawater or vertical infiltration of seawater or meltwater with atmospheric deposit may affect algal growth [*Ackley and Sullivan*, 1994; *Granskog et al.*, 2003; *Vancoppenolle et al.*, 2010]. Nutrient limitation changes significantly the metabolism of ice algae (e.g., leading to the production of high carbon-weight molecules [*Lee et al.*, 2008], which then can alter the rates at which algal debris sink, their potential to form

aggregates, and thus *in fine*, the potential for carbon export to the deep ocean once the microorganisms are released in seawater following the ice melt.

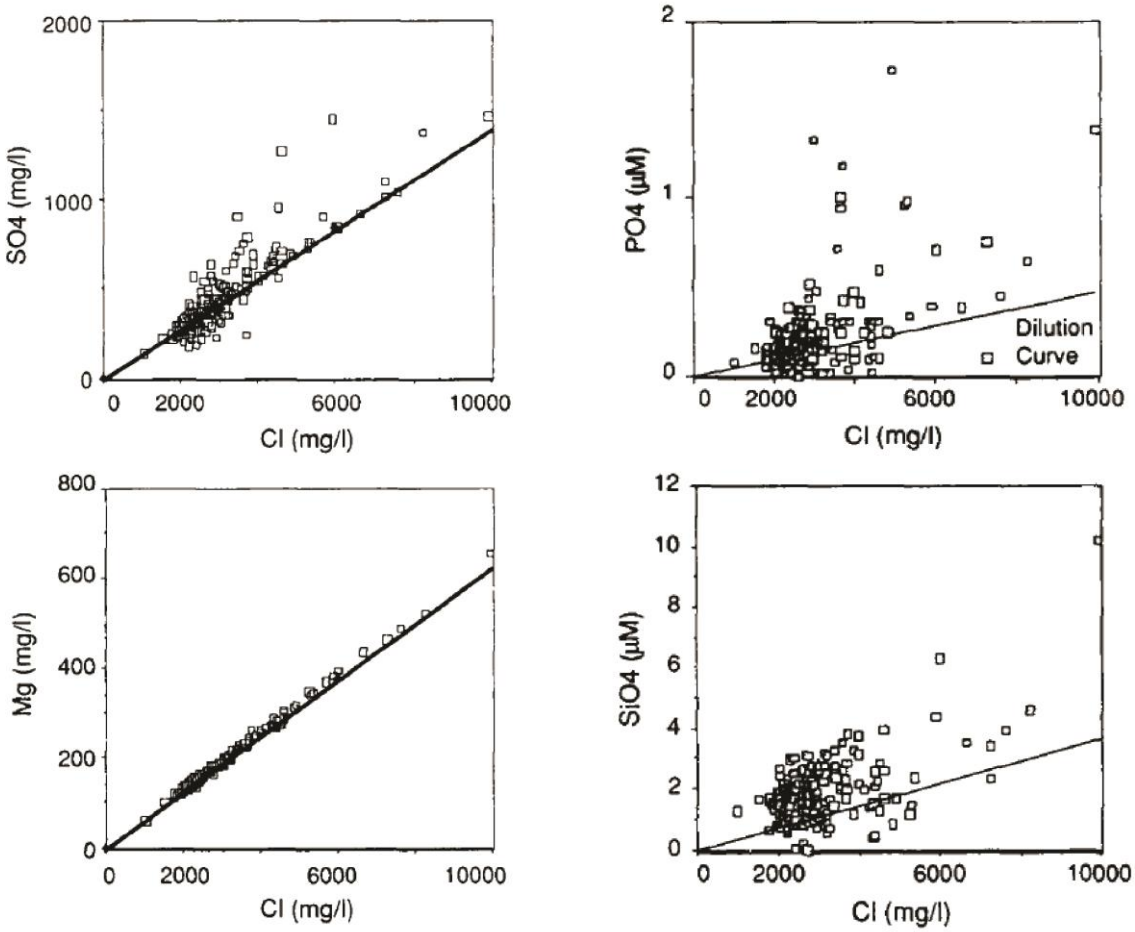

Figure 10 Concentrations of sulphate, phosphate, silicate and magnesium (clockwise from the top-left corner) in first-year sea ice in comparison with their dilution curve (note that here, chlorine concentration is used as a proxy of the salinity [*Meese*, 1989, p. 46-47]). Magnesium is conservative, but not phosphate and silicate (due to biological activities) or sulphate (due to mineral precipitation of differential diffusion (section 5.1.1)).

- **Micro-nutrients**

Some trace metals are micro-nutrients that are essential for the metabolic cycle; the most widely discussed micro-nutrient in sea ice is iron (Fe). Because Fe availability limits phytoplankton growth in regions like Southern Ocean and North Pacific, observations showing that Fe concentrations are orders of magnitude higher in sea ice than in the water column [*Aguilar-Islas et al.*, 2008; *Lannuzel et al.*, 2007; *Lannuzel et al.*, 2010] suggest that the Fe release that goes along with the sea ice melt triggers phytoplankton blooms in surface seawater, where Fe is limited [*Lancelot et al.*, 2009].

Because Fe is bio-essential for the metabolism of the micro-organisms in sea ice, they are expected to be generally non-conservative to salinity as for the macro-nutrients [*Lannuzel et al.*, 2011]. However, the transport pathway is much more complex than that of the macro-nutrients. First, Fe is present in sea ice in either the dissolved (dFe) or the particulate form (pFe). While biological assimilation may convert dFe into pFe, and cell-lysis and heterotrophic activity convert pFe back to dFe (as for the macronutrients) [*Hassler and Schoemann*, 2009], photo-reduction also participates to the conversion of pFe to dFe [*Kim et al.*, 2010; *Rijkenberg et al.*, 2008]. Second, the incorporation of dissolved "free" Fe is unexpected in contrast to the macro-nutrients, because most of the dFe and pFe present in seawater are complexed by organic ligands [*Boye et al.*, 2001]. Third, because of that complexation process, brine drainage should be less efficient in removing dFe in comparison to the other macro-nutrients which have no complexation properties [*Vancoppenolle et al.*, 2010].

5.2.2 Organic matter

The microorganisms in sea ice produce a large variety of dissolved and particulate organic matters (DOM and POM respectively). The distinction between DOM and POM may be unclear over a certain range of size, because dissolved organic matter is usually defined as smaller than 0.2 µm, but the characterization of DOM is generally done after the filtration through precombusted GF/F glass fiber filters of 0.7 µm [*Thomas et al.*, 2010] or 0.45 µm [*McMinn et al.,* 2009] in practice.

DOM availability in sea ice has many ecological implications. For instance, labile DOM is a food source for the microbial foodweb within sea ice. In addition, DOM includes some chelating agents that may affect the bio-availability of Fe in sea ice, and the coloured DOM (CDOM) alter the quality of the light penetrating through sea ice and serve as substrate for photochemical reactions [*Belzile et al.*, 2000; *Norman et al.*, 2011]. Further, and most importantly for this thesis, some DOM may spontaneously assemble into gel-like organic substances [*Chin et al.*, 1998], which then alter the effective porosity of sea ice and significantly impact the transport of the biogeochemical compounds in sea ice [*Krembs et al.*, 2011].

Extracellular polymeric substances (EPS) are part of these organic compounds that are produced by algae (and to a minor extent by bacteria) [*Passow*, 2002] and which can form gels, in particular with the presence of cations such as potassium, hydrogen and calcium

[*Verdugo et al.*, 2004]. EPS can undergo different phase transition (condensed or hydrated, DOM or gels) depending on the temperature, salinity and pH of the brine [*Riedel et al.*, 2008].

EPS plays a fundamental role for the microbial communities [*Krembs and Deming*, 2008]. It protects cells against changes associated with decreasing ice temperature and brine concentration [*Krembs et al.*, 2002], it represents a carbon-rich substrate for bacterial colonization and grazers [*Meiners et al.*, 2004; *Riedel et al.*, 2006; *Riedel et al.*, 2007], and its viscosity favours cell adherence to the brine wall [*Krembs et al.*, 2002] and affect the transport of salts [*Krembs et al.*, 2011] and ions [*Krembs and Deming*, 2008]. The increase of tortuosity due to the presence of EPS further offers a protection from grazers and improves sea ice habitability [*Krembs and Deming*, 2008]. Interestingly, EPS appears to remain in sea ice while the POM is released into the surface seawater during ice melt [*Juhl et al.*, 2011; *Riedel et al.*, 2006]; hence, there is a discontinuous export of organic matter from sea ice to the underlying seawater, and the quality and the quantity of that organic matter change across the melt season.

5.2.3 Biogas production and consumption

The most studied biogases in sea ice are O_2, CO_2 and dimethylsulphide (DMS). The study of O_2 dynamics is mainly motivated by the assessment of the net community production (NCP) in sea ice (i.e. the net balance of photosynthesis and respiration) [e.g., *McMinn and Ashworth*, 1998; *Mock et al.*, 2003], which is generally the sole source of fixed-carbon for the higher trophic level species in the ice-covered regions [*Arrigo et al.*, 2010]. Because of the tight relationship between O_2 and CO_2 during photosynthesis and respiration [*Laws*, 1991], assessing the net production of O_2 in sea ice helps to quantify the net uptake of CO_2 due to biological activity.

The dynamics of CO_2 is more complicated than the one of O_2, because it also depends on carbonate mineral precipitation and dissolution (section 5.1.1), in addition to the NCP and to the partitioning between CO_2, HCO_3^- and CO_3^{2-} [e.g., *Geilfus et al.*, 2012]. The partitioning of the CO_2 (in the form of CO_2 in gas bubbles or in the form of $CaCO_3$, i.e., as solid) has strong implications in the role of sea ice as a source or sink for the atmospheric CO_2 as described in *Delille et al.* [2014] and section 5.1.3.

DMS (dimethylsulfide) is a by-product of the degradation of DMSP (dimethylsulfoniopropionate). The latter is synthesized by some species of ice-algae and is

found in much larger concentrations in sea ice than in seawater [e.g., *Stefels et al.*, 2007]. When DMS is released to the atmosphere, the oxidation of DMS may produce aerosol particles, which affect the radiative properties of the atmosphere. Indeed, aerosols scatter the incoming solar radiation and may promote the formation of clouds which reflect part of the radiation [*Charlson et al.*, 1987].

In addition to O_2, CO_2 and DMS, the study of other biogases should gain interest in the coming years; these are methane (CH_4), nitrous oxide (N_2O) and halogen-organic compounds. CH_4 is a greenhouse gas which accounts for 20 % of the global radiative forcing of well-mixed greenhouse gases [*Myhre et al.*, 2013]. It potential emission from the destabilized permafrost and hydrates in the Arctic shelf regions, associated with the ongoing climate warming may have positive feedback on the climate, as it occured in the past [*O'Connor et al.*, 2010]. The role of sea ice in that scenario is uncertain. To date, CH_4 measurements in sea ice are scarce [*Lorenson and Kvenvolden*, 1995; *Shakhova et al.*, 2010b]. However, observations showing strong supersaturation of CH_4 relative to the atmosphere in the under-ice water, large mixing ratio of CH_4 in sea ice [*Shakhova et al.*, 2010a] and CH_4 emissions in the ice-covered central Arctic [*Kort et al.*, 2012] have raised questions (and speculations) on the role of sea ice in the exchange and the cycling of CH_4 in the polar regions. *Shakhova et al.* [2010a] have suggested that sea ice impedes air-sea exchange and allows CH_4 accumulation under the ice, while *He et al.* [2013] measured air-ice CH_4 fluxes and *Kitidis et al.* [2010] showed CH_4 oxidation under the ice based on incubations. Note that although many measurements have been carried out in the air, in seawater, and in the sediment, no study has yet discussed the CH_4 dynamics within sea ice. CH_4 production (methanogenesis) was thought to mainly occur in abiotic conditions (e.g., in anoxic sediment), but recent studies indicate that methanogenesis could also occur in aerobic seawater, as a result of DMSP degradation [*E. Damm et al.*, 2010; *Florez-Leiva et al.*, 2013; *Zindler et al.*, 2012]. Whether the same pathway could occur in sea ice, where large DMSP concentrations are found, has yet to be verified.

N_2O is a greenhouse gas and may be produced in Antarctic sea ice as a result of ammonium oxidation [*Priscu et al.*, 1990]. However, in the Arctic, N_2O production via denitrification appears to be limited to anaerobic micro-niches [*Kaartokallio*, 2001; *Rysgaard and Glud*, 2004]. Recent study on the dynamics of N_2O indicates that brine dilution leads to air-ice

fluxes of N_2O during ice decay [*Randall et al.*, 2012], but without any evidence of N_2O production in sea ice.

Finally, it is well known that active forms of bromine are responsible for the ozone depletion event during polar spring [e.g., *Simpson et al.*, 2007]. Sea ice has been suggested to be a source of bromine that participates to the ozone depletion events [e.g., *Simpson et al.*, 2007], because both Arctic and Antarctic sea ice algae produce a significant amount of halocarbons (volatile halogenated organic compounds), part of which may be converted photochemically into active forms of bromine [*Granfors et al.*, 2013a; *Granfors et al.*, 2013b; *Sturges et al.*, 1992; *Sturges et al.*, 1993]. However, since a recent study indicates that the catalytic reaction of ozone depletion requires an acidic reaction substrate, whereas sea ice brine has basic pH because of its salt content, the significance of sea ice contribution to the ozone depletion event still need to be assessed [*Pratt et al.*, 2013].

6 Constraints on observations and measurements

6.1 Demand for long-time survey

Biogeochemical measurements are currently scarce and sparse in time and in space. The study of biological and geochemical processes dates back to the beginning of the previous century [*Weeks*, 2010]. However, it has experienced a fast growth in the last 10-20 years, due to the recent technological development, which allows an easier access to the polar regions, and due to the growing demand for a better understanding of the future changes in the polar ecosystem, in the context of a warming climate [*Miller et al.*, under revision]. Ideally, our understanding of the incorporation and transport of bio-essential dissolved compounds (e.g., nutrients, DOM) and gases should reach the same levels of details as for salts, for accurate simulations of the future changes in sea ice primary production and the air-sea exchange of climate-active gases. While *Malmgren* [1927] described the evolution of the bulk salinity profile in sea ice across seasons, equivalent time-series do not exist for any of the biogeochemical compounds to date. Instead, current biogeochemical data are mainly limited to the ice decay, probably due to the more favourable navigation and sampling conditions [*Miller et al.*, under revision]. The eight-months long time series study, named International Circumpolar Flaw Lead System Study (CFL), which has been conducted in the Amundsen Gulf (Arctic), during the International polar year (IPY), 2007-2008, have provided interesting

results [e.g., *Carnat et al.*, 2013; *Geilfus et al.*, 2012] and calls for additional long time-series studies, and preferably in areas of low spatial variability.

6.2 Spatial variability

Spatial variability is important for process studies, as it partly determines the uncertainty of the results. Indeed, assuming that we measure a variable and its changes over time, how relevant is a change of 30 % between two ice cores collected at different time, in the same area, if the spatial variability already accounts for 50 % (i.e., if there is a difference of 50% between two ice cores collected at the same time)? While mean salinity generally shows low standard deviations between cores [*Eicken et al.*, 1991; *Tucker et al.*, 1984], large standard deviation (up to one order of magnitude) has been observed for chlorophyll-a [*Eicken et al.*, 1991]. The problem of spatial variability also exists at a smaller scale due to the heterogeneous structure of sea ice. For instance, when measuring the salinity of two ice samples from the same ice core and ice depth, the results may be different if one contains a large brine channel while the other one does not [*Cottier et al.*, 1999]. To avoid the issues related to the small-scale heterogeneity of the ice, it is therefore crucial to measure a representative ice volume, i.e., a sufficiently large ice sample with a representative φ [*Miller et al.*, under revision]. For the large-scale spatial variability, it would be valuable to measure the standard deviation of the variable among multiple ice cores [*Eicken et al.*, 1991; *Miller et al.*, under revision], unless we aim at describing temporal and spatial trends rather than obtaining absolute values as in *Meiners et al.* [2012].

6.3 Measurement methods

The heterogeneous structure imposes different constraints to the measurement methods. The most relevant methods and limitations are described here, based on the review of *Miller et al.* [under revision]. Because most of the methods for the measurements of biogeochemical compounds in sea ice directly derived from existing methods for seawater, ice samples are generally melted before the measurements. Melting the ice results in an addition of freshwater in brine, hence, a dilution of the brine content, because most of the biogeochemical compounds are concentrated in brine, while the surrounding ice matrix is almost pure. The associated abrupt change of salinity is known to cause osmotic shock to the microorganisms [*Garrison and Buck*, 1986; *Kottmeier and Sullivan*, 1988], induce artificial conversion of DMSP into DMS [*Stefels et al.*, 2012] and dissolve mineral precipitates like calcium carbonate. Because melting the ice inevitably alters bulk ice biogeochemistry, an

alternative would be to measure the concentrations of the solutes in brine rather than in the melted ice samples. To collect brine, we simply need to make a half-core hole (or sackhole) and let the brine percolates into it. However, the measurements in brine have two main drawbacks: first, if the ice temperature is very low, the brine pockets may be disconnected, or it may take a long time before obtaining the required volume; second, if some compounds are adsorbed at the surface of the sticky EPS, their concentrations will be underestimated in the brine samples. Currently, there is no ideal solution for the measurements of the dissolved compounds in sea ice; one needs to do with the caveats underlying each method.

Gas concentrations may also be underestimated in brine samples, because gas exchange may occur between the percolated brine and the atmosphere during the sampling. There are however four others methods for gas measurements in ice. (1) The oldest method is wet extraction; it requires melting the ice and refreezing the meltwater from the bottom so that the whole gas content are expelled in the headspace above the refrozen ice [*Tison et al.*, 2002]. For insoluble gases at high concentrations, the refreezing step is not necessary. We simply need to equilibrate the meltwater with a volume of gas standard, and measured the equilibrated volume of gas. (2) Dry-extraction involves the crushing of ice samples with stainless steel balls under vacuum [*Stefels et al.*, 2012; *Tison et al.*, 2002], and the measurements of the released gases by gas chromatography. However, that method does not suit for CH_4 measurements because the metal-metal friction during the crushing process artificially release of CH_4 [*Higaki et al.*, 2006]. The method of dry-crushing also requires a step of pre-concentration if we aim to measure trace gases like DMS [*Stefels et al.*, 2012]. (3) For CO_2 measurements, where melting and vacuum disrupts the equilibrium of the carbonate system, the ice samples may be equilibrated with a small volume of gas standard, which will be analyzed by gas chromatography [*Geilfus et al.*, 2012]. (4) In situ probes has been used for determining O_2 concentrations in sea ice [*McMinn et al.*, 2009], based on photochemical detection. However, the results vary depending on whether the probes are inserted in gas bubbles, brine, or microbial biofilms [*Mock et al.*, 2002]. In addition, unless the probes can be deployed before the freezing, their installation within the ice requires disturbing the ice cover.

Chapter III – Objectives

The main question we aim to answer is: “What are the most relevant processes affecting the dynamics of solutes and gases in sea ice?”

That general question may be divided into three sub-questions:

1. **How does the concentration of solutes and gases in sea ice change with depth and time?**
2. **How do these changes compare to those of the physical properties of the ice?**
3. **How do these changes compare to those of the biological properties of the ice?**

Indeed, in order to identify the most relevant processes that affect the dynamics of solutes and gases in sea ice, it is first important to describe the dynamics themselves, hence, how their concentrations vary with depth and across seasons (Question 1). Then, because the state of the art shows that both the physical and biological properties of the ice affect the changes of solutes and gases in sea ice, it appears necessary to compare the observed changes with the changes in the physical properties (Question 2) and the biological properties of the ice (Question 3), in order to identify the most relevant processes.

Chapter IV – Thesis outline

1 Manuscript presented in the present thesis

This thesis comprises four manuscripts (Chapters V to VIII). All of them describe the vertical distribution of different biogeochemical compounds in sea ice, from ice growth to ice decay (Question 1), in parallel with the physical properties (Question 2), and the biological properties of the ice (Question 3). The aims and the original findings of the manuscripts are synthesized here below, and on table 1.

Table 1 Comparison of the manuscripts presented in the thesis, based on the location and the duration of the sampling, and the analyzed compounds.

	Location, duration	**Analyzed compounds (in addition to temperature, salinity)**
Chapter V	Indoor experiment in Hamburg, 19 days	• Inorganic nutrients, DOC • Bacterial abundance, bacterial activity
Chapter VI	Barrow, field survey from Jan- June 2009	• Inorganic nutrients • Water stable isotopes • Chlorophyll a • Argon
Chapter VII		• Methane
Chapter VIII		• Oxygen, argon, nitrogen

The first manuscript (Chapter V) describes the evolution of nutrients, DOM, bacterial activity and abundance, in two series of mesocosms from ice growth to ice decay during a 19-day experiment in Hamburg (Germany). One series was filled with seawater, and the other one, with seawater and river water. The main aim was to identify the potential differences in sea ice biogeochemistry due to the additional riverine dissolved organic matter (DOM). We found that most of the dissolved compounds were more enriched in sea ice than we would expect if they were conservative against salinity, and the enrichment of DOM was more

important in the mesocosms with river water. This indicates that the physico-chemical properties of the DOM themselves may affect the incorporation efficiency. The addition of riverine DOM slightly boosted the bacterial abundance and bacterial activity. However, although bacterial abundance was the highest at the bottom of the ice, bacterial impact on the dissolved compounds was not obvious there. This is likely to be the result of brine convection, i.e., brine exchange with seawater, which tended to draw the concentrations of the dissolved compounds back to the conservative behaviour.

1. **Zhou, J.,** B. Delille, H. Kaartokallio, G. Kattner, H. Kuosa, J-L. Tison, R. Autio; G. S. Dieckmann, K-U. Evers, L. Jørgensen, H. Kennedy, M. Kotovitch, A-M. Luhtanen, C. A. Stedmon, D. N. Thomas, (2014) Physical and biological controls on the distribution of inorganic nutrients and DOC in sea ice during an experimental ice growth and decay cycle. *Marine Chemistry, 166*, 59-69, doi: http://dx.doi.org/10.1016/j.marchem.2014.09.013

My contribution: I did the sampling, measured temperature and salinity, and calculated the other physical parameters presented in the manuscript. I led the writing of the manuscript.

In contrast to the previous manuscript, the second manuscript (Chapter VI) deals with natural ice cores that were collected in Barrow, Alaska from February to June 2009. It aimed to compare the behaviour among the dissolved (nutrients and $\delta^{18}O$, δD), particulate (chlorophyll-a) and gaseous (argon) compounds with respect to the increase of sea ice permeability and brine drainage. Argon clearly responded different to brine dynamics than the other biogeochemical compounds; we attributed that contrast to the impact of gas bubble formation on gas transport compared to the other analyzed compounds.

2. **Zhou, J.**, B. Delille, H. Eicken, M. Vancoppenolle, F. Brabant, G. Carnat, N.-X. Geilfus, T. Papakyriakou, B. Heinesch, *and* J.-L. Tison *(*2013*).* Physical and biogeochemical properties in landfast sea ice (Barrow, Alaska): Insights on brine and gas dynamics across seasons, *J. Geophys. Res. Oceans, 118,* doi:10.1002/jgrc.20232.

My contribution: I did all the measurements (except the water stable isotopes). I led the writing of the manuscript.

The third paper (Chapter VII) also deals with natural ice cores that were collected in Barrow, Alaska from February to June 2009, but focuses on the dynamics of methane (CH_4), which is a biogas of low solubility with a high global warming potential. The release of CH_4 from the Arctic shelf regions potentially causes positive feedback on current global warming. However, the role of sea ice in the exchange of CH_4 between seawater and the atmosphere is

unclear. This manuscript aims at improving our understanding of the role of sea ice, by describing the changes of CH_4 in sea ice, brine and seawater, over time. Our main conclusion is that sea ice mainly act as a temporary storage for the CH_4 in seawater; the biological impact on the CH_4 in sea ice was likely negligible in comparison to the physical impact.

3. **Zhou, J.**, J.-L. Tison, G. Carnat, N.-X. Geilfus, B. Delille (2014) Physical controls on the storage of methane in landfast sea ice. *The Cryosphere, 8,* 1019-1029, doi:10.5194/tc-8-1019-2014.

My contribution: I did all the sea-ice related measurements. I led the writing of the manuscript.

The fourth paper (Chapter VIII) also deals with natural ice cores that were collected in Barrow, Alaska from February to June 2009, but compares the dynamic of O_2, a biogas, with that of N_2 and Ar, which are here considered as inert. We further discussed in that paper the potential of using N_2 and Ar to correct the physical contribution to O_2 variations, and thus, to determine the biological production of O_2 in sea ice. That manuscript has two main originalities: first, we analyzed the total O_2 content in the ice (gaseous and dissolved), while current studies mainly focus on the dissolved O_2 concentrations. Second, we discussed on an innovative method for determining biological production, which does not require to melt the ice or to deploy in situ probes. Therefore, we avoid obtaining biased biological production related to the ice melt or because the probes are inserted in gas bubbles or biofilms.

4. **Zhou, J.**, B. Delille, F. Brabant, J-L. Tison. Insights into oxygen transport and net community production in sea ice from oxygen, nitrogen and argon concentrations, *Biogeosciences Discuss., 11,* 2045-2081, doi:10.5194/bgd-11-2045-2014, 2014.

My contribution: I did all the measurements. I led the writing of the manuscript.

Following the four manuscripts, Chapter IX synthesizes the findings of the present thesis and provides concluding comments and insights on how current transport and biogeochemical processes likely evolve in the future.

2 Additional contribution to the peer-reviewed literature

In addition to the four manuscripts presented in the thesis, I also participated to 6 other publications, which are directly related to the topic of the thesis.

5. Carnat, G., T.N. Papkyriakou, N.-X. Geilfus, F. Brabant, B. Delille, M. Vancoppenolle, G. Gilson, **J. Zhou**, and J.-L. Tison (2013). Year-round investigations of Arctic first-year sea ice physical and textural properties in the Amundsen Gulf (IPY-CFL system study). *Journal of Glaciology, 59 (217)*, pp. 819-837.

My contribution: I participated to the discussion related to the physical properties of the ice, and I provided comments and suggestions at various stages of the manuscript preparation.

Interests: That manuscript provides a long-time dataset of sea ice physical properties in the Amundsen Gulf. We point out that the evolution of the ice temperature and other ice physical properties are more closely linked to the evolution of the air temperature rather than the spatial distribution of the sampling. In addition, the temporal evolution of the ice physical properties is similar to that observed in Barrow (Chapter VI-VIII); this suggests our findings in Barrow may be valid for Amundsen Gulf and all of the ice covers that experience the same temperature regime.

6. Carnat, G., **J. Zhou**, T. Papakyriakou, B. Delille, T. Goossens, T. Haskell, V. Schoemann, J.-L. Tison. Physical and biological controls on DMS, P dynamics in ice shelf‐influenced fast ice during a winter‐spring and a spring-summer transitions, *J. Geophys. Res. Oceans*, 119, doi: 10.1002/2013JC009381.

My contribution: I participated to the field samplings (4-5 months in Antarctica, including two months in winter), I measured some of the concentrations of DMS,P, in ice and water; I also did the filtration and some of the measurements of chlorophyll a. I computed the temperature and salinity-dependent parameters; this includes writing the Matlab routine for the calculation of Rayleigh number. I provided comments and suggestions at various stages of the manuscript preparation.

Interests: We presented the interactions between the physical and biological controls on the DMS,P cycle in ice. We highlighted the complexity to interpret the DMS(P) concentrations in parallel with the chlorophyll-a concentrations, when neglecting the physical framework. Indeed, in winter, platelet ice formation incorporated dinoflagellates, which are strong DMSP

producers. In winter-spring transition, increasing solar radiation stimulated the synthesis of DMSP, before the increase in the abundance of diatoms further increases DMSP concentrations in ice. In spring-summer transition, drastic changes in brine dynamics released DMS to the under-ice water and redistributed DMSP in the ice, without affecting the chlorophyll-a distribution.

7. Moreau M., M. Vancoppenolle, **J. Zhou**, J.-L. Tison, B. Delille, H. Goosse, (2014). Modeling argon dynamics in first-year sea ice, *Ocean Modelling, 73*, doi: 10.1016/j.ocemod.2013.10.004

My contribution: I participated to the discussions on the components to implement to the models; I provided the data for the validation of the model; I provided comments and suggestions at various stages of the manuscript preparation.

Interests: While model efforts have mainly focused on the dissolved compounds (e.g salt), Moreau et al. (2014) have implemented, a component that describes the incorporation and the transport of argon in ice, to a 1D-model for dissolved compounds in ice. The model simulations confirm that the formation of gas bubbles impacts the gas content in ice (as we have suggested in Chapter VI). Neglecting gas bubble formation (i.e., by taken into account only the dissolved gas compounds) could lead to an underestimation of the argon content in sea ice up to 70 %.

8. Moreau, S., M. Vancoppenolle, B. Delille, J-L. Tison, **J. Zhou**, M. Kotovitch, D.N. Thomas, N-X. Geilfus, H. Goosse, Drivers of inorganic carbon dynamics in first-year sea ice: a model study, *Under review in Journal of geophysical Research.*

My contribution: I participated to the discussion on the components to implement to the models; I provided the data for the validation of the model; I provided comments and suggestions at various stages of the manuscript preparation.

Interests: Following the model simulations on argon (manuscript #7 hereabove), we further developed model simulations on the dynamics of CO_2 in sea ice. The results were validated against some data obtained in both natural and experiment ice cores. In contrast to argon (Chapter VI), CO_2 may mainly remain in the dissolved state (in the form of DIC, dissolved organic carbon), because of the equilibria of the CO_2 system. A significant part of the DIC in

sea ice is released to the under-ice water, through brine drainage; but how much of this DIC is exported to the deep ocean remains uncertain.

9. Miller, L., F. Fripiat, B.G.T. Else, J. S. Bowman, K. A. Brown, R. E. Collin, M. Ewert, A. Fransson, M. Gosselin, D. Lannuzel, K.M. Meiners, C. Michel, J. Nishioka, D. Nomura, S. Papadimitriou, L.M. Russell, L.L. Sørensen, D.N. Thomas, J-L. Tison, M.A. van Leeuwe, M. Vancoppenolle, E.W. W., **J. Zhou**. Methods for Biogeochemical Studies of Sea Ice: the state of the art, caveats and recommendations. Under review in Elementa.

My contribution: I participated to the writing of the section related to gases in sea ice. I also provided comments and suggestions at various stages of the manuscript preparation for the other sections.

Interests: This manuscript reviews the existing methods for sea ice biogeochemical studies. Sea ice biogeochemistry has experienced a fast growth in the last 10 to 20 years, due to the recent technological development, and the growing demand for a better understanding of the future changes in the polar regions. Specialists have come from different disciplines, and used diverse methods for their measurements. As a result, it is not only complicate to compare the data, but also, to choose the appropriate method to use. That manuscript reviews the existing methods, and highlighted their caveats and limitations.

10. Vancoppenolle, M., D. Notz, F. Vivier, J.-L. Tison, B. Delille, G. Carnat, **J. Zhou**, F. Jardon, P. Griewank, A. Lourenço, and T. Haskell (2013). Technical Note: On the use of the mushy-layer Rayleigh number for the interpretation of sea-ice-core data, *The Cryosphere Discuss., 7*, 3209-3230, doi:10.5194/tcd-7-3209-2013.

My contribution: I provided comments and suggestions at various stages of the manuscript preparation.

Interests: This manuscript contains recommendations on the parameterization and the interpretation of the Rayleigh number (Ra). My co-authors and I realized that different parameterizations have been used for the computation of the Ra. As a result, it makes it difficult to compare the Rayleigh number from one study to another. In addition, we noticed that the Ra computed from field study were generally lower than those obtained from experiments, with in-situ salinity measurements. In that paper, we discussed on the change in Ra related to the different parameterization, and suggested to interpret the Ra qualitatively when it is computed from field data, because brine drainage, and the snapshot character of the sampling may lead to an underestimation of the Ra.

Chapter V - Physical and bacterial controls on the distribution of inorganic nutrients and DOC in sea ice during an experimental ice growth and decay cycle

Marine Chemistry, 166, 59-69, doi: 10.1016/j.marchem.2014.09.013

Zhou J.[1,2], B. Delille[2], H. Kaartokallio[3], G. Kattner[4], H. Kuosa[3], J-L. Tison[1], R. Autio[3], G. S. Dieckmann[4], K-U. Evers[5], L. Jørgensen[6,7], H. Kennedy[8], M. Kotovitch[1,2], A-M. Luhtanen[3,9], C. A. Stedmon[7], D. N. Thomas[3,8]

[1] Laboratoire de glaciologie, DSTE, Université Libre de Bruxelles, Belgium

[2] Unité d'océanographie chimique, MARE, Université de Liège, Belgium

[3] Marine Research Centre, Finnish Environment Institute (SYKE), Helsinki, Finland

[4] Alfred Wegener Institute Helmholtz Center for Polar and Marine Research, Bremerhaven, Germany

[5] Arctic Technology Department, HSVA, Germany

[6] Department of Biology, Marine Biological Section, University of Copenhagen, Denmark

[7] National Institute for Aquatic Resources, Technical University of Denmark, Denmark

[8] School of Ocean Sciences, Bangor University, Menai Bridge, United Kingdom

[9] Department of Biosciences, University of Helsinki, Finland

Abstract

We investigated how physical incorporation, brine dynamics and bacterial activity regulate the distribution of inorganic nutrients and dissolved organic carbon (DOC) in artificial sea ice during a 19-day experiment that included periods of both ice growth and decay. The experiment was performed using two series of mesocosms: the first consisted of seawater (SW) and the second consisted of seawater enriched with humic-rich river water (SWR). We grew ice by freezing the water at an air temperature of -14 °C for 14 days after which ice decay was induced by increasing the air temperature to -1 °C. Using the ice temperatures and bulk ice salinities, we derived the brine volume fractions, brine salinities and Rayleigh numbers. The temporal evolution of these physical parameters indicates that there were two main stages in the brine dynamics: bottom convection during ice growth, and brine stratification during ice decay. The major findings are: (1) the incorporation of dissolved compounds (nitrate, nitrite, ammonium, phosphate, silicate, and DOC) into the sea ice was not conservative (relative to salinity) during ice growth, which is different to commonly held assumptions. Brine convection clearly influenced the incorporation of the dissolved compounds, since the non-conservative behavior of the dissolved compounds was particularly pronounced in the absence of brine convection. (2) Bacterial activity further regulated nutrient availability in the ice: ammonium and nitrite accumulation was evidently a consequence of remineralization processes, although bacterial production was too low to induce major changes in DOC concentrations. (3) Different forms of DOC have different properties and hence incorporation efficiencies. In particular, the terrestrially-derived DOC from the river water was less efficiently incorporated into sea ice than the DOC in the seawater. Therefore the main factors regulating the distribution of the dissolved compounds within sea ice are clearly a complex interaction of brine dynamics, biological activity and in the case of DOM the physico-chemical properties of the dissolved constituents themselves.

1 Introduction

Sea ice is formed from the freezing of seawater, and therefore the dissolved inorganic and organic nutrient concentrations in sea ice depend on those of the parent water [*Petrich and Eicken*, 2010; *Weeks*, 2010]. Most of these compounds are concentrated in the brine inclusions, as they are not incorporated within the matrix of pure ice crystals [*Weeks*, 2010].

The two principal regions of sea ice production, the Arctic and Southern Oceans, differ widely in the concentrations of nutrients and dissolved organic matter (DOM) present in the surface waters from which sea ice is formed. The waters of the Arctic Ocean have comparatively lower nutrient concentrations (e.g, nitrate and phosphate), except the Pacific water inflow, but higher input of riverine particulates and DOM, as well as silicate [*Dittmar et al.*, 2001; *Wheeler et al.*, 1997]. In contrast, the Southern Ocean generally has high inorganic nutrient concentrations [*Gleitz et al.*, 1994], whereas DOM is of oceanic origin and at comparatively low concentrations [*Hansell et al.*, 2009]. A consequence of this fundamental difference is that Arctic sea ice can be expected to have a higher DOM content than ice produced in the Southern Ocean [*Stedmon et al.*, 2011; *Stedmon et al.*, 2007], and as such may promote greater bacterial production, leading to higher pCO_2 concentrations in the brines [*Geilfus et al.*, 2012]. In turn, this could result in the air-ice CO_2 exchange in the Arctic and Antarctic being fundamentally different, although this hypothesis is yet to be verified.

In addition to bacterial production, other mechanisms may regulate differences in the dynamics of dissolved constituents (nutrients and DOM) in sea ice. Previous studies have indicated selective incorporation of DOM during sea ice formation [*Aslam et al.*, 2012; *Giannelli et al.*, 2001; *Müller et al.*, 2013], raising the question as to whether or not there is a segregation among dissolved compounds during the incorporation phase, and in particular, whether the incorporation is comparable between Arctic and Antarctic sea ice because of the different compositions of DOM in the parent waters. Secondly, various physical mechanisms induce changes in the nutrient pools in ice after the initial incorporation. Among these, brine convection is the most important [*Notz and Worster*, 2009; *Vancoppenolle et al.*, 2010], since its impact lasts over the whole ice growth period and episodically during spring sea ice decay [*Carnat et al.*, 2013; *Zhou et al.*, 2013]. Other mechanisms exist, but are thought to be of minor importance in comparison to brine convection (e.g., brine expulsion, and migration of individual pockets) [*Notz and Worster*, 2009], or are only effective during the ice melt period (e.g., infiltration of snow meltwater [*Granskog et al.*, 2003], flooding of seawater [*Fritsen et al.*, 1998; *Fritsen et al.*, 2001], and infiltration of gap water in internal ice layers [*Ackley et al.*, 2008; *Haas et al.*, 2001]).

The aim of the present study was to better understand the differences in sea ice biogeochemistry and bacterial activity, related to additional allochthonous riverine DOC

during a whole cycle of sea ice formation, consolidation and subsequent decay. In our mesocosm experiment, we reproduced ice growth and ice decay on two series of mesocosms: One consisting of North Sea seawater and another consisting of North Sea seawater amended with 10% natural DOM-rich river water. The latter was designed to simulate the dissolved organic matter conditions that occur in Arctic shelf waters where much ice formation occurs. We hypothesized that the dissolved compounds of the parent waters would be predominantly incorporated conservatively into the ice (relative to salinity), and would then deviate from the conservative behavior due to bacterial activity, given that there was no autotrophic component in the experiment. We also expected that a deviation from the conservative behavior would be higher in the river-water amended mesocosms because the higher organic matter content would stimulate increased bacterial activity, if the riverine DOM is bioavailable.

2 Material and methods

2.1 Experimental setting and sampling routine

The 19-day experiment took place in the Hamburg Ship Model Basin (www.hsva.de). We used 21 polyethylene experimental mesocosms with a volume of 1.2 m³ each. Eleven of the mesocosms were filled with 1000 L of seawater from the North Sea (referred here after as SW), and the remaining 10 were filled with 900 L of seawater from the North Sea and 100 L of river water (referred here after as SWR). The North Sea water was collected on 24 May 2012 (54°7'N 7°54'E near Helgoland) and transported to Hamburg where the mesocosms were filled within 24 hours of collection. The river water was collected during spring freshet in mid May 2012 from River Kiiminkijoki (NW Finland), just before it enters the estuary, stored one week in the cold (4 °C), filtered through 0.2 µm using Durapore 10 inch (Millipore) and Clariflow G 10 inch (Parker) cartridge filters and added to the mesocosms 2 days afterwards.

As there was a slight temperature gradient in the main test basin, the mesocosms were distributed only partially randomly. As shown in Figure 1, the units were first randomly positioned into rows, but the respective manipulations (SW and SWR) were located at the same or adjacent row. The unit SW11 was reserved for instrumentation and it was excluded from all subsequent calculations and analysis due to possible contamination from instrumentation that was placed inside it.

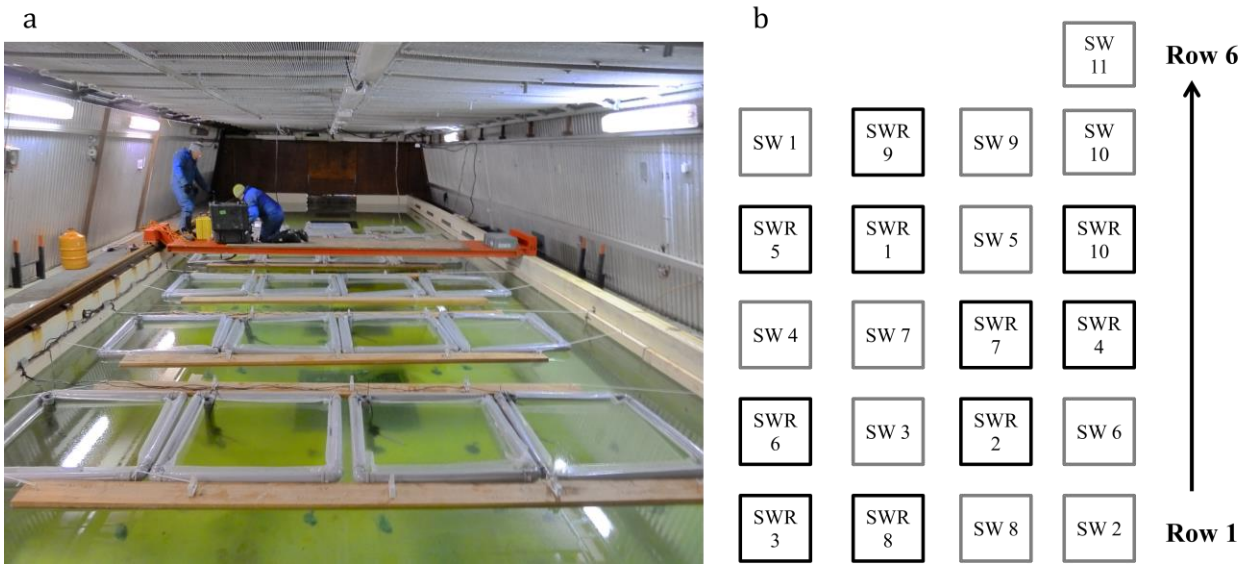

Figure 1. (a) The experimental basin at HSVA, (b) The spatial distribution of the SW and SWR mesocosms. Note that SW11, although sampled, was not included into the data set, because it was reserved for continuous physical measurements.

The salinities of the SWR mesocosms were adjusted to the SW values by adding aquarium standard salt (Tropic Marin®). Nitrate (NO_3^-) and phosphate (PO_4^{3-}) were also adjusted to concentrations that did not limit bacterial growth in both series of mesocosms. The addition of river water caused large difference in dissolved silicate ($Si(OH)_4$) and DOC concentrations between the SW and SWR mesocosms (Table 1), while nitrite (NO_2^-) and ammonium (NH_4^+) concentrations were similar.

Table 1 reports the mean and standard deviation of the starting conditions of both SW and SWR mesocosms (i.e, day 0). Differences in the mean starting conditions between SW and SWR were less than 10 % (which was about the range of standard deviation within each series of mesocosms), except for $Si(OH)_4$, DOC and bacterial production derived from leucine (BP Leu) and thymidine (BP TdR) incorporation, which were about 4, 1.7, 1.3 and 1.2 times higher in SWR, respectively.

Table 1. Mean and standard deviation (stdv) of the parameters measured at the beginning of the experiment (day 0) in SW and SWR mesocosms. Bact. Refers to bacterial abundance, BP Leu and BP TdR, to leucine-based and thymidine-based bacterial production respectively.

	S	**NO_3^-**	**NO_2-**	**$Si(OH)_4$**	**PO_4^{3-}**	**NH_4^+**	**DOC**	**Bact.**	**BP Leu**	**BP TdR**
		µmol L^{-1}	*µmol L^{-1}*	*µmol L^{-1}*	*µmol L^{-1}*	*µmol L^{-1}*	*µmol L^{-1}*	*10^6 cell ml^{-1}*	*µgC $L^{-1}h^{-1}$*	*µgC $L^{-1}h^{-1}$*
Mean										
SW	**31.1**	**27.4**	**0.2**	**3.0**	**1.9**	**1.9**	**140.7**	**1.0**	**0.9**	**0.8**
SWR	**30.6**	**27.2**	**0.2**	**12.3**	**1.9**	**1.9**	**245.8**	**0.9**	**1.2**	**0.9**
Stdv										
SW	0.0	4.4	0.0	0.7	0.1	0.1	4.3	0.2	0.1	0.2
SWR	0.1	3.5	0.0	1.1	0.1	0.1	21.7	0.1	0.2	0.0

The adjusted NO_3^- and PO_4^{3-} concentrations (27.2 – 27.4 and 1.9 µmol L^{-1} respectively: Table 1) are clearly higher than the maxima observed in the coastal Arctic Ocean during summer (3 and 0.5 µmol L^{-1} respectively [*Dittmar et al.*, 2001], but were realistic compared to Southern Ocean values [e.g., *Becquevort et al.*, 2009; *Gleitz et al.*, 1994]). DOC concentrations in both SW and SWR (141 and 246 µmol L^{-1} respectively) were consistent with the range observed in coastal Arctic Ocean [*Dittmar and Kattner*, 2003] for a similar salinity as in the present study, and were also consistent with the range of DOC in surface waters of the Weddell Sea (50-60 µmol L^{-1}) [*Hansell et al.*, 2009; *Lechtenfeld et al.*, 2014; *Norman et al.*, 2011]. Therefore, the outcome of our experiment on the incorporation of DOC and the consequence on sea ice biogeochemistry may be pertinent to areas in both Arctic and Southern Oceans, where NO_3^- and PO_4^{3-} are not limiting for bacterial growth.

Ice was grown from day 0 to 14, during which the air temperature was maintained at -14 °C, and then the air temperature was increased to -1 °C to trigger a decay phase. The resulting changes in ice thickness are shown in Figure 2 for each row of the mesocosms. Water and ice sample were collected at regular intervals from day 0 to day 1 respectively (Table 2). Brine samples were collected from day 8 onwards (at 6 cm of ice depth from the top), when the ice was thick enough to avoid lateral infiltration of seawater. The brines were collected 15 to 30 minutes after drilling (depending on the percolation rate) using a portable peristaltic pump

(Master Flex®, E/S portable sampler). Once the ice in a mesocosm was sampled it was considered to be compromised and not used again in the experiment.

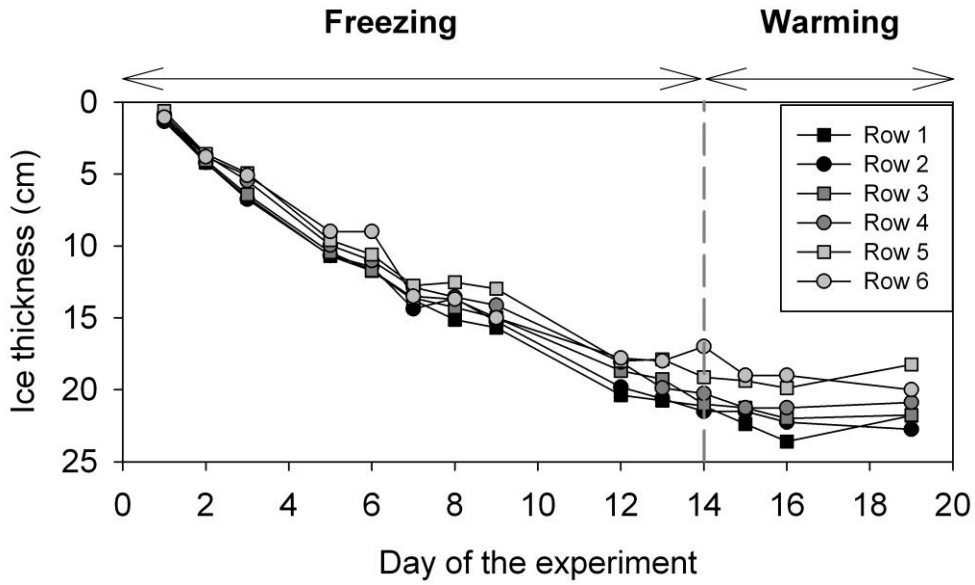

Figure 2. Evolution of the ice thickness during the experiment. The ice thickness is given per row. Row 1 refers to the bottommost row of mesocosms (Figure 1), while row 6 refers to the topmost row of mesocosms in Figure 1. The vertical dashed line represent the day when we increased the air temperature from -14 to 0 °C.

Table 2. Days of the experiment with samplings and the associated sampled mesocosms. For all the mesocosms, available data in ice, under-ice water and brine are marked with a cross, while unavailable data are marked with a minus.

Day of the experiment	**1**	**2**	**5**	**7**	**8**	**12**	**14**	**15**	**16**	**19**
Mesocosms (SW and SWR)	2	3	6	8	4	7	1	5	9	10, 11
Ice and under-ice water	x	x	x	x	x	x	x	x	x	x
Brine	-	-	-	-	x	x	x	x	x	x

A PVC tube was set at the corner of each mesocosm to maintain pressure equilibrium between the water and the atmosphere, and this was cleared of ice daily to relieve pressure

and as a portal for sampling under-ice waters. Ice thickness was measured on all sampling days outside, but adjacent to, the mesocosms in order not to disturb the ice growth in the mesocosms before the sampling. The absence of active photoautotrophic organisms in ice and underlying waters was verified on all sampling days using epifluorescence microscopy, which would reveal the existence of functioning chloroplasts.

2.2 Physical characteristics of the ice

Ice temperature was measured using a calibrated probe (Testo 720), immediately after the extraction of the ice core. The probe was inserted into holes (matching the diameter of the probe) drilled perpendicular to the ice core axis with a depth resolution of 2 cm. The precision of the probe was ± 0.1 °C. Bulk ice salinity was measured using two approaches: first, with melting of ice sections; and second, with employing the approach of *Cottier et al.* [1999], which limits possible brine drainage and where ice was frozen with under-ice water, and then, sectioned. The latter method was used together with temperature to derive brine volume fraction and brine salinity, following the relationships of *Cox and Weeks* [1983] (neglecting the air volume fraction). Measurements of the bulk ice salinity were performed on 2 or 4 cm vertical core sections. Salinities were measured with a portable conductivity meter (SEMAT Cond 315i/SET salinometer with WTW Tetracon 325 probe) on melted ice samples at room temperature. The precision was ± 0.1. This salinity was used to normalize the dissolved compounds to salinity (see section 2.6).

For the brine calculations we assumed that the sea ice was permeable for a brine volume fraction exceeding 5 % [*Golden et al.*, 1998], since the thin sections showed columnar ice structures (not shown). The derived brine salinity was comparable to the brine salinity measured on collected brine samples (data not shown). We therefore used temperature, bulk ice salinity, derived brine salinity and brine volume fraction to calculate the Rayleigh number (Ra), which is a proxy for brine convection as described by *Notz and Worster* [2008]. Theoretically, convection is possible in an ice layer (of a thickness h) when Ra exceeds 1 and decreases from the top to the bottom of that layer. However, critical Ra of 10 [*Notz and Worster*, 2008] and up to 8 [*Zhou et al.*, 2013] was observed in experimental study and natural conditions respectively. Because the calculation of Ra depends on the gradient of brine salinity, salt loss by drainage during ice core extraction, or the sampling resolution may lead to different Ra values. As there is currently no consensus on the critical value of Ra, we simply assume the critical Ra being 1 following the theoretical consideration.

2.3 Nutrients and DOC

Samples for inorganic nutrient analyses were stored frozen in 50 mL PE bottles. Inorganic nutrients (NO_3^-, NO_2^-, NH_4^+, PO_4^{3-} and $Si(OH)_4$) were measured with an autoanalyzer system (Evolution III, Alliance Instruments) according to slightly modified seawater standard methods [e.g.,*Grasshoff et al.*, 1999; *Kattner and Becker*, 1991]; NH_4^+ concentrations were measured according to *Kérouel and Aminot* [1997]).

Samples for the determination of dissolved organic carbon (DOC) were stored frozen (-20 °C) in glass vials (Wheaton; precombusted at 500 °C, 5 h) and determined by high temperature catalytic oxidation and subsequent non-dispersive infrared spectroscopy (TOC-VCPN, Shimadzu). After each batch of five samples, one reference standard (DOC-DSR, Hansell Research Lab, University of Miami, US), one ultrapure-water blank and one potassium hydrogen phthalate standard were measured. The accuracy of the DOC measurements was ± 5 %.

2.4 Bacterial abundance and production

Bacterial abundance was determined by flow cytometry after *Gasol et al.* [1999] and *Gasol and Del Giorgio* [2000]. Samples for bacterial abundance were fixed with particle-free (0.2 μm-filtered) paraformaldehyde (final concentration of 1 %) and stored at -80 °C. Cells were stained with SYBR Green I (Molecular Probes) and counted on an LSR II flow cytometer (BD Biosciences, San Jose, USA) using a 488 nm laser. CountBright beads (Molecular Probes) with known concentration were added to each sample to calculate the measured volume. The bacterial counts were acquired for 1 minute, and the cell populations identified from bivariate plots of green fluorescence versus side scatter. Gating analysis was performed using FACS Diva software (BD Biosciences). The bacterial abundance counted (in cells mL^{-1}) was calculated from the sample flow rates and number of events recorded. All samples were analyzed during one measurement session.

For the bacterial production measurements, samples containing a known amount of crushed ice and sterile-filtered seawater [*Kaartokallio*, 2004] were prepared as follows: Each intact 5–10 cm ice core section was crushed using a spike and electrical ice cube crusher. Approximately 10 mL of crushed ice was weighed in a scintillation vial. To better simulate the brine pocket salinity and ensure an even distribution of labeled substrate, 2–4 mL of sterile filtered (through 0.2 μm filter) seawater from the sample bags was added to the

scintillation vials. All the work was carried out in a cold room.

Bacterial production was measured immediately after sample collection using simultaneously the ^{14}C-leucine [*Kirchman et al.*, 1985] and ^{3}H-thymidine [*Fuhrman and Azam*, 1980; 1982] incorporation methods. Two aliquots and a formaldehyde-fixed absorption blank were amended with L-[U-^{14}C] leucine (PerkinElmer, USA, sp. act. 310 mCi mmol^{-1}) and [methyl-3H] thymidine (PerkinElmer, USA, specific activity 20 Ci mmol^{-1}). For thymidine, the concentrations were 30 nmol L^{-1} for all sample types; for leucine, the concentrations were 1000 nmol L^{-1} for ice samples, 330 nmol L^{-1} for water samples and 670 nmol L^{-1} for brine samples. The samples were incubated in the dark at -0.6°C on crushed ice in an insulated container according to the projected level of activity: ice samples were incubated 19-22 h, and water and brine samples 4-6 h. The incubations were stopped by the addition of formaldehyde and samples were processed using the standard cold-TCA extraction and filtration procedure. Labeled macromolecules were collected on 0.2 μm mixed cellulose ester membrane filters (Osmonics) and placed in clean scintillation vials. A Wallac WinSpectral 1414 counter and InstaGel (Perkin-Elmer) cocktail were used in scintillation counting. Bacterial production was calculated using a cell conversion factor of 2.09×10^{18} cells mol^{-1} [*R H Smith and Clement*, 1990], a cell volume of 0.3 μm^3 [*Kaartokallio*, 2004; *R H Smith and Clement*, 1990] and a carbon conversion factor of 0.12 pg C μm^3 [*Nagata and Watanabe*, 1990; *Pelegri et al.*, 1999] for thymidine, leucine-based bacterial production was calculated using a factor of 3.0 kg C mol^{-1} [*Bjornsen and Kuparinen*, 1991].

2.5 Data normalization and enrichment factor

In order to compare the nutrients and DOC concentrations between SW and SWR mesocosms, we needed to remove the effect of bulk ice salinity on the nutrient and DOC concentrations, and to take into account the variability of the starting conditions between the individual mesocosms. Therefore the data was normalized to both salinity and the starting conditions, according to the following equation:

$$X_{t\_n}^{m} = \overline{X_0} * \frac{X_t^m * S_0^m}{S_t^m * X_0^m} \qquad \text{(Eq.1)}$$

Where $X_{t\_n}^{m}$=normalized concentration of the mesocosms *m* for a given time *t*.

X_t^m =concentration of the sample (water, brine or ice) for mesocosm *m* at time *t*

S^m_t =salinity of the sample (water, brine or ice) in mesocosm *m* at time t

S^m_0=salinity of the parent water in mesocosm *m* at time 0, which is 30.9

X^m_0=concentration in the parent water in mesocosm *m* at time 0

$\overline{X_0}$ =mean start concentrations of SW (or SWR) if the sample was collected from SW (or SWR) mesocosms

The data that have been normalized are referenced hereafter with "_n" after the name of the variable. The equation 1 without $\overline{X_0}$ provides the enrichment factor.

3 Results

3.1 Ice thickness

The ice thickness increased until day 16, reaching a maximum ice thickness of 24 cm, and then stabilized or slightly decreased towards the end of the experiment (Figure 2). Overall, there was a general trend in the basin where the ice thickness decreased from row 1 to row 6. The difference was particularly obvious at the end of the experiment (4.5 cm of difference between row 1 and row 5 on day 19). The maximum difference of ice thickness between adjacent rows was 2.6 cm. The majority of mesocosms sampled on the same day were generally located on the same row (e.g., SW8 and SWR8) or adjacent rows (e.g. SW3 and SWR3) (Figure 1), which minimized the influence of this cross-basin gradient.

3.2 Physical properties of the ice

There was an increasing temperature gradient between the top and the bottom of the ice from day 1 to 15 (the freezing phase). In the subsequent melting phase the ice temperatures became more vertically homogeneous, approaching -1.8 °C on day 19 (Figure 3).

The salinity of the bulk ice was homogeneous until day 3, before developing a typical c-shape profile with a higher salinity at the top and the bottom of the ice compared to the ice interior. From day 3 to 15, the bulk ice salinity ranged between 4.6 and 23.5. In the bottom ice horizons salinities of the SW ice were up to 3.9 times higher than those of SWR between day 8 and day 14. From day 15 onwards, the salinity decreased in both the top and the bottom and ranged between 4.6 and 10.5.

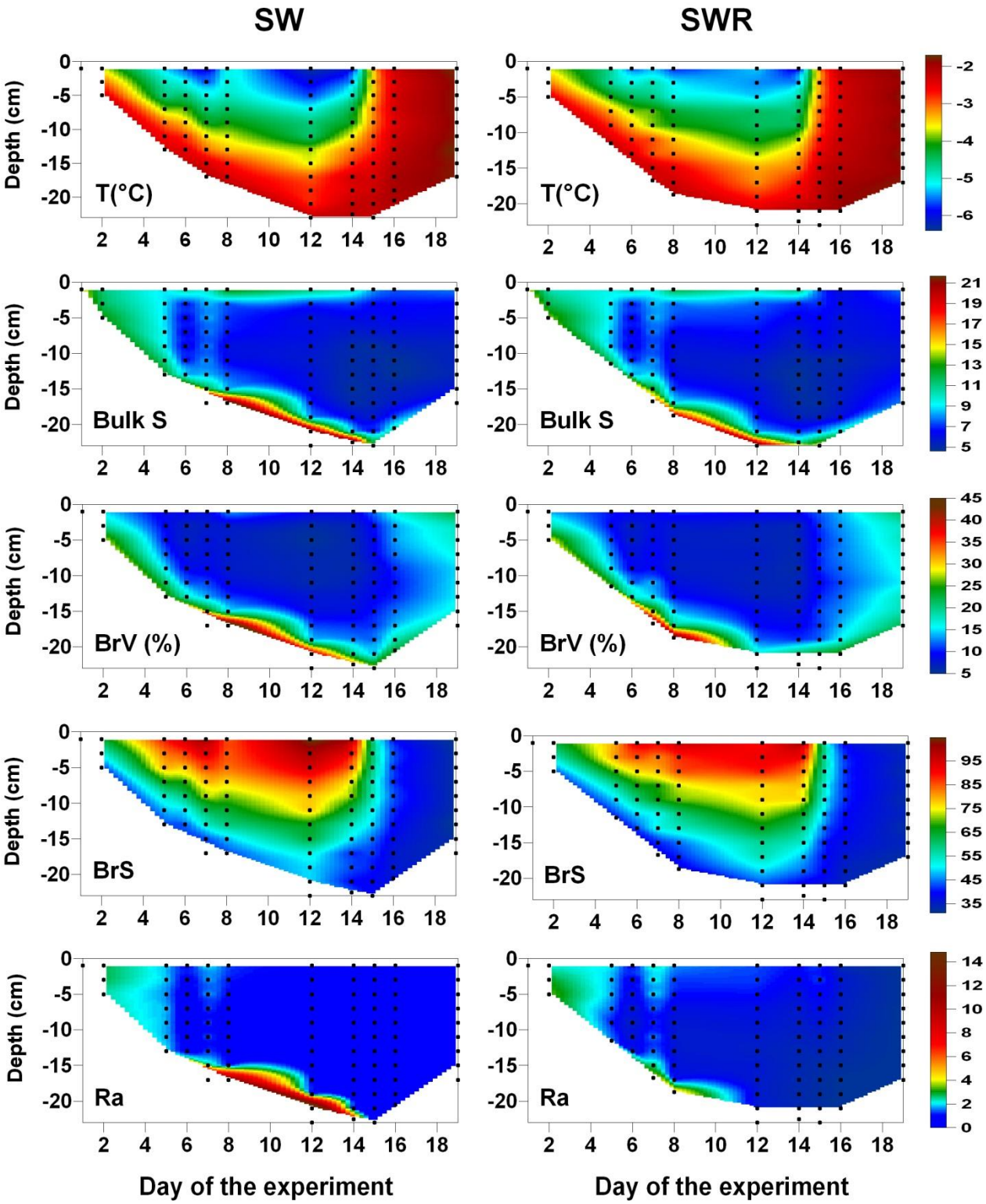

Figure 3. Ice temperature (T), salinity (Bulk S), brine volume fraction (BrV), brine salinity (BrS) and Rayleigh number (Ra) for both SW and SWR mesocosms. Each black dot refers to one data point, the color in between results of interpolation.

The brine volume fraction remained above 5 % during the whole experiment in both SW and SWR mesocosms. The bottom of the ice always had a larger brine volume fraction compared with the upper ice layers, except between day 17 and 19 when the estimated brine volume fractions were homogeneous over the whole ice cover. As for the bulk ice salinity, the brine volume fractions at the bottom of SW ice were higher than in SWR between day 8 and 14.

The calculated brine salinities decreased from the top to the ice bottom from day 1 to 16 in both SW and SWR mesocosms. During the final melting stage brine salinities became more homogeneous throughout the ice cover. On day 19, they approached 32, which was lower than the salinity in the under-ice water (36.7).

The temporal changes of Ra were similar to those in the bulk salinity: Ra exceeded 1 throughout the ice of both SW and SWR between day 1 and 3. From day 3 to 15, there was a sharp contrast of the Ra between the ice bottom and the ice interior: Ra was as high as 17.9 in the bottom of SWR and contrasted with the 0.1 value in the ice interior. The differences in salinity and brine volume fractions at the ice bottom between SWR and SW was particularly evident in Ra: On day 8, when the difference in salinity was 3.9, the difference in Ra reached 7.3. Ra dropped below 0.5 on day 15 and was equal to 0 at all ice depths on day 19.

It is worth noting the difference of up to 3.9 in salinity and up to 7.3 in Ra between SW and SWR in the very bottom ice layer on day 8. We observed a salinity of 23.5 in the ice bottom of SW, which is higher than the salinity measured on ice blocks that were obtained under similar conditions (salinity of 9 in *Cottier et al.* [1999]). However, since there is a continuum of salinity between the ice and the under-ice water [*Notz et al.*, 2005], a salinity of 23.5 (i.e., below 30.9, the salinity of the under-ice water) may be realistic. Furthermore, the resolution of the cutting was clearly different for the last layer (2 cm for SW but 3 cm for SWR). Because ice salinity increased sharply in the last few centimeters of the ice [*Notz et al.*, 2005], lower resolution sampling naturally results in higher ice salinities. The differences in salinity resulted in a difference in Ra [*Vancoppenolle et al.*, 2013a], but does not influence our interpretation since the qualitative interpretation of Ra (e.g., *Zhou et al.* [2013]) is sufficient to describe the brine dynamics.

3.3 Nutrients and DOC

Figure 4 presents the normalized concentrations of the dissolved compounds in ice, brine and seawater (and the corresponding EF) for both SW and SWR mesocosms. If the nutrients had

behaved conservatively with respect to salinity, they would exhibit an EF of 1. Therefore, Figure 4 shows that, with the exception of the dissolved compounds in the under-ice water, all nutrients in ice and brine were not conservative. This observation was true for both SW and SWR mesocosms.

For NO_3^-_n, PO_4^{3-}_n, NO_2^-_n and NH_4^+_n, the EFs varied similarly in both treatments: NO_3^-_n in ice approached an EF of 2 for both mesocosms, while PO_4^{3-}_n reached an EF of 1.4. NO_2^-_n and NH_4^+_n in ice approached an EF of 6, but local NO_2^-_n in brine, and NH_4^+_n in ice may reach an EF up to 10 in SWR. This contrasts with the NO_3^-_n in brine that was only half of the concentration of the starting water concentrations (EF = 0.5).

The normalized dissolved compounds did not show obvious changes over time, with the exception of: NO_2^-_n, which increased until day 7 and then remained constant. NH_4^+_n and DOC_n increased until day 19 in SW, but peaked already on days 12-14 and thereafter decreased in SWR.

In contrast to all the previous dissolved compounds, $Si(OH)_4$_n and DOC_n had different EFs in both treatments. Although $Si(OH)_4$ and DOC concentrations were both higher in SWR than in SW in the parent waters, the EFs in ice were lower in SWR than SW (Figure 5). Figure 5 also indicates a similarity between $Si(OH)_4$_n and DOC_n: their EF decreased from the top to the bottom of the ice, where the EFs generally approached a value of 1.

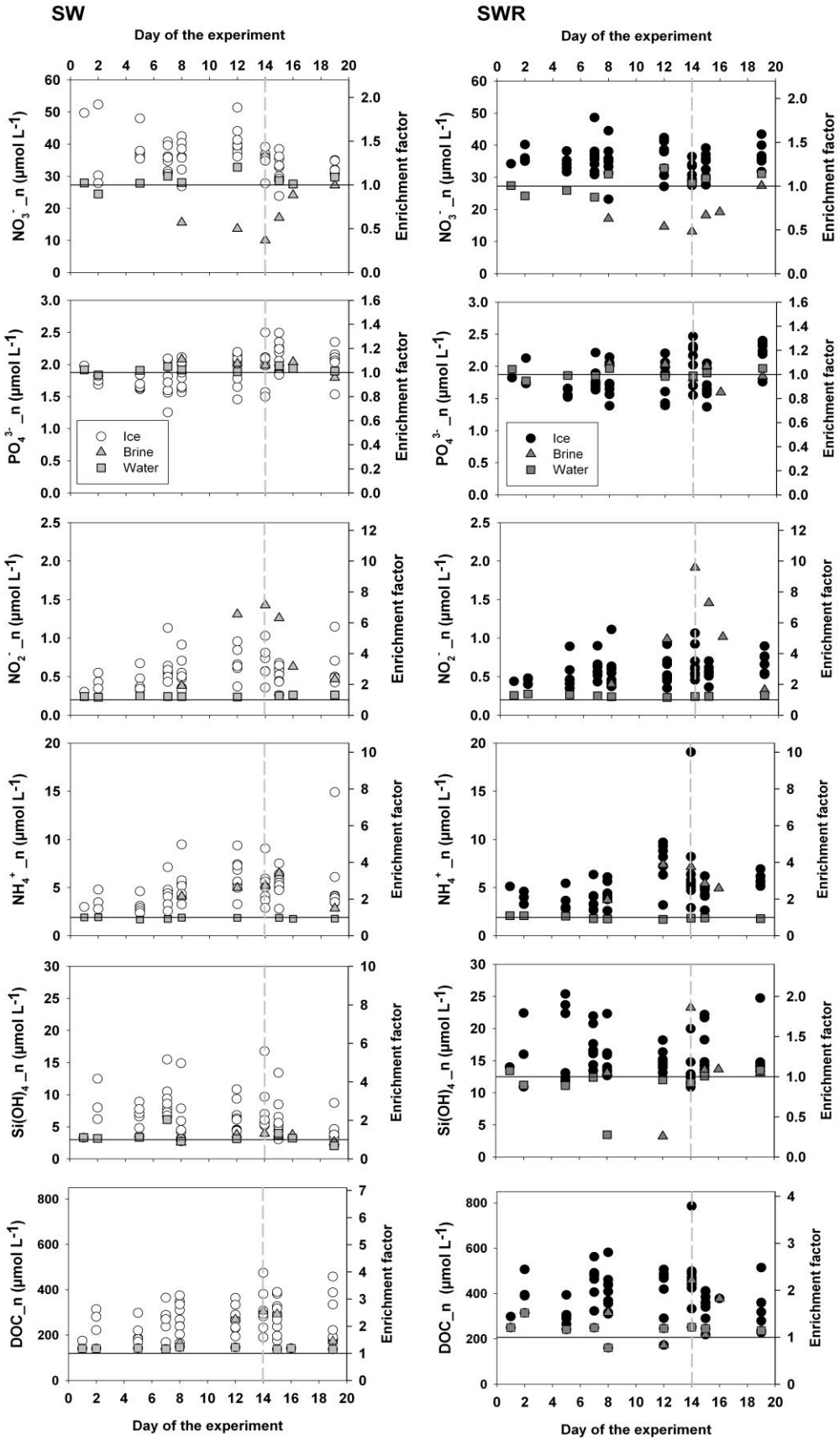

Figure 4. Normalized concentrations and enrichment factor in ice (circle), brine (triangle), and under-ice water (square), in both SW (left) and SWR (right). The horizontal lines indicate the mean starting concentration for all the mesocosms, and thus represent an enrichment factor of 1. The vertical dashed lines refer to day 14, the beginning of the warming stage of the experiment.

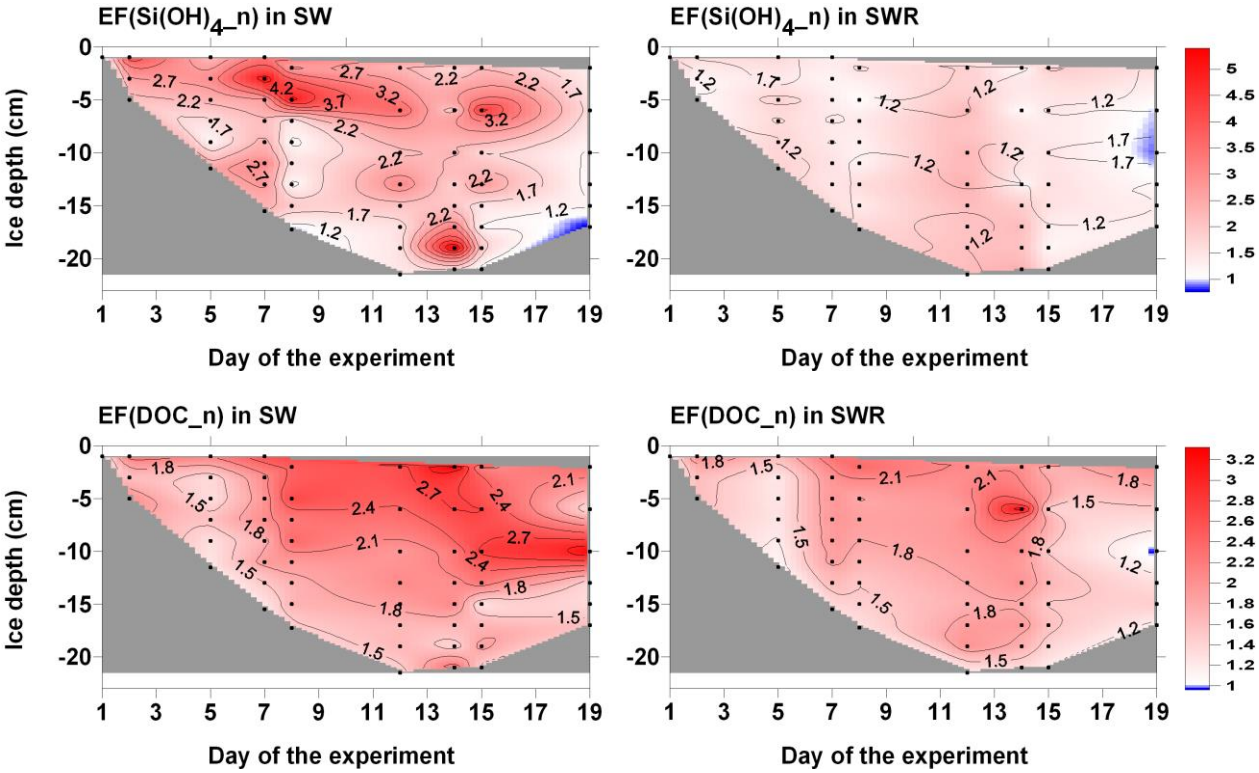

Figure 5. Evolution of the enrichment factor (EF) of $Si(OH)_4$_n and DOC_n in ice, between SWR and SW mesocosms. The black dots are depth-interpolated data points, while the colors in between are interpolations (natural neighbor).

3.4 Bacterial abundance and production

In both mesocosm series, bacterial abundance in ice (ca. 0.1 to 0.8 x 10^6 cells mL^{-1}) (Table 3) was lower than in the parent water (0.9 to 1.0 x 10^6 cells mL^{-1}) (Table 1). Figure 6 shows the temporal evolution of bacterial abundance and its vertical variability. During the ice growth phase (day 0 to 14), bacterial abundance was higher in the beginning and in the bottom of the ice, in comparison to the ice interior. During the ice decay phase, bacterial concentrations decreased, and the ice bottom maximum observed during ice growth phase disappeared.

In order to compare the bacterial activity in both treatments, without the effect of bacterial abundance, we compared both Leu and TdR incorporation per cell (Figure 6), rather than per volume of ice. It is evident that : (1) all the values in ice were lower than those in the parent water at the starting conditions, but (2) both Leu and TdR incorporation per cell increased from day 14 onwards in parallel with the increase of air temperature, and (3) they were both higher in SWR than in SW.

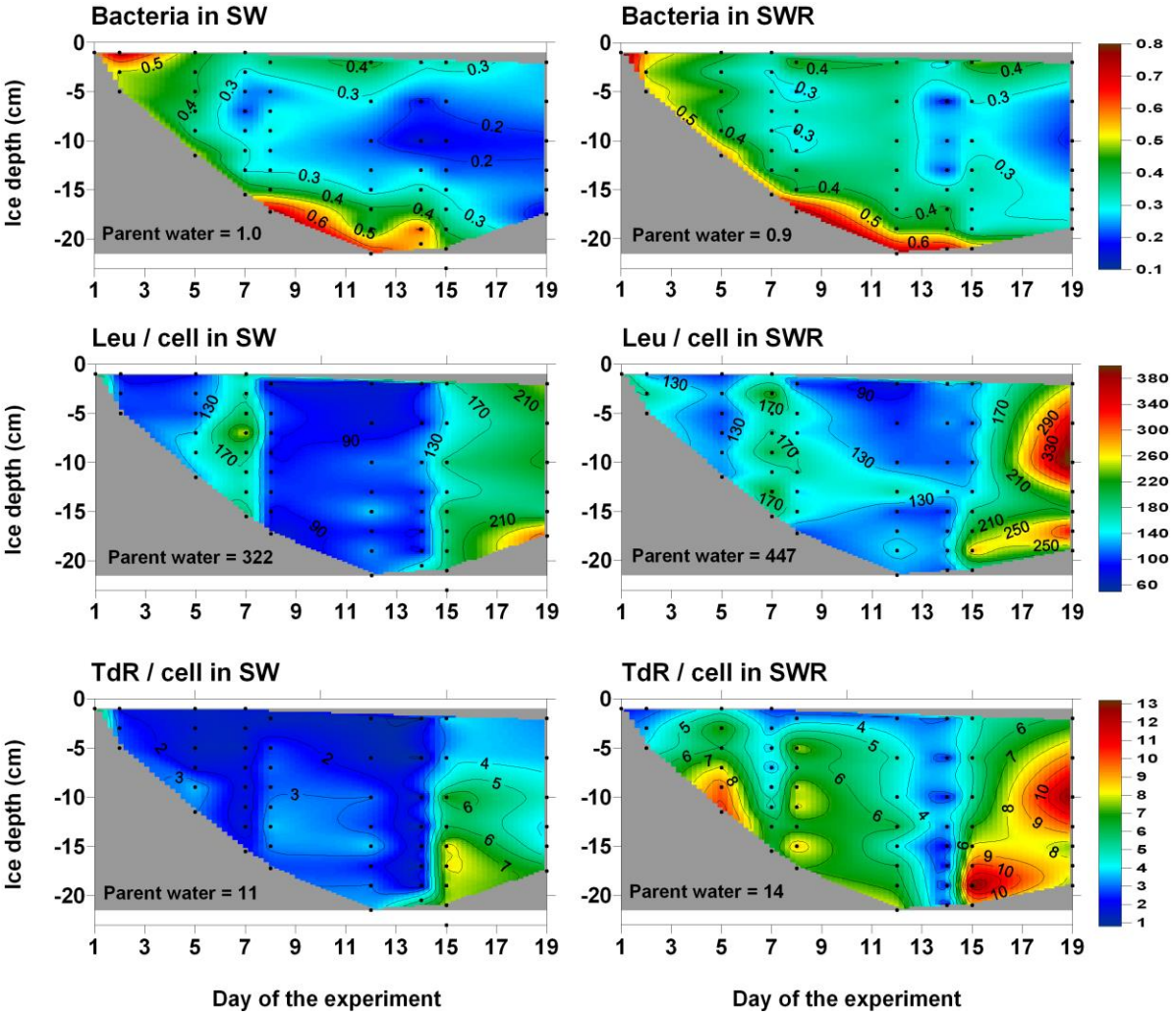

Figure 6. Evolution of the bacterial abundance (Bacteria) in 10^6 cells ml^{-1}, cell-specific leucine and thymidine incorporation (in 10^{21} mol $cell^{-1}$ h^{-1}) in ice, in SW and SWR mesocosms. The black dots are depth-interpolated data points, while the colors in between are interpolations (natural neighbor). For each category, the corresponding value in the parent water is mentioned for comparison. (10^6 cells ml^{-1})

For comparison with the literature, we also calculated bacterial production from both Leu and TdR incorporation. Overall leucine-based bacterial production rates ranged between 0.04 and 0.47 µg C $L^{-1}h^{-1}$ and TdR-based bacterial production rates between 0.01 and 0.47 of µg C $L^{-1}h^{-1}$ (Table 3). The median Leu/TdR ratio was 44 in SW and 26 in SWR.

Table 3. Minimum and maximum of of the parameters measured in ice, brine and under-ice water, and in both SW and SWR mesocosms. Bact. Refers to bacterial abundance, BP Leu and BP TdR, to leucine-based and thymidine-based bacterial production respectively.

	Ice		Brine		Under-ice water	
	SW	SWR	SW	SWR	SW	SWR
Salinity*	**5.3 - 15.1**	**5.9 - 14.7**	**36.0 - 104.6**	**36.6 - 100.4**	**31.1 - 39.8**	**29.0 - 39.6**
NO_3^- *$\mu mol\ L^{-1}$*	**4.9 - 21.9**	**5.4 - 16.7**	**29.3 - 41.6**	**28.8 - 41.5**	**26.0 - 48.6**	**25.6 - 43.5**
NO_2- *$\mu mol\ L^{-1}$*	**0.1 - 0.3**	**0.1 - 0.3**	**0.5 - 4.4**	**0.4 - 5.4**	**0.3**	**0.3**
$Si(OH)_4$ *$\mu mol\ L^{-1}$*	**0.7 - 5.3**	**2.4 - 7.9**	**4.9 - 12.8**	**13.7 - 68.0**	**2.9 - 6.6**	**11.5 - 19.8**
PO_4^{3-} *$\mu mol\ L^{-1}$*	**0.3 - 1.0**	**0.3 - 0.9**	**2.2 - 6.8**	**2.1 - 6.3**	**1.9 - 2.6**	**1.8 - 2.5**
NH_4^+ *$\mu mol\ L^{-1}$*	**0.8 - 3.1**	**0.8 - 3.8**	**3.7 - 16.8**	**7.5 - 25.5**	**1.8 - 2.4**	**1.9 - 2.4**
DOC *$\mu mol\ L^{-1}$*	**32 - 131**	**46 - 170**	**209 - 892**	**602 - 1334**	**145 - 19**	**247 - 347**
Bact. *$10^6\ cell\ ml^{-1}$*	**0.14 - 0.76**	**0.17 - 0.84**	**0.74 - 3.59**	**1.51 - 4.23**	**0.77 - 1.96**	**0.84 - 2.72**
BP Leu *$\mu gC\ L^{-1}h^{-1}$*	**0.04 - 0.37**	**0.06 - 0.47**	**0.1**	**0.18 - 0.90**	**0.61 - 1.25**	**0.61 - 1.25**
BP TdR *$\mu gC\ L^{-1}h^{-1}$*	**0.01 - 0.37**	**0.03 - 0.47**	**0.04**	**0.23 - 0.72**	**0.21 - 1.08**	**0.53 - 1.87**

* extraction of the ice following Cottier et al. [1999]

4 Discussion

4.1 Physical imprints on nutrient incorporation

There were no significant differences in the physical parameters of SW and SWR (Figure 3), except small differences in ice thickness (Figure 2), and the vertical changes of the physical properties of the ice from growth to decay were consistent with observations from Arctic sea ice [*Carnat et al.*, 2013; *Zhou et al.*, 2013]. We identified two main stages in brine dynamics, which affected the incorporation of nutrients. From day 1 to day 2, the homogeneous bulk salinity throughout the ice indicates that convection had occurred. However, sea ice has to reach a thickness of about 5 cm for gravity drainage to occur [*Worster and Wettlaufer*, 1997], while our samples were all thinner than 5 cm. We therefore suggest that we may have artificially induced convection while sawing the ice during the sampling. From day 2 to day 15, the Ra profile only suggests brine convection at the ice bottom, although the brine volume fraction remained above 5 % at all depths (i.e., permeable [*Golden et al.*, 1998]). Finally, from day 15 to the end of the experiment, the increase of air temperature (Figure 2) increased the ice temperature. As a consequence brine salinity decreased and Ra dropped below 1 and brine convection stopped.

It is noteworthy that we did not observe full-depth brine convection at the beginning of the warming phase, as found in natural ice covers by *Carnat et al.* [2013] and *Zhou et al.* [2013]. This is likely to be a result of the temperature not being low enough at the ice surface to promote a strong brine salinity gradient (a requirement for full-depth brine convection).

The impact of brine dynamics on nutrient distribution was clear (Figure 5): Because convection favors the exchange of nutrients between the brine and the under-ice water [*Vancoppenolle et al.*, 2010], the EF of $Si(OH)_4$ approached 1 in the bottom of the ice, but increased towards the top of the ice, where convection was limited (Ra close to 0.1). Ice melt implies an addition of freshwater to the brine, which will dilute the nutrient concentrations; however, brine dilution was not seen in our data, since they were all double-normalized (including normalization to salinity).

A solute that is solely subject to physical incorporation should behave conservatively with respect to salinity (i.e., concentrations evolve in parallel with salinity, on a dilution curve [*Thomas et al.*, 2010]). If other processes such as biological uptake or regeneration occur, solute concentrations will deviate from the dilution curve. This will materialize as an EF that

differs from 1. All measured parameters had an ice EF between 1.1 and 1.8 during initial freezing (day 1 to 2) indicating a net production or preferential incorporation (relative to salinity). This is in agreement with earlier results from natural sea ice for most of the nutrients, as opposed to other major ions [*Meese*, 1989].

One explanation is that the direct incorporation favors the accumulation of dissolved compounds in sea ice, although this has only been shown for DOC [*Giannelli et al.*, 2001; *Müller et al.*, 2013] and NH_4^+ [*Zhou et al.*, 2013]. This explanation is at least true for fluorescent DOM, since optical measurements performed during this experiment showed a selective incorporation of different fluorescent DOM fractions in sea ice (i.e., amino-acid-like and humic-like fluorescent DOM [*Jørgensen et al.*, submitted]. Our range of EF for DOC is consistent with the one previously presented for artificially produced DOM (1.0 – 2.7) under similar ice growth conditions [*Müller et al.*, 2013].

Another explanation for the EFs above 1 is that the compounds were initially incorporated as particulate, and then converted to DOM after incorporation. This could occur if organisms and particulate organic matter (POM) were incorporated in the ice: Algal and bacterial lyses and POM degradation may have then increased the concentrations of the dissolved compounds in sea ice, leading to EFs above 1. This hypothesis is valid for DOC as it may originate from the degradation of POM [*Thomas et al.*, 1995]. It is valid for $Si(OH)_4$ as well: Although no functioning chloroplast was observed, we cannot exclude the possible existence of dead algal cells and their fragments, and other POMs in the parent water, because the seawater had not been filtered (see Material and methods). Further, because of the relative abundance of carbon, silicon, nitrogen and phosphorus in algae (i.e., Redfield-Brzezinski ratio for diatoms), it is not surprising to observe the highest EF for DOC and $Si(OH)_4$, and the lowest for PO_4^{3-} on day 2.

NO_3^- showed a negative EF in brine, in contrast to all the other compounds, suggesting either a consumption of NO_3^- in sea ice or an adsorption of NO_3^- to the ice crystals [*Bartels et al.*, 2002] (i.e., parts of the NO_3^- were not collected in brine). Potential pathways for NO_3^- consumption are NO_3^- respiration to NO_2^- and/or denitrification [*Kaartokallio*, 2001; *Rysgaard et al.*, 2008] with production of NO_2^-, N_2O and N_2. However, NO_2^- in ice (Table 3) or N_2O in brine (data not shown) did not increase significantly, suggesting that NO_3^- reduction and denitrification were minor. Therefore, the adsorption of NO_3^- is more likely the

factor responsible for the observed negative EF. This is also coherent with the observation of positive NO_3^- EFs in the ice.

4.2 Bacterial growth, production and imprints on nutrient concentrations

Our Leu- and TdR-based bacterial production estimates are convergent, pointing to the reliability of the results. Overall BP Leu and TdR in ice were low, but were comparable to those of *Kuparinen et al.* [2011] obtained on predator-free batch cultures from melted 2-week-old sea ice. The bacterial abundance and ice salinities were in the same range to other studies measuring bacterial production in sea ice in the Southern Ocean [*Grossmann and Dieckmann*, 1994; *Helmke and Weyland*, 1995], the Arctic Ocean [*Kaartokallio et al.*, 2013; *Nguyen and Maranger*, 2011] and the Baltic Sea [*Kuparinen et al.*, 2007]. Unlike many studies done in natural sea ice, algae and other typical larger sea ice organisms were absent in our experiment, which may have led to lower bacterial production, since ice algae may be a source of autochtonous DOM in ice [*Thomas et al.*, 2001] .

Overall, cell-specific Leu and TdR were lower in ice than in parent water, indicating different physiological adaptations required in these two adjacent environments. The dynamics in bacterial activity appeared to be associated with three different stages in cell-specific Leu and TdR and bacterial abundance. At the beginning of the experiment, the majority of bacteria in ice were probably not well-acclimated to the sea ice environment and possibly undergoing a community shift [*Eronen-Rasimus et al.*, 2014], resulting in higher cell-specific Leu and TdR and a decrease in abundance throughout the ice before day 7. After day 7, cell-specific Leu and TdR were generally stable, but bacterial abundance increased in the bottom ice sections and decreased in the ice interior, pointing to active bacterial growth in the lower ice layers also subject to brine convection before day 15. After day 15, corresponding to the onset of the melting phase, bacterial abundance decreased throughout the ice column and a sharp increase in cell-specific Leu and TdR occurred. This points to a direct effect of physical changes on the bacterial physiology, most likely to be initiated by a sudden change in brine salinity and ice temperature or decreasing nutrient supply due to brine stratification. Brine dilution and direct cell loss from bottom ice during the melting phase could explain the decrease of bacterial abundance.

While cell-specific Leu showed a similar pattern in both treatments, TdR was higher in SWR (compared to SW) both in ice and parent water. This indicates that DOC addition had a

positive impact on bacterial growth, which is also in agreement with the slightly higher bacterial abundance and overall higher bacterial production in SWR series (Table 3).

Bacterial activity impacted NH_4^+ and NO_2^- concentrations in sea ice, but had no notable effect on NO_3^- and DOC. Indeed, NH_4^+ and NO_2^- further accumulated in sea ice (on day 7) after their physical incorporation into sea ice, in SW and SWR. The accumulation of NH_4^+ and NO_2^- likely indicates bacterial remineralization. Remineralization of DOC was almost negligible because bacterial productions were low in comparison to the large pool of DOC in sea ice. Indeed, median bacterial production was 0.16 µg C L^{-1} h^{-1}, which is equivalent to 0.013 µmol C L^{-1} h^{-1}, and this is several orders lower than the DOC concentrations (up to 170 µmol L^{-1}) (Table 3). As a consequence, the difference in bacterial productions could not explain the difference in the EFs of DOC between SW and SWR.

4.3 The particular cases of $Si(OH)_4$ and DOC

All the dissolved compounds showed similar EF in both SW and SWR with the exception of $Si(OH)_4$ and DOC. We did not expect a difference in the brine convection as possible explanation since the physical conditions were comparable between the two treatments. Also, bacterial production might not have affected DOC and $Si(OH)_4$ concentrations significantly, as it was too low in comparison to the large DOC pool, and as bacterial activity is not known to affect $Si(OH)_4$.

A possible explanation for the difference in EF for $Si(OH)_4$ is the degradation of algal cells that were incorporated into the ice (see section 4.1), which may have induced a bias in the EF. Adding the same amount of $Si(OH)_4$ in both SW and SWR would have induced a higher EF in SW than SWR, because the $Si(OH)_4$ in the parent water was lower in SW than SWR.

To verify the hypothesis of particulate silicate (PSi) conversion into $Si(OH)_4$ (DSi), we calculated the deviation of mean $Si(OH)_4$ in ice at the mean ice salinity of 8 from the dilution curve: The mean $Si(OH)_4$ in sea ice was 1.9 and 4.3 µmol L^{-1} in SW and SWR respectively, while it should be 0.8 and 3.2 µmol L^{-1} if it behaved conservatively. Thus, the deviation from the dilution curve was 1.1 µmol DSi L^{-1} for both SW and SWR. This deviation is the additional of $Si(OH)_4$ that we attribute to PSi degradation. Because DSi_n increased considerably on day 2 and then remained constant, the PSi degradation rate should approach 0.55 µmol L^{-1} d^{-1} and then became negligible. This PSi degradation rate corresponds to a dissolution rate constant of PSi of 0.15 d^{-1} (assuming a first order reaction). Similar PSi

degradation rate (0.52 – 0.6 µmol L^{-1} d^{-1} [*Fripiat et al.*, 2009] and dissolution rate constants (0.16 d^{-1} [*Demarest et al.*, 2009], 0 - 0.2 d^{-1} [*Beucher et al.*, 2004]) were found in seawater. In addition, similar rapid decreases in the dissolution rate constants was also observed in *Demarest et al.* [2009], and was attributed to the decrease of overall reactive surface area and the increase of the proportion of less soluble structure as dissolution proceeded.

For DOC, a possible explanation for the differences in incorporation is its molecular composition and the affinity to the other compounds in sea ice. In contrast to the other parameters measured, DOC represents a complex mixture of compounds spanning a range in physical characteristics (e.g. hydrophobicity and size). The addition of river water in the SWR mesocosms resulted in a higher DOC concentration and higher contribution of terrestrial DOC than in the SW mesocosms. Terrestrial DOM is generally composed of older soil-derived and younger vegetation-derived material of which the former is less degradable. We therefore conclude that the addition of riverine DOC, being half of the total DOC, notably changed the composition compared to the prevailing marine (mainly phytoplankton-derived) DOC in the seawater. Thus, the SWR mesocosms contained a higher proportion of refractory DOM than SW. Our data agree with the report that the more labile form of DOC are better retained in sea ice than the refractory form (e.g., humic acids) [*Jørgensen et al.*, submitted; *Müller et al.*, 2013], and that the DOC_n concentrations in ice may be even lower than in the under-ice water when the water contains higher concentrations of soil-derived DOC [*Granskog et al.*, 2005; *Hagström et al.*, 2001]. Furthermore, *Dittmar and Kattner* [2003] referred to the intra-molecular contraction and coiling of humic acids with increasing salinity to explain differences in their chromatographic behavior. Therefore, even among different types of humic acids, there may be differences in the incorporation efficiency.

4.4 Conclusion and perspectives

The aim of our experiments was to better understand the difference in sea ice biogeochemistry from ice growth to ice decay related to additional DOC contribution and bacterial production. We reproduced two main stages in brine dynamics that affect the biogeochemistry in natural sea ice (i.e., bottom convection and brine stratification) despite the short duration of the experiment (19 days).

The experiment has shown that dissolved compounds do not necessarily behave conservatively in relation to salinity during ice formation, consolidation and melt. Particulate organic matter incorporated into sea ice may rapidly be converted to dissolved compounds,

thereby inducing a deviation from the conservative dilution curve. Such deviation from the conservative behavior is however reduced at the bottom of the ice where brine convection occurs.

Three distinct phases in bacterial abundance and carbon production were identified corresponding to physical changes. The overall cell-specific bacterial production was lower than in the starting waters, but increased one week after as a response to the bacterial growth in the ice cover. The initiation of a melting phase seemed to introduce unfavorable growth conditions for bacteria, presumably due to sudden change in brine salinity. Our results demonstrate that there is a direct regulation of bacterial activity by ice physical processes (brine stability and melting) and suggest that the length, and periodicity of freeze-melt cycles may be important for the functioning of bacterial communities in sea ice. Although NH_4^+ and NO_2^- accumulations are consequences of bacterial activity, the bacterial carbon demand was too low to significantly impact the overall DOC pool in sea ice during the experiment.

This experiment has provided evidence that the inter-hemispheric difference of DOC dynamics and bacterial respiration are more complex than initially hypothesized. Indeed, although DOC concentrations are higher in the Arctic Ocean compared to those in the Southern Ocean, Arctic DOC may be less efficiently incorporated into sea ice (because of the properties of terrestrially-derived DOC). The difference in sea ice biogeochemistry between the Arctic and Southern Oceans may also depend on the amount of bio-available DOC (arising from POM in parent seawater) and the associated bacterial production, rather than the total input of allochtonous riverine DOC in seawater.

Acknowledgments

The work described in this publication was supported by the European Community's 7th Framework Programme through the grant to the budget of the Integrated Infrastructure Initiative HYDRALAB-IV, Contract no. 261520. We are grateful to C. Burau and K.-U. Ludwichowski for nutrient and DOC measurements. The authors would like to thank the Hamburg Ship Model Basin (HSVA), especially the ice tank crew, for their hospitality, technical and scientific support and the professional execution of the test program in the Research Infrastructure ARCTECLAB. We also thank the two anonymous reviewers for their thorough comments, which have improved the quality of the manuscript. JZ and BD are

respectively a research fellow and a research associate of the Fonds de la Recherche Scientique –FNRS. The work was supported by a FiDiPro award by the Academy of Finland (grant no. 127097), the Walter and Andree Nottbeck Foundation, the Danish Strategic Research Council to the project NAACOS (grant no. 10-093909) and the Belgian BELSPO-BIGSOUTH grant (# SD/CA/05A). This is a Mare contribution 279.

Chapter VI - Physical and biogeochemical properties in landfast sea ice (Barrow, Alaska): Insights on brine and gas dynamics across seasons

Journal of geophysical Research – Ocean, 118(6), 3172-3189, doi: 10.1002/jgrc.20232

Zhou J. [1,2], B. Delille[2], H. Eicken[3], M. Vancoppenolle[4], F. Brabant[1], G. Carnat[5], N-X. Geilfus[5], T. Papakyriakou[5], B. Heinesch[6] and J-L. Tison[1]

[1] Laboratoire de glaciologie, DSTE, Université Libre de Bruxelles, Belgium

[2] Unité d'océanographie chimique, MARE, Université de Liège, Belgium

[3] Geophysical Institute, University of Alaska Fairbanks, United States

[4] Laboratoire d'Océanographie et du Climat, CNRS, France

[5] Department of Environment and Geography, CEOS, University of Manitoba, Canada

[6] Unité de physique des biosystèmes, Gembloux Agro-Bio Tech, Université de Liège, Belgium

Physical and biogeochemical properties in landfast sea ice (Barrow, Alaska): Insights on brine and gas dynamics across seasons

Jiayun Zhou,[1,2] Bruno Delille,[2] Hajo Eicken,[3] Martin Vancoppenolle,[4] Frédéric Brabant,[1] Gauthier Carnat,[5] Nicolas-Xavier Geilfus,[5] Tim Papakyriakou,[5] Bernard Heinesch,[6] and Jean-Louis Tison[1]

Received 19 August 2012; revised 22 April 2013; accepted 5 May 2013; published 26 June 2013.

[1] The impacts of the seasonal evolution of sea-ice physical properties on ice-ocean biogeochemical exchanges were investigated in landfast ice at Barrow (Alaska) from January through June 2009. Three stages of brine dynamics across the annual cycle have been identified based on brine salinity, brine volume fraction, and porous medium Rayleigh number (Ra). These are sea-ice bottom-layer convection, full-depth convection, and brine stratification. We further discuss the impact of brine dynamics on biogeochemical compounds in sea ice: stable isotopes of water (δD, δ^{18}O), nutrients (NO_3^-, PO_4^{3-}, NH_4^+), microalgae (chlorophyll-a), and inert gas (argon). In general, full-depth convection events favor exchanges between sea ice and seawater, while brine stratification limits these exchanges. However, argon responds differently to brine dynamics than the other biogeochemical compounds analyzed in this study. This contrast is attributed to the impact of bubble nucleation on inert gas transport compared to the other biogeochemical compounds. We present a scenario for argon bubble formation and evolution in sea ice and suggest that a brine volume fraction approaching 7.5–10% is required for inert gas bubbles to escape from sea ice to the atmosphere.

Citation: Zhou, J., B. Delille, H. Eicken, M. Vancoppenolle, F. Brabant, G. Carnat, N.-X. Geilfus, T. Papakyriakou, B. Heinesch, and J.-L. Tison (2013), Physical and biogeochemical properties in landfast sea ice (Barrow, Alaska): Insights on brine and gas dynamics across seasons, *J. Geophys. Res. Oceans*, *118*, 3172–3189, doi:10.1002/jgrc.20232.

1. Introduction

[2] Sea ice covers up to 6% of the Earth's oceans at its maximum extent [*Comiso*, 2010]. Beside its effects on albedo, polar water mass stratification and vertical mixing, and heat and moisture exchange between the atmosphere and the ocean [*Dieckmann and Hellmer*, 2010], sea ice also plays a key role in the polar marine ecosystem [e.g., *Eicken*, 1992; *Lizotte*, 2001]. It has been shown that the ice cover hosts microbial communities during the winter and spring [e.g., *Horner et al.*, 1992; *Thomas and Dieckmann*, 2002]. It is also well established that sea ice melting in summer frequently triggers phytoplankton blooms at retreating sea ice margins [*Smith and Nelson*, 1986]. In contrast, exchanges between sea ice and seawater and their impact on biota before the melt season are less well documented.

[3] As sea ice forms, impurities (e.g., salt and microorganisms) in seawater are trapped in brine liquid inclusions within the ice [*Petrich and Eicken*, 2010]. Both ice temperature and salinity control the brine volume fraction [*Cox and Weeks*, 1983; *Hunke et al.*, 2011] and, therefore, the connectivity of the brine network. Columnar ice permeability in the vertical direction increases drastically for fluid transport when the brine volume fraction exceeds approximately 5% [*Golden et al.*, 1998; *Pringle et al.*, 2009].

[4] Recent modeling studies suggest a direct link between brine convection (also referred as gravity drainage or convective overturning [*Notz and Worster*, 2009; *Notz et al.*, 2005]) and sea ice biogeochemistry. For instance, *Vancoppenolle et al.* [2010] have shown how brine convection ensures nutrient supply from seawater to sea ice, therefore controlling sea ice algal growth. Experimental studies suggest that unstable brine density profiles lead to convection in permeable sea ice. The porous-medium Rayleigh number (Ra) is an indicator of the propensity of brine convection to occur [*Notz and Worster*, 2008]. Convection is found to occur once Ra exceeds a critical value, typically 10 for young sea ice [*Notz and Worster*, 2008]. When convection develops near the ice bottom, exchanges between

[1]Laboratoire de glaciologie, DSTE, Université Libre de Bruxelles, Bruxelles, Belgium.
[2]Unité d'océanographie chimique, MARE, Université de Liège, Liège, Belgium.
[3]Geophysical Institute, University of Alaska, Fairbanks, Alaska, USA.
[4]Laboratoire d'Océanographie et du Climat, Institut Pierre-Simon Laplace, CNRS/IRD/UPMC/MNHN, Paris, France.
[5]Department of Environment and Geography, CEOS, University of Manitoba, Winnipeg, Canada.
[6]Unité de physique des biosystèmes, Gembloux Agro-Bio Tech, Université de Liège, Liège, Belgium.

Corresponding author: Jiayun Zhou, Laboratoire de glaciologie, DSTE, Université Libre de Bruxelles, 1050 Bruxelles, Belgium. (jiayzhou@ulb.ac.be)

2169-9275/13/10.1002/jgrc.20232

sea ice and the underlying seawater occur [e.g., *Niedrauer and Martin*, 1979; *Notz and Worster*, 2008, 2009; *Weeks*, 2010]. Field studies also suggest that convective processes are necessary to explain changes observed in biogeochemical measurements [*Fritsen et al.*, 1994; *Lannuzel et al.*, 2008; *Tison et al.*, 2008], although no obvious link has yet been established between convection and changes in sea ice biogeochemistry.

[5] In this paper, we provide an integrated view of the link between sea ice physical properties and sea ice biogeochemistry. First, we combine field measurements and parameters derived from experimental studies for assessing ice permeability and brine convection; we examine changes in brine salinity and brine volume fraction in relation to changes in Ra. Second, we discuss the impact of permeability and convection on different biogeochemical compounds in sea ice (and specifically within the brine). The biogeochemical compounds were selected in order to represent impurities existing in different phases in sea ice: liquid (stable isotopes of water, nutrients), solid (chlorophyll-a), and gaseous (argon).

2. Material and Methods

2.1. Study Site and Sampling Scheme

[6] The study took place at Barrow, in Alaska, in collaboration with the International Polar Year Seasonal Ice Zone Observing Network (SIZONet) project (www.sizonet.org). The sampling was performed within a 2500 m^2. The northeastern corner of the square was located at 71° 22.013′ N, 156° 32.447′ W, 40 m away from the ice mass balance buoy of the Barrow sea ice observatory of the Geophysical Institute (University of Alaska Fairbanks) [*Druckenmiller et al.*, 2009] (Figure 1). The sampling period covered the ice-growth period and melt onset, from January to June 2009. Figure 2 relates the dates of the 10 sampling events (BRW1–BRW10) to the evolution of air temperature, snow depth, and sea ice thickness monitored at the Barrow Sea Ice observatory (data available at seaice.alaska.edu/gi/

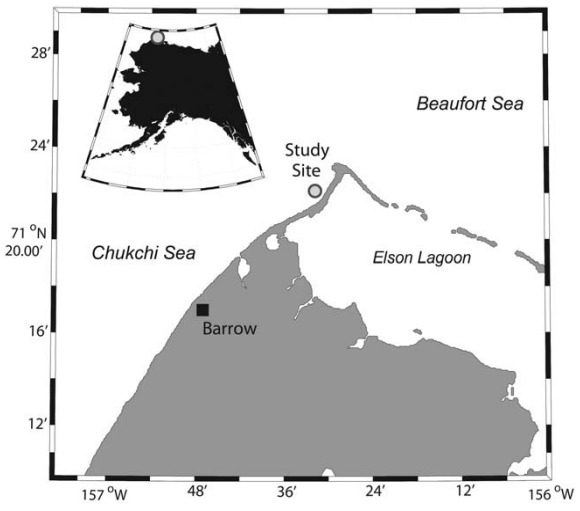

Figure 1. The study site, North of Barrow, Alaska, USA.

data). The ice cores were obtained in level landfast first-year sea ice using an electropolished stainless steel corer. Each sampling event took place within an area of 10 m by 10 m. Landfast ice at this site is immobile and is more homogeneous than drifting pack ice. It is thus better suited for temporal studies, because most of the contrasts between samples can be attributed to the temporal evolution rather than the spatial variability [*Druckenmiller et al.*, 2009]. Directly after extraction, the ice cores were stored and kept at −35°C in the dark. This ensures brine and gas immobilization and inhibits biological activity. Sea ice freeboard was positive during the whole sampling period. Water depth was 9 m. We collected seawater at the ice/seawater interface, 1 and 6 m below the ice cover.

2.2. Thin Sections

[7] Thin sections show ice crystal texture and gas bubble content. They provide information about the conditions during sea ice formation [*Weeks*, 2010]. The preparation and analysis of thin sections took place in a cold room that was held at −25°C. Vertical ice core sections of about 1.5 cm thickness were cut using a band saw, then subdivided into 5–8 cm long sections. Each section was then stuck on a glass plate, by freezing a small amount of distilled water (4°C) along its perimeter. Ice sections were thinned to a few millimeters, using a microtome (Leica SM2400). They were then detached from the glass plate by controlled warming, turned over and reattached through melting and refreezing of a thin interfacial film that does not alter the ice crystallographic properties. Ice sections were then thinned down to 700 μm. The sections were examined between crossed polarizers, and photographs were obtained on the Universal Stage system [*Langway*, 1958].

2.3. Ice Temperature and Salinity

[8] Ice temperature was measured using a calibrated probe (Testo 720). The probe was inserted into holes (matching the diameter of the probe) drilled perpendicular to the ice core axis with a depth resolution of 5 cm. Precision of the probe was ±0.1°C. Though temperature measurements were completed within 5 min after ice core extraction as recommended by *Pringle and Ingham* [2009], some temperature measurements on extracted ice cores were still depressed toward the air temperature near cracked or open-faced ends of the core (Figure 3). This contrasts with the smooth profiles measured by the in situ thermistors (40 m away from our sampling area). The mean temperature difference between in situ thermistors and our own temperature profiles was 0.1°C with a standard deviation of 0.6°C. The temperature measurements were, therefore, smoothed to reduce small-scale temperature deviations, which we assume to be artifacts of the core extraction and measurement process. Remaining differences between the smoothed temperatures and those measured by in situ thermistors could be due to differences in snow thickness. Since ice temperatures impact both sea ice physical and biogeochemical properties, we felt more appropriate to use the smoothed temperatures (Figure 5a) in the calculations of brine salinity, brine volume fraction, Ra, and argon (Ar) solubility (see later sections). Contour plots of physical parameters were created using Surfer® package ("natural neighbor" method).

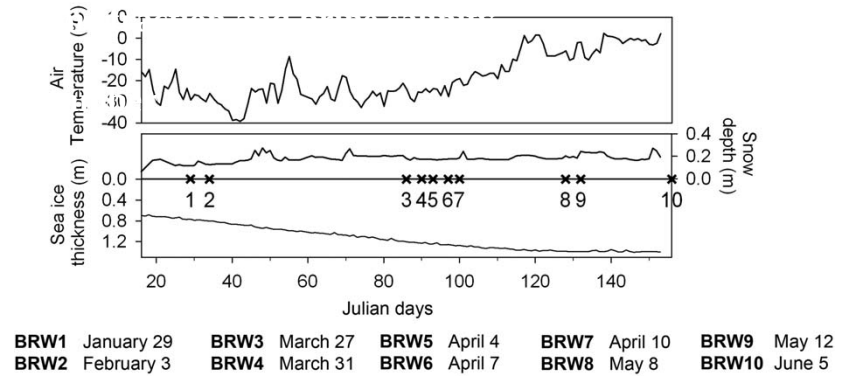

Figure 2. The 10 sampling events (BRW1 to BRW10) referred to the continuous monitoring of air temperature, snow depth, and sea ice thickness at the Barrow sea ice observatory.

[9] Bulk ice salinity measurements were performed on 5 cm vertical core sections obtained from the ice core that was used for temperature measurements. The core was immediately sectioned in the field, stored in polyethylene containers, and left to melt in the Barrow facility laboratories. Salinities were measured with a portable conductimeter (Orion Star Series Meter WP-84TP) on melted ice samples, at room temperature. The precision was ±0.1.

2.4. Brine Volume Fraction and Brine Salinity

[10] Sackholes were drilled into the ice floe surface down to 30, 75, and 95 cm depth, to allow gravity-driven brine collection [*Thomas et al.*, 2010]. Each sackhole remained covered with a plastic lid to minimize atmospheric contamination. Brines were collected after 15–45 min (depending on percolation rate) using a portable peristaltic pump (Master Flex®, E/S portable sampler) and were used for brine salinity, stable isotopes of water, chlorophyll-a (chl-a), and nutrient analyses. Theoretical brine volume fraction and brine salinity were calculated from ice temperature and bulk salinity, neglecting the air volume fraction and using the relationships of *Cox and Weeks* [1983].

2.5. Rayleigh Number

[11] Rayleigh number (Ra) is used as a proxy for gravity drainage (i.e., brine convection). Ra expresses the ratio between the negative buoyancy in the brines and dissipation [*Notz and Worster*, 2008]. At a given depth z within sea ice, Ra is given by:

$$Ra = \frac{g \cdot (h_i - z) \cdot \rho_w \cdot \beta_w \cdot [\sigma(z) - S_w] \cdot \Pi(e_{min})}{\kappa \cdot \eta} \quad (1)$$

where g is the gravity acceleration $g = 9.81$ m·s^{-2}, $[\sigma(z) - S_w]$ is the difference between the brine density at the level z and that at the ice-seawater interface, ρ_w is the density of pure water, β_w is the haline expansion coefficient of seawater, with both ρ_w and β_w taken at 0°C from *Fofonoff* [1985]. $\Pi(e_{min})$ is the effective ice permeability (m^2), which is computed using the formula of *Freitag* [1999, eq. 2.19, p. 48] as a function of the minimum brine volume e_{min} between the level z and the ice-ocean interface. For brine volume fraction, we used the equations given in *Notz and Worster* [2009]. The dynamic viscosity and the thermal

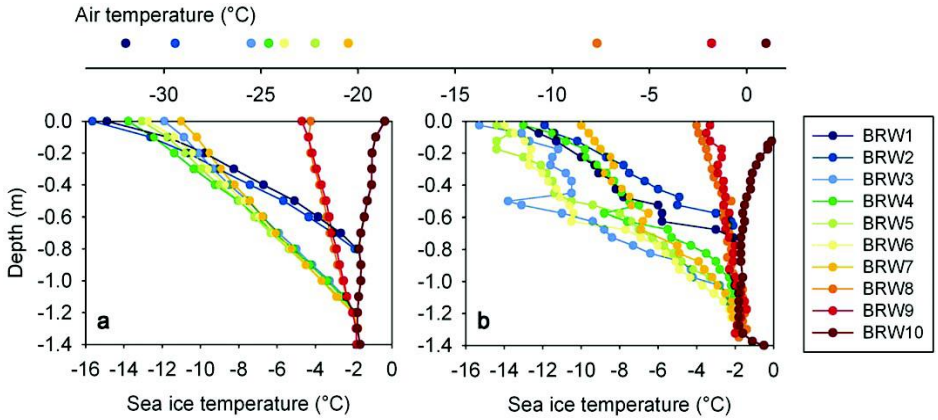

Figure 3. (a) Ice cover temperature profile as obtained from thermistor chain measurements at the Barrow Sea ice observatory versus (b) ice core temperature profiles for the 10 sampling events.

diffusivity of brine are $\eta = 2.55 \times 10^{-3}$ kg·(m·s)$^{-1}$ and $\kappa = 1.2 \times 10^{-7}$ m·s^{-2}, respectively, following *Notz and Worster* [2008].

[12] It is noteworthy that the formulation of *Freitag* [1999] for ice permeability was developed for young sea ice (<30 cm), and a more appropriate formula would be the one of *Eicken et al.* [2004] derived from first-year ice at Barrow. However, we chose to compute permeability using the formulation of *Freitag* [1999] for consistency and comparison with previous work [*Notz and Worster*, 2008].

2.6. Stable Isotopes of Water

[13] We determine δD and δ^{18}O [*Weston*, 1955] in 15 mL aliquots of the melted ice samples (used for the bulk salinity measurements), brine, and seawater samples. Stable isotope measurements were carried out at the Stable Isotope Ratio for Environmental Research Laboratory at the University of Utah using a thermochemical elemental analyzer (TCEA) coupled to a Thermo Finnigan Delta Plus XL Isotope Ratio Mass Spectrometer (measured against Vienna Standard Mean Ocean Water (VSMOW)) at a precision of 0.03‰ for δ^{18}O and 0.4‰ for δD.

2.7. Nutrient and Chl-a

[14] Ice core sections, brine, and seawater samples were melted in the dark at 4°C and filtered through 0.4 μm polycarbonate filters, within 24 h after ice extraction. Inorganic nutrients were analyzed by colorimetry according to the methods described in *Grasshoff et al.* [1983]. To avoid matrix effect, standards used for calibration were prepared in artificial seawater solutions with salinities similar to those of the samples analyzed. For chl-a measurements, the ice samples were melted in the dark, in 0.2 μm filtered seawater (1:4 volume ratio) to avoid osmotic stress. We used 10 and 0.8 μm polycarbonate filters in a sequence in order to distinguish larger microalgae species from the smaller ones. Extractions and calculations were made following the procedure of *Arar and Collins* [1997]. We then calculated the standing stock of chl-a, i.e., we integrated the concentrations vertically to obtain the chl-a content per square meter of ice.

2.8. Argon

[15] Argon (Ar) is an inert gas and is therefore not involved in biogeochemical processes. We used the dry-crushing technique as developed for gas measurements in continental ice [*Raynaud et al.*, 1982]. The measurements have been carried out back in Belgium within 15 months after the survey. Each ice core was cut every 5 cm, and 60 g of sample was introduced into a vessel, with seven stainless steel balls. We evacuated the vessel to 10^{-3} torr, and then fixed it to an ice crusher as described in *Stefels et al.* [2012]. After the crushing at −25°C, the vessel was kept at −50°C in a cold ethanol bath, and was connected to the gas chromatograph equipped with a thermal conductivity detector for concentration analyses [*Skoog et al.*, 1997]. We used Alphagaz™ 2 He (Air Liquide–P0252) as carrier gas and a 22 mL packed column (Mole Sieve 5A 80/100; 5 m × 1/8″). The reproducibility of the analyses was 97.8%.

[16] The amount of gas collected includes both the gas bubbles in the ice and the dissolved phase within liquid brine. Therefore, we compared the evolution of Ar concentration ([Ar]) in bulk ice to its theoretical solubility in ice at saturation. The latter represents the maximum [Ar] that we may find in the dissolved phase, if no supersaturation exists. It is obtained by calculating the solubility of Ar [*Hamme and Emerson*, 2004] using temperature and salinity in brine and weighting it by the brine volume fraction in the ice. The difference between observed concentration in bulk ice and the theoretical solubility in ice at saturation provides a maximum estimate of the Ar content in gas bubble.

[17] It is noteworthy that the relationship of *Hamme and Emerson* [2004] was established for temperatures between 0°C and 30°C and for salinities between 0 and 34.5. We thus assumed in our calculations of Ar solubility that this relationship holds for the ranges of temperature and salinity found in our brine samples. This assumption seems reasonable, because we compared the inventory of Ar solubility calculated as described above with that from an alternative calculation with temperature and salinity fixed at 0°C and 34.5, respectively (the lowest temperature and highest salinity for which Ar solubility is experimentally known [*Hamme and Emerson*, 2004]), and the appropriate brine volume at each depth: the mean difference between both calculations was only 0.059 μmol·L^{-1}. This result indicates that calculations of Ar solubility are much more sensitive to changes in brine volume fraction than to the dependance of Ar solubility on temperature and salinity as expressed by *Hamme and Emerson* [2004].

3. Results

3.1. Physical Framework

[18] The stratigraphy of representative cores from each sampling event is shown in Figure 4. The sampling area was highly homogeneous, with similar textures for BRW1–BRW9: granular ice (~2 cm thick) and columnar ice down to the ice bottom, with a transition layer ("transition ice") with both granular and columnar ice in between (~10 cm thick). From BRW1 to BRW9, the boundary between the transition ice and the columnar ice was particularly bubble rich (Figure 4b). The bubbles were a few millimeters in diameter. Porous ice with larger bubbles and pores (~2 cm diameter), interleaved with superimposed ice layers [*Haas et al.*, 2001], was observed from 0 to 20 cm at BRW10. Maximum snow depth was measured at BRW4 (40 cm) with no snow at BRW10.

[19] Figure 5 shows the evolution of temperature, bulk ice salinity, brine salinity, brine volume fraction, and Ra, within the ice cover, interpolated from the 10 sampling events (dots on Figure 5). The evolution of temperature can clearly be divided into three stages: (1) a cold stage, from BRW1 to BRW7, where ice temperature decreased from the seawater freezing point at the ice base to colder values near the top; (2) a transition stage (BRW7–BRW9) where the temperature near the surface increased and the temperature gradient weakened; (3) a warm stage (BRW9–BRW10) where the temperature profile was nearly isothermal, with a slight temperature increase from the base to the top of the ice.

[20] During the cold stage, all salinity profiles exhibited a typical c-shape, with higher salinities in the top and bottom ice layers compared to those in the ice interior. The bulk ice salinity profiles (Figure 5b) showed a marked transition between BRW7 and BRW8. From BRW8 onward,

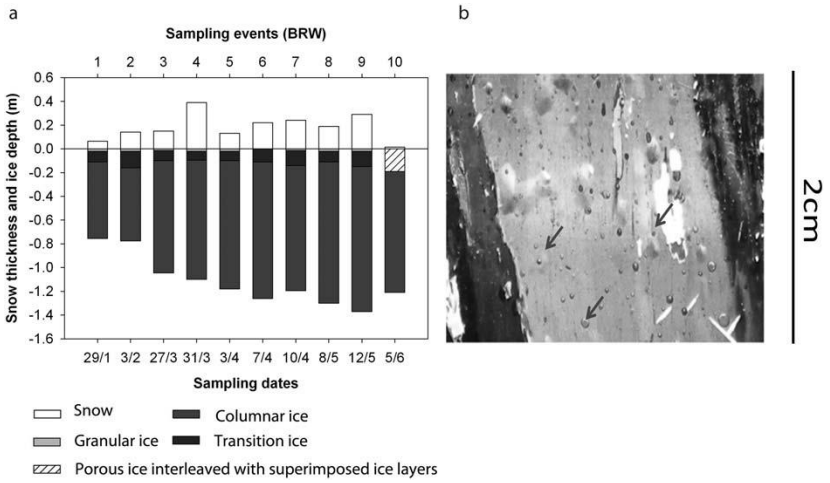

Figure 4. (a) Snow thickness and ice depth shown with respect to the snow-ice interface. Ice texture is shown with different shading of bars. (b) Thin section close up at the transition level (15–17 cm) on BRW4. The arrows point to selected bubbles.

the surface salinity decreased, particularly at BRW10 where the salinity at the top approached 0.

[21] As brine salinity depends solely on temperature, calculated brine salinity (Figure 5c) is the mirror image of the temperature profile. During the cold stage, brine salinity was higher at the top of the sea ice than at the bottom. Then during the transition stage, the differences between the top and the bottom layers greatly diminished. Brine salinity was closer to seawater salinity (32) for these sampling events. Finally, during the warm stage, brine salinity was lower at the top than at the bottom.

[22] The brine volume fraction (Figure 5d) also showed a sharp shift between BRW7 and BRW8. During the cold stage, only the bottom ice layer had a brine volume fraction above 5%, considered as a permeability threshold for fluid transport through sea ice, according to *Golden et al.* [1998] and *Pringle et al.* [2009]. The brine volume fractions exceeded 5% throughout the ice cover from BRW8 onward. We can make a further distinction among the fully permeable ice cores. During the transition stage (BRW8 and BRW9), the brine volume fraction increased downwards. During the warm stage (BRW10), because of high temperatures and despite the low bulk sea ice salinity, brine volume fraction increased upwards, approaching nearly 30% at the ice surface.

[23] The Ra (Figure 5e) was always close to 0.5 to 1 at the sea ice bottom. In the ice interior, Ra was always close to 0 except during the transition stage (BRW8 and BRW9) (Ra up to 8). Although Ra was higher than average at these sampling events, Ra never exceeded the critical convection threshold value of 10. This is rather surprising because during the transition stage, a high fluid permeability (brine volume fraction above 5%) was observed and the unstable brine salinity gradient was reduced; these observations suggest potential brine convection and drainage.

3.2. Isotopic Composition

3.2.1. Sea Ice Isotopic Composition

[24] Figure 6 shows data on isotopic composition of bulk ice, snow and seawater. Ice δD and δ^{18}O profiles appear similar. We observe five main common features related to the ice δD and δ^{18}O depth profiles: (1) 0–5 cm depth: there appears a wide range with contrasting signatures. Late in the season, δD and δ^{18}O reached the lowest values (-67.2‰ and -8.2‰, respectively); (2) 5–20 cm depth: the values scatter around a mean value of -2.0‰ δD and -0.2‰ δ^{18}O; (3) 20–40 cm: there is a transition zone, with local minima at 30 cm (δD = -4.0‰ to -10‰ and δ^{18}O = -0.4‰ to -1.3‰) then rising to maximal observed values at 40 cm (δD = $+8.0$‰ to $+2.0$‰ and δ^{18}O = $+0.8$‰ to $+1.2$‰); (4) 40–90 cm: while the earlier sampling events (BRW2 and BRW4) showed a slight decrease of δ values from 40 to 90 cm, the later samplings (BRW7, BRW8, and BRW10) showed relatively constant δ values (δD = -1.0‰ to $+8.0$‰ and δ^{18}O = $+0.1$‰ to $+1.2$‰); (5) bottom section (bottommost 40 cm): we observe a steeper gradient of decreasing δ values, corresponding to the layer of sharp brine volume increase (Figure 5d).

3.2.2 Brine Isotopic Composition

[25] We hypothesized that the isotopic composition measured on bulk sea ice is due to the contribution of both brine and pure ice.

$$\delta D_{\text{bulk ice}} = (V_{\text{brine}} \cdot \delta D_{\text{brine}}) + (V_{\text{pure ice}} \cdot \delta D_{\text{pure ice}}) \quad (2)$$

[26] $\delta D_{\text{pure ice}}$ only depends on processes occurring during freezing and should not evolve over time. Indeed, solid-state diffusion is not relevant at seasonal timescales, and no fractionation occurs in the solid on melting. Any temporal variation of $\delta D_{\text{bulk ice}}$ is hence due to changes in the relative volume fractions of pure ice and brine ($V_{\text{pure ice}}$ and V_{brine}) and changes in δD_{brine}. The pure ice volume fraction $V_{\text{pure ice}}$ and the brine volume fraction V_{brine} can be derived from temperature and salinity data [*Cox and Weeks*, 1983; *Petrich and Eicken*, 2010], yielding δD_{brine} according to:

$$\delta D_{\text{brine}} = \frac{\delta D_{\text{bulk ice}} - (V_{\text{pure ice}} \cdot \delta D_{\text{pure ice}})}{V_{\text{brine}}} \quad (3)$$

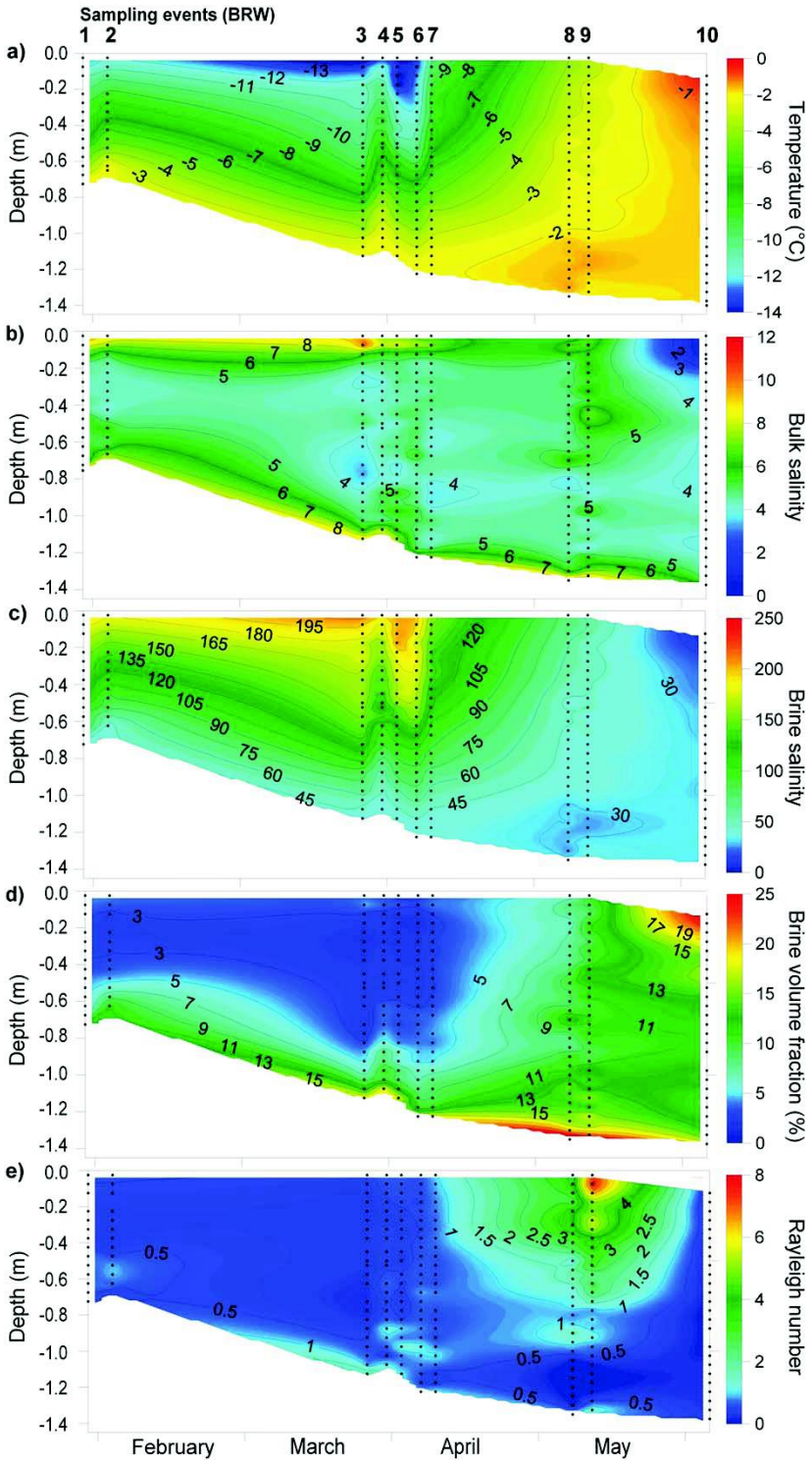

Figure 5. The evolution of (a) temperature, (b) salinity, (c) brine salinity, (d) brine volume fraction, and (e) Rayleigh number computed with *Freitag* [1999] formulation of effective ice permeability. Plots are produced from "natural neighbors" interpolation of field measurements and derived data (dots).

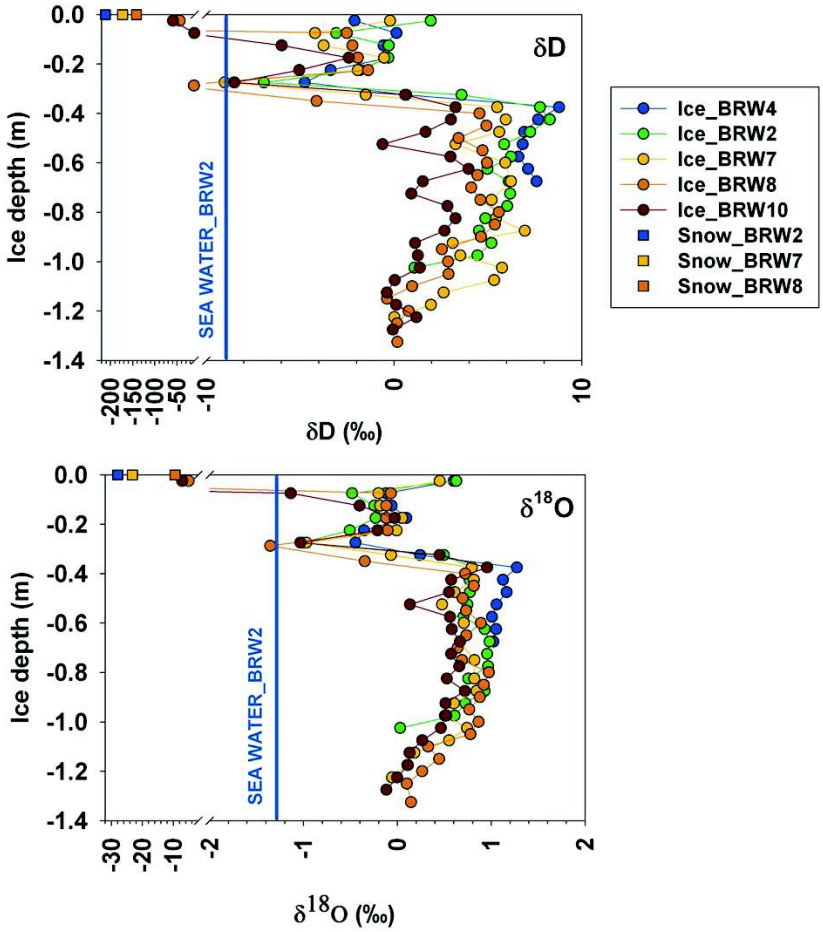

Figure 6. Evolution of $\delta^{18}O$ and δD profiles in bulk sea ice and snow. Seawater value at BRW2 (typical seawater of the main growth period) is also shown.

[27] We hypothesized that isotopic variation in the brine (δD_{brine}) is controlled by internal phase changes and brine drainage processes with subsequent infiltration of snow meltwater or replenishment by seawater. Therefore, in an attempt to track the brine dynamics, we reconstructed the evolution of δD_{brine} and compared it to that of δD values of snow and seawater. Similar calculations could be done for $\delta^{18}O$. However, we focused the discussion on δD because the fractionation factor is larger for δD [*Weston*, 1955], hence changes of δD_{brine} would be more obvious than those of $\delta^{18}O_{brine}$.

[28] The δD_{brine} at BRW7, BRW8, and BRW10 were estimated using equation (3). Because the latest δD_{brine} is only available for BRW4, we used this value to estimate the $\delta D_{pure\ ice}$ at BRW4 ($\delta D_{pure\ ice\ 4}$) and we assumed that it is the same for BRW7, BRW8, and BRW10 at the respective depth levels in the ice. The thickness of BRW4 hence constrained further calculations to a maximum depth of about 1 m. Rearranging equation (3) for this specific use, we then calculated $\delta D_{brine\ 7,8,10}$ from:

$$\delta D_{brine\ 7,8,10} = \frac{\delta D_{bulk\ ice\ 7,8,10} - \left(V_{pure\ ice\ 7,8,10} \cdot \delta D_{pure\ ice\ 4}\right)}{V_{brine\ 7,8,10}} \quad (4)$$

[29] The results are plotted in Figure 7, and only for depths below 40 cm depth (given contrasting signature in the top 40 cm—as discussed below). Measured δD_{brine} from sackholes represents an integration of δD_{brine} in the ice above the sackhole depth. The reconstructed δD_{brine} profiles may, therefore, not be accurate, but their relative temporal trend is still of interest. δD_{brine} profiles increased in homogeneity over time (standard deviations of δD_{brine} at BRW7, BRW8, and BRW10 were 48.0, 14.7, and 11.9‰, respectively). From BRW7 to BRW8, values approached the seawater level, while they drifted toward lower δD_{brine} between BRW8 and BRW10.

3.3. Nutrients

[30] Bulk ice nutrient concentrations are compared to the dilution curve for seawater at BRW2, typical seawater of the main growth period (Figure 8). Any deviation from the dilution curve can be attributed to biological activity [*Thomas et al.*, 2010]. Nitrate (NO_3^-) and phosphate (PO_4^{3-}) show a similar relationship to salinity, and that relationship appears to differ between the cold stage (BRW2 and BRW7) and the transition and warm stage (BRW8 and BRW10). During the cold stage, NO_3^- and

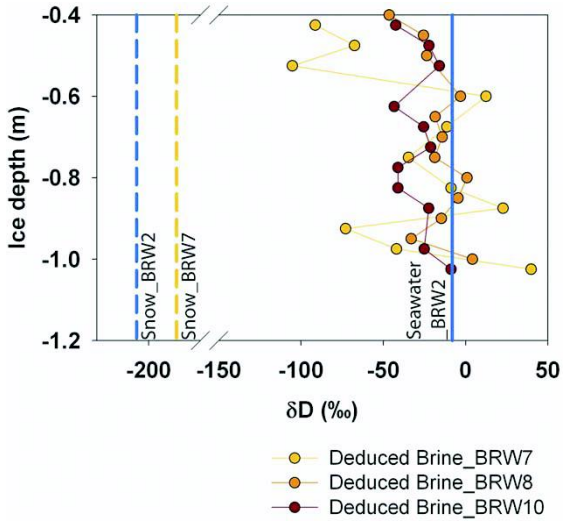

Figure 7. Calculated δD changes in brine below 40 cm depth at BRW7, BRW8, and BRW10 (see equation (4) in the text). δD in seawater, snow, and brines are plotted for comparison.

PO_4^{3-} first scatter around the dilution curve (BRW2) and then increase slightly above the dilution curve (BRW7). With the transition stage, data points fall below the dilution curves. Ammonium (NH_4^+) concentrations in bulk ice were always higher than the dilution curve with a maximum at BRW7.

[31] Nutrients in snow, brine, and seawater were normalized at a salinity of 5 for comparison with bulk sea ice concentrations. All nutrients in snow were above the dilution curve. While [PO_4^{3-}] and [NH_4^+] in snow were similar to those in bulk ice, [NO_3^-] in snow exceeded largely the concentrations observed in bulk ice. In brine, [NO_3^-] and [PO_4^{3-}] were both close to concentrations observed in bulk ice at BRW7, but then decreased at BRW8. As the nutrient concentrations in the brine dropped, we observed a corresponding rise in their concentration within the underlying seawater. The values in seawater then remained stable.

[32] [NH_4^+] did not follow the trend observed for [NO_3^-] and [PO_4^{3-}]. At BRW7, when [NO_3^-] and [PO_4^{3-}] in brine and seawater were close to their concentrations in bulk ice, [NH_4^+] in brine and seawater were well below their concentrations in bulk ice. Then, while changes were observed for [NO_3^-] and [PO_4^{3-}] between BRW7 and BRW8, [NH_4^+] remained close to 0 and well below the dilution curve for both BRW7 and BRW8. In contrast, [NH_4^+] in brine increased at BRW10 and was found above the dilution curve, when [NO_3^-] and [PO_4^{3-}] in brine were below the dilution curve and were close to 0.

3.4. Chlorophyll-a

[33] The total chl-a (standing stock) increased from BRW1 (0.3 mg·m^{-2}) to BRW10 (8.3 mg·m^{-2}), with two decreases (BRW4 and BRW8) and subsequent resumption of the trend toward increasing values (Figure 9). Large

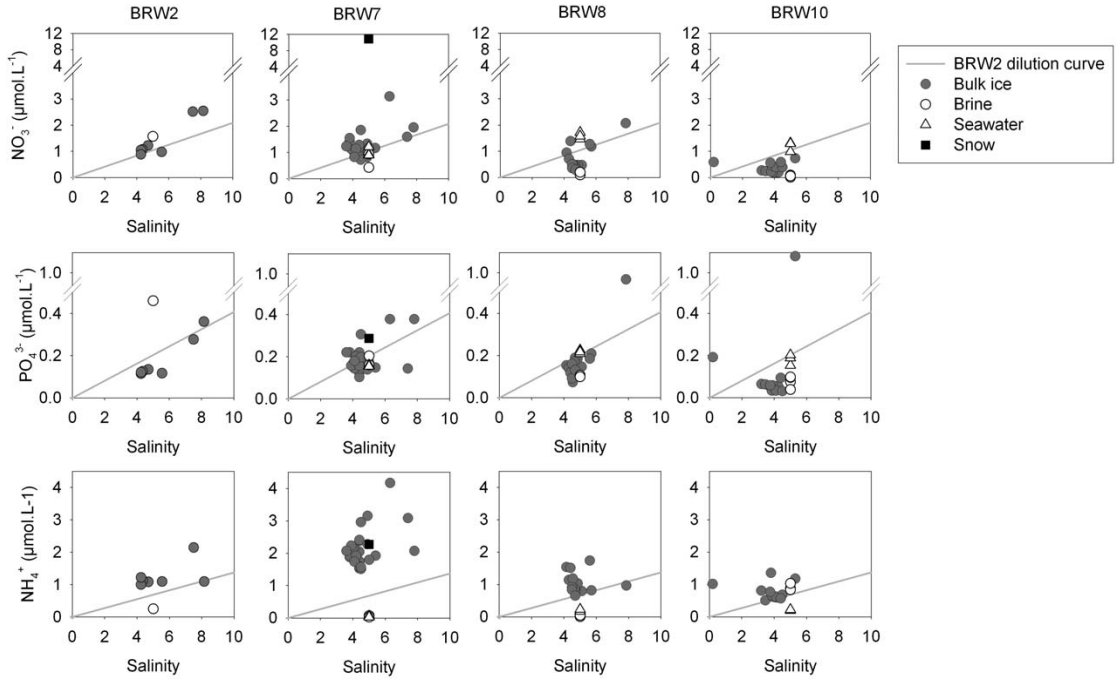

Figure 8. NO_3^-, PO_4^{3-}, and NH_4^+ concentrations in bulk ice (gray dots) compared to the dilution curve for seawater at BRW2, typical seawater of the main growth period. Nutrient concentrations in brine (white dots), seawater (triangles), and snow (squares) have been standardized at a salinity of 5 for comparison.

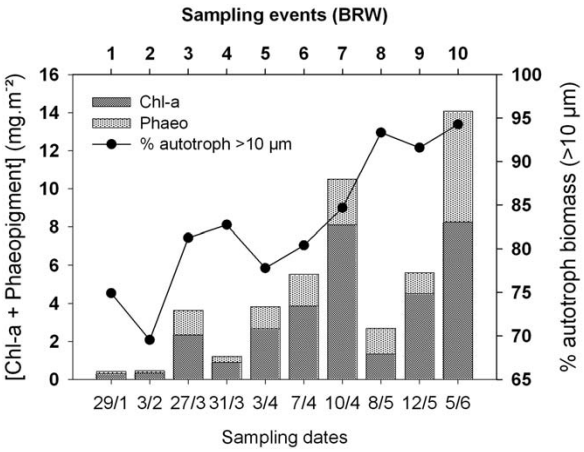

Figure 9. Evolution of the total chl-a, total phaeopigment (phaeo), and percentage of small autotrophs.

species were always dominant in the sea ice. Their dominance within sea ice increased with time (Figure 9).

[34] Figure 10 shows chl-a concentration ([chl-a]) in ice in the upper box, and [chl-a] in seawater in the lower box. In both cases, we differentiate two groups of autotrophs based on cell size, 0.8–10 µm and above 10 µm (Figure 10, black and gray bars, respectively). The colored dots are values for algae in the brines or snow. The distribution of [chl-a] in sea ice showed large vertical variability, with as expected the highest concentrations being observed in the bottommost layers [e.g., *Arrigo et al.*, 2010; *Horner et al.*, 1992]. Prior to BRW7, the [chl-a] in sea ice (generally above 0.5 $\mu g \cdot L^{-1}$) was higher than that in seawater (0.1 $\mu g \cdot L^{-1}$). By BRW8, we observed a sharp decrease of [chl-a] throughout the ice cover, corresponding to an increase in the seawater (0.5 $\mu g \cdot L^{-1}$). The [chl-a] further increased in both sea ice and seawater at BRW9 and BRW10. [chl-a] in brine was always close to 0, except in the permeable layers of BRW7 and BRW9 (Figure 5d).

3.5. Argon

[35] The evolution of Ar concentration ([Ar]) in bulk sea ice (filled dots) is compared to the theoretically determined concentration based on Ar solubility in sea ice using temperature and salinity in brine (crosses) and temperature and salinity fixed to 0°C and 34.5, respectively (empty dots, see section 2) (Figure 11). The [Ar] measured in bulk sea ice integrates both dissolved Ar and Ar content in gas inclusions (gas bubbles) in sea ice. [Ar] scattered around 5 $\mu mol \cdot L_{ice}^{-1}$

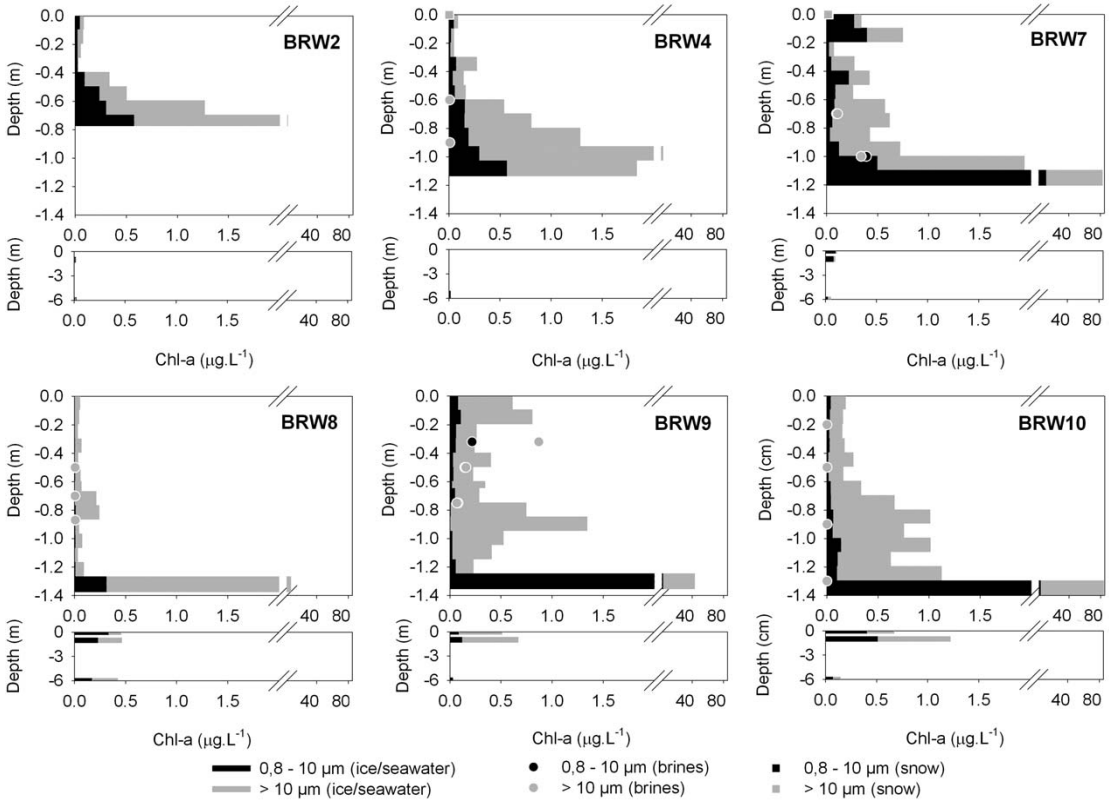

Figure 10. Individual chl-a profiles at selected sampling events. The upper boxes refer to sea ice and the lower boxes to seawater. Gray stacked bars refer to chl-a of bulk ice or seawater, color points refer to chl-a in brines and snow.

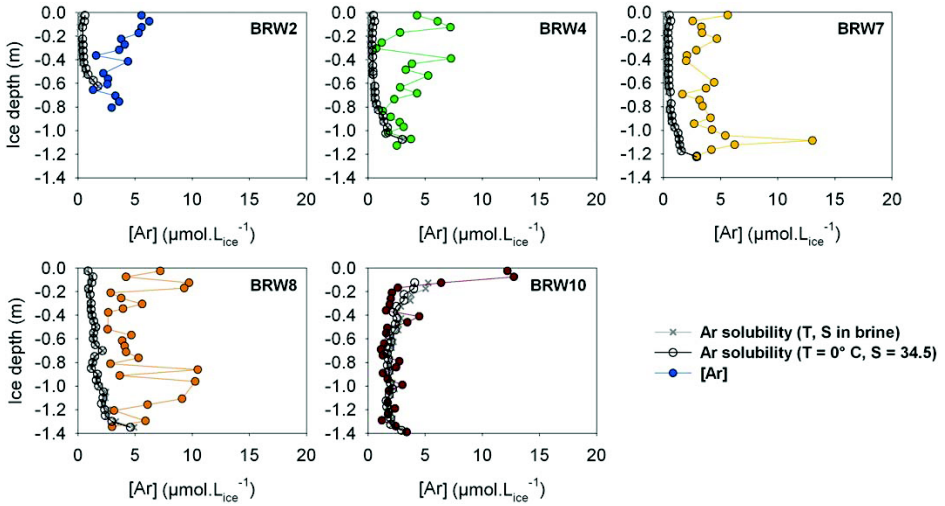

Figure 11. Evolution of Ar concentration ([Ar]) in bulk sea ice (dots) as compared to the solubility limits in sea ice calculated using temperature and salinity in brine (crosses) or temperature and salinity fixed at 0°C and 34.5, respectively (empty dots). Deviation of [Ar] in bulk ice to the solubility limit indicates potential bubble content, while [Ar] in bulk ice at the solubility limit indicates that the gas is dissolved in brine.

and were generally higher than the theoretical solubility values. Maximum [Ar] was ~13 µmol·L_{ice}^{-1} and was observed at sea ice bottom of BRW7 and at the top of BRW10, within the layer of porous ice interleaved with superimposed ice layers. Maximum supersaturation (measured [Ar] divided by the solubility) for the analyzed sampling events was however observed ~12 cm depth and ranged between 2200% and 3800%. [Ar] always corresponded to the theoretical solubility value (~3 µmol·L_{ice}^{-1}) in the bottom layer and at all depths beneath the superimposed ice layers at BRW10. If gas bubble nucleation occurred once dissolved Ar exceeds the theoretical solubility value, the results would suggest that gaseous Ar represented the largest fraction of total Ar in sea ice until BRW8.

4. Discussion

4.1. Physical Framework

[36] The predominance of columnar ice throughout the ice column at all sites indicates that sea ice growth occurred in calm conditions [*Weeks*, 2010]. The homogeneity of the ice stratigraphy and ice texture between samples also supports the conjecture that most trends in the observed variables result from temporal rather than spatial variability. The temporal evolution of sea ice thickness, temperature, and salinity gradients is consistent with those from previous studies in the same area [e.g., *Backstrom and Eicken*, 2006; *Lee et al.*, 2008; *Pringle et al.*, 2007].

[37] The evolution of temperature and salinity (and derived brine volume fraction and brine salinity) can be divided into three main stages: (1) a cold stage (BRW1–BRW7) with ice temperature decreasing from the bottom to the top of the sea ice cover, and the salinity characterized by a C-shape profile; (2) a transition stage (from BRW7 to BRW9) with ice temperature evolving toward isothermal brine volume fractions of 5% and surface brine salinity starting to decrease, and (3) a warm stage (BRW9–BRW10) with ice nearly isothermal, brine volume maximal at the surface with temperature approaching 0°C, bulk ice salinity approaching 0, and brine salinity converging toward seawater salinity in the lower half of the ice cover.

[38] During the cold stage, Ra in the ice interior was close to 0. The brine volume fraction was below 5%, except in the bottom ice layer. The lack of pore connectivity within the brine network [*Golden et al.*, 2007; *Pringle et al.*, 2009] prevented brine percolation despite unstable brine density gradients, by maintaining low permeabilities which in turn kept Ra close to 0. At the other extreme, during the warm stage, brine volume fraction was well above 5%. However, convection was not possible because the brine salinity decreased upwards (Figure 5c); the brine system was stratified. Ra was, therefore, also close to 0. Between the cold and the warm stage, we have identified a transition stage when the brine salinity gradient was unstable and brine volume fraction exceeded 5% throughout the ice. The brine network was hence expected to be sufficiently connected for sea ice permeability to increase to levels that would allow vertical brine mixing. At this time, the Ra value had increased, reflecting more favorable conditions for convection to occur.

[39] Ra in this study never exceeded 10, neither in sea ice bottom layer as in the experimental study of *Notz and Worster* [2008], nor in the ice interior during the transition stage despite the favorable conditions for convection to occur. We suggest that ice-core based derivations (from core salinity and temperature data) underestimate Ra, and that convection may occur for apparent values of Ra less than 10. First, Ra is a function of brine salinity and effective ice permeability (equation (1)). Salt loss by drainage during ice core extraction may have led to an underestimation of sea ice salinity, particularly near the ice bottom where others [e.g., *Notz et al.*, 2005] have reported salinity

to be underestimated by 1–5 and sometimes greater than 10. Such errors in ice salinity lead to an underestimation in Ra in the range of 2–10. Second, sampling only gives a snapshot of variables that are highly time dependent. For instance, supercritical Ra values which take several weeks to buildup over the full depth of the ice vanish within 1 or 2 days due to convection [*Vancoppenolle et al.*, 2010]. For the two reasons outlined above, detecting critical Ra values from ice core data is inherently challenging. However, we believe that Ra change with depth and time may provide insight into whether or not conditions are becoming more favorable for convection. In our case, this would more likely occur in the bottom ice layer from the cold stage to the transition stage, and in the ice interior during the transition stage (Figure 5e). These findings are consistent with those of *Pringle et al.* [2007]. The authors have indeed characterized two types of convective events based on thermal conductivity measurements: The ones occurring near the base of the ice during winter and those occurring further up in the ice interior, late in the season.

[40] The three stages in the evolution of temperature and salinity (and derived brine salinity and brine volume fraction) thus correspond to three stages in sea-ice brine dynamics. (1) The cold stage was associated with sea-ice bottom-layer convection; there is no convection in the ice interior because of the low permeability. (2) The transition stage was associated with full-depth convection because sea ice permeability and brine salinity gradients were both favorable for convection to occur. (3) The warm stage was associated with a complete lack of convection due to brine stratification. The evolution of biogeochemical compounds discussed in the following section supports the characterization of brine dynamics.

4.2. Isotopic Composition

4.2.1. Sea Ice Isotopic Composition

[41] In general, the $\delta^{18}O$ isotopic range in the ice is similar to data collected at the Barrow site in 2006–2008 (−1.5‰ to 1‰; seaice.alaska.edu/gi/data). However, rather than a regular increase of the isotopic composition from the surface to the bottom of sea ice, as generally observed in landfast sea ice [e.g., *Eicken*, 1998], our data show a large variation of the isotopic composition at the surface and a sharp transition ~20–40 cm. Three processes control the profiles of $\delta^{18}O$ and δD: the freezing rate, the isotopic composition of the seawater from which sea ice originated and potential postgenetic disturbance [*Eicken*, 1998; *Souchez and Jouzel*, 1984]. The latter is generally associated with rafting, seawater seepage, or (snow) meltwater seepage, and hence implies changes in salinity.

[42] The minimum value observed at the surface of BRW10 is explained by postgenetic modification in the form of admixture of snow meltwater. Indeed, the bulk isotopic signature at the ice surface was close to that observed in snow (Figure 6), and the fact that ice salinity approached 0 (Figure 5b) suggests snow melting and flushing [*Eicken et al.*, 2004; *Vancoppenolle et al.*, 2007]. Moreover, the observation of superimposed ice formation (Figure 4a) implies seepage of snow meltwater and subsequent freezing on contact with sea ice [*Haas et al.*, 2001].

[43] A sharp transition in $\delta^{18}O$ and δD at ~20–40 cm was found in all cores analyzed for isotopic composition. The thin sections showed no visible disruption in the core stratigraphy or crystal texture at this depth level, suggesting undisturbed growth and the absence of postgenetic disturbance. As sea ice thickens, the freezing rate declines, which would result in a gradual increase of the respective δ values [*Eicken*, 1998; *Souchez and Jouzel*, 1984]. However, at the Barrow site, changes in the sea ice growth rate at depths below 40 cm were small such that any signal due to changing growth rate was likely overwhelmed by changes in the composition of the parent water mass.

[44] Changes in the isotopic signatures of the parent water can be explained by freshwater input or changes in isotopic composition due to advection of different water masses. There are no major rivers in the vicinity of the site, but discharge from Elson Lagoon just east of the sampling site may explain lower isotopic signatures in the early growth season (top 20 cm). *Johnson* [1989] and *Weingartner et al.* [2005] report that Barrow coastal waters are impacted by the combined actions of (1) mean seawater flow coming from the Bering Strait and the Herald Valley forced by the sea-level slope, (2) prevailing southwestward winds, and (3) growth of the sea ice cover. The mean current opposes the prevailing winds and, depending on the balance of both factors, Barrow coastal water is influenced by southwestward or northeastward flows [*Weingartner et al.*, 2005]. We suggest that at the onset of ice growth, water with lower $\delta^{18}O$ (−2‰ to −8‰) advected in response to wind forcing from the Beaufort Sea [*Yamamoto-Kawai et al.*, 2010]. Moreover, remnant surface water containing higher proportions of surface runoff may still have prevailed as well. Once the sea ice reached a thickness of 20–30 cm, wind influence dropped and flow to the Northeast prevails, raising the $\delta^{18}O$ (−1‰ to −2‰) [*Yamamoto-Kawai et al.*, 2010]. In addition, increased mixing of inshore waters due to ice formation and brine discharge may have contributed to diluting the signatures of isotopically light surface water layers impacted by surface runoff.

4.2.2. Brine Isotopic Composition

[45] At BRW8, brine volume fraction and Ra increased sharply (Figures 5d and 5e), suggesting that convection within the sea ice brine system may have been active. The fact that the δD_{brine} homogenized toward seawater values at BRW8 (Figure 7) supports the prospect of mixing between the sea ice brine system and seawater, with partial brine replacement by seawater. This observation supports the occurrence of convection, particularly at BRW9, where higher Ra values were observed (Figure 5e). The later drift of δD_{brine} toward lower values between BRW8 and BRW10 further supports that snow melting was generalized, with active flushing during the warm stage.

[46] Finally, δD_{brine} in the bottom 10–20 cm was always at seawater value. The steeper drop of $\delta D_{bulk\ ice}$ through the bottom 10–20 cm at nearly all the sampling events coincided with the increase in brine volume fraction in sea ice bottom (Figure 6). Higher brine volume fraction means a larger seawater contribution, which drives down the $\delta D_{bulk\ ice}$.

4.3. Nutrients

[47] Our data range is consistent with those of *Krembs et al.* [2002] and *Lee et al.* [2008] obtained in Barrow

landfast ice as well. The comparison of individual data points with the dilution curve (Figure 8) provides insight into the balance between physical and biological processes active in the brine. [NO_3^-], [PO_4^{3-}] at the beginning of the cold stage (BRW2) align along the dilution curve when plotted against the salinity, indicating that physical processes (nutrient incorporation in sea ice and subsequent transport within the brine system) dominate over biological nutrient turnover. In contrast, nutrient concentrations at the end of the cold stage (BRW7) point to dominant heterotrophic processes with recycling and accumulation of by-products from the activity of bacterial metabolism (dots above the dilution curve). However, from the transition stage to the warm stage (BRW8 and BRW10), [NO_3^-] and [PO_4^{3-}] decreased which we attribute to convection and biological consumption as outlined below.

[48] An incursion of seawater into the brine network at BRW8 would have resulted in a slight lowering of nutrient concentrations. We explore this possibility through the use of theoretical nutrient concentrations ([NO_3^-] and [PO_4^{3-}]) in bulk sea ice. Our theoretical estimate assumes that the nutrient concentrations at the sea ice/seawater interface at BRW7 (5.3 and 1.0 $\mu mol \cdot L^{-1}$ for NO_3^- and PO_4^{3-}, respectively) fills between 5% and 30% of bulk ice throughout the sea ice vertical profile at BRW8. The percentages were defined given the brine volume fractions at BRW8 (Figure 5). In the estimate, we neglect potential biological consumption, which we feel is valid given the low [chl-a] measured at BRW8 (Figure 10). Resulting concentrations in ice range from 0.3 to 1.6 $\mu mol \cdot L^{-1}$ for NO_3^- and 0.05 to 0.3 $\mu mol \cdot L^{-1}$ for PO_4^{3-}. These values cover the measured range of sea ice nutrient content at BRW8 (Figure 8), supporting our hypothesis that seawater had replaced the brine. It is noteworthy that brine drainage induced fewer changes in nutrients than in δD_{brine}. This is because nutrient concentrations in seawater were already close to those in brine, while isotopic fractionation led to larger difference between δD in brine and δD in seawater.

[49] At BRW10, [NO_3^-] and [PO_4^{3-}] further decreased in bulk ice, brine, and surface seawater. The decrease in the bulk of the ice indicates internal nutrient consumption, with limited resupply from seawater. Convection processes at that time were indeed unlikely (see section 3.1); hence nutrient resupply from seawater was limited. We believe that nutrient supply at this time was mainly through remineralization [*Lee et al.*, 2008] and diffusion from seawater [*Vancoppenolle et al.*, 2010]. Nutrient consumption may have supported the increase in algal biomass from BRW8 to BRW10 (Figures 9 and 10) in bulk ice and seawater.

[50] The temporal evolution of [NH_4^+] differed from those of [NO_3^-] and [PO_4^{3-}] but parallels those observed in previous studies [e.g., *Lee et al.*, 2008]. At first sight, the evolution of [NH_4^+] reflects the balance between bacterial degradation and the uptake by phytoplankton [*Becquevort et al.*, 2009; *Lee et al.*, 2008]. However, the results further showed that bulk ice had conspicuously higher [NH_4^+] than brine (not observed for [NO_3^-] and [PO_4^{3-}]). This phenomenon has also been reported in *Becquevort et al.* [2009] for Antarctic sea ice. Two processes that can lead specifically to higher [NH_4^+] in bulk ice than in brines: NH_4^+ incorporation in the pure ice matrix and NH_4^+ adsorption on exopolymer substances (EPS) [e.g., *Gradinger and Ikävalko*, 1998; *Krembs et al.*, 2002]. First, NH_4^+ is indeed one of the few chemical compounds that can be incorporated into the ice crystal through substitution [*Weeks*, 2010]. If this occurred, ice melting during the warm stage would transfer NH_4^+ from the ice matrix to the brine and foster sea ice algae growth. Second, the acidic nature of EPS favors cation adsorption [*Hart et al.*, 2001]. If NH_4^+ adhered to the walls of brine inclusions, just like chl-a during the cold stage (see the next section), its drainage into brine sackholes would be unlikely. We believe that this second process was predominant at BRW7, since [NH_4^+] in bulk ice increased significantly but NH_4^+ production in the pure ice matrix is unlikely.

[51] Nutrient concentrations in snow were above the dilution curve at BRW7 (Figure 8). In particular, [NO_3^-] in snow was well above the respective concentration in bulk ice. This indicates that NO_3^- in snow was due to atmospheric supply rather than brine expulsion. Atmospheric supply of NO_3^- through snow deposit has also been observed in the Baltic Sea, where it likely affects the biological productivity in sea ice and in under-ice water through gravity drainage [*Granskog et al.*, 2003].

4.4. Chlorophyll-a

[52] The proportion of large phototrophic organisms increased within sea ice from January to June (Figure 9), as found in previous studies at the site [e.g., *Horner and Schrader*, 1982; *Krembs et al.*, 2001]. Also in agreement with previous findings [*Gradinger et al.*, 1991; *Juhl and Krembs*, 2010], our study suggests an impact of snow cover on algal biomass in sea ice. Although total [chl-a] increased from BRW1 (0.3 $mg \cdot m^{-2}$) to BRW10 (8.3 $mg \cdot m^{-2}$) (Figure 10), this range is well below biomass levels found in earlier studies in the same area (e.g., 27 $mg \cdot m^{-2}$) in 2003 [*Lee et al.*, 2008]). This may be explained in part by the comparatively deep snow cover in 2009. For comparison, although the snow depth was only between 10 and 15 cm in 2003 [*Jin et al.*, 2006], it ranged between 13 and 39 cm in the present study. Heavier snow cover attenuates light and hence lowers photosynthetic activity [*Gradinger et al.*, 1991; *Juhl and Krembs*, 2010; *Mundy et al.*, 2005].

[53] While snow cover may have impacted the overall range of total [chl-a] in sea ice, gravity and convective drainage impacted total [chl-a] in specific ice cores. The gradual increase of total [chl-a] over the study period was punctuated by two apparent reductions in biomass. At BRW4, the drop in [chl-a] could be related to spatial variability or to the loss of bottom biomass by gravity drainage during sample extraction. Since microorganisms were mainly concentrated near the bottom (Figure 10), loss by gravity drainage could have drastically impacted the total [chl-a]. At BRW8, the decrease of [chl-a] was not limited to the bottom layers, but occurred throughout the entire ice thickness (Figure 10). A twin ice core has been melted and variation in total [chl-a] did not exceed 5%. Moreover, since the decrease of [chl-a] was coupled to the increases of Ra and of [chl-a] at the ice-seawater interface, we interpret the [chl-a] decrease at BRW8 as the result of convective overturning, rather than spatial variability.

[54] Linking [chl-a] decreases in sea ice to convective processes implies that microalgae could be drained from sea ice. However, it has been shown that microalgae

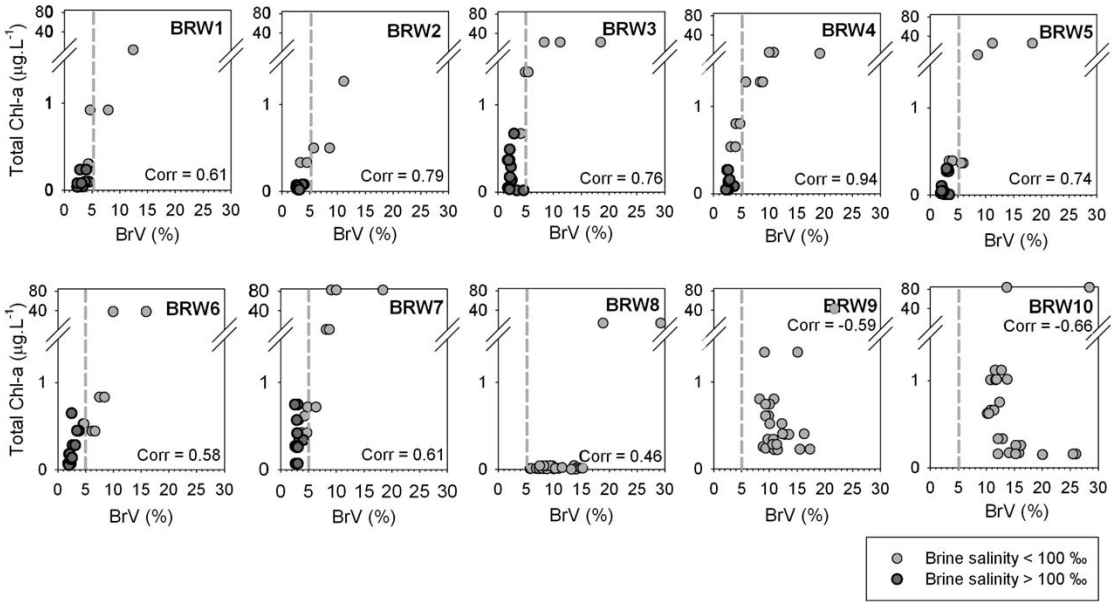

Figure 12. Total chl-a plotted versus brine volume fraction (BrV). The dashed line at 5% of brine volume fraction refers to the threshold for fluid permeability. The correlation coefficient is calculated with omission of the last 20 cm where the dynamic is clearly different from that in the rest of sea ice.

produce exopolymer substances (EPS) that favor their attachment to the walls of brine inclusions [e.g., *Gradinger and Ikävalko*, 1998; *Krembs et al.*, 2002]. Low [chl-a] in brine collected from sackholes supports this suggestion. Figure 12 describes the relationship between the total chl-a and the brine volume fraction and may help resolve this apparent contradiction. There is a positive correlation between both parameters in BRW1–BRW7, suggesting that larger brine volume fractions, characteristic of the bottom layers, favors higher standing stocks. Possible explanations of this observation include: (1) higher nutrient supply, (2) more space within which algal communities can develop high biomass, or (3) high salinities (typically above 100, dark gray dots) and low temperatures inhibit algae growth at small brine volumes. The transition to brine volume fractions above 5% (increasing the permeability of the internal layers above the percolation threshold), combined with convective processes associated with the increase of Ra, result in a complete obliteration of the chl-a and brine volume relationship. This suggests that these processes can overwhelm the EPS-binding mechanism, leading to biomass drainage and removal, increasing their concentration at the ice-seawater interface. *Krembs et al.* [2001] and *Gradinger et al.* [1991] have also suggested that sea ice permeability and brine drainage could impact ice algal buildup.

[55] Our study further recorded rapid chl-a resumption, despite low nutrient concentrations (Figures 8 and 9). This contrasts with the results of *Jin et al.* [2006], suggesting that convective process increases nutrient supply supporting algal growth at Barrow at the same period. Total chl-a was 1.5 mg chl-a·m^{-2} at BRW8, but 4.0 mg chl-a·m^{-2} at BRW9, 4 days later. According to *Arrigo et al.* [2010], carbon (C):chl-a ratio is between 20 and 40. We applied the ratio of 30 to BRW8 and BRW9 and got 45 and 120 mg C·m^{-2}, respectively. The inferred carbon uptake rate is 19 mg C·m^{-2}·d^{-1}, which is consistent with that reported by *Lee et al.* [2008] at Barrow (16 mg C·m^{-2}·d^{-1} the 28th of April). The authors have also noticed algal growth despite of nutrient depletion; this was associated with the increase of carbon allocation into algal lipids. In addition, the increase in the proportion of large species throughout the annual cycle may suggest that these species were more adapted to large brine volumes and low nutrient conditions.

4.5. Argon

[56] Our data range (0.7–13.0 µmol·L_{ice}^{-1}) is consistent with the results of *Matsuo and Miyake* [1966]. Ar profiles are different from those of the other analyzed inert compounds (salt via salinity and isotopes). First, the increase in [Ar] at the base of the transition zone between granular and columnar ice was not observed in all the profiles of the other compounds. Second, while chl-a and nutrients decreased with convective brine drainage during the transition stage (BRW8), Ar further accumulated in sea ice. Third, when chl-a increased again during the warm stage (BRW10), [Ar] dropped to ice solubility values in most of the profile. We suggest that bubble nucleation and migration were the main drivers for the observed differences, because in contrast to the other compounds Ar may be present in the form of gas bubbles. We first discuss how gas bubbles could form in sea ice and how their formation led to the observed Ar profiles.

[57] Within a closed sea ice system, the ratio between the dissolved and the bubble state of Ar depends on the gas solubility in the liquid. [Ar] in the bottom ice layer was always at the solubility limit, suggesting that Ar incorporation at the ice-seawater interface occurred close to the solubility value. Once incorporated into the ice cover, Ar is

exposed to a decrease in temperature and an increase in brine salinity. Decreasing temperature increases Ar solubility but the salinity effect dominates so that Ar solubility in brine (and, therefore, in bulk ice) decreased after incorporation [*Hamme and Emerson*, 2004]. As a consequence, a portion of the dissolved gas is forced out of solution and into bubble. Within a closed system however, the total amount of Ar per unit mass of ice (dissolved + bubble state) should remain constant. We therefore expect a more or less constant value of 3 $\mu mol \cdot L_{ice}^{-1}$ as near the sea ice bottom. The increasing deviation of the measured [Ar] from the solubility limit moving from the ice bottom to the surface (at BRW2 and BRW4) therefore requires the addition of Ar.

[58] Bubble nucleation due to solubility decrease in an open system (i.e. connected to the seawater) could explain the rise in [Ar] in bulk ice. First, on nucleation bubbles may rise due to their buoyancy [*Frank et al.*, 2007], until they are blocked from further migration by reductions in ice permeability. Second, in an open system, brine replacement by seawater through convective processes will increase the Ar content in sea ice given at saturation in brine is lower than [Ar] at saturation in seawater. Ar solubility in the "new" brine would be subject to a lower temperature and higher salinity, resulting in the formation of new bubbles through the lowering of brine solubility for Ar. Repeated convective events may then be effective at raising bulk Ar concentration in sea ice (Figure 13).

[59] Although further laboratory experiments are needed to assess the suggested scenario, we cannot exclude bubble formation within sea ice. Indeed, the highest Ar supersaturations for the presented sampling events ranged between 2200% and 3800%. This range is consistent with the supersaturation level at which *Killawee et al.* [1998] observed nitrogen bubble formation. Moreover, the highest Ar supersaturations were found at the base of the transition level where thin sections showed high bubble content. Furthermore, first results of model simulations indicate at least 50% underestimation of the Ar content within sea ice if the process of bubble formation is not taken into account (S. Moreau et al., Modeling argon dynamics in first-year sea ice, submitted to *Ocean Modelling*, 2013).

[60] Bubble nucleation due to the decrease of solubility contributed significantly to bubble accumulation within sea ice in winter, because of the strong temperature (hence brine salinity) gradient between the top and the bottom of the permeable layers. Since this gradient weakened as the sea ice thickened and its surface temperature increased (Figure 5). Other processes need to be considered to explain the additional incorporation of Ar at the sea ice bottom of BRW7 and BRW8.

[61] Bubble nucleation can also occur at low supersaturation [*Jones et al.*, 1999]. The requirements are (1) preexisting gas cavities in the surface of the substrate and (2) local fluctuations in the gas-supersaturated liquid. These requirements were satisfied at BRW8. The gas cavities

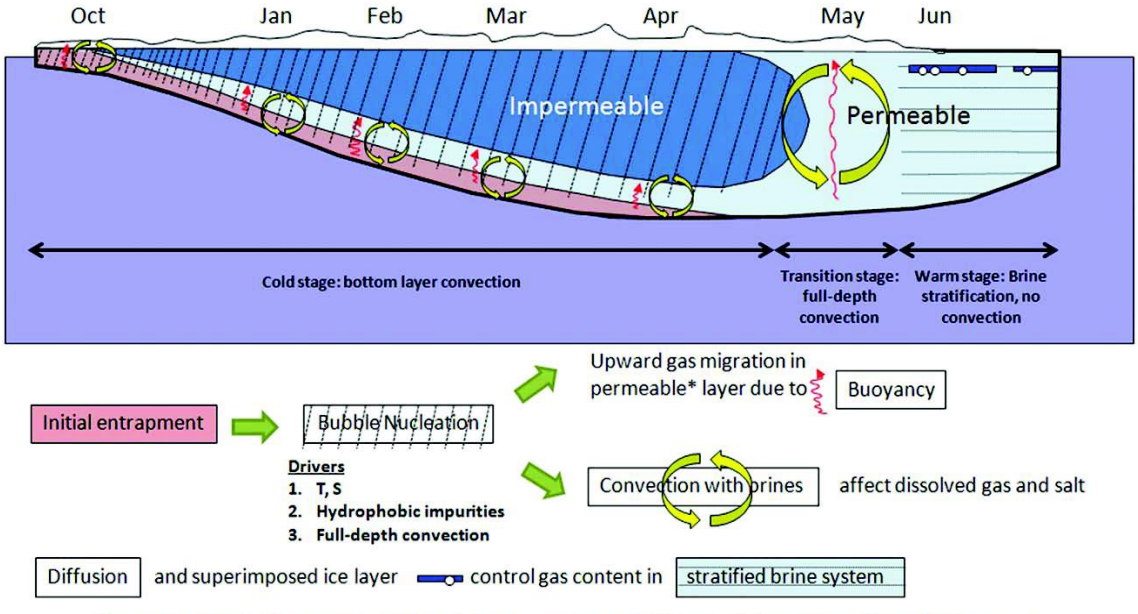

Figure 13. Schematic view of gas entrapment and evolution in sea ice through the three stages of brine dynamics described in the manuscript. After the entrapment, changes in temperature (*T*) and salinity (*S*), the presence of hydrophobic impurities, and full-depth convection contribute to bubble nucleation. Bubbles could then migrate upward in permeable layers due to their buoyancy compared to the brines, while gas dissolved in brine would migrate as salt does, due to brine convection. Diffusion [*Loose et al.*, 2010] and the formation of superimposed ice layers may also control gas content in permeable sea ice.

Table 1. Synthesis on the Evolution of the Physical Properties of Landfast Sea Ice and Their Impacts on Brine Dynamics and Atmosphere-Ice-Ocean Exchanges of Biogeochemical Compound

			Cold Stage	Transition Stage	Warm Stage
Physical Parameters		Texture	• Dominance of columnar ice	• Dominance of columnar ice	• Dominance of columnar ice, and superimposed ice formation at the ice surface
		Temperature, salinity	• Strong temperature gradient, c-shape salinity profile	• Nearly isothermal temperature profile, decrease of surface salinity	• Isothermal temperature profile, salinity close to 0 at the ice surface
		Brine salinity, brine volume fraction	• Unstable brine density profile associated with low ice permeability (brine volume fraction < 5%) in the ice interior	• Unstable brine density profile associated with permeable ice cover (brine volume fraction > 5%) at all depths	• Stable brine density profile associated with permeable ice cover (brine volume fraction > 10%) at all depths
		Ra	• 0 in the ice interior, 1 at the ice bottom	• Ra decreases from the ice surface (1 to 8) to the bottom (ca. 1)	• 0 at all depths
		Interpretation	*Active Ice Growth/Sea-Ice Bottom-Layer Convection*	*Late Ice Growth/Brine Drainage or Full-Depth Convection*	*Ice Melt/No Convection or Brine Stratification*
Biogeochemical Compounds	Dissolved	δD, $\delta^{18}O$	• Physical control only (e.g., parent water mass, isotopic fractionation)	• δD_{brine} approaches the values in seawater	• Decrease of surface δD_{brine} due to snow melt
		Nutrients	• Both physical (e.g., incorporation and rejection) and biological controls (e.g., remineralization).	• Slight decrease in bulk ice nutrient concentration	• Slow/no exchange between brine and under-ice water, but potential input of NO_3^- through snow melt
	Particle	Chl-a	• Physical parameters constrain algal distribution (e.g., low temperature, high brine salinity and limited nutrient supply)	• Drainage of microorganisms from sea ice to under-ice water with rapid resumption and potential changes in species	• Algal growth under low nutrient concentration conditions
	Gaseous	Ar	• Gas bubble formation allows Ar accumulation in sea ice, large Ar supersaturation compared to Ar solubility in ice is observed	• Further Ar accumulation	• No more supersaturation. Gas should have escaped for brine volume fraction approaching 7.5 to 10%
	Interpretation in parallel with the physical processes		*Sea ice is mainly impermeable. The ice interior acts as a close system, which allows accumulations of Ar and NH_4^+. Physical constraints on algae are strong.*	*Sea ice permeability increases (semiopen system) and allows important exchanges with the under-ice water through brine drainage. While dissolved compounds and particles are partially transferred to the under-ice water, gas further accumulates.*	*Sea ice permeability further increases (open system). The exchanges between brine and seawater slow down due to brine stratification, but gas exchanges between brine and the atmosphere is possible. Snow/ice melt and superimposed ice formation locally impact the concentrations of biogeochemical compounds.*

were gas inclusions trapped within brine-filled pores and the local fluctuations were provided by the full-depth convection events. Hence, in addition to solubility-driven bubble nucleation, gas may further accumulate in sea ice through convection-driven bubble nucleation. Further, heterogeneous nucleation may also favor bubble nucleation [*Jones et al.*, 1999] at the ice base with a large content of hydrophobic composites. Since the sea ice bottom at BRW7 was characterized by one of the highest chl-a contents (i.e., potentially high algal biomass) in the dataset, and since algae can synthesize hydrophobic composites [*Underwood et al.*, 2010], the high [Ar] observed at the sea ice bottom of BRW7 may be related to the presence of hydrophobic composites. Further laboratory experiments are however needed for assessing these conjectures.

[62] Our study further suggests that the permeability threshold for gaseous Ar transport in sea ice could be different from that for brine. Indeed, brine volume fractions exceeded 5% at BRW8 and BRW10 (Figure 5d). If Ar behaved as brine, sea ice would be permeable for Ar at these porosities. However, accumulation of Ar below 85 cm at BRW8 indicates that Ar was trapped by impermeable sea ice. In contrast, [Ar] at solubility values (beneath the superimposed ice layers) at BRW10 indicates that a significant amount of bubbles escaped. The comparison of the layers above 85 cm between both sampling events reveals that the brine volume fraction in these layers was below 7.5% at BRW8, but above 10% at BRW10. Therefore, the critical porosity threshold for upward transport of Ar (and possibly other gases as bubbles) in our study may be between 7.5% and 10% of brine volume fraction. These brine volume fractions are associated with temperatures of −3.5 and −2.5°C, respectively, for a bulk ice salinity of 5. The present study thus moderates the statement of *Gosink et al.* [1976] suggesting gas migration through sea ice for temperatures above −10°C. It is however in agreement with the findings of *Loose et al.* [2010], showing gas diffusion through young sea ice (<15 cm thick) between 6.1% and 7.9% of brine volume fraction.

[63] If Ar bubbles escape from sea ice for brine volumes approaching 10%, such escape should have occurred between BRW9 and BRW10 (Figure 5d) and have led to a decrease of [Ar]. Finding [Ar] up to 13 $\mu mol \cdot L_{ice}^{-1}$ at the ice surface of BRW10 is then surprising. There are three potential explanations for this observation: (1) The [Ar] originated from a direct input of atmospheric air. Since sea-ice freeboard was positive, atmospheric air could have filled the ice pores, following brine drainage, and increased [Ar]. (2) The [Ar] originated from bubble upward migration. Indeed, superimposed ice layers were observed at BRW10, and these could impede gas exchange between sea ice and the atmosphere [*Tison et al.*, 2008]. Providing that superimposed ice layers were formed between BRW9 and BRW10 and that bubble upward migration was slow, superimposed ice layers could have blocked the bubbles rising up throughout the brine network; (3) The [Ar] was related to superimposed ice formation itself, as a result of snow melt with subsequent rapid freezing at the ice interface. This explanation is supported by the following statements: First, the observed high [Ar] was found within the superimposed ice layers but not underneath, which would have been the case if it was due to bubble upward migration. Second, the measured concentration is equivalent to 0.29 mL $Ar \cdot L_{ice}^{-1}$ in STP, which is similar to that obtained from instant freezing of seawater (0.23 mL $Ar \cdot L_{ice}^{-1}$, assuming 1% of Ar in total gas content) [*Matsuo and Miyake*, 1966]. Third, the measured concentration is consistent with the solubility of snow and ice meltwater. Indeed, hypothesizing equilibrium between meltwater and the atmosphere and taking into account the bulk salinity of the ice surface (0–5 cm), which was 0.2, we computed the solubility of Ar at 0°C [*Hamme and Emerson*, 2004] and found 22 $\mu mol \cdot L^{-1}$. The measured concentration (13 µmol $Ar \cdot L_{ice}^{-1}$) is slightly lower than the computed solubility; this is likely due to the matrix of pure ice (meltwater only filled pores within the pure ice matrix). Therefore, during the warm stage, despite large brine volume fraction, gas accumulation in sea ice seems possible through superimposed ice formation.

5. Conclusion and Perspectives

[64] The present study focuses on the physical properties of landfast sea ice, and their impacts on brine dynamics and ice-ocean-atmospheric exchanges of biogeochemical compounds, during an annual cycle of ice growth and decay (from January to June 2009) at Barrow (Alaska). The main findings are summarized in Table 1. We have identified three main stages in the evolution of physical properties (temperature, salinity, brine salinity, and brine volume fraction, Ra): a cold stage (BRW1–BRW7), a transition stage (BRW7–BRW8), and a warm stage (BRW9–BRW10). These stages corresponded to three stages in sea-ice permeability and brine dynamics: (1) the cold stage was associated with low permeability in the ice interior and sea-ice bottom-layer convection; (2) the transition stage was associated with full-depth convection due to the combined effect of permeable ice cover and unstable brine density profile. (3) The warm stage was associated with a complete lack of convection, despite permeable ice cover, due to brine stratification.

[65] Ra was used qualitatively because detecting critical Ra values from ice core data appears to be challenging. Nondestructive, in situ measurements of temperature and bulk salinity (the latter through approaches such as those outlined by *Notz et al.* [2005] or *Backstrom and Eicken* [2006]) can help address this issue. Similarly, temperature traces from time series collected by thermistor arrays may also provide evidence for the onset of convection [*Pringle et al.*, 2007].

[66] The analyzed biogeochemical compounds showed distinct behavior during each of the brine dynamic stages. During the cold stage, the temperature gradient was steep with an effectively impermeable ice interior and a highly permeable sea-ice bottom layer. Within the impermeable layer, concentrations of the biogeochemical compounds at the beginning of the cold stage depend strongly on the conditions of sea ice formation and the dominance of physical controls. δD and $\delta^{18}O$ suggest regional changes in water mass properties; nutrient distribution along the dilution curve indicates that physical processes dominate over biological turnover. Chl-a concentrations that correlate well with brine volume fractions suggest that the size of brine inclusions may constrain the distribution of microorganisms

(through the associated temperature, brine salinity, and nutrient supply). Ar accumulation within the ice is related to changes in gas solubility and subsequent bubble formation at incorporation. At the end of the cold stage, biological control of the biogeochemical compounds increased: total chl-a increased, and nutrients accumulated in the ice interior due to remineralization. Such an accumulation confirms that the ice interior was impermeable with a lack of exchange between the ice interior and the under-ice water. In contrast to the impermeable ice interior, convection occurred throughout the whole cold stage within the permeable sea-ice bottom layer. This ensured nutrient supply and contributed to the high [chl-a] observed near the sea ice bottom.

[67] During the transition stage, brine volume fractions increased throughout the ice cover. This, in combination with the unstable brine salinity gradient, favored full-depth convection, which then impacted all the biogeochemical compounds. Dissolved compounds reflect brine drainage with partial seawater replenishment: δD_{brine} approached seawater values; NO_3^- and PO_4^- returned to values set by the dilution curve. The solid fraction (chl-a) was also flushed out of the ice. This seeding of nutrients and organic matter likely boosts microorganism growth in the under-ice water, where concomitant chl-a increases was indeed observed. *Arrigo et al.* [2012] have also reported such an under-ice phytoplankton growth in the Chukchi Sea northeast of Barrow. While both dissolved (isotopes and nutrients) and solid (chl-a) fractions were flushed from the ice, chl-a showed a rapid resumption. Sharp changes in brine volume fraction and in nutrient concentrations, associated with the transition stage, should promote changes in the ice algal community. As a potential consequence, the proportion of larger microorganisms within the ice was observed to increase during the transition stage. In contrast to the other compounds, Ar further accumulated in sea ice. We relate this behavior to its presence in the gaseous phase, and suggest that the formation of bubbles (through convection processes and heterogeneous nucleation) and the subsequent rise due to buoyancy promote Ar accumulation within the ice. Therefore, in contrast to the cold stage, where sea ice interactions with seawater are limited to the bottom layers, during the transition stage such interactions take place throughout the ice column.

[68] Finally, during the warm stage, the brine within the ice column was well stratified, precluding convection. Isotopes indicated downward percolation of snow meltwater into the ice. Nutrient concentrations further decreased since consumption outweighed supply, sustaining the increase of chl-a standing stock through the melt season, with potential contributions of NO_3^- from snow melt and NH_4^+ from ice melt. These observations need to be properly simulated by models of sea ice primary production that rely on a tight link between nutrient supply and ice algal growth. In contrast to the two other stages, interactions between sea ice and seawater are more limited during the warm stage, which is characterized mainly by diffusive rather than convective transport. At the same time, exchange between the ice cover and the atmosphere is more intense. Thus, Ar dropped to the solubility value during this warm stage, suggesting the release of the bubble content to the atmosphere. We estimate that the threshold for significant Ar bubble migration in the brine system is at brine volume fractions of between 7.5% and 10%. Our study, therefore, shows that gases can accumulate in sea ice and persist longer than what would be expected based on brine migration behavior. This finding has potential implications for the biological impact of the dynamics of climate-active gases like CO_2 [*Delille et al.*, 2007] and CH_4 [*Shakhova et al.*, 2010] that are incorporated into sea ice.

[69] **Acknowledgments.** The authors thank C. Petrich and the sea ice group of the Geophysical Institute of the University of Alaska Fairbanks for installing and maintaining the sea ice mass balance buoy. We are indebted to the Barrow Arctic Science Consortium and the North Slope Borough for their logistical support. We thank L. Chou and S. El Amri for their efficient help in laboratory work. We gratefully acknowledge the helpful comments and suggestions of the four anonymous reviewers. This research was supported by the F.R.S-FNRS (contract 2.4584.09), the National Science Foundation (project OPP-0632398 (SIZONet)), the University of Alaska Fairbanks and the Belgian Science Policy (contract SD/CA/03A), and the NCE ArcticNet and National Science and Engineering Research Council (NSERC). N.X.G. and F.B. got a PhD grant from F.R.S.-FRIA. J.Z. is a research fellow of F.R.S.-FNRS, B.D. is a research associate of F.R.S.-FNRS. This is MARE contribution 245.

Chapter VII - Physical controls on the storage of methane in landfast sea ice

The Cryosphere, 8, 1019-1029, doi:10.5194/tc-8-1019-2014

Zhou J.[1, 2], J-L. Tison[1], G. Carnat[1], N-X. Geilfus[3] and B. Delille[2]

[1]Laboratoire de glaciologie, DSTE, Université Libre de Bruxelles, Brussels, Belgium

[2]Unité d'Océanographie chimique, MARE, Université de Liège, Liège, Belgium

[3]Arctic Research Center, Aarhus University, Aarhus, Denmark

Physical controls on the storage of methane in landfast sea ice

J. Zhou[1,2], J.-L. Tison[1], G. Carnat[1], N.-X. Geilfus[3], and B. Delille[2]

[1]Laboratoire de glaciologie, DSTE, Université Libre de Bruxelles, Brussels, Belgium
[2]Unité d'Océanographie chimique, MARE, Université de Liège, Liège, Belgium
[3]Arctic Research Center, Aarhus University, Aarhus, Denmark

Correspondence to: J. Zhou (jiayzhou@ulb.ac.be)

Received: 13 November 2013 – Published in The Cryosphere Discuss.: 6 January 2014
Revised: 17 April 2014 – Accepted: 22 April 2014 – Published: 3 June 2014

Abstract. We report on methane (CH_4) dynamics in landfast sea ice, brine and under-ice seawater at Barrow in 2009. The CH_4 concentrations in under-ice water ranged from 25.9 to 116.4 nmol L_{sw}^{-1}, indicating a supersaturation of 700 to 3100 % relative to the atmosphere. In comparison, the CH_4 concentrations in sea ice ranged from 3.4 to 17.2 nmol L_{ice}^{-1} and the deduced CH_4 concentrations in brine from 13.2 to 677.7 nmol L_{brine}^{-1}. We investigated the processes underlying the difference in CH_4 concentrations between sea ice, brine and under-ice water and suggest that biological controls on the storage of CH_4 in ice were minor in comparison to the physical controls. Two physical processes regulated the storage of CH_4 in our landfast ice samples: bubble formation within the ice and sea ice permeability. Gas bubble formation due to brine concentration and solubility decrease favoured the accumulation of CH_4 in the ice at the beginning of ice growth. CH_4 retention in sea ice was then twice as efficient as that of salt; this also explains the overall higher CH_4 concentrations in brine than in the under-ice water. As sea ice thickened, gas bubble formation became less efficient, CH_4 was then mainly trapped in the dissolved state. The increase of sea ice permeability during ice melt marked the end of CH_4 storage.

1 Introduction

Methane (CH_4) is a well-mixed greenhouse gas. Its concentration in the atmosphere is much lower than that of its oxidation product (CO_2) (1.9 vs. 397 ppm respectively) (http://www.esrl.noaa.gov/gmd/aggi/). However, since the CH_4 global warming potential is 28 times higher than that of CO_2 over a 100-year frame, it accounts for 20 % of the global radiative forcing of well-mixed greenhouse gases (Myhre et al., 2013).

Global ocean emission of CH_4 is estimated at 19 Tg per year (Kirschke et al., 2013), which is about 3 % of the global tropospheric CH_4 input. Of that marine contribution, 75 % is from coastal regions (Bange et al., 1994). CH_4 supersaturation relative to the atmosphere in estuaries (Borges and Abril, 2011; Upstill-Goddard et al., 2000) and coastal shelves (Kvenvolden et al., 1993; Savvichev et al., 2004; Shakhova et al., 2005, 2010) is indeed larger than that in the open ocean (Bates et al., 1996; Damm et al., 2007, 2008, 2010).

Methanogenesis in submarine sediments is thought to be the main process causing CH_4 efflux in the Arctic shelf regions. Nonetheless, other sources could also be significant: CH_4 seepage from coastal ice-complex deposits (Romanovskii et al., 2000) and from deeper seabeds (Judd, 2004), and CH_4 dissociation in the shallow hydrates (Reagan and Moridis, 2008; Westbrook et al., 2009). Recently, aerobic CH_4 production in the water column related to dimethylsulfoniopropionate (DMSP) degradation was reported for the central Arctic (Damm et al., 2010), tropical upwelling areas (Florez-Leiva et al., 2013) and tropical oligotrophic areas (Zindler et al., 2013). However, the significance of that process over the Arctic shelf still needs to be assessed.

Ongoing global warming is likely to affect the various sources of CH_4 cited above, with positive feedback on the climate. Indeed, a rise in sea temperature should increase methanogenic activities, leading to a more efficient conversion of organic matter to CH_4 (Zeikus and Winfrey, 1976). In addition, the induced seawater stratification is likely to change the nutrient ratio, which favours aerobic CH_4 production (Karl et al., 2008). Moreover, warmer seawater is likely to weaken the coastal ice complex (including subsea

permafrost) (Lawrence et al., 2008) and to displace the gas hydrate stability zones (Reagan and Moridis, 2008), increasing gas seepage. Significant CH_4 escape has recently been detected via acoustic surveys along the Spitsbergen continental margin (Westbrook et al., 2009), suggesting that changes in the CH_4 storage system are ongoing. Since CH_4 has a high global warming potential, its release will enhance global warming, which in turn will enhance methanogenic activities and gas seepages. This positive feedback has contributed to rapid and significant climate warming in the past (O'Connor et al., 2010).

Understanding the current CH_4 budget is thus important in order to better simulate future climate scenarios. Many CH_4 measurements have been carried out in sediments and seawater throughout the coastal Arctic areas (Kvenvolden et al., 1993; Savvichev et al., 2004; Shakhova et al., 2005, 2010). These observations have led to speculations about potential CH_4 accumulation (Shakhova et al., 2010) and/or oxidation (Kitidis et al., 2010) under sea ice cover. Other studies further brought forward the role of sea ice in the exchange of CH_4 between seawater and the atmosphere (He et al., 2013; Kort et al., 2012). However, to the best of our knowledge, no study has yet discussed the physical controls on the storage of CH_4 in sea ice and its exchange at the atmosphere–ice–ocean interfaces. For instance, CH_4 mixing ratios up to 11 000 ppmV have been measured in sea ice bubbles (Shakhova et al., 2010), but the mechanisms leading to the incorporation of those gas bubbles within the ice have not been discussed. Similarly, He et al. (2013) suggested CH_4 consumption in the ice, based on CH_4 fluxes above sea ice. However, they did not discuss the impact of sea ice permeability or ice melt on their results, although these parameters have been shown to affect other gas dynamics in sea ice (see, e.g., Loose et al. (2009) for O_2 and SF_6, Geilfus et al. (2012) and Nomura et al. (2010) for CO_2, and Zhou et al. (2013) for Ar). Therefore, we felt it necessary to highlight the physical controls on CH_4 dynamics in sea ice, from ice growth to ice melt. We have done this by investigating the annual evolution of CH_4 concentrations in sea ice, in parallel with sea ice physical properties, and CH_4 concentrations in seawater. To the best of our knowledge, we report here the first detailed time series of CH_4 concentrations in sea ice across seasons.

2 Materials and methods

2.1 Study site and physical framework

Sea ice and under-ice seawater samples were collected during a field survey in the Chukchi Sea near Barrow (Alaska) (Fig. 1) from January through June 2009. The sampling was performed on level first-year landfast sea ice, within a square of 50 m by 50 m. The north-eastern corner of the square was located at 71°22.013′ N, 156°32.447′ W. Seawater depth at the location was about 6.5 m (http://seaice.alaska.edu/gi/observatories/barrow_sealevel). Ice cores were extracted and kept in darkness in the laboratory at −35 °C to prevent brine drainage and to limit biological activity. Temperature recorders indicated that the samples were always kept below −20 °C during transport. All of the analyses were completed within the following year. A complete physical framework of the present study is presented and discussed in Zhou et al. (2013). We have selected six sampling events to illustrate the evolution of CH_4 concentrations at our location: one in the winter (BRW2; 3 February), four in early spring (BRW4, BRW5, BRW6 and BRW7; corresponding to 31 March, 3, 7 and 10 April respectively), and the final one in late spring (BRW10; 5 June). The first five sampling events occurred during ice growth, the last one during ice decay.

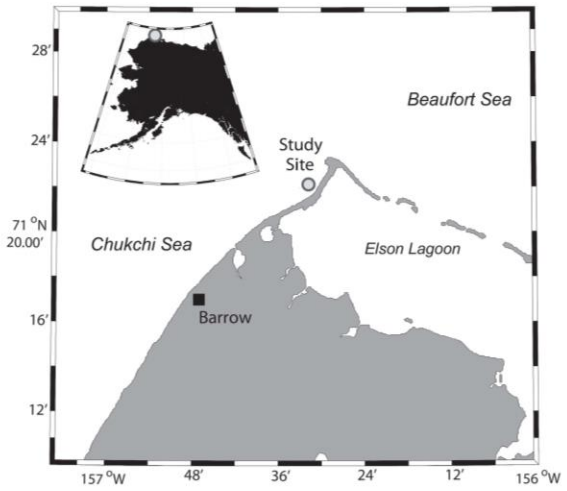

Figure 1. The study site (north of Barrow, Alaska, USA).

2.2 CH_4 concentrations in seawater

CH_4 concentrations in seawater were determined by gas chromatography (GC) with flame ionization detection (SRI 8610C GC-FID) (Skoog et al., 1997) after creating a 30 mL headspace with N_2 in 70 mL glass serum bottles, following the procedure described by Abril and Iversen (2002). After creating the N_2 headspace, samples were vigorously shaken for 20 min and were placed in a thermostatic bath overnight at −1.6 °C. The following day, the samples were shaken again for 20 min before starting the GC analysis. $CH_4 : CO_2 : N_2$ mixtures (Air Liquide, Belgium) of 1, 10 and 30 ppm CH_4 were used as standards. The concentrations were then computed using the CH_4 solubility coefficient given by Yamamoto et al. (1976). The accuracy of the measurements was within 1 %.

We calculated the solubility of CH_4 in seawater that is in equilibrium with the atmosphere, following Wiesenburg and Guinasso (1979). The ratio between the measured CH_4

concentration in seawater and the calculated solubility in equilibrated seawater determines the supersaturation factor.

2.3 CH_4 concentrations in bulk ice and brine

We used the wet extraction method to extract CH_4 from sea ice, as described in Raynaud et al. (1982) for continental ice. Briefly, 80 g of ice sample were put in a small container, using a 5 cm vertical resolution. The ice sample was then melted in the container under vacuum (10^{-3} torr), using a "bain-marie". It was then slowly refrozen from the bottom, using an ethanol (96 %) bath that was cooled to −80 °C by the addition of liquid N_2. After refreezing, the whole gas content (both dissolved and in the bubbles) was expelled into the headspace of the container. The expelled gas was then injected through a 22 mL packed column (Mole Sieve 5 A 80/100; 5 m × 1/8″) into a gas chromatograph (Trace GC) equipped with a flame ionization detector for CH_4 measurement. The reproducibility of the measurement, based on triplicate analysis of five different standards, was 99.6 %.

The method described here above gives CH_4 concentrations in bulk ice. Providing that there is no CH_4 in the pure ice matrix (Weeks, 2010) and, hence, that the entire amount of CH_4 (dissolved or in gas bubbles) is found within the ice pores (i.e. brine channels), CH_4 concentration in bulk ice divided by the brine volume fraction (Cox and Weeks, 1983) gives the deduced CH_4 concentration in brine.

Dissolved CH_4 concentration in brine was also measured for brine samples collected using the sackhole technique (e.g. Gleitz et al., 1995; Papadimitriou et al., 2007). Sackholes (partial core holes) were drilled at different depths, ranging from 20 to 130 cm. Brines, from adjacent brine channels and pockets, seeped into the sackholes and were collected after 10 to 60 min using a peristaltic pump (Cole Palmer, Masterflex® – Environmental Sampler). Each sackhole remained covered with a plastic lid to minimize mixing with the free atmosphere. Brines were collected in 70 mL glass serum bottles, filled to overflowing, poisoned with 100 µL of saturated $HgCl_2$ and sealed with butyl stoppers and aluminium caps. The measured CH_4 concentration in brine is an integrated value of the CH_4 in brine from all the ice layers above the sampling depth. Therefore, the vertical resolution is lower than that of the CH_4 concentrations in brine that is deduced from the CH_4 concentrations in bulk ice. It is also noteworthy that the relative contribution of the various depth levels is unknown and dependent on the brine volume changes with depth. However, it is of interest to compare the measured CH_4 concentrations in brine with those deduced from the bulk ice values, as discussed later on.

For data interpretation, we calculated CH_4 solubility in brine and in ice (i.e. potential CH_4 concentration dissolved in brine and in bulk ice respectively). The solubility of CH_4 in brine was calculated using the same temperature and salinity-dependent solubility of Wiesenburg and Guinasso (1979) as for seawater. This is possible providing that the relationship of Wiesenburg and Guinasso (1979) is valid for the ranges of brine temperature and brine salinity. As for the conversion of CH_4 concentrations in bulk ice into the deduced CH_4 concentrations in brine, we simply multiplied the solubility of CH_4 in brine by the brine volume fraction to get the solubility of CH_4 in bulk ice. Brine salinity and brine volume (used in the calculations) were derived from the relationship of Cox and Weeks (1983). The ratio between the observed CH_4 concentration in ice or brine to their respective calculated solubility determines the supersaturation factor.

In addition, we computed the standing stock of CH_4, i.e. the total amount of CH_4 within the ice cover. To do so, we integrated the concentrations of CH_4 in bulk ice vertically to obtain the CH_4 content per square metre of ice.

For further comparison with the literature, we also computed CH_4 mixing ratios. They are usually obtained by dividing the number of moles of CH_4 by the total gas content. However, since we did not measure the total gas content, we used the sum of measured atmospheric-dominant gases (O_2, N_2 and Ar; data not shown) instead.

3 Results

3.1 CH_4 concentrations in ice

CH_4 concentrations in bulk ice ranged from 3.4 nmol L_{ice}^{-1} to 17.2 nmol L_{ice}^{-1}. Mean CH_4 concentration increased from BRW2 (6.4 nmol L_{ice}^{-1}) to BRW7 (7.8 nmol L_{ice}^{-1}) and decreased to 5.5 nmol L_{ice}^{-1} at BRW10. This evolution parallels that of the standing stocks of CH_4, which increased from BRW2 (5070 to 5430 nmol m^{-2}) to BRW7 (9200 nmol m^{-2}), then decreased at BRW10 (7580 nmol m^{-2}) (Fig. 2). For data interpretation, sea ice thickness is also shown in Fig. 2. It appears that the mean CH_4 concentration and the standing stock increased as sea ice thickened from BRW2 to BRW7, but decreased at BRW10 despite the fact that sea ice was thicker there.

The individual profiles of CH_4 concentrations in bulk ice (Fig. 3a) for each sampling event further highlight the contrasts between BRW10 and all the previous sampling events (BRW2 to BRW7): all the CH_4 concentration profiles in ice from BRW2 to BRW7 can be divided into three main zones. The first one ranged from 0 to 25 cm, where a peak of CH_4 concentration was found at 15 to 25 cm. CH_4 concentration measurements made on a twin ice core of BRW2 (duplicate) show that spatial variability in the 15 to 25 cm layer could reach 60 %. The second zone was found in the ice interior and ranged from 25 cm to the upper limit of the permeable layers (shaded area), where CH_4 concentrations were close to 5 nmol L_{ice}^{-1}. The third zone corresponds to the permeable layers where CH_4 concentration increased again toward the sea ice bottom, with values ranging from 5 to 10 nmol L_{ice}^{-1}. At BRW10, as the whole ice cover became permeable (shaded area at all depths), the whole profile flattened: the peak of

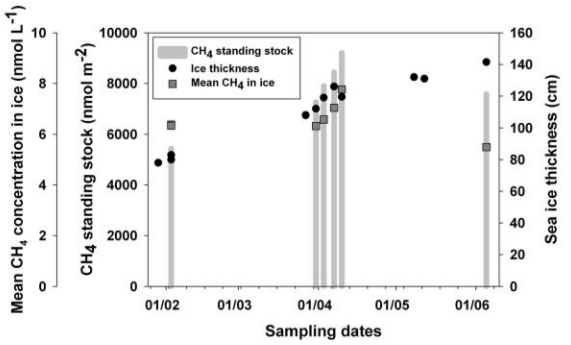

Figure 2. CH_4 standing stock for selected samplings events (vertical bars, from left to right, BRW2, BRW4, BRW5, BRW6, BRW7 and BRW10) in parallel with mean CH_4 concentration in sea ice and sea ice thickness.

CH_4 concentration around 15 to 25 cm disappeared, the ice interior still has a baseline at 5 nmol L_{ice}^{-1} and the increase of CH_4 concentration at the bottom was less obvious than in the previous sampling events.

Beside the strong vertical variation, CH_4 concentrations in bulk ice were always higher than the solubility values in surface seawater that would have been in equilibrium with the atmosphere (3.8 nmol L_{sw}^{-1}) and the theoretical solubility in ice at all depths (Fig. 3a – white dots). CH_4 concentrations in bulk ice were on average 1.8 times higher than that in surface seawater and 75 times higher than the theoretical solubility in ice. The highest supersaturation factor reached 396 and was measured in BRW6, at a depth of 20 to 25 cm. Again, BRW10 differed from all the other sampling events, with a lower supersaturation factor (mean supersaturation and standard deviation were 11 ± 4 versus 86 ± 68 for BRW2 to BRW7).

The CH_4 mixing ratio (not shown) was also calculated for BRW2, BRW4, BRW7 and BRW10. It ranged from 5.8 to 105.3 ppmV. The maximum mixing ratio was found in BRW4, at a depth of 15 to 20 cm; this is 3.6 times higher than the mean mixing ratio of 29 ppmV.

To summarize, BRW10 differed from all the other samplings events by its lower mean CH_4 concentration and its flatter CH_4 concentration profiles. Although all the ice samples were supersaturated relative to surface seawater, larger supersaturations were observed from BRW2 to BRW7 (less permeable ice cores) compared to BRW10 (entirely permeable ice core), especially at a depth of 15 to 25 cm where both CH_4 concentrations and CH_4 mixing ratios were found to be the highest.

3.2 CH_4 concentrations in brine

Deduced CH_4 concentrations in brine (using CH_4 concentrations in ice) ranged from 13.2 nmol L_{brine}^{-1} to 677.7 nmol L_{brine}^{-1}. These are thus much higher than the range of CH_4 concentrations measured in brine sackholes (10.0 to 36.2 nmol L_{brine}^{-1}) (Fig. 3 – triangles) and in seawater (25.9 and 116.4 nmol L_{sw}^{-1}).

The evolution of CH_4 concentrations in brine across seasons was rather similar to that of CH_4 concentrations in bulk ice, except in the bottom layers. Indeed, from BRW2 to BRW7, high CH_4 concentrations in brine were also observed at a depth of 15 to 20 cm; but from that level, CH_4 concentration in brine decreased and reached the lowest values at the sea ice bottom, where it is similar to observed CH_4 values in seawater. There was thus no increase of CH_4 concentration in brine at the sea ice bottom as observed in the CH_4 concentrations in bulk ice. The profile of CH_4 concentrations in brine flattened at BRW10, with values ranging between 13.2 and 87.0 nmol L_{brine}^{-1}, which were less variable and much closer to both the solubility values in brine and the actual measured CH_4 concentrations in brine than the ranges of values in the previous sampling events (35.6 nmol L_{brine}^{-1} and 677.7 nmol L_{brine}^{-1}). The minimum CH_4 concentration in brine was calculated at 12.5 cm. Temperature data were missing at the very surface, so that we could not compute CH_4 concentrations in brine above 12.5 cm.

3.3 CH_4 concentrations in seawater

Measured CH_4 concentrations in seawater ranged from 25.9 to 116.4 nmol L_{sw}^{-1} (Fig. 3c). This is 7 to 31 times higher than seawater in equilibrium with the atmosphere (3.8 nmol L^{-1} for a salinity of 35 at 0 °C) (Wiesenburg and Guinasso, 1979).

Measurements of CH_4 concentrations in seawater were homogenous in time from BRW2 to BRW7, with a mean value and standard deviation of 42.0 ± 2.4 nmol L_{sw}^{-1} for BRW2 and 37.5 ± 6 nmol L_{sw}^{-1} for BRW4 to BRW7. They then increased at all depths at BRW10 and reached a mean value and standard deviation of 77.4 ± 27.8 nmol L_{sw}^{-1}.

4 Discussion

The present paper aims at understanding the physical controls on the CH_4 concentrations in sea ice. Discussing the physical controls only makes sense if the variations of CH_4 concentration due to biological activity are negligible compared to those due to physical processes. Therefore, we will first assess the importance of biological activity on the variation of CH_4 concentrations in sea ice and brine (Sect. 4.1) before discussing the physical controls (Sect. 4.2).

4.1 Impact of biological activity on CH_4 concentrations

To assess the impact of biological activity on CH_4 concentrations, we recalculated the standing stocks of BRW4 to BRW7 (Fig. 3), by considering every 5 cm ice sample in the 25 to 80 cm depth layers. These choices are motivated by the

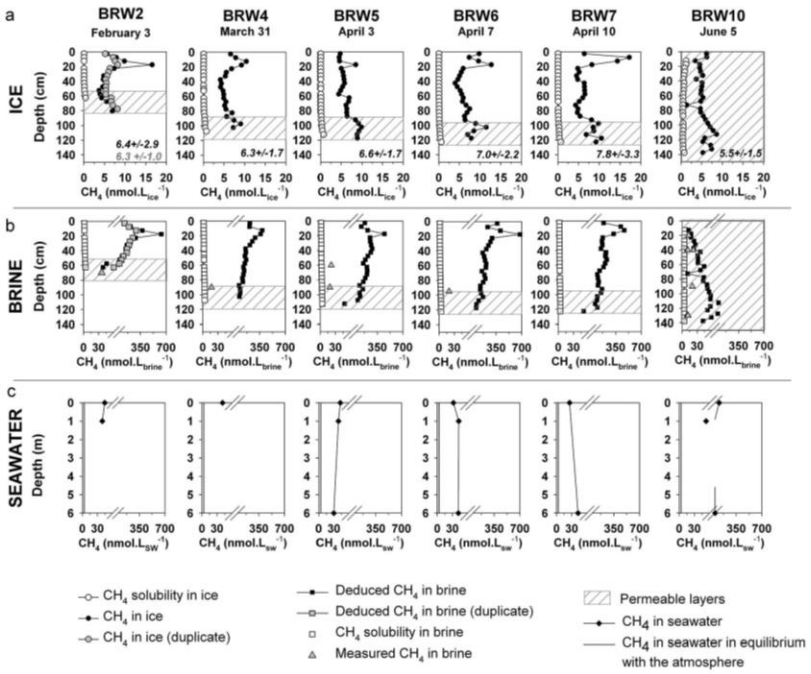

Figure 3. Evolution of CH_4 concentration in **(a)** bulk ice, **(b)** brine and **(c)** seawater (black dots, squares and diamonds respectively), compared to CH_4 solubility in ice, brine and seawater that is in equilibrium with the atmosphere (white dots, white squares and black straight lines respectively). Grey dots and grey squares are measurements made on duplicate samples of BRW2. Grey triangles in **(b)** are CH_4 measurements in brine sackholes. The break in the x axes of **(b)** and **(c)** is set at 60 nmol L. Dashed areas are permeable layers (i.e. layers with a brine volume fraction above 5 %).

following reasons: first, we suggest focusing on the standing stocks of the impermeable layers (i.e. layers that have a brine volume fraction below 5 % (Golden et al., 1998); layers above the shaded areas on Fig. 3a, b). These layers are considered as a closed system in terms of brine dynamics and are therefore suitable for assessing biological transformation of CH_4. Second, we felt it appropriate to ignore the upper layer (0 to 25 cm), since spatial variability could be important in these layers (up to 60 % the 15 to 25 cm depth layer) as shown in Fig. 3a – BRW2. Third, we only focused on the sampling events that were collected at short time intervals (three or four days), i.e. BRW4 to BRW7 rather than BRW2 to BRW4 (56 days). This is mainly due to the similar physical properties of the ice cores collected at short time intervals (i.e. in terms of ice core length, ice temperature and ice salinity profiles).

Deduced CH_4 standing stocks in the 5 cm ice samples (in the 25 to 80 cm ice layer, from BRW4 to BRW7) varied between 198 and 375 nmol m^{-2}, with a mean and standard deviation of 271 ± 41 mol m^{-2}. We performed an ANalysis Of VAriance (ANOVA) test on these standing stocks ($n = 44$) and differences between the samplings were not significant enough to exclude the possibility of random sampling variability.

In addition, we plotted chlorophyll a concentrations against CH_4 concentrations in bulk ice and phosphate concentrations against CH_4 concentrations in bulk ice to investigate potential in situ production of CH_4 in both permeable and impermeable ice layers (see Appendix A). The rationale is that previous studies have shown a strong correlation between these variables (Damm et al., 2008, 2010) where CH_4 production was found to occur. As there is no obvious correlation between the presented variables (see Appendix A), we surmise that the pathway of CH_4 production that was observed in Damm et al. (2008, 2010) may not have occurred in the present study.

Furthermore, the turnover time for CH_4 oxidation in the Arctic Ocean exceeds 1.5 years (Griffiths et al., 1982, and Valentine et al., 2001), which is much longer than the lifetime of first-year landfast ice. If we assumed that the turnover time is similar in landfast sea ice, then we would not expect to find major CH_4 oxidation in our ice samples.

Because CH_4 production is unlikely in sea ice and CH_4 oxidation may be slow, we conclude that biological transformation of CH_4 is negligible in comparison with the amount of

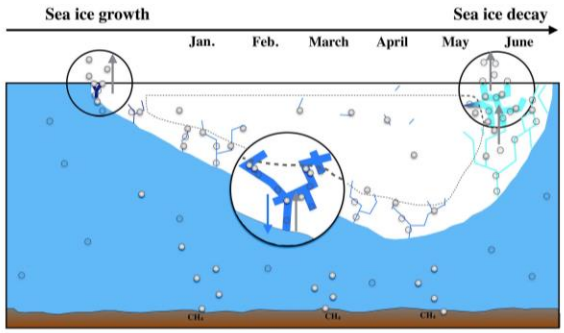

Figure 4. Schematic figure of CH_4 incorporation and release in sea ice. Sizes are intentionally disproportionate to highlight processes better. The area above the dotted line represents the impermeable layers. The small filled and empty circles represent CH_4 in gas bubbles and in dissolved state respectively. Upward grey arrows indicate the upward transport of gas bubbles due to their buoyancy, while downward blue arrows indicate the removal of dissolved gas through brine drainage. Large black circles zoom in on particular processes described in the text (Sect. 4.2): gas exchanges at the beginning of ice growth, gas accumulation predominantly under the impermeable layers and gas bubble escape during ice decay. Dark blue, light blue and cyan strokes in ice represent brine channels with high, moderate or low salinity respectively.

CH_4 that was physically incorporated in the impermeable ice layers; this is consistent with the findings derived from the standing stocks. Therefore, the discussion below will mainly focus on the physical processes that regulate CH_4 concentrations in sea ice.

4.2 Impact of physical processes on CH_4 concentrations

4.2.1 Range of CH_4 concentrations in sea ice and seawater, comparison with the literature

Our CH_4 concentrations in sea ice (3.4–17.2 nmol L_{ice}^{-1}) were slightly lower than those of Lorenson and Kvenvolden (1995) (15 to 40 nmol L_{ice}^{-1}). The deduced mixing ratios (5.8 to 105.3 ppmV) were, however, much lower than the 11 000 ppmV of Shakhova et al. (2010). We attribute the observed differences to (1) the CH_4 concentrations in seawater and (2) ebullition processes (i.e. the seepage of CH_4 bubbles from the seafloor and their rising through the water column).

First, our CH_4 concentrations in seawater (25.9 and 116.4 nmol L_{sw}^{-1}) are consistent with those reported in northern Alaska (10.7 to 111.8 nmol L_{sw}^{-1}; Kvenvolden et al., 1993) and shallow shelf areas with CH_4 release from sediment and/or destabilized gas hydrate (2.1 to 154 nmol L_{sw}^{-1}; Shakhova et al., 2005), but are much lower than the measurements reported by Shakhova et al. (2010) (1.8 to 2880 nmol L_{sw}^{-1}). The differences in CH_4 concentrations in seawater lead to contrasting CH_4 supersaturations (700 % and 3100 % in the present study versus 100 % to 160 000 % in Shakhova et al., 2010). Assuming similar incorporation rates in both studies, lower CH_4 supersaturation in seawater leads to lower CH_4 incorporated into sea ice and hence a lower CH_4 mixing ratio in sea ice.

Second, ebullition is a process associated with rapid bubble ascension, limiting gas equilibration with the surrounding water mass (Keller and Stallard, 1994). Therefore, in shallow locations, CH_4 bubbles released from the seafloor could reach the seawater surface (Keller and Stallard, 1994; McGinnis et al., 2006). We believe that ebullition could increase CH_4 at the sea-ice–water interface and lead to larger CH_4 incorporation into sea ice than if the ebullition was absent. Ebullitions were clearly observed in the Siberian Arctic Shelf (Shakhova et al., 2010) and, in that particular case, centimetre-sized bubbles were found within the ice (Shakhova et al., 2010). Since we did not find any literature reporting ebullition processes at Barrow and since our ice cores generally showed millimetre-sized bubbles (Zhou et al., 2013), we believe that ebullition processes were much less important in our study than in Shakhova et al. (2010).

4.2.2 Mechanisms responsible for the evolution of the vertical profiles of CH_4 concentrations in bulk ice and brine during ice growth

Although the CH_4 source was seawater, CH_4 concentrations in bulk ice from BRW2 to BRW7 did not show a C-shaped profile, as would salinity for growing sea ice (Petrich and Eicken, 2010). For instance, instead of a surface maximum for salt, we observed a subsurface maximum for CH_4. As discussed below, we propose three abiotic mechanisms to explain the salient features of the vertical profiles of CH_4 concentration in Barrow bulk ice: (1) gas escape during the initial ice growth phase in the surface layer, (2) predominant gas accumulation in the subsurface and (3) brine volume fraction effect for the bottom layer.

We assume that CH_4, similarly to CO_2, could escape from the ice to the atmosphere at the beginning of the ice growth (Geilfus et al., 2013; Nomura et al., 2006) (Fig. 4). In addition, once sea ice is consolidated, changes in temperature and in the volume of brine pockets are likely to fracture the ice, causing the expulsion of brines (Notz and Worster, 2009) and air bubbles (Untersteiner, 1968) at the ice surface. These two processes could explain the decrease of CH_4 concentrations in bulk ice right at the surface of sea ice (Fig. 3).

Predominant gas accumulation during ice growth has been described for argon (Ar) in Zhou et al. (2013): in addition to brine concentration, temperature and salinity changes in brine at sea ice formation lead to a sharp decrease of CH_4 solubility that favours bubble nucleation in sea ice. Once formed, the bubbles migrate upward due to their buoyancy. They are trapped under the impermeable surface layer, leading to gas accumulation (Fig. 4). Such a process is supported by two characteristics: the presence of bubbles and the occurrence of large supersaturation levels (compared to the rest of

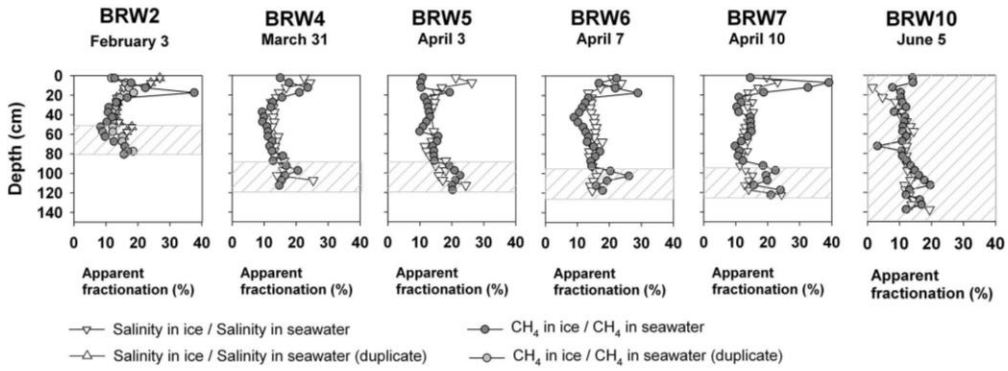

Figure 5. Comparison between the apparent fractionation of salinity in ice (the ratio between ice salinity and seawater salinity (32)) and the apparent fractionation of CH_4 (the ratio between CH_4 in ice and CH_4 in seawater ($44\,\mathrm{nmol\,L_{sw}^{-1}}$)). The seawater salinity and CH_4 in seawater that are chosen as references were the values obtained from BRW2. Dashed areas are permeable layers (i.e. layers with a brine volume fraction above 5 %).

the ice core). The presence of bubbles was observed in thin sections by Zhou et al. (2013) and is also consistent with the large difference between the deduced CH_4 in brine (which includes both CH_4 in bubbles and CH_4 that is dissolved in brine) (Fig. 3b, squares) and the actual measurements of CH_4 in brine (only CH_4 that is dissolved in brine) (Fig. 3, triangles). Moreover, the largest CH_4 supersaturations relative to CH_4 solubility in ice were always found at a depth of 15 to 25 cm, which corresponds to the ice depth where Zhou et al. (2013) have observed bubble accumulation and Ar supersaturation up to 2900 %. Therefore, the mechanism of predominant gas accumulation suggested for Ar may be relevant for CH_4 as well. Larger CH_4 supersaturation as compared to Ar supersaturation is likely due to the difference in CH_4 and Ar solubility; CH_4, which is less soluble than Ar, would be more affected by temperature and salinity changes. It is also noteworthy that this process of bubble formation in sea ice led to large spatial variability as witnessed by the duplicate of BRW2, which showed up to 60 % of CH_4 variation at a depth of 15 to 25 cm.

As the freezing front progresses, the temperature gradient in the permeable layer reduces; bubble nucleation due to solubility decrease is less efficient. As a consequence, CH_4 accumulates less and CH_4 concentration in brine decreases towards the bottom. Such a decrease is however not observed for CH_4 concentration in bulk ice. We attribute this to the brine volume fraction effect: a larger brine volume may contain a larger amount of CH_4 molecules, which induces higher CH_4 concentrations in bulk ice. The fact that CH_4 in brine did not show an increase at the bottom of the ice supports this suggestion.

An alternative explanation for the predominant gas accumulation due to solubility changes would be that of a direct bubble incorporation after a sudden but intense release of CH_4 bubbles from the sediment to the ice bottom. CH_4 release from sediment is possible since our CH_4 concentrations in seawater are consistent with those found in areas where CH_4 release from sediment and/or gas hydrate destabilization likely occurs (see Sect. 4.2.1). However, this process does not explain the slow decrease of CH_4 concentration in brine from a depth of 15 to 25 cm to the sea ice bottom (Fig. 3b), and we may also wonder why the ebullition only occurred once during the whole sampling period.

The contribution of in situ bubble formation in the retention of CH_4 in sea ice is assessed in Fig. 5. We calculated the ratio between CH_4 in ice and the CH_4 in seawater at BRW2 ($44\,\mathrm{nmol\,L_{sw}^{-1}}$) and the ratio between brine salinity and the salinity of seawater at BRW2 (32) at each ice depth for all the sampling events. The CH_4 in seawater and the salinity of seawater of BRW2 were chosen as references for the sake of consistency with Zhou et al. (2013). Similar apparent fractionation means that CH_4 is retained (incorporated and transported) in sea ice in the same way to salt, while a difference in the apparent fractionation means a difference in their retention processes.

Four main observations can be made with regard to Fig. 5. First, the apparent fractionation averaged 15 % but never reached 100 %. This is due to the rejection of impurities during sea ice formation (Weeks, 2010). Our study therefore suggests that sea ice rejects about 85 % of its impurities, but retains 15 % of them. This is in agreement with Petrich and Eicken (2010), who suggested that sea ice brine allows a retention of 10 to 40 % of seawater ions in the ice. Second, the highest apparent fractionation of CH_4 (up to 39 %) was observed at a depth of 15 to 25 cm; in that layer, the retention of CH_4 could be higher than that of salt by a factor of 2. This supports the previous suggestion about predominant gas accumulation: the presence of gas bubbles allows higher retention of CH_4 than salt. Third, the apparent fractionation of CH_4 was lower than that of salt at the surface

of all the sampling events, except at BRW10. That lower apparent fractionation may be related to the large permeability of the ice during its formation and/or the formation of some cracks at the ice surface (during the cold period), which have allowed gas to escape from sea ice to the atmosphere, as explained earlier in this section. The lower CH_4 concentrations in bulk ice at these sampling events (Fig. 3a) tends to support the conjecture of gas escape. Fourth, below the top layer of about 25 cm of ice, both CH_4 and salt enrichment values are similar, indicating that, in these ice layers, CH_4 was mainly incorporated in the dissolved state in the same way as salt.

4.2.3 Sea ice permeability controls CH_4 concentrations in bulk ice and brine during sea ice decay

At BRW10, both CH_4 concentrations in bulk ice and deduced CH_4 concentrations in brine decreased and became less variable than the previous samplings (BRW2 to BRW7). In addition, CH_4 standing stocks decreased by ca. 1600 nmol m^{-2} from BRW7 to BRW10, and the deduced CH_4 concentrations in brine approached the measured concentrations. These measurements suggest that there is an enhanced gas transport through the ice and that gas bubbles have escaped from sea ice to the atmosphere. Gas escape was possible given that sea ice was permeable at all depths (Fig. 3a, b, shaded area). Concomitant Ar bubble escape was suggested in Zhou et al. (2013). However, in contrast to Ar that was then at saturation, CH_4 was still supersaturated compared to the solubility in brine. This could be related to a slow exchange between the atmosphere, brine and the supersaturated seawater through diffusion.

CH_4 concentrations in brine at BRW10 (13.2 to 87.0 nmol L_{brine}^{-1}) were lower than the CH_4 concentration at the ice/water interface (116.4 nmol L_{sw}^{-1}), but higher than the theoretical CH_4 solubility in surface seawater that is in equilibrium with the atmosphere (3.8 nmol L_{sw}^{-1}). Although the CH_4 concentrations in brine right at the surface (0–12.5 cm) could not be retrieved, we can hypothesize that the gradient of CH_4 concentrations between the ice/seawater interface and the ice surface led to CH_4 diffusion from the ice/seawater interface to the ice surface and therefore maintained CH_4 supersaturation in ice after gas bubble escape. Since the source of CH_4 came from supersaturated seawater, CH_4 concentrations in brine were slightly higher at the sea ice bottom than at the top.

5 Conclusions and perspectives

We reported on the evolution of CH_4 concentrations in landfast sea ice, brine and under-ice water from February through June 2009 at Barrow (Alaska). Our CH_4 concentrations in sea ice in seawater are consistent with records from the area with CH_4 release from sediment and gas hydrate destabilization (Kvenvolden et al., 1993; Lorenson and Kvenvolden, 1995; Shakhova et al., 2010).

We suggest that brine concentration and strong solubility decrease triggered gas bubble formation, which favoured CH_4 accumulation in ice. As a result, CH_4 retention in the ice was twice as efficient as that of salt. However, as summarized in Fig. 4, gas exchange likely took place during initial ice growth between sea ice and the atmosphere, and the formation of cracks could also lead to a decrease of CH_4 right at the surface of the ice. Also, as sea ice thickened, temperature and brine salinity gradient were no longer sufficient to trigger bubble nucleation, and CH_4 was then trapped in the dissolved state in the same was as salt. The subsequent evolution of CH_4 concentrations in sea ice layers mainly depended on physical processes, as chlorophyll *a* and phosphate concentrations did not support in situ CH_4 production and as CH_4 oxidation was likely insignificant. Abrupt changes in CH_4 concentrations in sea ice occurred when sea ice became permeable; these were associated with the release of gas bubbles to the atmosphere. Therefore, the main role of our landfast sea ice in the exchange of CH_4 from seawater to the atmosphere was its control of the amount of CH_4 that it is able to store in its impermeable layers and the duration of such storage.

Although gas incorporation and sea ice permeability were two dominant factors driving CH_4 concentrations in sea ice in our study site, the magnitude of these processes may be different in other polar seas. Indeed, the contribution of the ebullition fluxes of CH_4 from sediment to the concentration of CH_4 in bulk ice, the transport of CH_4 through the ice and the significance of physical and biological controls on CH_4 dynamics rely on the nature of the sediment, the water depth, the physical parameters of the ice and biological activity within the ice, which may vary depending on the location.

In the case of a higher mix of physical and biological controls on CH_4 concentrations in bulk ice, we would recommend measuring: (1) the carbon and hydrogen isotopes of CH_4 in sea ice, as isotopic fractionation is highly sensitive to biological processes; and (2) the same isotopes in the sources (e.g. organic matter). Indeed, previous studies have suggested that the carbon isotopic values of biogenic CH_4 within anoxic sediments may be as negative as −110 ‰ (Whiticar, 1999) in comparison to those resulting from CH_4 oxidation (−10 to −24 ‰; Damm et al., 2008; Schubert et al., 2011), but few of them have considered that the measured isotopic values in the sediment or in seawater also depend on the isotopic composition of the sources.

Appendix A: Relationships between chlorophyll *a* and CH_4 concentrations and between phosphate and CH_4 concentrations in sea ice

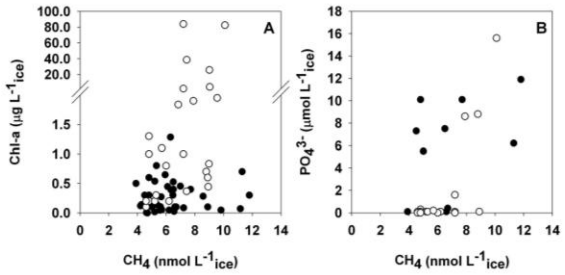

Figure A1. Relationships between **(A)** chlorophyll *a* (Chl *a*) and methane (CH_4) concentrations, and **(B)** phosphate (PO_4^{3-}) and CH_4 concentrations in sea ice. Open and closed circles indicate respectively permeable and impermeable ice layers (i.e. a brine volume fraction above or below 5 %). Chl *a* and PO_4^{3-} data are from Zhou et al. (2013); Chl *a* data were available for all the sampling events that are presented here, while PO_4^{3-} data were only available for BRW2, BRW7 and BRW10.

Acknowledgements. The authors would like to thank Hajo Eicken, the rest of the sea ice group of the Geophysical Institute of the University of Alaska Fairbanks, Tim Papakyriakou, Bernard Heinesch, Michel Yernaux, Frédéric Brabant, Thomas Goossens, Noémie Carnat and Rodd Laing for their help during fieldwork. We are indebted to the Barrow Arctic Science Consortium and the North Slope Borough for their logistical support. We also thank Saïda El Amri and Arnaud Rottier for their efficient help with laboratory work, Ceri Middleton for language help and Célia Sapart and Neige Egmont for their comments. Our gratitude also goes to the three anonymous reviewers as their comments have greatly improved the quality of the manuscript. This research was supported by the F.R.S-FNRS (contract 2.4584.09), the National Science Foundation (project OPP-0632398 (SIZONet)), the University of Alaska Fairbanks and the Belgian Science Policy (contract SD/CA/03A), the NCE ArcticNet and National Science and Engineering Research Council (NSERC). N.-X. Geilfus received a PhD grant from F.R.S.-FRIA and acknowledges the Canada Excellence Research Chair Program and the Arctic Science Partnership (ASP). J. Zhou is a research fellow of F.R.S.-FNRS, and B. Delille is a research associate of F.R.S.-FNRS. This is MARE contribution no. 265.

Edited by: L. Kaleschke

Chapter VIII - Insights into oxygen transport and net community production in sea ice from oxygen, nitrogen and argon concentrations

Biogeosciences, 11, 5007-5020, doi: 10.5194/bgd-11-2045-2014

Zhou J.[1, 2], B. Delille[2], F. Brabant[1] and J-L. Tison[1]

[1]Laboratoire de glaciologie, DSTE, Université Libre de Bruxelles, Brussels, Belgium}

[2]Unité d'Océanographie chimique, MARE, Université de Liège, Liège, Belgium}

Abstract

We present and compare the dynamics (i.e., changes in standing stocks, saturation levels and concentrations) of O_2, Ar and N_2 in landfast sea ice, collected in Barrow (Alaska), from February through June 2009. The comparison suggests that the dynamic of O_2 in sea ice strongly depends on physical processes (gas incorporation and subsequent transport). Since Ar and N_2 are only sensitive to the physical processes in the present study, we then discuss on the use of O_2/Ar and O_2/N_2 to correct for the physical contribution to O_2 supersaturations, and to determine the net community production (NCP). We conclude that O_2/Ar suits better than O_2/N_2, due to the relative abundance of O_2, N_2 and Ar, and the lower biases when gas bubble formation and gas diffusion are maximized. We further estimate NCP in the impermeable layers during ice growth, which ranged from -6.6 to 3.6 µmol O_2 L^{-1} d^{-1}, and the concentrations of O_2 due to biological activity in the permeable layers during ice decay (3.8 to 122 µmol O_2 L^{-1}). We finally highlight the key issues to solve for more accurate NCP estimates in the future.

1 Introduction

Sea ice is a composite material with a matrix of pure ice and inclusions of brine [*Weeks*, 2010]. The latter concentrates most of the impurities of the ice, including dissolved compounds, gas bubbles, and micro-organisms that are able to survive at high salinities and low temperatures [*Thomas and Dieckmann*, 2002]. The net community production (NCP), i.e. the net carbon fixation due to photosynthesis and respiration of the microorganisms in sea ice is a crucial measurement in polar ecological studies, because it is generally the sole source of fixed carbon for the higher trophic-level species in ice-covered oceans [*Arrigo et al.*, 2010; *Brierley*, 2002; *Michel et al.*, 1996].

However, the measurement of NCP in sea ice is challenging due to the composite structure of sea ice. A traditional standard technique is to measure the accumulation of algal biomass and its temporal change via the measurements of chlorophyll a (chl a) or particulate organic carbon (POC). Another traditional standard technique is to measure the maximum photosynthetic rate and photosynthetic efficiency in a laboratory, and then to deduce the changes of biomass based on the concentration of chl a and the light intensity from the field, assuming that the photosynthetic parameters obtained in laboratory still hold for field measurements. Both standard techniques have one major limitation: they require the

extraction and the melting of sea ice, which inevitably modify the growth environment of the microorganisms (e.g. sudden change of brine salinity due to bulk ice melting).

The more recent techniques for NCP measurement favor in-situ measurements with minimized disturbance on sea ice. These include pulse amplitude modulated (PAM) fluorometry [*Glud et al.,* 2002], O_2 microelectrodes [*McMinn and Ashworth,* 1998], O_2 micro-optodes [*Mock et al.,* 2002] and ice/water interface O_2 eddy correlation [*Long et al.,* 2012]. Nonetheless, the results still depend on the composite structure and the physical properties (i.e., permeability and brine dynamics) of sea ice. For instance, the PAM fluorescence depends on the spatial distribution of the algal biomass and the optical properties of the ice [*Glud et al.,* 2002]. Another example is that the amount of O_2 measured using microsensors depends on whether the sensors were set in brine, ice, gas bubbles or bacterial films [*Mock et al.,* 2002] and whether the ice permeability allows the diffusion of O_2 to the microsensors [*Glud et al.,* 2002]. Although the ice/water O_2 eddy correlation seems promising, because of its large footprint in comparison to the other techniques, it may be sensitive to the additional input of O_2 from sea ice due to brine convection and ice melt [*Long et al.,* 2012]. In that context, understanding the dynamics of O_2 within the ice will better constrain the O_2 fluxes at the ice-water interface, obtained from eddy correlation.

The present study first aims to describe the dynamics of O_2 in sea ice, based on a time-series of O_2 concentrations within sea ice from ice growth to ice decay. The O_2 measurements were obtained from ice crushing, which allow the measurement of both dissolved and gaseous O_2 (i.e. O_2 in brine and gas bubbles), in both permeable and impermeable sea ice layers (i.e., ice layer with brine volume fraction above and below 5 % respectively [*Golden et al.,* 1998]). Since current studies have mainly focused on the dissolved O_2 in the permeable ice layers [*Glud et al.,* 2002; *Mock et al.,* 2002], our study undeniably extends the current knowledge on O_2 dynamic.

Second, as it is well-know that gas diffusion and brine convection affect the measured O_2 concentrations in sea ice [e.g. *Glud et al.,* 2002; *Long et al.,* 2012], we will also discuss the possibility to correct the imprints of these physical processes on O_2, using nitrogen (N_2) and argon (Ar) and to determine NCP. Some recent studies yielded the NCP in seawater from the measurements of O_2/Ar ratio [*Cassar et al.,* 2009; *Castro-Morales et al.,* 2013; *Hendricks et al.,* 2004; *Reuer et al.,* 2007], while others have proven that O_2/N_2 was sensitive to the biological activity in basal continental ice [e.g., *Souchez et al.,* 2006]. These approaches

consider Ar and N_2 as inert to biogeochemical processes (hence, not affected by NCP), where the use of O_2/Ar and O_2/N_2 ratios allows for the correction of physical processes (e.g., temperature, salinity or pressure changes and bubble effects).

2 Materials and methods

2.1 Sampling area and sampling events

The ice cores were collected on landfast sea ice, off Barrow (Figure1), from January through June 2009. The sampling area covered a surface of 50 m by 50 m. The north-eastern corner of the square was located at 71° 22.013' N, 156° 32.447' W. The ice cores were extracted by drilling and then stored at -30 °C in the dark, to prevent brine drainage and to limit biological activity. All of the analyses were completed within the following year. The physical framework has been presented and discussed in *Zhou et al.* [2013]. In brief, all of the ice cores had similar crystallographic structure, with a dominance of columnar ice that suggests low spatial variability.

In the present paper, five sampling events (out of ten) were selected to illustrate the temporal evolution of chl a, O_2, O_2/Ar and O_2/N_2 at our location: one in winter (BRW2 - February 3), two in early spring (BRW4, BRW7 - corresponding to March 31 and April 10 respectively), one in mid spring (BRW8 - May 8), and the last one in late spring (BRW10 - June 5). The first four sampling events occurred during ice growth, the last one during ice decay. As discussed in *Zhou et al.* [2013], full-depth convection occurred in BRW8, leading to the drainage of the dissolved compounds in brine, and a partial replenishment by seawater. This contrasted with the sampling events prior to BRW8, where convection only occurred in the permeable bottom ice layers. Finally, in BRW10, the increase of air temperature led to ice melt, full permeability, brine stratification, and the formation of 20 cm of superimposed ice at the surface of the ice. The formation of superimposed ice indicates that seeping snow meltwater had frozen on contact with sea ice [*Haas et al.*, 2001].

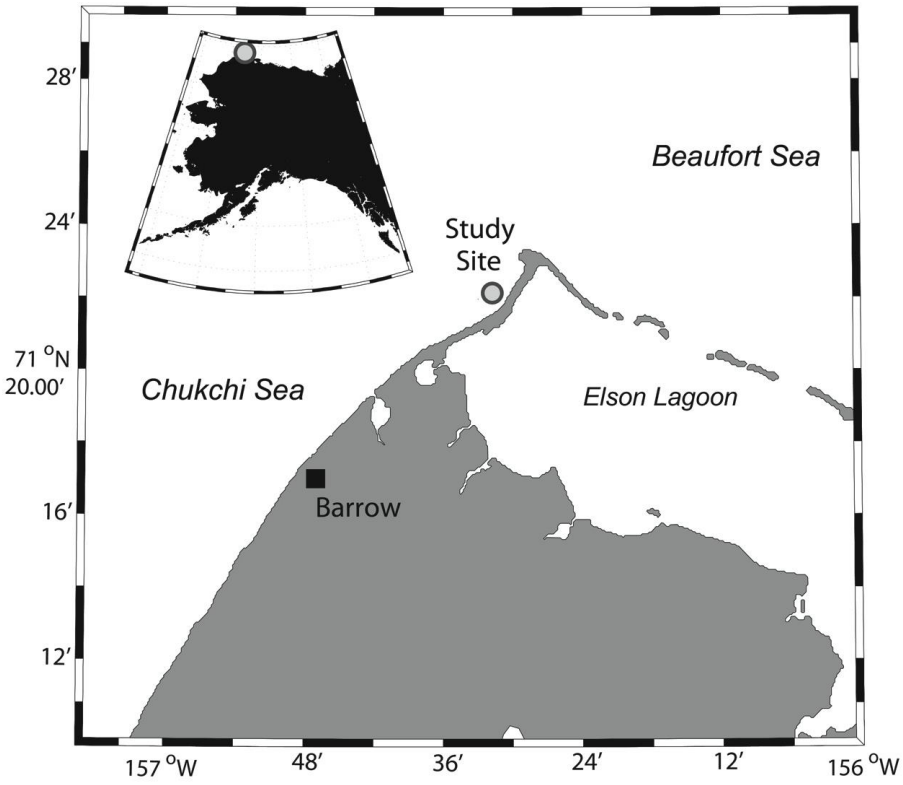

Figure 1 The study site, North of Barrow (Alaska, USA).

2.2 Chlorophyll *a* and phaeopigment

The ice samples were melted in the dark, in 0.2 µm filtered seawater (1:4 volume ratio) to avoid osmotic stress. We used 10 µm and 0.8 µm polycarbonate filters in a sequence in order to distinguish larger micro-algae species from the smaller ones. Extractions and calculations were made following the procedure of *Arar and Collins* [1997]. The standing stocks of chlorophyll a (chl a) were calculated by integrating the chl a concentrations over the whole ice length and have been discussed in *Zhou et al.* [2013]. The percentage of phaeopigment was obtained by dividing the concentration of phaeopigment by the sum of both chl a and phaeopigment concentrations. As phaeopigments result from chl a degradation, a high percentage of phaeopigments indicates strong grazing pressure (i.e. strong impact of respiration on NCP), and/or high algal mortality.

2.3 O_2, Ar and N_2 concentrations in ice and their respective solubility

We used the dry-crushing technique developed for gas measurements in continental ice [*Raynaud et al.*, 1982] to extract O_2, Ar and N_2 from the ice samples. This technique extracts the gas bubbles in the ice and the gas in the dissolved state within liquid brine. Each ice core

was cut every 5 cm, and about 60 g of sample was introduced into a vessel, with 7 stainless steel balls. The ice was crushed in the vessel, under vacuum (10^{-3} torr), as described in *Stefels et al.* [2012] at -25 °C. Subsequently, the vessel was kept at -50 °C in a cold ethanol bath, and was connected to the gas chromatograph equipped with a thermal conductivity detector for concentration analyses [*Skoog et al.,* 1997]. We used AlphagazTM2 - He (Air Liquide – P0252) as carrier-gas and a 22 ml packed column (Mole Sieve 5A 80/100; 5 m x 1/8"). The reproducibility of the analyses (i.e., the precision of the gas chromatograph) was 99.3 % for O_2, 97.8 % for Ar and 99.9% for N_2. It corresponds to 100 % minus the variation coefficient (in %) obtained from triplicate analysis of four different standards (2, 3, 5, 10 torrs of injection pressures). In addition, diel O_2 production/respiration may account for 3 to 6 % of variations in our O_2 concentrations, as all the ice cores were not sampled at the same time of the day; more details on the error estimates are given in the supplementary material (S1).

To compute the saturation levels (i.e. the deviation from saturation) of O_2, Ar and N_2 in ice and for further calculations (sections 2.4 and 2.5), we also determined the theoretical solubility of each gas in ice at saturation. The solubility in brine was calculated using temperature and salinity in brine following the relationship of *Garcia and Gordon* [1992] for O_2 and the relationship of *Hamme and Emerson* [2004] for N_2 and Ar. This value weighted by the brine volume fraction consitutes the solubility in ice. Weighting is necessary, as most of the impurities (including gases) are concentrated within the brine structure, but not in the pure ice matrix [*Weeks,* 2010]. It is noteworthy that the relationship of *Hamme and Emerson* [2004] was established for temperatures between 0 °C and 30 °C and salinities between 0 and 34.5, and the relationship of *Garcia and Gordon* [1992] for temperatures between 0 and 40 °C and salinities between 0 and 42. We thus assumed in our calculations of gas solubility that

(S1) Estimate of bias on O_2 concentrations due to diel O_2 production/respiration

Since the ice cores were not always sampled at the same time of the day, but between 11AM and 3PM, we estimated the potential bias on the measured O_2 concentrations as following: According to the incubation experiments of Mar Fernández Méndez (https://www.mpi-bremen.de/Binaries/Binary16430/M.Sc._Thesis_Mar_Fern%C3%A1ndez.pdf, p.27), the net primary production (NPP) of F. *cylindrus* (a typical cold-water species that can be found in Arctic and Antarctic seawater and sea ice) was 1.73 µmol O_2 $L_{incubation\ water}^{-1}$ h^{-1}. Assuming a 12 hours of daylight, we may expect a NPP of 20.76 µmol O_2 L_{brine}^{-1} d^{-1} in the field. Because brine volume fraction approach 20 % in the bottom of the ice where the highest chlorophyll-a concentrations was observed (Figure 3), we may expect a NPP of 20.76 * 20 % µmol O_2 L_{ice}^{-1} d^{-1}, hence 4.15 µmol O_2 L_{ice}^{-1} d^{-1}. This accounts for 3 to 6 % of the mean O_2 concentrations in bulk ice (ranging from 67.4 to 122.4 µmol O_2 L_{ice}^{-1}).

those relationships still hold for the range of temperature and salinity found in our brine samples.

Gas saturation levels are described following *Craig and Hayward* [1987] for seawater as:

$$\Delta C_i = \frac{C_i}{C_{eq}} - 1 \qquad (1)$$

where Ci is the measured concentration of the gas i in bulk ice and C_{eq} the solubility of gas i in bulk ice at equilibrium with the atmosphere, calculated at in situ temperature, salinity and pressure as described above. Note that for comparison with the literature, gas saturations are given in percentage in the text. Supersaturation and undersaturation are therefore represented by positive and negative percentage values respectively.

2.4 O_2/Ar and O_2/N_2

The use of O_2/Ar and O_2/N_2 is only valid if both Ar and N_2 are inert. Ar is a noble gas, i.e. inert and not affected by any biogeochemical processes. N_2 is affected by denitrification, which was found to occur in sea ice [*Rysgaard et al.*, 2008], but whose impact on N_2 concentrations should be negligible in the present study. The maximum reported denitrification rate (23 nmol N_2 L^{-1} d^{-1}) was 4 orders of magnitude lower than the average bulk ice N_2 concentrations (248 µmol N_2 L^{-1}) presented here. The correlation between N_2 and Ar with a r^2 of 0.98 (Figure 2) further supports that N_2 can be treated as inert like Ar, and used to trace physical processes.

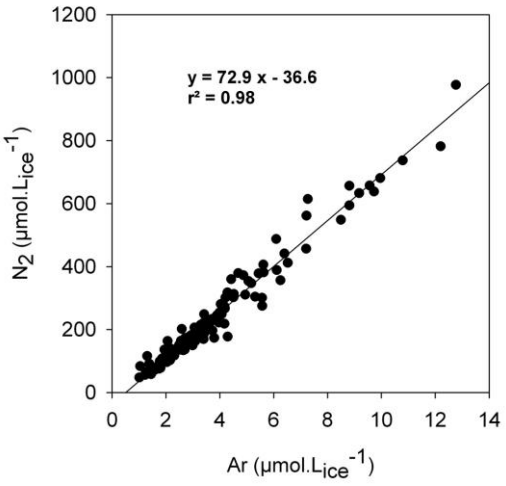

Figure 2 Concentrations of N_2 in ice plotted against the concentrations of Ar in ice. The equation and r^2 are calculated assuming a linear regression between both gas concentrations.

O_2/Ar and O_2/N_2 ratios were calculated from the concentrations of O_2, Ar and N_2 in ice, and were compared with their respective ratios in seawater and the atmosphere. The relative solubility of O_2/Ar in seawater (at 0°C, with 32 of salinity) is 20.48 [*Garcia and Gordon*, 1992; *Hamme and Emerson*, 2004]. However, even in abiotic conditions, the gas ratios in sea ice after gas incorporation and before sea ice consolidation (i.e. being impermeable) may differ from that in seawater due to diffusion process at the ice/seawater interface [*Killawee et al.*, 1998; *Tison et al.*, 2002]. We thus applied the relative diffusion coefficient of O_2 and Ar (1.2/0.8 = 1.5) [*Broecker and Peng*, 1982] to our relative solubility of O_2/Ar to obtain a value of O_2/Ar with maximized diffusion processes at the bottom of sea ice (13.65) as described below. Note that different diffusion coefficients exist in the literature (Table 1) for temperature close to 0 °C or below, for seawater, water or ice; we chose to use the diffusion coefficients of *Broecker and Peng* [1982] because it is the most recent peer-reviewed study that provides diffusion coefficients for O_2, Ar and N_2 near the freezing temperature. Salinity is not given in *Broecker and Peng* [1982], but one may expect a maximum decrease of 4.9 % of the diffusion coefficient per 35.5 of salinity increase [*Jähne et al.*, 1987].

Table 1 Diffusion coefficients of O_2, Ar and N_2 found in the literature for different medium (water, seawater and sea ice) for temperature at or below 0 °C. Salinity is given when available. The diffusion coefficients in use in the present study are those of *Broecker and Peng* [1982] (in bold).

	Medium	**Temperature**	**Salinity**	**O_2**	**Ar**	**N_2**
		°C		$10^{-5}cm^2s^{-1}$	$10^{-5}cm^2s^{-1}$	$10^{-5}cm^2s^{-1}$
Broecker and Peng [1974]	Water	0	?	1.17	0.88	0.95
Broecker and Peng [1982]	**Seawater**	**0**	**?**	**1.2**	**0.8**	**1.1**
Ferrell and Himmelblau [1967], Jahne et al. [1987]	Seawater	0	35	1.18*	-	0.94*
Loose et al. [2010]	Ice	-12 to -4	3.78 - 6.58	3.9	-	-
Crabeck et al. [submitted]**	Ice	-3.8 to -0.8	3.2	1.6-1.8	1.6-1.8	2.5

* Computed solubility using the matlab code available on http://web.uvic.ca/~rhamme/download.html

** The values are gas diffusivities which should take into account the geometry of the brine structure.

The initial values of O_2/Ar could range between 13.65 and 20.48, based on the magnitude of gas diffusion at the ice/seawater interface. Further, as O_2/Ar in the atmosphere is 22.5, gas input from the atmosphere (during frazil ice formation or when sea ice is permeable) and gas bubble formation in the permeable ice should pull the bulk ice O_2/Ar towards 22.50. Therefore, if both dissolved and gaseous states exist in the ice, O_2/Ar could range between 13.65 and 22.50 due to physical processes, hereafter referred to abiotic range of O_2/Ar.

We applied the same calculation to O_2/N_2. The relative solubility in seawater is 0.56 [*Garcia and Gordon,* 1992; *Hamme and Emerson,* 2004]. Since the relative diffusion coefficient between O_2 and N_2 is 1.09 [*Broecker and Peng*, 1982], the relative solubility with maximized diffusion processes is 0.51. Given that the atmospheric ratio of O_2/N_2 is 0.27, the abiotic range of O_2/N_2 in ice is 0.27 – 0.51. O_2/N_2 that is above or below this abiotic range is attributed to an impact of biological activity [*Souchez et al.*, 2006].

2.5 Deviation of the O_2/Ar from saturation

The deviation of O_2/Ar from saturation, $\Delta(O_2/Ar)$ (which is referred to as "biological O_2 supersaturation" in seawater studies [e.g., *Castro-Morales et al.*, 2013]) is formulated as in equation 2, and we define the O_2 concentrations associated with the in situ biological activity ($[O_2]_{bio}$) as in equation 3:

$$\Delta(O_2/Ar) = \frac{[O_2]/[Ar]}{[O_2]_{eq}/[Ar]_{eq}} - 1 \quad (2)$$

$$[O_2]_{bio} = [O_2]_{eq}\Delta(O_2/Ar) \quad (3)$$

For seawater, $[O_2]_{eq}$ and $[Ar]_{eq}$ are respectively the solubility of O_2 and Ar at saturation. In ice, however, $[O_2]_{eq}$ and $[Ar]_{eq}$ may differ from these solubilities due to physical processes such as bubble nucleation, diffusion and convection (sections 2.4 and 4.6).

Multiplying the $[O_2]_{bio}$ obtained in equation 3 (in mol O_2 L_{ice}^{-1}) by the ice thickness of the samples (generally 5 cm) gives a production of O_2 in mol O_2 m^{-2}. With an O_2/C ratio of 1.43 [*Glud et al.*, 2002] and the molar mass of C, we can calculate the equivalent C uptake in gC m^{-2}. The change of that C uptake over time is the NCP. Since NCP is derived from the comparison of C uptake obtained in distinct ice cores that are separated by a certain time interval, how nutrient and light availability locally affect the C uptake is not taken into consideration.

3 Results

3.1 A general overview from the standing stocks

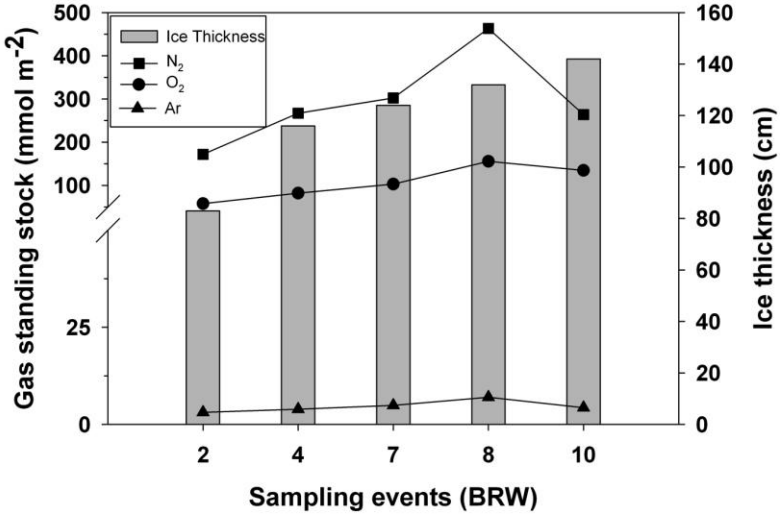

Figure 3 Evolution of the standings stocks of N_2, O_2 and Ar (squares, circles and triangles respectively) compared to the evolution of sea ice thickness (vertical grey bars). The break in gas standing stocks is set at 50 mmol m^{-2}.

Figure 3 shows the standing stocks of Ar, O_2 and N_2, in parallel with the ice thickness, for the different sampling events. N_2 has the largest standing stocks among the three gases, followed by O_2 and then Ar. The temporal variation of the three gas standing stocks were similar, but differed from that of the ice thickness: while sea ice continuously thickened from BRW2 (82 cm) to BRW10 (142 cm), the gas standing stocks increased from BRW2 to BRW8 but decreased at BRW10.

3.2 Gas saturation levels

The saturation levels of N_2, O_2 and Ar decreased with increasing brine volume fraction (Figure 4). The highest supersaturation of N_2, O_2 and Ar (7030, 3180 and 2960 % respectively) corresponded to the lowest brine volume fraction (2.2 %), while the lowest undersaturations (-33, -52 and -54 % respectively) corresponded to the largest brine volume fraction (29.3 %). In addition, N_2 saturation levels contrasted with those of O_2 and Ar: for similar brine volume fraction, N_2 generally reached higher supersaturation levels than O_2 and Ar, which have much similar saturation levels.

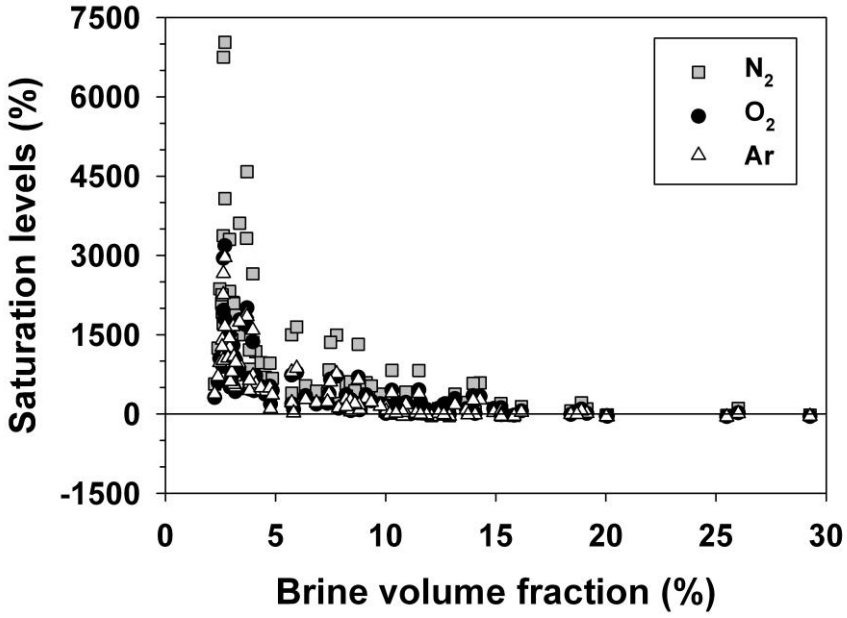

Figure 4 Saturation levels (ΔC_i in Eq. 1, in percentage) of N_2, O_2 and Ar (squares, circles and triangles respectively) compared to the brine volume fraction.

3.3 O_2 concentrations

Figure 5a shows the concentration of O_2 in bulk ice [O_2], compared to the solubility of O_2 in ice. The dashed areas refer to the permeable ice, i.e., layers with brine volume fraction above 5 %, while the non-dashed areas right above refer to the impermeable layers, i.e., with brine volume fraction below 5 % [*Golden et al.*, 1998]. Mean [O_2] increased from BRW2 (67.4 µmol L_{ice}^{-1}) to BRW8 (122.4 µmol L_{ice}^{-1}) and decreased at BRW10 (93.4 µmol L_{ice}^{-1}). At BRW2 and BRW4, [O_2] generally exceeded the solubility of O_2 in the impermeable layers, but reached the solubility values in the permeable layers. The trends changed from BRW7 onwards: in BRW7 and BRW8, [O_2] was higher than the solubility at all depths, except in the 5 last centimeters of the ice core. In BRW10, [O_2] was close to the solubility of O_2 in the upper layers (from 12.5 to 72.5 cm), but exceeded the solubility of O_2 below these layers.

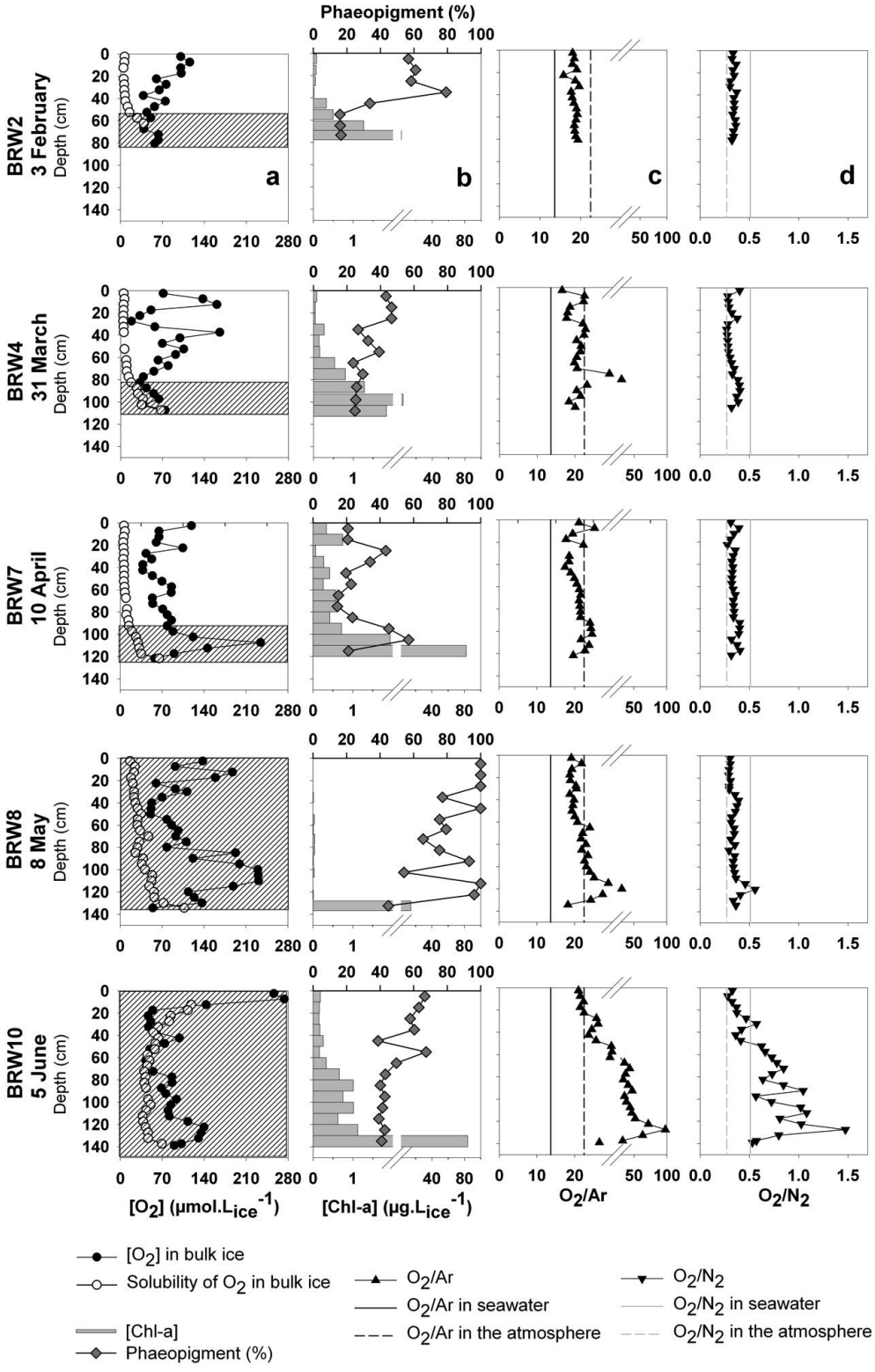

Figure 5 (a) O_2 concentration in bulk ice (black dots) compared to its solubility in ice (white dots), the dashed areas refer to permeable ice layers (i.e. with a brine volume fraction above 5%); (b) Chl *a* concentrations (horizontal bars) with a break at 2 µg L_{ice}^{-1} compared to the percentage of phaeopigments (diamonds); (c) O_2/Ar in ice (upside triangles) with a break at 25, compared to the same ratios in seawater (straight black line) and in the atmosphere (dashed black line); (d) O_2/N_2 in ice (downside triangles) compared the same ratios in seawater (straight grey line) and in the atmosphere (dashed grey line).

3.4 Chlorophyll *a* and phaeopigment concentrations

The concentrations of chl *a* [chl *a*] varied largely with depth (Figure 5b) and ranged from 0 to 83.9 µg L_{ice}^{-1} over all the sampling events. The highest [chl *a*] were always in the ice bottom, except in BRW4. Above the bottom layer, the [chl *a*] was generally below 1 µg L_{ice}^{-1}. Drastic changes occurred in BRW8 when sea ice permeability increased sharply: [chl *a*] dropped at all depths, and particularly in the ice interior. [chl *a*] increased again at BRW10, showing a vertical profile and standings stocks similar to those of BRW7.

The percentage of phaeopigment also varied strongly with depth in BRW2, with over 60% of phaeopigments in the upper ice layers but less than 20 % at the ice bottom. It varied between 20 and 40 % in BRW4 and BRW7, and increased drastically in BRW8 (with phaeopigments reaching 100% in some layers). In BRW10, the percentage of phaeopigments varied between about 40 and 70%, with generally higher values in the upper ice layers.

3.5 O_2/Ar and O_2/N_2

O_2/Ar in ice ranged between 15.8 and 97.6 (Figure 5c) and O_2/N_2, between 0.3 and 1.5 (Figure 5d). Both O_2/Ar and O_2/N_2 ratios are compared to their respective values in the atmosphere (22.5 and 0.3) and in seawater with maximized diffusion processes (13.7 and 0.5).

O_2/Ar in ice at BRW2 was highly homogeneous at all depths, with a mean and standard deviation of 18.49 +/- 0.84. These ratios were found between the value of O_2/Ar in the atmosphere and that in seawater with maximized diffusion processes. Over the next sampling events, O_2/Ar in ice increased on average, exceeding the O_2/Ar in the atmosphere (the upper limit of O_2/Ar that can be explained by abiotic processes), and became more variable vertically (Figure 5c). It is also noteworthy that from BRW4 onwards, the maximum O_2/Ar in each sampling event was found in the lower part of the ice, but never coincided with the maximum of [chl a], even at BRW10 where the whole profile of O_2/Ar clearly mimicked the one of [chl a].

Although both O_2/N_2 and O_2/Ar in ice have similar coefficient of variation (respectively, 49 and 46%, n=121), O_2/N_2 only exceeded once its abiotic range between BRW2 and BRW8, while O_2/Ar exceeded its abiotic range from BRW4 onwards (Figs. 5c and 5d). Similarities between O_2/Ar and O_2/N_2 became more obvious in BRW10: both ratios were close to their respective atmospheric values at the ice surface, and they exceeded their respective abiotic

range in the ice interior, with a maximum in the lower part of the ice that did not coincide with the maximum in [chl a].

4 Discussion

4.1 Overview on the dynamic of O_2 in comparison to those of Ar and N_2

Since N_2 and Ar are only sensitive to physical processes in the present study, the fact that O_2 standing stocks varied in the same way as N_2 and Ar over time (Figure 3) indicates that the physical controls on O_2 standing stocks dominated over the biological ones. Two main physical processes affect the standing stocks of gases in ice: the incorporation during ice growth and the subsequent gas transport within the ice. Gas incorporation during ice growth would result in similar changes in gas standing stock and ice thickness, while subsequent gas transport within the ice could result in decoupled changes.

Figure 6 compares the changes in gas standing stocks and ice thickness in all the sampling events relative to BRW2. Increasing standing stocks and ice thickness in one sampling event (relative to BRW2) will result in a value of changes above 1. Further, if the gas standing stocks increased solely due to ice growth, gas standing stocks and ice thickness will show a similar value of changes. Therefore, the changes of gas standing stocks that (almost) evolve in the same way as the ice thickness from BRW2 to BRW7 indicate that gas incorporation was (mainly) associated with ice growth, while the significant differences in BRW8 and BRW10 indicate subsequent gas transport.

Subsequent gas transport may have occured in BRW8 and BRW10 because both ice cores were permeable (brine volume fraction above 5%) at all depths. However, the processes leading to the subsequent gas transport were different in both sampling events, as the changes relative to BRW2 increased in BRW8 for all the gases (indicating an addition of gases), but decreased in BRW10 (indicating a removal of gases), and more particularly for N_2 and Ar than for O_2 (Figure 6).

Therefore, the temporal changes of the standing stocks indicate 3 distinct stages in the gas dynamics: (1) gas incorporation during ice growth from BRW2 to BRW7, (2) gas accumulation in BRW8 despite the increase of ice permeability at all depths, and (3) gas removal in BRW10, but with larger removal of Ar and N_2 than O_2.

4.2 Gas incorporation during ice growth

If the entrapment of gases in sea ice was constant during ice growth, we should expect a constant [O_2] in ice with depth. The slight decreasing [O_2] in ice from the surface to the bottom of the impermeable ice layers (2 to 4.9 % of brine volume fraction) (Figure 5) then indicate a decrease in the entrapment efficiency during ice growth. That decrease in the incorporation efficiency has been suggested for Ar in *Zhou et al.* [2013] and is also valid for CH_4 [*Zhou et al.*, 2014b]. Briefly, when sea ice forms, gas concentration increases in parallel with salinity (this is the so-called "brine concentration"). At the same time, because of the temperature gradient at the beginning of ice growth, brine salinity increases above seawater salinity, leading to the decrease of gas solubility in brine. Both increasing gas concentration and decreasing gas solubility lead to gas supersaturation, and eventually gas bubble formation. Whatever the ice depth where gas bubble formation take place, the formed gas bubbles may then ascend due to their buoyancy and accumulate under the impermeable ice layers. Because gas bubbles move upwards due to their buoyancy, while dissolved compounds are subject to gravity drainage (i.e., downward movement), gas bubble formation favors gas accumulation in sea ice in contrast to the dissolved compounds. However, as sea ice thickens, the temperature gradient (i.e., brine salinity gradient) decreases in the ice, and gas bubble formation due to solubility changes becomes less efficient. This mechanism explains the slight decreasing trend in [O_2] in ice from the surface to the bottom of the impermeable ice layers.

The presence of gas bubbles in the impermeable ice layers is confirmed by ice thin sections [*Zhou et al.,* 2013], and the large N_2 supersaturations also indicate the presence of gas bubbles in our ice samples. Indeed, N_2 supersaturation reached up to 7000 % in the impermeable ice layers, while supersaturation of 2200 % already corresponds to gas bubble formation [*Killawee et al.,* 1998].

Because the accumulation of gas bubbles occurred at the beginning of the ice growth, i.e., in the upper ice layers, which are also associated with high brine salinity (hence low gas solubility) and low brine volume fractions at the sampling, it is not surprising to observe high O_2, Ar and N_2 supersaturation at low brine volume fractions (Figure 4).

4.3 Gas accumulation subsequent to ice formation

4.3.1 Gas bubble formation due to biological activity

The changes in gas standing stocks that deviated from the changes in ice thickness in BRW8 (relative to BRW2) indicate an addition of gases. The addition of gases may be counter-intuitive because BRW8 was permeable at all depths; hence, gas exchanges (diffusion and/or convection) should tend to alleviate the supersaturation that is formed during ice growth (see previous section), leading to a decrease of the standing stocks, rather than an accumulation of gases as it is observed.

Further, the simultaneous addition of O_2, Ar and N_2 (Supplementary material S2) was only possible through gas bubble formation and accumulation in sea ice. Since full-depth convection occurred in BRW8 (section 2.1), additional dissolved gases would be drained out of the ice through convection, while additional gas bubbles may remain in the ice due to their buoyancy despite brine convection. The resulting questions are then: how do these gas bubbles form in sea ice and how can they accumulate in the permeable ice layers?

One explanation for the accumulation of gas bubbles could be the growth of gas bubbles from pre-existing gas cavities, triggered by local supersaturation fluctuations [*Jones et al.,* 1999]. Because [O_2] in bulk ice was at solubility in the bottom 30 cm of the ice in BRW2 and BRW4, but became locally supersaturated in BRW7 when [chl a] increased sharply (Figure 5), we postulate that biological activity in BRW7 created O_2 supersaturation and possibly gas bubbles [*Tsurikov,* 1979] in some local micro-niches (i.e. confined pores created by microbial excretion and/or structure), forming the so-called "pre-existing gas cavities". Then, the increasing ice permeability and full-depth convection in BRW8 allowed the local supersaturation fluctuation, which favored the growth of gas bubbles [*Jones et al.,* 1999] and supports the observed O_2 accumulation. Once the O_2 gas bubbles are formed, other dissolved gases (e.g. N_2 and Ar) may diffuse from brine into the gas bubbles, because the partial pressure of N_2 and Ar in brine is higher than that in the O_2 gas bubbles [e.g. *Lubetkin,* 2003]. This process eventually allows the accumulation of all the gases in sea ice, and more particularly N_2 rather than Ar (see the larger changes in N_2 than in Ar in Figure 6), because the partial pressure of N_2 is higher than that of Ar (see the range of [N_2] and [Ar] in the supplementary material S2).

Supplementary material S2

Gas concentrations in bulk ice (black dots) compared to their solubility in ice (white dots). From left to right, O2, Ar and N2 concentrations. The dashed areas refer to ice layers with brine volume fraction above 5 %.

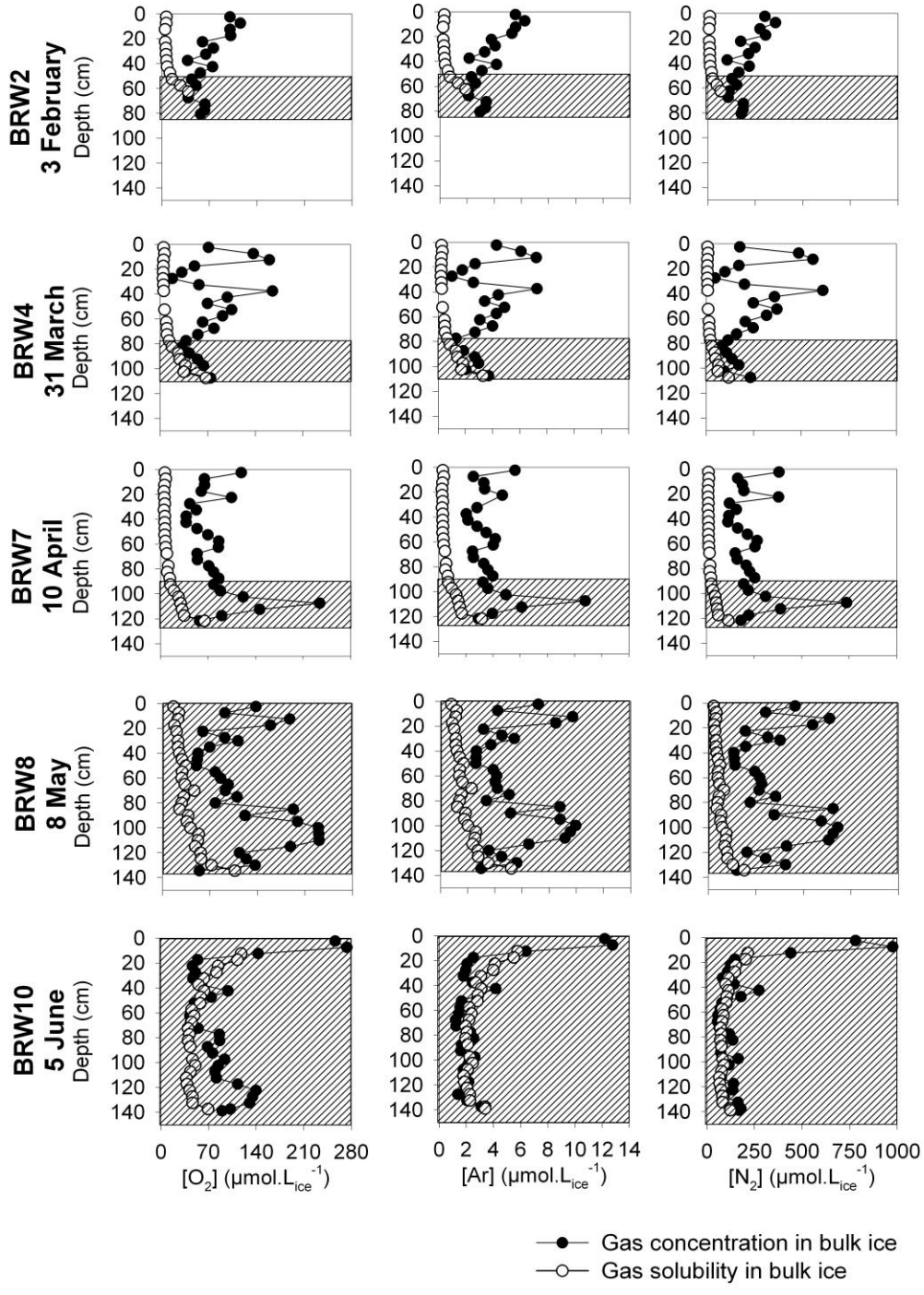

Theoretically, the formed gas bubbles should rise through the brine channels and escape from the permeable ice. The fact that we observed an accumulation of gases in BRW8 indicates that the process of gas bubble escape was not instantaneous. The geometry of the brine network or tortuosity [e.g. *Golden et al.*, 2007], the impurities in brine [*Liger-Belair,* 2005], the presence of biogenic exopolymer substances [*Krembs et al.*, 2011] and the intensity of brine drainage [*Moreau et al.*, 2014] may all slow down the ascension of gas bubbles through the brine network, i.e. increasing the duration needed for gas equilibrium.

4.3.2 Void formation in warming sea ice

Another explanation for gas bubble formation in warming sea ice (BRW 8) is the formation of voids, caused by the melting of the pure ice which has a lower density than brine [*Light et al.,* 2003; *Tsurikov,* 1979]. Although void formation in sea ice inevitably leads to gas exsolution from brine, these voids had to form before brine convection for significant gas bubble formation. Otherwise, brine convection may fill the voids in sea ice, impeding the process of exsolution.

4.3.3 Superimposed ice formation

Superimposed ice formation was found in the 20-first cm at the surface of BRW10 [*Zhou et al.*, 2013], which implies the seepage of snow meltwater and subsequent freezing on contact with sea ice [*Haas et al.*, 2001]. The mechanism leading to gas accumulation in or right below the superimposed ice is unclear, but there are 3 potential explanations for this observation according to *Tsurikov* [1979]: (1) direct input of atmospheric air in the ice pores (because of the positive freeboard) before the formation of the superimposed ice layers, (2) accumulation of gas bubbles that have risen through the brine network, or (3) accumulation of gases associated with the rapid freezing of snow meltwater (see *Zhou et al.* [2013] for a more extensive discussion).

4.4 Difference in the changes of standing stocks between O_2 and both Ar and N_2

The changes of the standing stocks (relative to BRW2) decreased between BRW8 and BRW10 (Figure 6) for all the gases, indicating the removal of gases from sea ice. The fact that both [Ar] and [N_2] dropped to their respective solubility in ice (below the superimposed ice layers) (Supplementary material S2) is a result of prolonged gas exchange (through gas bubble escape and gas diffusion). The addition of snow- and ice meltwater likely have further drawn down [Ar] and [N_2] to below their respective solubility in ice. Previous analyses of

water stable isotopes in brine, nitrate concentrations and ice texture [*Zhou et al.*, 2013] support the suggestion of snow- and ice meltwater infiltration.

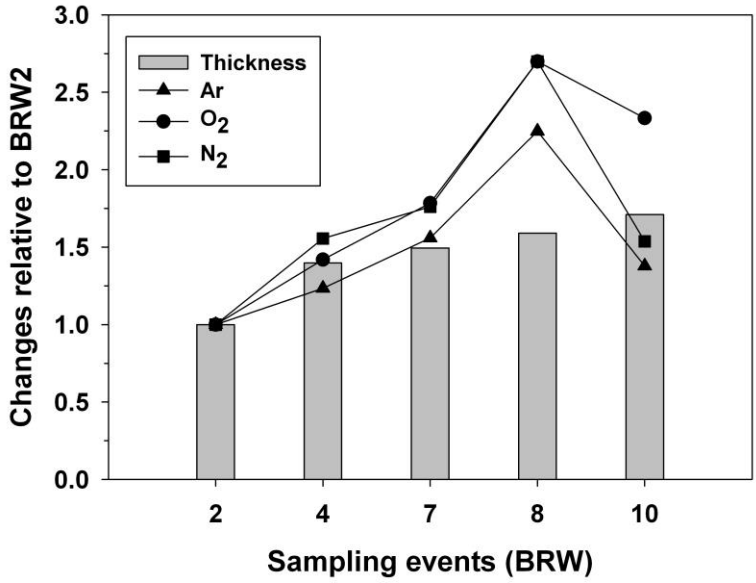

Figure 6 Changes of ice thickness, Ar, O_2 and N_2 concentrations for each sampling event relative to BRW2. Value above, equal to or below 1, indicates an observed change that is respectively higher, equal to or lower than the value in BRW2.

In the layers comprised between 20 cm (i.e. below the superimposed ice layer) and 75 cm of BRW10, [O_2] also approached the saturation as for [N_2] and [Ar], indicating that all the gases are likely dissolved in brine. Dividing the observed [O_2] in ice by the brine volume fraction, and assuming a density of the brine of 1 (because brine salinity was close to seawater salinity), we obtain the range of [O_2] in brine, which range from 232 to 647 µmol kg^{-1}, with a mean of 400 µmol kg^{-1}. That range is close to that presented in *Papadimitriou et al.* [2007] (212 to 604 µmol kg^{-1}) where the loss of O_2 from ice was also evident.

In contrast to [Ar] and [N_2], [O_2] was supersaturated at the bottom of BRW10 (Supplementary material S2), and the changes of O_2 standing stocks (relative to BRW2) decreased with a lower magnitude than Ar and N_2 (Figure 6). The reason is that biological O_2 production partly compensated the loss of O_2 due to gas exchange. [O_2] higher than the solubility were indeed found in the lower part of BRW10 – where high [chl-a] were also observed.

We made a simple calculation to estimate the changes of saturation associated with the biological O_2 production, between BRW8 and BRW10. Mean Ar solubility in the whole ice column has increased from 1.9 (in BRW8) to 2.8 µmol L_{ice}^{-1} (in BRW10), i.e. by 50 %. Similarly O_2 solubility has increased from 38 to 57 µmol L_{ice}^{-1}, i.e. also by 50 %. Therefore, in a closed system, the saturation levels of both Ar and O_2 should have decreased by 50 %. Meanwhile, mean Ar saturation has decreased from 263 to -15 %, i.e. by 106 %. Hence, the 50 % of changes in Ar solubility are not large enough to explain the changes in the saturation levels, and about 56 % of the decrease in Ar saturation is associated to the escape of gas bubble escape, gas diffusion – and possibly the addition of snow meltwater that contributed to the Ar saturation levels down to -15 %. Mean O_2 saturation has decreased from 180 to 58 %, i.e. by 79 %, which was lower than the 106 % observed for Ar. The difference (106 % – 79 % = 27 %) is likely the contribution of biological activity to the O_2 supersaturation.

There is one fundamental difference between BRW8 and BRW10 that is worth to discuss: why did biological activity trigger gas accumulation in BRW8, but not in BRW10? One simple reason would be the larger brine volume fraction in the upper layers of BRW10 (10 to 30%) in comparison to BRW8 (7.5 to 10 %), which allowed the evacuation of the formed gas bubbles. Another explanation would be that gas bubbles were more difficult to nucleate in BRW10. Indeed, the production of O_2 in BRW8 occurred at the beginning of the increase of ice permeability, when both gas cavities and supersaturated gases were present, and when brine convection allowed the fluctuations of local supersaturations. In contrast, in BRW10, low N_2 and Ar supersaturation due to prolonged gas equilibration between the atmosphere and brine (Figure 4), in combination with brine stratification (i.e, absence of local supersaturation fluctuations due to brine convection), could have made it more difficult to form gas bubbles from O_2 production in BRW10.

4.5 Gas exchange at the bottom of the ice

Although ice-algae produce O_2, the maximum of [chl a] did not coincide with the maximum of [O_2] over all the sampling events. The low phaeopigment percentage (20-30 %) in those bottom layers (Figure 5b) suggests low algal degradation, and hence low consumption of O_2 by the heterotrophs in comparison to the algal production. A potential pathway that allows the removal of the produced O_2 in these bottom permeable ice layers is the transport through diffusion and convection. The fact that [O_2], [Ar], [N_2] in ice all reached the solubility in the

bottom of the ice supports the suggestion of gas exchange with seawater – where all the gases are assumed to be at saturation.

4.6 Caveats and uncertainties when calculating NCP from O_2/Ar with O_2/N_2 in sea ice

Recent studies have determined NCP in seawater, using Ar to correct for the physical contribution in the variation of O_2 [*Cassar et al.*, 2009; *Castro-Morales et al.*, 2013; *Hendricks et al.*, 2004; *Reuer et al.*, 2007], while O_2/N_2 was shown to be sensitive to the biological activity in basal continental ice [e.g. *Souchez et al.*, 2006]. In this section, we will discuss caveats and uncertainties related to the calculation of NCP from O_2/Ar or O_2/N_2 in sea ice.

4.6.1 O_2/N_2 and O_2/Ar trends in this study

The range of O_2/N_2 from BRW2 to BRW7 (0.27 and 0.41) remained within the abiotic range (0.27-0.51), indicating that we cannot exclude the possibility that these were solely associated with physical processes. Indeed, the observed range is consistent with those obtained from ice growth experiments in abiotic conditions (0.37 – 0.45) [*Killawee et al.*, 1998], or with negligible bacterial activity (0.32 – 0.44) [*Tison et al.*, 2002]. In contrast, the increase of O_2/N_2 up to 1.47, i.e., beyond the abiotic range, in BRW10, indicates that the contribution of biological activity to the [O_2] dominated over that of the physical processes. This is in agreement with what we have observed from the changes of gas standing stocks over time (section 4.4).

To the best of our knowledge, O_2/Ar has never been measured in ice before. However, the range of O_2/Ar observed in the present study (15.8 - 97.6) is comparable to (if not higher than) the range of O_2/Ar in seawater studies (10 – 55) [*Nemcek et al.*, 2008; *Shadwick et al.*, in press.], pointing to the reliability of our results. Further, since O_2/Ar and O_2/N_2 evolve similarly toward higher values over the sampling events, the sharp increase of O_2/Ar in BRW10 likely indicates, as for O_2/N_2, the switch from a situation where the physical contribution to O_2 supersaturation dominated to a situation where the biological contribution dominated.

The main difference between O_2/Ar and O_2/N_2 (Figs. 5c and 5d) was their variability with depth: O_2/Ar exceeded the abiotic range from BRW4 onwards (versus BRW8 for O_2/N_2). That difference may result from (1) the relative abundance of O_2 compared to those of Ar and

N_2, (2) the relative solubilities of the gases and (3) the relative diffusion rates of the gases. Firstly, since $[O_2]$ is about 20 times higher than [Ar], but about 3 times lower than $[N_2]$, adding the same amount of O_2 (due to biological activity) will induce a higher increase in the O_2/Ar ratio than in the O_2/N_2 ratio. Secondly, N_2 solubility in brine was clearly different from that of O_2 and Ar, as suggested by the larger supersaturation of N_2 in comparison to O_2 and Ar (Figure 4). That difference in gas solubility impacts the partitioning of gases between brine and gas bubbles, which then affect differently the O_2/Ar and O_2/N_2 ratios. Thirdly, although there is currently no consensus on the diffusion coefficient of O_2, Ar, and N_2 in brine (Table 1), it is well established that O_2/Ar and O_2/N_2 ratios will change if diffusion occurs in the permeable bottom ice layers [*Killawee et al.,* 1998].

4.6.2 Biases on $[O_2]_{eq}/[Ar]_{eq}$ and $[O_2]_{eq}/[N_2]_{eq}$ due to physical processes

Before calculating NCP from equations 2 and 3, we first assess the potential biases on NCP associated with the impact of gas diffusion and gas bubble nucleation on $[O_2]_{eq}/[Ar]_{eq}$ and $[O_2]_{eq}/[N_2]_{eq}$. The presence of gas bubbles will draw $[O_2]_{eq}/[Ar]_{eq}$ from 20.48 (solubility in seawater) to 22.5 (ratio in gas bubbles) and $[O_2]_{eq}/[N_2]_{eq}$ from 0.56 to 0.27 (section 2.4). Gas diffusion privileges the loss of O_2 in comparison to Ar and N_2 by a factor of 1.5 and 1.1 respectively, if one considers the ratio of diffusion coefficient following *Broecker and Peng* [1982]. But if one considers the work of *Crabeck et al.* [submitted], the ratio of diffusion coefficient for O_2/Ar will change by a factor of 0.9 to 1.1 and for O_2/N_2, by a factor of 0.6 to 0.72 (Table 1). The expected changes (given in percentage in Table 2) thus range between -9.2 to -33.3 % for $[O_2]_{eq}/[Ar]_{eq}$ and between -8.9 to +66 % for $[O_2]_{eq}/[N_2]_{eq}$ depending on whether we consider the work of *Broecker and Peng* [1982] or *Crabeck et al.* [submitted]. Considering the lower range of bias on $[O_2]_{eq}/[Ar]_{eq}$ in comparison to $[O_2]_{eq}/[N_2]_{eq}$, we suggest using the former in the calculation of $[O_2]_{bio}$ and NCP.

We estimated the propagation of errors on $[O_2]_{bio}$ (calculated from equation 3), using the Monte Carlo procedure and neglecting the error on gas diffusion (i.e., assuming equivalent diffusivities for O_2 and Ar in sea ice as in *Crabeck et al.* [submitted]), we used random values of the measured parameters (T, S and O_2/Ar) between the mean ± standard deviation over 1000 iterations, assuming a maximum error of 9.9 % on $[O_2]_{eq}/[Ar]_{eq}$ due to gas bubble formation and an absolute error of 0.1 for T and S (Table 2). The calculated maximum uncertainty of $[O_2]_{bio}$ is then 34 %.

Table 2 Synthesis on the trends of changes of O_2/Ar and O_2/N_2 at the ice-water interface. An upward arrow indicates that the process increases the ratio, while a downward arrow indicates that the process decreases the ratio. The percentages in brackets indicate the maximal changes of the ratio associated with the physical processes (section 4.6.2).

	O_2/Ar	**O_2/N_2**
Photosynthesis	↑	↑
Respiration	↓	↓
Gas bubble formation	↑ (+9.9 %)	↓ (-51.8 %)
Diffusion (1)	↓ (-33.3 %)	↓ (-8.9 %)
Diffusion (2)	? (-9.2 to +11 %)	↑ (+39 to +66%)

(1) *Broecker and Peng* [1982] ; (2) *Crabeck et al.* [submitted]

4.6.3 Biases on $[O_2]_{eq}$ due to physical processes

Equation 3 implicitly assumes that $[O_2]$ equals to $[O_2]_{eq}$ in the absence of biological activity. However, as discussed in section 2.5, $[O_2]_{eq}$ prior to biological activity may be higher than the gas solubility calculated at in situ temperature and salinity following *Garcia and Gordon* [1992] and *Hamme and Emerson* [2004], because of gas bubble accumulation (section 4.2). Indeed, Ar supersaturation approached 500 % for brine volume fraction of 5 % (the transition from permeable to impermeable layers) (Figure 4) – in comparison to 1 % of supersaturation reported in seawater studies [*Hamme and Severinghaus*, 2007], and 564 % in Antarctic lake ice [*Hood et al.*, 1998]. Similarly, $[O_2]_{eq}$ at sea ice consolidation, may be supersaturated as well: at least 500 % if we assume similar solubility for O_2 and Ar [*Weiss*, 1970], and even more if we take into account the O_2 production in the bottom ice layers.

4.7 Estimate of $[O_2]_{bio}$ and NCP and in sea ice

4.7.1 The impermeable layers

Previous sections have shown how physical processes and biological activity both influence $[O_2]$ in sea ice. Therefore, NCP calculations from $[O_2]$ require removing the physical imprints. Since we assume that the impermeable ice layers are closed systems, only biological activity could change O_2 concentration in these layers over time. Thus, theoretically, the changes of the standing stocks of O_2 in the impermeable layers (0-50 cm) from BRW2 to BRW7 (Table 3 – O_2 meth column) should be equal to NCP. However, since BRW2, BRW4 and BRW7

refer to different sampled ice cores, rather than the changes in the same ice core over time, spatial variability affects the calculated NCPs. For instance, the simultaneous drop in [O_2], [Ar] and [N_2] to the solubility values in BRW4, between 20 and 40 cm depth, (Supplementary material S2) points to spatial variability rather than NCP changes. That spatial variability was likely associated with changes in water masses, as water stable isotopes also showed anomalies at the same ice depths [*Zhou et al.,* 2013]. NCP calculated following equation 3 should then correct for spatial variability, because it corrects for O_2 variations using Ar, which evolved under the same physical conditions (i.e., experiencing the same spatial variability).

Table 3. NCP in the impermeable ice layers (0 to 50 cm depth) from BRW2 to BRW4 and from BRW4 to BRW7, in µmol O_2 L^{-1} d^{-1} The columns entitled "O_2 meth." refer to the NCP derived from the standing stocks of [O_2] in bulk ice, while the columns entitled "O_2/Ar" refer to the NCP derived using the O_2/Ar (see Eqs. (2) and (3), considering 500 to 3000 % of supersaturation). The latter could be further affected by a maximum uncertainty of 35 % (section 4.6.2).

	BRW2-BRW4		BRW4-BRW7	
Ice depth (cm)	O_2 meth.	O_2/Ar meth.	O_2 meth.	O_2/Ar meth.
0-10	1.0	0 – 0.1	-1.2	0.6 – 3.6
10-20	1.9	-0.1 – 0	-4.3	-0.2 – 1.3
20-30	0.4	-0.1 – 0	4.9	0.2 – 1.0
30-40	2.0	0 – 0.3	-6.6	-0.6 – 3.3
40-50	1.5	0 – 0.2	-3.9	-3.3 – -0.5

We further multiplied the NCP (calculated following equation 3) by a factor of 5 to 30 to take into account the full range of observed O_2 supersaturation when the ice became impermeable (Figure 4 and section 4.6.3). Dividing the obtained values by the number of days between the sampling events then provides NCP (Table 3 – O_2/Ar meth). Note that, as demonstrated in section 4.6.2, these ranges have a maximum uncertainty of 40 % due to the impact of physical processes on $[O_2]_{eq}/[Ar]_{eq}$ (34 %, section 4.6.2) and the sampling time (up to 6 %, section 2.3 and Supplementary material S1).

Both positive and negative NCP from BRW4 to BRW7 indicate that heterotrophic and autotrophic processes coexist in sea ice; this is possible due to the presence of micro-niches

in sea ice [*Rysgaard et al.*, 2008]. The change from a net autotrophic (BRW2-BRW4) to a both autotrophic and heterotrophic system (BRW4-BRW7) is also in agreement with previous results suggesting increased remineralisation (i.e., net heterotrophic processes) in BRW7 [*Zhou et al.*, 2013].

Measurements of NCP in the ice interior are scarce, which limit the comparison of our values with the literature. However, the positive NCPs reported here (0 – 3.6 µmol O_2 L^{-1} d-1, which are equivalent to 0 to 1.3 mgC m^{-3} h^{-1}) are consistent with those measured in the melt ponds in the Canada Basin in 2005 (0.03 and 2.12 mgC m^{-3} h^{-1}) [*Lee et al.*, 2012], with similar [chl a] (0.02 and 0.7 mg Chl a m^{-3} in the present study versus 0.1 and 0.6 mg Chl a m^{-3} in *Lee et al.* [2012]). The negative NCPs (-0.2 to -6.6 µmol O_2 L_{ice}^{-1} d^{-1}) are comparable to the range of O_2 consumption rates measured in the bottom of sea ice in Franklin Bay (0 - 3 µmol O_2 L_{ice}^{-1} d^{-1}) [*Rysgaard et al.*, 2008].

4.7.2 The permeable layers

In the permeable layers, $[O_2]_{eq}$ should be closer to the gas solubility calculated at in situ temperature and salinity following *Garcia and Gordon* [1992] than in the impermeable layers. However, brine convection and diffusion may have affected $[O_2]_{eq}/[Ar]_{eq}$. Beside the fact that a large range of diffusion coefficients exist in the literature (Table 1), our present understanding of brine dynamics and gas transport does not allow assessing the frequency or the impact of the convection on the variations of $[O_2]$ over the sampling period (e.g., not in BRW8). Therefore, rather than calculating NCP based on the change of $[O_2]$ between BRW8 and BRW10, and neglecting the differential impact of brine convection and permeability on $[O_2]$ in both sampling events (section 4.4), we simply provide a conservative estimate of $[O_2]_{bio}$ in BRW10, where brine convection was absent and hence, when only biological activity and diffusion took place.

In contrast to the impermeable layers, we simply consider $[O_2]_{eq}$ at saturation (hence no supersaturation), since all the gas bubbles have escaped from the ice (section 4.4). The maximum uncertainty is 21 %: This was calculated following the procedure described in section 4.6.2, but neglecting the 9.9 % of error due to gas bubble accumulation (because of the absence of gas bubbles), and adding the 6 % of error due to diel O_2 production/respiration.

The calculated $[O_2]_{bio}$ varies between 5.4 and 174.5 µmol O_2 L_{ice}^{-1} (Figure 7), which is equivalent to a carbon uptake (or autotrophic organic carbon production) of 3.8 - 122 µmol C

L_{ice}^{-1}, considering the O_2/C ratio of 1.43 [*Glud et al.*, 2002]. This minimum estimate is comparable to the range of POC found in the bottom of Barrow sea ice, in May (105 – 212 µmol C L^{-1}) [*Juhl et al.*, 2011].

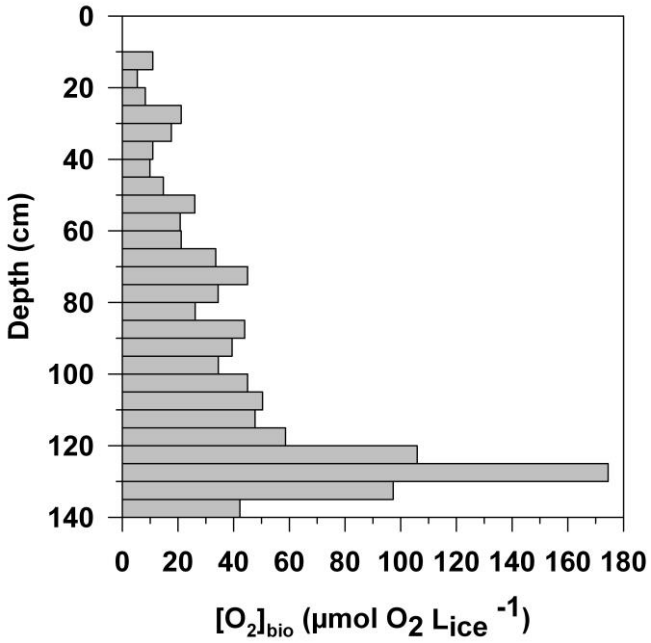

Figure 7 $[O_2]_{bio}$ in BRW10 calculated following equation 3. The results may be converted into C uptake, assuming a photosynthetic quotient O_2/C of 1.43 [*Glud et al.*, 2002].

Integrating $[O_2]_{bio}$ leads to a standing stock of 52.3 mmol O_2 m^{-2} due to biological activity, which is equivalent to 36.6 mmol C m^{-2}, or 438.9 mgC m^{-2}. This fits within the range of integrated sea-ice POC reported in the Chukchi and Beaufort Seas during May/June 2002 (200 – 2000 mg C /m^2) [*Gradinger,* 2009]. Given that the chl a standing stocks were 8.3 mg m-² [*Zhou et al.*, 2013], our calculation provides a C:Chla ratio of 52, which compares well with the 57 used in *Jin et al.* [2006] and obtained from their observations (Jin, personal communication). The consistency of C:chl a with the literature and the similarity between $[O_2]_{bio}$ with POC in the literature, in spite of neglecting diffusion, suggest that diffusion occurred at a much lower rate than NCP.

5 Conclusion and perspectives

We presented the first time-series of O_2, Ar and N_2 measurements in natural landfast sea ice, collected in Barrow from February through June 2009. The gases were extracted from ice

crushing – a technique that allows the measurement of O_2 from both brine and gas bubbles, both in impermeable and permeable layers. The results thus extend our current knowledge, which is limited to dissolved O_2 in the bottom permeable ice layers.

We have highlighted 3 distinct stages in the dynamics of O_2 as compared to Ar and N_2: (1) gas incorporation in the form of gas bubbles or dissolved gases. In the latter situation, gas standing stocks increase with increasing ice thickness; (2) gas accumulation subsequent to ice growth, through the formation of gas bubbles due to biological activity, voids and superimposed ice; (3) gas removal due to prolonged gas exchange in permeable ice layers. However, the gas removal was less marked for O_2 than for Ar and N_2, because biological O_2 production partly compensated the loss of O_2 due to gas exchange (gas bubble escape and gas diffusion).

The dynamics of O_2 in landfast sea ice was highly sensitive to physical processes: gas incorporation and subsequent transport. Brine concentration and decreasing solubility (associated with decreasing temperature and increasing brine salinity) cause a non-linear relationship between gas saturation levels and brine volume fraction. In particular, supersaturations of O_2 up to 500 % were still observed in the permeable layers (where brine volume fraction exceeds 5 %), probably due to the formation of gas bubbles and/or slow gas equilibrium. It still remains unclear how O_2 supersaturation affect the O_2 dissolved in brine and its diffusion at the ice/water interface, but solving this issue will be crucial for the estimate of NCP based on O_2 diffusion (e.g. under-ice eddy covariance [*Long et al.,* 2012], and O_2 optode measurements [*Mock et al.,* 2002]).

Finally, we discussed the possibility to correct for the physical imprints (including spatial variability) on O_2 variations using Ar and N_2. The main problem associated with gas measurements in sea ice is the uncertainty of gas exchange within the permeable sea ice. $[O_2]_{eq}$ upon sea ice consolidation is indeed uncertain. Also, the wide range of diffusion coefficients for O_2, Ar and N_2 found in the literature, and the uncertainty of how both brine convection and diffusion affect the O_2/Ar signal in sea ice have to be solved for accurate NCP estimates. We acknowledge the limitations of our pioneering study, but as our conservative estimate of NCP and $[O_2]_{bio}$ are comparable to the literature, NCP calculation using O_2/Ar appear promising – especially in cases like BRW10, where brine convection was absent and diffusion probably negligible in comparison to NCP.

Acknowledgements

The authors would like to thank Dr. Hajo Eicken, the rest of the sea ice group of the Geophysical Institute of the University of Alaska Fairbanks, Nicolas-Xavier Geilfus, Gauthier Carnat, Tim Papakyriakou, Bernard Heinesch, Michel Yernaux, Thomas Goossens, Noémie Carnat and Rodd Laing for their help in field work. We are indebted to the Barrow Arctic Science Consortium and the North Slope Borough for their logistical support. We also thank Saïda El Amri for her efficient help in laboratory work, Neige Egmont for her comments and Roberta Hamme for sharing the matlab script on gas diffusion. This research was supported by the F.R.S-FNRS (contract 2.4584.09), the National Science Foundation (project OPP-0632398 (SIZONet)), the University of Alaska Fairbanks and the Belgian Science Policy (contract SD/CA/03A), the NCE ArcticNet and National Science and Engineering Research Council (NSERC). FB was a research fellow of F.R.S.-FRIA, JZ a research fellow of F.R.S.-FNRS, and BD, a research associate of F.R.S.-FNRS. This is MARE contribution no. XXX.

Chapter IX – Conclusions

1 The most relevant processes affecting the dynamics of solutes and gases in sea ice

The overarching objective of the thesis was to identify the most relevant processes affecting the dynamics of solutes and gases in sea ice. To fulfil that objective, we raised three questions. How this thesis contributed to address these questions is summarized hereafter.

1. **How does the concentration of solutes and gases in sea ice change with depth and time?**

We analyzed different inorganic macronutrients, dissolved organic carbon (DOC), and different gases in sea ice. Most of them were not conservative against salinity in the ice.

In the Interice V experiment (Chapter V), the dissolved compounds were 4 to 6 times more enriched in the ice than what we would expect if they were transported as salts. The enrichment factors of most of the compounds decrease from the top, to the bottom of the ice, where they approach 1. The enrichment of DOC in ice was higher in the mesocosms with seawater than in the mesocosms with the addition of river water.

Gases in natural ice cores showed much larger enrichment factors in the ice (Chapter VI-VIII) than the inorganic nutrients and DOC in the experiment ice. N_2 reached 7000 % of supersaturation, which means that it was 70 times more enriched in the ice that it would have been if it were only dissolved in brine, and no supersaturation existed. O_2, Ar and CH_4 were also supersaturated, reaching about 3000 % of supersaturation. The maximum supersaturation was reached in the upper ice layer (about 15-25 cm depth), where the brine volume fraction was lowest (2%) and where large gas bubble accumulation was observed in thin sections. Inert gas concentrations (N_2 and Ar) were close to their solubility values at the bottom of the ice, and at all depths when the ice became fully permeable, except when a superimposed ice layer forms at the ice surface. In contrast, CH_4 was always supersaturated, in both permeable and impermeable ice layers; O_2 was supersaturated in the bottom permeable layers, but only in late spring.

2. How do these changes compare to those of the physical properties of the ice?

We have shown that the physical properties of the ice exert a strong influence on the distribution of the (dissolved and gaseous) biogeochemical compounds in sea ice, as they influence ice permeability and brine dynamics, and gas bubble formation.

Increasing **ice permeability** affects both the dissolved and the gaseous compounds: it allows the infiltration of snow meltwater, which may affect the nutrients and $\delta^{18}O$ in brine (chapter VI); it also allows gas exchange between the atmosphere and the ice, and between the ice and seawater (chapters VI-VIII). Gas exchange through sea ice generally tends to draw gas concentrations in sea ice toward their solubility values, as we have observed for Ar and N_2, except when there is in situ production, as for O_2, and when the under-ice is supersaturated, as for CH_4.

Brine dynamics affect the dissolved compounds. When brine convection occurs, it tends to draw the concentrations of nutrients, DOM and $\delta^{18}O$ in brine towards their respective concentrations in seawater. The reach of brine convection in the ice depends on the **stages of brine dynamics**, and we have identified three of them in our studies. (1) Gravity-driven bottom convection lasts during most of the ice growth period. Because decreasing air temperature reduces the permeability in the ice interior, convection is limited to the bottom of the ice, although brine salinity decreases with depth. (2) Gravity-driven full-depth convection may then take place (or not) depending on the competing effect between the potential energy for gravity drainage and the dissipation of the energy as the brine moves downward. (3) Finally, brine stratification develops when further temperature increase triggers internal ice melt, which eventually stabilizes the brine density profile, slowing down the exchange of nutrients between brine and seawater.

The **formation of gas bubbles** affects the transport pathway of gases in sea ice, because while dissolved gases tend to move downward due to gravity drainage (as with the other dissolved compounds), gas bubbles tend to move upward due to buoyancy. This difference in the transport pathways between the dissolved and gaseous compounds explains the larger accumulation of gases in sea ice, in comparison to salts and the other dissolved compounds.

3. **How do these changes compare to those of the biological properties of the ice?**

In our study, the largest bacterial abundance and chlorophyll-a concentrations were found at the bottom of the ice. However, because brine convection was also generally the most intense at the bottom of the ice, it was difficult to assess the biological impact based on the changes of the biogeochemical compounds only. In other words, there was a competing effect between the biological impact and the physical impact. As a result, the maximum O_2 concentration was not observed at the same depth as the maximum chlorophyll-a, but slightly above, where brine convection was limited and diffusion was slow.

In addition, biological impacts on the changes of biogeochemical compounds were only obvious when the biological production or consumption rate is larger than the initial pool. As a result, because of the large initial DOC concentrations, bacterial respiration did not significantly affect the concentrations of DOC.

To the general question **"what are the most relevant processes affecting the dynamics of solutes and gases in sea ice?"**, the answer is that **physical processes** induced the most significant changes in the **observed stocks** of the biogeochemical compounds analysed in this thesis.

Brine convection tends to pull the concentrations of the biogeochemical compounds to conservative behaviour (and override any potential biological impacts), while **gas bubble formation,** due to brine concentration and gas solubility decrease, induces a selective retention for gases. Increasing **permeability** enhances gas exchange through sea ice; this could induce a drastic decrease in gas standing stocks, which may be partly compensated for by in situ biological production (O_2) and external input (CH_4).

2 Implications of our findings on regional scale and in a climate change perspective

The findings from this work have not only helped to identify the most relevant processes affecting gas and solute dynamics in sea ice, they may also have larger scale implications.

2.1 Sea ice retains the more labile form of DOC

In the Interice V experiment (Chapter V), we have observed that there was a significant enrichment of DOC in the ice, and that enrichment was higher in the mesocosms filled with seawater than in the mesocosms filled with seawater and river water. Because riverine DOC contains older soil-derived material, which is more refractory than the marine DOC (mainly phytoplankton-derived), our results suggest that the more labile forms of DOC are better retained in sea ice than the refractory forms. This is in agreement with the results of *Müller et al.* [2013] and *Jørgensen et al.* [submitted].

Through the selective retention of the labile form of DOC in sea ice, sea ice plays an important role in the carbon cycle. By selectively retaining the labile form of DOC, sea ice growth likely drives segregation of the microorganism species between the ice and the under-ice water, hence, different community development and production in sea ice and in seawater.

In the context of a warming climate, sea ice may play a more significant role in the carbon cycling in the Arctic. In the coastal regions, if the riverine input of refractory DOC increased (e.g., because warmer temperature increases higher bacterial respiration), carbon cycling could be more efficient in sea ice than in the under-ice water, because sea ice would contain a larger fraction of labile DOC.

2.2 Gas bubble formation enhances gas accumulation in sea ice, and possibly gas transfer towards the atmosphere

In Chapter VI – VIII, we suggested that the formation of gas bubbles in sea ice is a mechanism leading to the accumulation of gases in sea ice. As a result, argon responded differently to brine dynamics than the other dissolved biogeochemical compounds (Chapter VI). Model simulations support this suggestion: *Moreau et al.* [2014] described the incorporation and the transport of argon in ice. Our results indicate that neglecting gas bubble formation (i.e., by taking into account only the dissolved gas compounds) would lead to an underestimate of the argon content in sea ice of 40 to 60 %.

However, the impact of the gas bubble formation in the retention of the gases may vary depending on the gases. For instance, for the soluble gas CO_2, because of the equilibria of the CO_2 system, CO_2 in gas bubbles only represent 5 % of the total CO_2 content [*Moreau et al.*, submitted].

2.3 The 3 main stages of brine dynamics from ice growth to ice decay

We described 3 main stages of brine dynamics from ice growth to ice decay: (1) Bottom convection which lasts during most of the ice growth period, (2) Full-depth convection in early spring, and (3) brine stratification when further temperature increase triggers internal ice melt and stabilizes the brine density profile. Since the different stages of brine dynamics mainly depend on the unstable brine density profile and the ice permeability, which are both a function of the ice temperature, all the areas with similar physical constraints (air temperature and water salinity) should experience the same successive stages in brine dynamics. This suggestion is at least pertinent for the Canadian Arctic basin: *Carnat et al.* [2013] have indeed observed the 3 same stages in their field study, despite the large spatial coverage of the sampling.

2.4 The role of sea ice in the CH_4 cycle

Chapter VII presented the first time-series of CH_4 in sea ice, in parallel to the physical properties of the ice; the results improved our understanding on the role of sea ice in the exchange of CH_4 between seawater and the atmosphere. This is important, because CH_4 is a greenhouse gas with a high global warming potential, and its release from the Arctic coastal waters potentially causes positive feedback on current global warming. However, there is not yet consensus on the role of sea ice in the methane cycle.

Our results indicate that Barrow landfast sea ice mainly acts as a temporary storage for the CH_4 release from the seafloor, and that biological impacts on the CH_4 concentrations should be minor in comparison to the physical incorporation. These results may be pertinent for the other Arctic shelf regions with shallow water depths.

However, our results can probably not be generalized to the whole Arctic, or Antarctica. *Kort et al.* [2012] measured significant fluxes of CH_4 over the ice-covered central Arctic. Because the water depth is deeper in the central Arctic than the coastal regions, the CH_4 released from the seafloor could be oxidized before reaching the surface water. Therefore, ice-air CH_4 fluxes in the central Arctic must indicate a production of CH_4 in the ice or in the under-ice water (with emission of CH_4 via leads). CH_4 production in aerobic water has been found in the Pacific side of the central Arctic [*E. Damm et al.*, 2008]. Whether the same process could occur in sea ice remains an open question.

2.5 O_2/Ar, a new method for studying net community production in sea ice

The manuscript presented in Chapter VIII has two main originalities: first, we measured the total O_2 content in the ice (gaseous and dissolved), while current studies mainly focus on the dissolved O_2 concentrations. Second, we discussed the use of inert gases N_2 and Ar to correct the physical contribution to O_2 variations, and thus, to determine the net community production in sea ice. This method does not require melting the ice or deploying in situ probes; we therefore avoid obtaining biased net community production related to the ice melt or because the probes are inserted in gas bubbles or biofilms. Although this is a pioneer study, and further improvements are required (e.g, equations describing the diffusion of O_2 at the ice-water interface), the method seems promising.

3 Revision of the processes regulating the distribution of gases in sea ice

Because the previous review on the processes regulating the distribution of gases in sea ice dates back to 1979 [*Tsurikov*, 1979] and was mainly based on theoretical considerations, we here present an update of the processes with references to observations supporting each of the processes (Table 1). While all the processes could occur in both Arctic and Antarctic sea ice, the entrapment of CH_4 gas bubbles (an example of process2) should be more common in the Arctic shelf regions, like the East Siberian shelf, with a large input of terrestrial organic matter, shallow water depths, and melting sub-sea permafrost. Because positive freeboards are more generally encountered in the Arctic; and negative freeboards in the Antarctic, the substitution of air for brine due to positive freeboard (process3) should be more common in the Arctic, while the capture of air during the formation of snow ice (process5) should be more common in Antarctica.

Table 1 Review of the processes regulating gas concentrations in sea ice

PROCESSES			EXAMPLE(S)
Entrapment	1	The entrapment of the dissolved gases	*Tsurikov* [1979]; *Tison et al.* [2002]
	2	The entrapment of gas bubbles (e.g., CH_4)	*Tsurikov* [1979]; *Perovich and Gow* [1996]; *Shakhova et al.* [2010b]; *Zhou et al.* [2014b]
	3	Air replacing the downward moving brine in permeable ice pores above the freeboard	*Tsurikov* [1979]; *Perovich and Gow* [1996]
	4	Superimposed ice formation : The entrapment of the air contained in the snow	*Zhou et al.* [2013]
	5	Snow ice formation : The entrapment of the air in snow and the dissolved gases in seawater	*Tsurikov* [1979]
Transport	6	Gas transport with brine movement	*Moreau et al.* [2014] for brine drainage; *Geilfus et al.* [2013] for brine expulsion
	7	Air-ice and ice-ocean exchanges	*Delille et al.* [2014]; *Loose and Schlosser* [2011]; *Nomura et al.* [2010] ; *Rysgaard et al.* [2011]
	8	Gas bubble rise due to buoyancy	*Moreau et al.* [2014]; *Zhou et al.* [2013]
Nucleation and dissolution	9	Brine concentration (cooling) and brine dilution (warming)	*Zhou et al.* [2013] ; *Zhou et al.* [2014a] ; *Zhou et al.* [2014b]
	10	Changes in gas solubility	*Zhou et al.* [2013] ; *Zhou et al.* [2014a] ; *Zhou et al.* [2014b]
	11	Pressure changes (e.g., void formation due to internal ice melt)	*Tsurikov* [1979]; *Light et al.* [2003] and *Zhou et al.* [2014a] for void formation
Biogeochemical processes	12	Biological production and consumption	*Zhou et al.* [2014a] for O_2; *Carnat et al.* [2014] for DMS; *Delille et al.* [2007] for CO_2
	13	Mineral precipitation and dilution (e.g., calcium carbonate)	*Delille et al.* [2007]; *Geilfus et al.* [2013]

4 Research perspectives

4.1 Multi-year sea ice

Our work has mainly focused on the study of first-year ice. Although it has brought lots of interesting results, we need to compare them with results obtained from multi-year sea ice, in order to better predict the changes in the global biogeochemical cycles. This is particularly pertinent in the Arctic, where the proportion of first sea ice is increasing, and the proportion of multi-year ice is decreasing.

For instance, we found that the labile forms of DOC are better retained in first-year sea ice than the more refractory forms. Because the incorporation and retention is related to sea ice formation, we may expect the DOC enrichment to be more pronounced in first-year ice than in multi-year ice. This conjecture needs to be verified with measurements on multi-year ice. If it is verified, then, carbon cycling will likely be enhanced in Arctic sea ice, with the increasing proportion of first-year sea ice.

Another interest in measuring multi-year sea ice is related to the CH_4 cycle. Significant ice-air CH_4 fluxes that have been measured in the central Arctic (Kort et al., 2010) indicate a production of CH_4 in the ice or in the under-ice water (with emission of CH_4 via leads). Measuring CH_4 in the multi-year ice of the central Arctic would help to better understand the contribution of sea ice to the observed fluxes.

4.2 Exchanges at the ice-water and ice-air interfaces

Our work has shown that brine convection affect the vertical distribution the dissolved compounds (e.g., inorganic nutrients, DOC) in sea ice. How frequent and how far is the reach of brine convection within the ice is still in need of quantification. Monitoring changes of salinity at fine vertical resolution and at high frequency (time-intervals) using in-situ salinity probes should help to better quantify the impact of brine convection on the ice. The results would help to better parameterize ice algal growth within the ice.

In addition to brine convection, more work could also be done with respect to the diffusive transport. In the absence of turbulence (e.g., waves and tides), purely diffusive transport regime could occur between two episodes of convection, at the bottom of the ice, when the Ra increases but has not yet reached the critical number, It could also occur when the ice pack growth reaches a steady state, because salt rejection is then reduced and brine

convection limited. We have shown that diffusion affect the estimate of the biological O_2 stock at the bottom of the ice (Chapter VIII). A better understanding of the ice-water exchanges will improve our estimate of the biological O_2 stock and thus net community production.

Finally, because of the potential emission of climate active gases (CO_2, DMS, CH_4, N_2O) from the ice to the atmosphere, it would be valuable to better budget gas fluxes through sea ice. Our work highlighting the different transport pathways of gases and their dependence to gas solubility is a first step. Formulating gas solubility equations for the range of ice temperature and brine salinity in sea ice, determining more gas diffusion coefficients, and finding a good parameterization for the ice permeability for upward gas transport should further help to improve our assessment of gas fluxes through sea ice.

REFERENCES

Abril, G., and N. Iversen (2002), Methane dynamics in a shallow non-tidal estuary (Randers Fjord, Denmark), *Marine Ecology-Progress Series*, *230*, 171-181.

Ackley, S. F., and C. W. Sullivan (1994), Physical controls on the development and characteristics of Antarctic sea ice biological communities— a review and synthesis, *Deep Sea Research Part I: Oceanographic Research Papers*, *41*(10), 1583-1604.

Ackley, S. F., M. J. Lewis, C. H. Fritsen, and H. Xie (2008), Internal melting in Antarctic sea ice: Development of "gap layers", *Geophysical Research Letters*, *35*(11), L11503.

Aguilar-Islas, A. M., R. D. Rember, C. W. Mordy, and J. Wu (2008), Sea ice-derived dissolved iron and its potential influence on the spring algal bloom in the Bering Sea, *Geophysical Research Letters*, *35*(24), L24601.

Arar, E. J., and G. B. Collins (1997), In vitro Determination of Chlorophyll a and Pheophytin a in Marine and Freshwater Algae by Fluorescence (Method 445.0)*Rep.*, National Exposure Research Laboratory - U.S. Environmental Protection Agency, Ohio.

Arrigo, K. R., T. Mock, and M. P. Lizotte (2010), Primary Producers and Sea Ice, in *Sea ice*, edited by D. N. Thomas and G. S. Dieckmann, pp. 283-325, Blackwell Publishing Ltd, UK.

Arrigo, K. R., et al. (2012), Massive Phytoplankton Blooms Under Arctic Sea Ice, *336*(6087).

Arzel, O., T. Fichefet, and H. Goosse (2006), Sea ice evolution over the 20th and 21st centuries as simulated by current AOGCMs, *Ocean Modelling*, *12*(3–4), 401-415.

ASCE (1996), *Hydrology Handbook*, American Society of Civil Engineers (ASCE), New York, NY, United States.

Aslam, S. N., G. J. C. Underwood, H. Kaartokallio, L. Norman, R. Autio, M. Fischer, H. Kuosa, G. S. Dieckmann, and D. N. Thomas (2012), Dissolved extracellular polymeric substances (dEPS) dynamics and bacterial growth during sea ice formation in an ice tank study, *Polar Biology*, *35*(5), 661-676.

Assur, A. (1958), Composition of sea ice and its tensile strength, in *Arctic Sea Ice*, edited, pp. 106-138, National Academy of Sciences-National Research Council.

Backstrom, L. G. E., and H. Eicken (2006), Capacitance probe measurements of brine volume and bulk salinity in first-year sea ice, *Cold Regions Science and Technology*, *46*, 167-180.

Bange, H. W., U. H. Bartell, S. Rapsomanikis, and M. O. Andreae (1994), Methane in the Baltic and North Seas and a Reassessment of the Marine Emissions of Methane, *Global Biogeochem. Cycles*, *8*(4), 465-480.

Bartels, T., B. Eichler, P. Zimmermann, H. W. Gäggeler, and M. Ammann (2002), The adsorption of nitrogen oxides on crystalline ice, *Atmospheric Chemistry and Physics*, *2*(3), 235-247.

Bates, T. S., K. C. Kelly, J. E. Johnson, and R. H. Gammon (1996), A reevaluation of the open ocean source of methane to the atmosphere, *Journal of Geophysical Research*, *101*(D3), 6953-6961.

Becquevort, S., I. Dumont, J. L. Tison, D. Lannuzel, M. L. Sauvee, L. Chou, and V. Schoemann (2009), Biogeochemistry and microbial community composition in sea ice and underlying seawater off East Antarctica during early spring, *Polar Biology*, *32*(6), 879-895.

Belzile, C., S. C. Johannessen, M. Gosselin, S. Demers, and W. L. Miller (2000), Ultraviolet attenuation by dissolved and particulate constituents of first-year ice during late spring in an Arctic polynya, *Limnology and Oceanography*, *45*(6), 1265-1273.

Bennington, K. O. (1963), Some crystal growth features of sea ice, *J. Glaciol.*, *4*(36), 669-688.

Beucher, C., P. Tréguer, A.-M. Hapette, R. Corvaisier, N. Metzl, and J.-J. Pichon (2004), Intense summer Si-recycling in the surface Southern Ocean, *Geophysical Research Letters*, *31*(9), L09305.

Bitz, C. M., and W. H. Lipscomb (1999), An energy-conserving thermodynamic model of sea ice, *Journal of Geophysical Research: Oceans (1978–2012)*, *104*(C7), 15669-15677.

Bjornsen, P. K., and J. Kuparinen (1991), Determination of bacterioplankton biomass, net production and growth efficiency in the Southern Ocean, *Marine Ecology Progress Series*, *71*, 185-194.

Borges, A. V., and G. Abril (2011), 5.04 - Carbon Dioxide and Methane Dynamics in Estuaries, in *Treatise on Estuarine and Coastal Science*, edited by W. Editors-in-Chief: Eric and M. Donald, pp. 119-161, Academic Press, Waltham.

Boye, M., C. M. G. van den Berg, J. T. M. de Jong, H. Leach, P. Croot, and H. J. W. de Baar (2001), Organic complexation of iron in the Southern Ocean, *Deep Sea Research Part I: Oceanographic Research Papers*, *48*(6), 1477-1497.

Brandon, M., and P. Wadhams (1999), The near surface hydrography beneath the Odden ice tongue, *Deep Sea Research Part II: Topical Studies in Oceanography*, *46*(6), 1301-1318.

Brierley, A. S. (2002), Antarctic krill under sea ice: elevated abundance in a narrow band just south of the ice edge, *Science*, *295*, 1890-1892.

Broecker, W. S., and T. H. Peng (1974), Gas exchange rates between air and sea, *Tellus*, *26*(1-2), 21-35.

Broecker, W. S., and T. H. Peng (1982), *Tracers in the Sea*, The Lamont-Doherty Geological Observatory, Columbia University, New York.

Brooks, J. M., M. E. Field, and M. C. Kennicutt (1991), Observations of Gas Hydrates in Marine-Sediments, Offshore Northern California, *Marine Geology*, *96*(1-2), 103-109.

Burton, J. A., R. C. Prim, and W. P. Slichter (1953), The Distribution of Solute in Crystals Grown from the Melt. Part I. Theoretical, *The Journal of Chemical Physics*, *21*(11), 1987-1991.

Carnat, G., T. Papakyriakou, N.-X. Geilfus, F. Brabant, B. Delille, M. Vancoppenolle, G. Gilson, J. Zhou, and J.-L. Tison (2013), Investigations on physical and textural properties of Arctic first-year sea ice in the Amundsen Gulf, Canada, November 2007–June 2008 (IPY-CFL system study), *Journal of Glaciology*, *59*(217), 819-837.

Carnat, G., J. Zhou, T. Papakyriakou, B. Delille, T. Goossens, T. Haskell, V. Schoemann, F. Fripiat, J.-M. Rintala, and J.-L. Tison (2014), Physical and biological controls on DMS,P dynamics in ice shelf-influenced fast ice during a winter-spring and a spring-summer transitions, *Journal of Geophysical Research: Oceans*, *119*(5), 2882-2905.

Cassar, N., B. Barnett, M. L. Bender, J. Kaiser, R. C. Hamme, and B. Tilbrook (2009), Continuous high-frequency dissolved O2/Ar measurements by Equilibrator Inlet Mass Spectrometry (EIMS), *Analytical Chemistry*, *81*(5), 1855-1864.

Castro-Morales, K., N. Cassar, D. R. Shoosmith, and J. Kaiser (2013), Biological production in the Bellingshausen Sea from oxygen-to-argon ratios and oxygen triple isotopes, *Biogeosciences*, *10*, 2273-2291.

Charlson, R. J., J. E. Lovelock, M. O. Andrea, and S. G. Warren (1987), Oceanic phytoplankton atmospheric sulphur, cloud albedo and climate, *Nature*, *326*(6114), 655-661.

Chin, W.-C., M. V. Orellana, and P. Verdugo (1998), Spontaneous assembly of marine dissolved organic matter into polymer gels, *Nature*, *391*(6667), 568-572.

Comiso, J. C. (2010), Variability and Trends of the Global Sea Ice Cover, in *Sea ice*, edited by D. N. Thomas and G. S. Dieckmann, pp. 205-246, Blackwell Publishing Ltd, UK.

Cota, G. F., and E. P. W. Horne (1989), Physical control of Arctic ice algal production, *Marine ecology progress series. Oldendorf*, *52*(2), 111-121.

Cota, G. F., S. J. Prinsenberg, E. B. Bennett, J. W. Loder, M. R. Lewis, J. L. Anning, N. H. F. Watson, and L. R. Harris (1987), Nutrient fluxes during extended blooms of Arctic ice algae, *Journal of Geophysical Research: Oceans (1978–2012)*, *92*(C2), 1951-1962.

Cottier, F., H. Eicken, and P. Wadhams (1999), Linkages between salinity and brine channel distribution in young sea ice, *Journal of Geophysical Research: Oceans*, *104*(C7), 15859-15871.

Cox, G. F. N., and W. F. Weeks (1975), Brine Drainage and Initial Salt Entrapment in Sodium Chloride Ice*Rep.*, Cold regions research and engineering laboratory, Hanover, New Hampshire.

Cox, G. F. N., and W. F. Weeks (1983), Equations for determining the gas and brine volumes in sea-ice samples, *Journal of Glaciology*, *29*(102), 306-316.

Cox, G. F. N., and W. F. Weeks (1988), Numerical simulations of the profile properties of undeformed first-year sea ice during the growth season, *Journal of Geophysical Research: Oceans (1978–2012)*, *93*(C10), 12449-12460.

Crabeck, O., B. Delille, S. Rysgaard, D. N. Thomas, N. X. Geilfus, B. Else, and J.-L. Tison (submitted), First "in situ" determination of gas transport coefficient (DO2, DAr, DN2) from bulk gas concentration measurements (O2, N2, Ar) in natural sea ice, *Journal of geophysical Research - Oceans*.

Craig, H., and T. Hayward (1987), Oxygen Supersaturation in the Ocean: Biological Versus Physical Contributions, *Science*, *235*(4785), 199-202.

Crocker, G. B., and P. Wadhams (1989), Modelling Antarctic fast-ice growth, *Journal of Glaciology*, *35*(119), 3-8.

Cross, J. N., J. T. Mathis, K. E. Frey, C. E. Cosca, S. L. Danielson, N. R. Bates, R. A. Feely, T. Takahashi, and W. Evans (2014), Annual sea-air CO2 fluxes in the Bering Sea: Insights from new autumn and winter observations of a seasonally ice-covered continental shelf, *Journal of Geophysical Research: Oceans*, n/a-n/a.

Damm, E., U. Schauer, B. Rudels, and C. Haas (2007), Excess of bottom-released methane in an Arctic shelf sea polynya in winter, *Continental Shelf Research*, *27*(12), 1692-1701.

Damm, E., R. P. Kiene, J. Schwarz, E. Falck, and G. Dieckmann (2008), Methane cycling in Arctic shelf water and its relationship with phytoplankton biomass and DMSP, *Marine Chemistry*, *109*(1-2), 45-59.

Damm, E., E. Helmke, S. Thoms, U. Schauer, E. Nöthig, K. Bakker, and R. P. Kiene (2010), Methane production in aerobic oligotrophic surface water in the central Arctic Ocean *Biogeosciences*, *7*, 1099-1108.

Delille, B. (2006), Inorganic carbon dynamics and air-ice-sea CO_2 fluxes in the open and coastal waters of the Southern Ocean PhD Thesis thesis, 297 pp, University of Liège.

Delille, B., B. Jourdain, A. V. Borges, J. L. Tison, and D. Delille (2007), Biogas (CO_2, O_2, dimethylsulfide) dynamics in spring Antarctic fast ice, *Limnology and Oceanography*, *52*(4), 1367-1379.

Delille, B., et al. (2014), Southern Ocean CO2 sink: the contribution of the sea ice, *Journal of Geophysical Research*, *119*(9), 6340-6355.

Demarest, M. S., M. A. Brzezinski, and C. P. Beucher (2009), Fractionation of silicon isotopes during biogenic silica dissolution, *Geochimica et Cosmochimica Acta*, *73*(19), 5572-5583.

Dempsey, D. E., and P. J. Langhorne (2012), Geometric properties of platelet ice crystals, *Cold Regions Science and Technology*, *78*(0), 1-13.

Dieckmann, G. S., and H. H. Hellmer (2010), The Importance of Sea Ice: An Overview, in *Sea Ice*, edited, pp. 1-22, Wiley-Blackwell.

Dieckmann, G. S., G. Rohardt, H. Hellmer, and J. Kipfstuhl (1986), The occurrence of ice platelets at 250 m depth near the Filchner Ice Shelf and its significance for sea ice biology, *Deep Sea Research Part A. Oceanographic Research Papers*, *33*(2), 141-148.

Dieckmann, G. S., G. Nehrke, C. Uhlig, J. Göttlicher, S. Gerland, M. A. Granskog, and D. N. Thomas (2010), Ikaite ($CaCO_3$*$6H_2O$) discovered in Arctic sea ice, *The Cryosphere*, *4*(2), 227-230.

Dieckmann, G. S., G. Nehrke, S. Papadimitriou, J. Göttlicher, R. Steininger, H. Kennedy, D. Wolf-Gladrow, and D. N. Thomas (2008), Calcium carbonate as ikaite crystals in Antarctic sea ice, *Geophysical Research Letters*, *35*.

Dittmar, T., and G. Kattner (2003), The biogeochemistry of the river and shelf ecosystem of the Arctic Ocean: A review, *Marine Chemistry*, *83*(3), 103-120.

Dittmar, T., H. P. Fitznar, and G. Kattner (2001), Origin and biogeochemical cycling of organic nitrogen in the eastern Arctic Ocean as evident from D- and L-amino acids, *Geochimica et Cosmochimica Acta*, *65*(22), 4103-4114.

Druckenmiller, M. L., H. Eicken, M. A. Johnson, D. J. Pringle, and C. C. Williams (2009), Toward an integrated coastal sea-ice observatory: System components and a case study at Barrow, Alaska, *Cold Regions Science and Technology*, *56*(2–3), 61-72.

Eicken, H. (1992), The role of sea ice in structuring antarctic ecosystems, *Polar Biology*, *12*(1), 3-13.

Eicken, H. (1994), Structure of under-ice melt ponds in the central Arctic and their effect on the sea-ice cover, *Limnol Oceanogr*, *39*(3), 682-694.

Eicken, H. (1998), Factors determining microstructure, salinity and stable-isotope composition of Antarctic sea ice: Deriving modes and rates of ice growth in the Weddell Sea, in *Antarctic Sea Ice*

Physical Processes, Interactions and Variability, edited by M. O. Jeffries, pp. 89-122, American Geophysical Union, Washington, USA.

Eicken, H., and M. A. Lange (1989), Development and properties of sea ice in the coastal regime of the southeastern Weddell Sea, *J. Geophys. Res.*, *94*(C6), 8193-8206.

Eicken, H., M. A. Lange, and G. S. Dieckmann (1991), Spatial Variability of Sea-Ice Properties in the Northwestern Weddell Sea, *Journal of Geophysical Research*, *96*(C6), 10603-10615.

Eicken, H., H. R. Krouse, D. Kadko, and D. K. Perovich (2002), Tracer studies of pathways and rates of meltwater transport through Arctic summer sea ice, *Journal of Geophysical Research: Oceans*, *107*(C10), 8046.

Eicken, H., T. C. Grenfell, D. K. Perovich, J. A. Richter-Menge, and K. Frey (2004), Hydraulic controls of summer Arctic pack ice albedo, *Journal of Geophysical Research : Oceans*, *109*(C8), C08007.

Eronen-Rasimus, E., H. Kaartokallio, C. Lyra, R. Autio, H. Kuosa, G. S. Dieckmann, and D. N. Thomas (2014), Bacterial community dynamics and activity in relation to dissolved organic matter availability during sea-ice formation in a mesocosm experiment, *MicrobiologyOpen*, *3*(1), 139-156.

Feltham, D. L., M. G. Worster, and J. S. Wettlaufer (2002), The influence of ocean flow on newly forming sea ice, *Journal of Geophysical Research: Oceans*, *107*(C2), 3009.

Ferrell, R. T., and D. M. Himmelblau (1967), Diffusion coefficients of nitrogen and oxygen in water, *Journal of Chemical & Engineering Data*, *12*(1), 111-115.

Florez-Leiva, L., E. Damm, and L. Farías (2013), Methane production induced by dimethylsulfide in surface water of an upwelling ecosystem, *Progress in Oceanography*, *112–113*(0), 38-48.

Fofonoff, N. P. (1985), Physical properties of seawater: A new salinity scale and equation of state for seawater, *Journal of Geophysical Research*, *90*(C2), 3332-3342.

Foldvik, A., and T. Kvinge (1974), Conditional instability of sea water at the freezing point, *Deep Sea Research and Oceanographic Abstracts*, *21*(3), 169-174.

Forster, P., et al. (2007), Changes in Atmospheric Constituents and in Radiative Forcing, in *Climate Change 2007: The Physical Science Basis. Contribution of Working Group I to the Fourth Assessment Report of the Intergovernmental Panel on Climate Change*, edited by S. Solomon, D. Qin, M. Manning, Z. Chen, M. Marquis, K. B. Averyt, M.Tignor and H. L. Miller, Cambridge University Press, Cambridge, United Kingdom.

Foster, T. D. (1968), Haline convection induced by the freezing of sea water, *Journal of Geophysical Research*, *73*(6), 1933-1938.

Frank, X., N. Dietrich, J. Wu, R. Barraud, and H. Z. Li (2007), Bubble nucleation and growth in fluids, *Chemical Engineering Science*, *62*, 7090-7097.

Freitag, J. (1999), Untersuchungen zur Hydrologie des arktischen Meereises-Konsequenzen für den kleinskaligen Stofftransport, *Ber. Polarforsch./Rep. Pol. Res.*, *325*, 48.

Fripiat, F., R. Corvaisier, J. Navez, M. Elskens, V. Schoemann, K. Leblanc, L. Andre, and D. Cardinal (2009), Measuring production-dissolution rates of marine biogenic silica by Si-30-isotope dilution using a high-resolution sector field inductively coupled plasma mass spectrometer, *Limnology and Oceanography-Methods*, *7*, 470-478.

Fritsen, C. H., S. F. Ackley, J. N. Kremer, and C. W. Sullivan (1998), Flood-Freeze Cycles and Microalgal Dynamics in Antarctic Pack Ice, in *Antarctic Sea Ice: Biological Processes, Interactions and Variability*, edited, pp. 1-21, American Geophysical Union.

Fritsen, C. H., S. L. Coale, D. R. Neenan, A. H. Gibson, and D. L. Garrison (2001), Biomass, production and microhabitat characteristics near the freeboard of ice floes in the Ross Sea, Antarctica, during the austral summer, *Annals of Glaciology*, *33*(1), 280-286.

Fuhrman, J. A., and F. Azam (1980), Bacterioplankton secondary production estimates for coastal waters of British Columbia, Antarctica, and California, *Applied and Environmental Microbiology*, *39*(6), 1085-1095.

Fuhrman, J. A., and F. Azam (1982), Thymidine incorporation as a measure of heterotrophic bacterioplankton production in marine surface waters: evaluation and field results, *Marine Biology*, *66*(2), 109-120.

Garandet, J. P., S. Corre, S. Kaddeche, and T. Alboussière (2000), The influence of convection on the duration of the initial solute transient in alloy crystal growth, *Journal of Crystal Growth*, *209*(4), 970-982.

Garcia, H. E., and L. I. Gordon (1992), Oxygen solubility in seawater: Better fitting equations, *Limnology and Oceanography*, *37*(6), 1307-1312.

Garrison, D. L., and K. R. Buck (1986), Organism losses during ice melting: A serious bias in sea ice community studies, *Polar Biology*, *6*(4), 237-239.

Garrison, D. L., S. F. Ackley, and K. R. Buck (1983), A physical mechanism for establishing algal populations in frazil ice, *Nature*, *306*(5941), 363-365.

Garrison, D. L., A. R. Close, and E. Reimnitz (1989), Algae concentrated by frazil ice - evidence from laboratory experiments and field-measurements, *Antarctic Science*, *1*(4), 313-316.

Gasol, J. M., and P. A. Del Giorgio (2000), Using flow cytometry for counting natural planktonic bacteria and understanding the structure of planktonic bacterial communities, *Scientia Marina*, *64*(2), 197-224.

Gasol, J. M., U. L. Zweifel, F. Peters, J. A. Fuhrman, and Å. Hagström (1999), Significance of size and nucleic acid content heterogeneity as measured by flow cytometry in natural planktonic bacteria, *Applied and Environmental Microbiology*, *65*(10), 4475-4483.

Geilfus, N.-X., G. Carnat, T. Papakyriakou, J. L. Tison, B. Else, H. Thomas, E. Shadwick, and B. Delille (2012), Dynamics of pCO2 and related air-ice CO2 fluxes in the Arctic coastal zone (Amundsen Gulf, Beaufort Sea), *Journal of Geophysical Research: Oceans*, *117*(C9), C00G10.

Geilfus, N.-X., G. Carnat, G. S. Dieckmann, N. Halden, G. Nehrke, T. Papakyriakou, J. L. Tison, and B. Delille (2013), First estimates of the contribution of CaCO3 precipitation to the release of CO2 to the atmosphere during young sea ice growth, *Journal of Geophysical Research: Oceans*, *118*(1), 244-255.

Giannelli, V., D. N. Thomas, C. Haas, G. Kattner, H. Kennedy, and G. S. Dieckmann (2001), Behaviour of dissolved organic matter and inorganic nutrients during experimental sea-ice formation, *Annals of Glaciology*, *33*, 317-321.

Gleitz, M., U. Bathmann, and K. Lochte (1994), Build-up and decline of summer phytoplankton biomass in the eastern Weddell Sea, Antarctica, *Polar Biology*, *14*(6), 413-422.

Glud, R. N., S. Rysgaard, and M. Kuhl (2002), A laboratory study on O-2 dynamics and photosynthesis in ice algal communities: quantification by microsensors,O-2 exchange rates, C-14 incubations and a PAM fluorometer, *Aquatic Microbial Ecology*, *27*(3), 301-311.

Golden, K. M., S. F. Ackley, and V. I. Lytle (1998), The percolation phase transition in sea ice, *Science*, *282*(5397), 2238-2241.

Golden, K. M., H. Eicken, A. L. Heaton, J. Miner, D. J. Pringle, and J. Zhu (2007), Thermal evolution of permeability and microstructure in sea ice, *Geophys. Res. Lett.*, *34*(L16501).

Gosink, T. A., J. G. Pearson, and J. J. Kelley (1976), Gas movement through sea ice, *Nature*, *263*(2), 41-42.

Gow, A. J., S. F. Ackley, J. W. Govoni, and W. F. Weeks (1998), *Physical and Structural Properties of Land-Fast Sea Ice in Mcmurdo Sound, Antarctica*, American Geophsyical Union, Washington, D.C.

Gradinger, R. (2009), Sea-ice algae: Major contributors to primary production and algal biomass in the Chukchi and Beaufort Seas during May/June 2002, *Deep Sea Research Part II: Topical Studies in Oceanography*, *56*(17), 1201-1212.

Gradinger, R., and J. Ikävalko (1998), Organism incorporation into newly forming Arctic sea ice in the Greenland Sea, *Journal of plankton research*, *20*(5), 871-886

Gradinger, R., M. Spindler, and D. Henschel (1991), Development of Arctic sea-ice organisms under graded snow cover, *Polar Research*, *10*(1), 295-307.

Granfors, A., A. Karlsson, E. Mattsson, W. O. Smith, and K. Abrahamsson (2013a), Contribution of sea ice in the Southern Ocean to the cycling of volatile halogenated organic compounds, *Geophysical Research Letters*, *40*(15), 3950-3955.

Granfors, A., M. Andersson, M. Chierici, A. Fransson, K. Gårdfeldt, A. Torstensson, A. Wulff, and K. Abrahamsson (2013b), Biogenic halocarbons in young Arctic sea ice and frost flowers, *Marine Chemistry*, *155*(0), 124-134.

Granskog, M. A., H. Kaartokallio, and K. Shirasawa (2003), Nutrient status of Baltic Sea ice: Evidence for control by snow-ice formation, ice permeability, and ice algae, *Journal of Geophysical Research*, *108*(C8), 3253.

Granskog, M. A., H. Kaartokallio, D. N. Thomas, and H. Kuosa (2005), Influence of freshwater inflow on the inorganic nutrient and dissolved organic matter within coastal sea ice and underlying waters in the Gulf of Finland (Baltic Sea), *Estuarine, Coastal and Shelf Science*, *65*(1–2), 109-122.

Grasshoff, K., M. Erhard, and K. Kremling (1983), *Methods of seawater analysis*, 2nd ed., Verlag-Chemie, Weinhem, Germany.

Grasshoff, K., K. Kremling, and M. Ehrhardt (1999), *Methods of Seawater Analysis*, Wiley-VCH Verlag, Weinheim, Germany.

Griewank, P. J., and D. Notz (2013), Insights into brine dynamics and sea ice desalination from a 1-D model study of gravity drainage, *Journal of Geophysical Research: Oceans*, *118*(7), 3370-3386.

Grossmann, S., and G. S. Dieckmann (1994), Bacterial standing stock, activity, and carbon production during formation and growth of sea ice in the Weddell Sea, Antarctica, *Applied and Environmental Microbiology*, *60*(8), 2746-2753.

Haas, C., D. N. Thomas, and J. Bareiss (2001), Surface properties and processes of perennial Antarctic sea ice in summer, *Journal of Glaciology*, *47*(159), 613-625.

Hagström, Å., F. Azam, J. Kuparinen, and U.-L. Zweifel (2001), Pelagic plankton growth and resource limitations in the Baltic Sea, in *A systems analysis of the Baltic Sea*, edited, pp. 177-210, Springer.

Hamme, R. C., and S. R. Emerson (2004), The solubility of neon, nitrogen and argon in distilled water and seawater, *Deep-Sea Research I - Oceanographic Research Papers*, *51*(11), 1517-1528.

Hamme, R. C., and J. P. Severinghaus (2007), Trace gas disequilibria during deep-water formation, *Deep Sea Research Part I: Oceanographic Research Papers*, *54*(6), 939-950.

Hansell, D. A., C. A. Carlson, D. J. Repeta, and R. Schlitzer (2009), Dissolved organic matter in the ocean: a controversy stimulates new insights, *Oceanography*, *22*(4), 202-211.

Hart, T. D., J. M. Lynch, and A. H. L. Chamberlain (2001), Anion exclusion in microbial and soil polysaccharides, *Biol Fertil Soil*, *34*, 201–209.

Hassler, C. S., and V. Schoemann (2009), Bioavailability of organically bound Fe to model phytoplankton of the Southern Ocean, *Biogeosciences*, *6*(10), 2281-2296.

He, X., L. Sun, Z. Xie, W. Huang, N. Long, Z. Li, and G. Xing (2013), Sea ice in the Arctic Ocean: Role of shielding and consumption of methane, *Atmospheric Environment*, *67*, 8-13.

Heinesch, B., M. Yernaux, M. Aubinet, N. X. Geilfus, T. N. Papakyriakou, G. Carnat, H. Eicken, J. L. Tison, and B. Delille (2009), Measuring air-ice CO_2 fluxes in the Arctic, *FluxLetter, the newsletter of FLUXNET*, *2*(2), 2.

Helmke, E., and H. Weyland (1995), Bacteria in sea ice and underlying water of the eastern Weddell Sea in midwinter, *Marine Ecology Progress Series*, *117*, 269-287.

Hendricks, M. B., M. L. Bender, and B. A. Barnett (2004), Net and gross O2 production in the southern ocean from measurements of biological O2 saturation and its triple isotope composition, *Deep Sea Research Part I: Oceanographic Research Papers*, *51*(11), 1541-1561.

Higaki, S., Y. Oya, and Y. Makide (2006), Emission of methane from stainless steel surface investigated by using tritium as a radioactive tracer, *Chemistry Letters*, *35*(3), 292-293.

Hobbs, P. V. (1974), Ice physics, *Oxford: Clarendon Press, 1974*, *1*.

Hood, E. M., B. L. Howes, and W. J. Jenkins (1998), Dissolved gas dynamics in perennially ice-covered Lake Fryxell, Antarctica, *Limnology and Oceanography*, *43*(2), 265-272.

Horner, R. A., S. F. Ackley, G. S. Dieckmann, B. Gulliksen, T. Hoshiai, L. Legendre, I. A. Melnikov, W. S. Reeburgh, M. Spindler, and C. W. Sullivan (1992), Ecology of sea ice biota. 1. Habitat, Terminology, and methodology *Polar Biology*, *12*(3-4), 417-427.

Hudier, E. J.-J., R. G. Ingram, and K. Shirasawa (1995), Upward flushing of sea water through first year ice, *Atmosphere-Ocean*, *33*(3), 569-580.

Hunke, E. C., D. Notz, A. K. Turner, and M. Vancoppenolle (2011), The multiphase physics of sea ice: a review for model developers, *The Cryosphere*, *5*, 989-1009.

Hunt, A. G., B. Ghanbarian, and R. Ewing (2014), *Percolation Theory for Flow in Porous Media*, Springer International Publishing, Cham.

Jacobs, S. S., H. H. Helmer, C. S. M. Doake, A. Jenkins, and R. M. Frolich (1992), Melting of ice shelves and the mass balance of Antarctica, *Journal of Glaciology*, *38*(130), 375-387.

Jähne, B., G. Heinz, and W. Dietrich (1987), Measurement of the diffusion coefficients of sparingly soluble gases in water, *Journal of Geophysical Research: Oceans*, *92*(C10), 10767-10776.

Jardon, F. P., F. Vivier, M. Vancoppenolle, A. Lourenço, P. Bouruet-Aubertot, and Y. Cuypers (2013), Full-depth desalination of warm sea ice, *Journal of Geophysical Research: Oceans*, *118*(1), 435-447.

Jeffries, M. O., W. F. Weeks, R. Shaw, and K. Morris (1993), Structural characteristics of congelation and platelet ice and their role in the development of Antarctic land-fast sea ice, *Journal of Glaciology*, *39*(132), 223-238.

Jeffries, M. O., K. Schwartz, K. Morris, A. D. Veazey, H. R. Krouse, and S. Gushing (1995), Evidence for platelet ice accretion in Arctic sea ice development, *Journal of Geophysical Research: Oceans*, *100*(C6), 10905-10914.

Jin, M., C. J. Deal, J. Wang, K.-H. Shin, N. Tanaka, T. E. Whitledge, S. H. Lee, and R. R. Gradinger (2006), Controls of the landfast ice-ocean ecosystem offshore Barrow, Alaska, *Annals of Glaciology*, *44*, 63-72.

Johnson, W. R. (1989), Current response to wind in the Chukchi Sea: A regional coastal upwelling event, *Journal of Geophysical Research*, *94*(C2), 2057-2064.

Jones, S. F., G. M. Evans, and K. P. Galvin (1999), Bubble nucleation from gas cavities - a review, *Advances in Colloid and Interface Science*, *80*, 27-50.

Jørgensen, L., C. A. Stedmon, H. Kaartokallio, M. Middelboe, and D. N. Thomas (submitted), Changes in the composition and bioavailability of dissolved organic matter during sea ice formation, *Limnology and Oceanography*.

Judd, A. G. (2004), Natural seabed gas seeps as sources of atmospheric methane, *Environmental Geology*, *46*(8), 988-996.

Juhl, A. R., C. Krembs, and K. M. Meiners (2011), Seasonal development and differential retention of ice algae and other organic fractions in first-year Arctic sea ice, *Marine Ecology Progress Series*, *436*, 1-16.

Kaartokallio, H. (2001), Evidence for active microbial nitrogen transformations in sea ice (Gulf of Bothnia, Baltic Sea) in midwinter *Polar Biology*, *24*(1), 21-28.

Kaartokallio, H. (2004), Food web components, and physical and chemical properties of Baltic Sea ice, *Marine Ecology Progress Series*, *273*, 49-63.

Kaartokallio, H., D. H. Søgaard, L. Norman, S. Rysgaard, J.-L. Tison, B. Delille, and D. N. Thomas (2013), Short-term variability in bacterial abundance, cell properties, and incorporation of leucine and thymidine in subarctic sea ice, *Aquatic Microbial Ecology*, *71*(1), 57-73.

Karl, D. M., L. Beversdorf, K. M. Bjorkman, M. J. Church, A. Martinez, and E. F. DeLong (2008), Aerobic production of methane in the sea, *Nature Geoscience*, *1*(7), 473-478.

Kattner, G., and H. Becker (1991), Nutrients and organic nitrogenous compounds in the marginal ice zone of the Fram Strait, *Journal of Marine Systems*, *2*(3), 385-394.

Kattner, G., D. N. Thomas, C. Haas, H. Kennedy, and G. S. Dieckmann (2004), Surface ice and gap layers in Antarctic sea ice: highly productive habitats, *Marine Ecology Progress Series*, *277*, 1-12.

Keller, M., and R. F. Stallard (1994), Methane emission by bubbling from Gatun Lake, Panama, *Journal of Geophysical Research*, *99*, 8307-8319.

Kennett, J. P., K. G. Cannariato, I. L. Hendy, and R. J. Behl (2000), Carbon Isotopic Evidence for Methane Hydrate Instability During Quaternary Interstadials, *Science*, *288*, 128-133.

Kérouel, R., and A. Aminot (1997), Fluorometric determination of ammonia in sea and estuarine waters by direct segmented flow analysis, *Marine Chemistry*, *57*(3), 265-275.

Killawee, J. A., I. J. Fairchild, J. L. Tison, L. Janssens, and R. Lorrain (1998), Segregation of solutes and gases in experimental freezing of dilute solutions: Implications for natural glacial systems, *Geochimica Et Cosmochimica Acta*, *62*(23-24), 3637-3655.

Kim, K., W. Choi, M. R. Hoffmann, H.-I. Yoon, and B.-K. Park (2010), Photoreductive dissolution of iron oxides trapped in ice and its environmental implications, *Environmental science & technology*, *44*(11), 4142-4148.

Kirchman, D., E. K'nees, and R. Hodson (1985), Leucine incorporation and its potential as a measure of protein synthesis by bacteria in natural aquatic systems, *Applied and Environmental Microbiology*, *49*(3), 599-607.

Kitidis, V., R. C. Upstill-Goddard, and L. G. Anderson (2010), Methane and nitrous oxide in surface water along the North-West Passage, Arctic Ocean, *Marine Chemistry*, *121*(1-4), 80-86.

Kort, E. A., et al. (2012), Atmospheric observations of Arctic Ocean methane emissions up to 82[deg] north, *Nature Geosci*, *5*(5), 318-321.

Kottmeier, S. T., and C. W. Sullivan (1988), Sea ice microbial communities (SIMCO) 9. Effects of temperature and salinity on rates of metabolism and growth of autotrophs and heterotrophs, *Polar Biology*, *8*, 293-304.

Krembs, C., and J. W. Deming (2008), The Role of Exopolymers in Microbial Adaptation to Sea Ice, in *Psychrophiles: from Biodiversity to Biotechnology*, edited by R. Margesin, F. Schinner, J.-C. Marx and C. Gerday, pp. 247-264, Springer Berlin Heidelberg.

Krembs, C., R. Gradinger, and M. Splindler (2000), Implications of brine channel geometry and surface area for the interaction of sympagic organisms in Arctic sea ice, *Journal of Experimental Marine Biology and Ecology*, *243*, 55-80.

Krembs, C., T. Mock, and R. Gradinger (2001), A mesocosm study of physical-biological interactions in artificial sea ice: effects of brine channel surface evolution and brine movement on algal biomass, *Polar Biology*, *24*(5), 356-364.

Krembs, C., H. Eicken, and J. W. Deming (2011), Exopolymer alteration of physical properties of sea ice and implications for ice habitability and biogeochemistry in a warmer Arctic, *PNAS*, *108*(9), 3653-3658.

Krembs, C., H. Eicken, K. Junge, and J. W. Deming (2002), High concentrations of exopolymeric substances in Arctic winter sea ice: implications for the polar ocean carbon cycle and cryoprotection of diatoms, *Deep-sea Research I*, *49*(12), 2163-2181.

Kuparinen, J., R. Autio, and H. Kaartokallio (2011), Sea ice bacterial growth rate, growth efficiency and preference for inorganic nitrogen sources in the Baltic Sea, *Polar Biology*, *34*(9), 1361-1373.

Kuparinen, J., et al. (2007), Role of sea-ice biota in nutrient and organic material cycles in the northern Baltic Sea, *Ambio*, *36*, 149-154.

Kvenvolden, K. A. (1995), A review of the geochemistry of methane in natural gas hydrate, *Organic Geochemistry*, *23*(11-12), 997-1008.

Kvenvolden, K. A., M. D. Lilley, and T. D. Lorenson (1993), The Beaufort Sea Continental Shelf as a seasonal source of atmospheric methane, *Geophys. Res. Lett.*, *20*(22), 2459-2462.

Lancelot, C., A. de Montety, H. Goosse, S. Becquevort, V. Schoemann, B. Pasquer, and M. Vancoppenolle (2009), Spatial distribution of the iron supply to phytoplankton in the Southern Ocean: a model study, *Biogeosciences*, *6*(12), 2861-2878.

Lange, M. A. (1988), Basic properties of Antarctic sea ice as revealed by textural analysis of ice cores, *Annals of Glaciology*, *10*, 95-101.

Lange, M. A., S. F. Ackley, P. Wadhams, G. S. Dieckmann, and H. Eicken (1989), Development of sea ice in the Weddell Sea, *Ann. Glaciol*, *12*, 92-96.

Lange, M. A., P. Schlosser, S. F. Ackley, P. Wadhams, and G. Dieckmann (1990), 18O concentrations in sea ice of the Weddell Sea, Antarctica *Journal of Glaciology*, *36*(124), 315-323.

Langhorne, P. J., and W. H. Robinson (1986), Alignment of crystals in sea ice due to fluid motion, *Cold Regions Science and Technology*, *12*(2), 197-214.

Langway, C. C. (1958), Ice fabrics and the universal stage*Rep. 62*, U.S. Snow, Ice and Permafrost Research Establishment, Wilmette, Illinois.

Lannuzel, D., V. Schoemann, J. de Jong, J. L. Tison, and L. Chou (2007), Distribution and biogeochemical behaviour of iron in the East Antarctic sea ice, *Marine Chemistry*, *106*(1-2), 18-32.

Lannuzel, D., A. R. Bowie, P. C. van der Merwe, A. T. Townsend, and V. Schoemann (2011), Distribution of dissolved and particulate metals in Antarctic sea ice, *Marine Chemistry*, *124*(1-4), 134-146.

Lannuzel, D., V. Schoemann, J. de Jong, L. Chou, B. Delille, S. Becquevort, and J. L. Tison (2008), Iron study during a time series in the western Weddell pack ice, *Marine Chemistry*, *108*(1-2), 85-95.

Lannuzel, D., V. Schoemann, J. de Jong, B. Pasquer, P. van der Merwe, F. Masson, J. L. Tison, and A. Bowie (2010), Distribution of dissolved iron in Antarctic sea ice: Spatial, seasonal, and inter-annual variability, *Journal of Geophysical Research-Biogeosciences*, *115*.

Lawrence, D. M., A. G. Slater, R. A. Tomas, M. M. Holland, and C. Deser (2008), Accelerated Arctic land warming and permafrost degradation during rapid sea ice loss, *Geophysical Research Letters*, *35*(11).

Laws, E. A. (1991), Photosynthetic quotients, new production and net community production in the open ocean, *Deep-Sea Research Part I*, *38*(1), 143-167.

Lechtenfeld, O. J., G. Kattner, R. Flerus, S. L. McCallister, P. Schmitt-Kopplin, and B. P. Koch (2014), Molecular transformation and degradation of refractory dissolved organic matter in the Atlantic and Southern Ocean, *Geochimica et Cosmochimica Acta*, *126*(0), 321-337.

Lee, S. H., T. E. Whitledge, and S. H. Kang (2008), Spring time production of bottom ice algae in the landfast sea ice zone at Barrow, Alaska, *Journal of Experimental Marine Biology and Ecology*, *367*(2), 204-212.

Lee, S. H., D. A. Stockwell, H.-M. Joo, Y. B. Son, C. Kang, and T. E. Whitledge (2012), Phytoplankton production from melting ponds on Arctic sea ice, *Journal of Geophysical Research: Oceans*, *117*(C4), C04030.

Lelieveld, J., P. J. Crutzen, and F. J. Dentener (1998), Changing concentration, lifetime and climate forcing of atmospheric methane, *Tellus Series B-Chemical and Physical Meteorology*, *50*(2), 128-150.

Leppäranta, M., and T. Manninen (1988), The brine and gas content of sea ice with attention to low salinities and high temperatures.

Levasseur, M., M. Gosselin, and S. Michaud (1994), A new source of dimethylsulfide (DMS) for the arctic atmosphere - ice diatoms, *Marine Biology*, *121*(2), 381-387.

Lewis, E., and R. Perkin (1983), Supercooling and energy exchange near the Arctic Ocean surface, *Journal of Geophysical Research: Oceans (1978–2012)*, *88*(C12), 7681-7685.

Liger-Belair, G. (2005), The Physics and Chemistry behind the Bubbling Properties of Champagne and Sparkling Wines: A State-of-the-Art Review, *Journal of Agricultural and Food Chemistry*, *53*(8), 2788-2802.

Light, B., G. Maykut, and T. Grenfell (2003), Effects of temperature on the microstructure of first-year Arctic sea ice, *Journal of Geophysical Research: Oceans (1978–2012)*, *108*(C2).

Lizotte, M. P. (2001), The contributions of sea ice algae to Antarctic marine primary production, *American Zoologist*, *41*(1), 57-73.

Long, M. H., D. Koopmans, P. Berg, S. Rysgaard, R. N. Glud, and D. H. Søgaard (2012), Oxygen exchange and ice melt measured at the ice-water interface by eddy correlation, *Biogeosciences Discuss.*, *9*, 1957-1967.

Loose, B., and P. Schlosser (2011), Sea ice and its effect on CO2 flux between the atmosphere and the Southern Ocean interior, *Journal of Geophysical Research: Oceans*, *116*(C11), C11019.

Loose, B., P. Schlosser, D. Perovich, D. Ringelberg, D. T. Ho, T. Takahashi, J. Richter-Menge, C. M. Reynolds, W. R. Mcgillis, and J. L. Tison (2010), Gas diffusion through columnar laboratory sea ice: implications for mixed-layer ventilation of CO2 in the seasonal ice zone, *Tellus B*, *63*(1), 23-39.

Lorenson, T. D., and K. A. Kvenvolden (1995), Methane in coastal seawater, sea ice and bottom sediments, Beaufort Sea, Alaska: U.S. Geological Survey Open-File Report 95-70*Rep.*, US Geological Survey, Menlo Park, CA.

Lubetkin, S. D. (2003), Why Is It Much Easier To Nucleate Gas Bubbles than Theory Predicts?, *Langmuir*, *19*(7), 2575-2587.

Macdonald, R. W., E. C. Carmack, and D. W. Paton (1999), Using the delta O-18 composition in landfast ice as a record of arctic estuarine processes, *Marine Chemistry*, *65*(1-2), 3-24.

Macdonald, R. W., D. W. Paton, E. C. Carmack, and A. Omstedt (1995), The freshwater budget and under-ice spreading of Mackenzie River water in the Canadian Beaufort Sea based on salinity and 18O/16O measurements in water and ice, *Journal of Geophysical Research*, *100*(C1), 895-919.

Maksym, T., and M. O. Jeffries (2000), A one-dimensional percolation model of flooding and snow ice formation on Antarctic sea ice, *Journal of Geophysical Research: Oceans*, *105*(C11), 26313-26331.

Malmgren, F. (1927), On the properties of sea-ice, in *The Norwegian North Polar Expedition with the "Maud" 1918-1925*, edited by H. U. Sverdrup, pp. 1-67, AS John Griegs Boktrykkeri, Bergen, Norway.

Marion, G. M., and R. E. Farren (1999), Mineral solubilities in the Na-K-Mg-Ca-Cl-SO4-H2O system: a re-evaluation of the sulfate chemistry in the Spencer-Møller-Weare model, *Geochimica et Cosmochimica Acta*, *63*(9), 1305-1318.

Martin, S., and P. Kauffman (1974), The evolution of under-ice melt ponds, or double diffusion at the freezing point, *Journal of Fluid Mechanics*, *64*(03), 507-528.

Matsuo, S., and Y. Miyake (1966), Gas composition in ice samples from Antarctica, *Journal of Geophysical Research*, *71*(22), 5235-5241.

Maus, S., S. Müller, J. Büttner, S. Brütsch, T. Huthwelker, M. Schwikowski, F. Enzmann, and A. Vähätolo (2011), Ion fractionation in young sea ice from Kongsfjorden, Svalbard, *Annals of Glaciology*, *52*(57), 301-310.

McGinnis, D. F., J. Greinert, Y. Artemov, S. E. Beaubien, and A. Wüest (2006), Fate of rising methane bubbles in stratified waters: How much methane reaches the atmosphere?, *Journal of Geophysical Research*, *111*(C9).

McMinn, A., and C. Ashworth (1998), Use of oxygen microelectrodes to determine the net production by an Antarctic sea ice algal community, *Antarctic Science*, *10*(1), 39-44.

McMinn, A., R. Gradinger, and D. Nomura (2009), Biogeochemical Properties of Sea Ice, in *Field Techniques for Sea Ice Research*, edited by H. Eicken, R. Gradinger, M. Salganek, K. Shirasawa, D. Perovich and M. Lepparanta, pp. 259-282, University of Alaska Press, Alaska.

Meese, D. A. (1989), The chemical and structural properties of sea ice in the southern Beaufort Sea*Rep.*, 1-97 pp, U.S. Army Cold Regions Research and Engineering Laboratory.

Meiners, K., R. Brinkmeyer, M. A. Granskog, and A. Lindfors (2004), Abundance, size distribution and bacterial colonization of exopolymer particles in Antarctic sea ice (Bellingshausen Sea), *Aquatic microbial ecology*, *35*(3), 283-296.

Meiners, K., M. Vancoppenolle, S. Thanassekos, G. S. Dieckmann, D. N. Thomas, J.-L. Tison, K. R. Arrigo, D. L. Garrison, A. McMinn, and D. Lannuzel (2012), Chlorophyll a in Antarctic sea ice from historical ice core data, *Geophysical research letters*, *39*(21).

Meredith, M., K. Heywood, P. Dennis, L. Goldson, R. White, E. Fahrbach, U. Schauer, and S. Østerhus (2001), Freshwater fluxes through the Western Fram Strait, *Geophysical Research Letters*, *28*(8), 1615-1618.

Michel, C., L. Legendre, R. G. Ingram, M. Gosselin, and M. Levasseur (1996), Carbon budget of sea-ice algae in spring: Evidence of a significant transfer to zooplankton grazers, *Journal of Geophysical Research*, *101*(C8), 18345-18360.

Miller, L. A., T. N. Papakyriakou, R. E. Collins, J. W. Deming, J. K. Ehn, R. W. Macdonald, A. Mucci, O. Owens, M. Raudsepp, and N. Sutherland (2011), Carbon dynamics in sea ice: A winter flux time series, *Journal of Geophysical Research*, *116*(C2), C02028.

Miller, L. A., et al. (under revision), Methods for Biogeochemical Studies of Sea Ice: The State of the Art, Caveats, and Recommendations, *Elementa: Oceans*.

Mock, T., M. Kruse, and G. Dieckmann (2003), A new microcosm to investigate oxygen dynamics at the sea ice water interface, *Aquatic Microbial Ecology*, *30*, 197-205.

Mock, T., G. S. Dieckmann, C. Haas, A. Krell, J. L. Tison, A. L. Belem, S. Papadimitriou, and D. N. Thomas (2002), Micro-optodes in sea ice: a new approach to investigate oxygen dynamics during sea ice formation, *Aquatic Microbial Ecology*, *29*(3), 297-306.

Moreau, S., M. Vancoppenolle, J. Zhou, J.-L. Tison, B. Delille, and H. Goosse (2014), Modelling argon dynamics in first-year sea ice, *Ocean Modelling*, *73*(0), 1-18.

Moreau, S., M. Vancoppenolle, B. Delille, J.-L. Tison, J. Zhou, M. Kotovitch, D. N. Thomas, N.-X. Geilfus, and H. Goosse (submitted), Drivers of inorganic carbon dynamics in first-year sea ice: a model study, *J. Geophys. Res.*

Müller, S., A. V. Vähätalo, C. A. Stedmon, M. A. Granskog, L. Norman, S. N. Aslam, G. J. C. Underwood, G. S. Dieckmann, and D. N. Thomas (2013), Selective incorporation of dissolved organic matter (DOM) during sea ice formation, *Marine Chemistry*, *155*, 148-157.

Mundy, C. J., D. G. Barber, and C. Michel (2005), Variability of thermal, physical and optical properties pertinent to sea ice algae biomass during spring, *Journal of Marine Systems*, *58*, 107-120.

Myhre, G., et al. (2013), Anthropogenic and Natural Radiative Forcing*Rep.*, Cambridge University Press, Cambridge, United Kingdom and New York, NY, USA.

Nagata, T., and Y. Watanabe (1990), Carbon-and nitrogen-to-volume ratios of bacterioplankton grown under different nutritional conditions, *Applied and Environmental Microbiology*, *56*(5), 1303-1309.

Nakawo, M., and N. K. Sinha (1981), Growth rate and salinity profile of first-year sea ice in the high Arctic, *Journal of Glaciology*, *27*, 315-330.

Nemcek, N., D. Ianson, and P. D. Tortell (2008), A high-resolution survey of DMS, CO2, and O2/Ar distributions in productive coastal waters, *Global Biogeochem. Cycles*, *22*(GB2009).

Neufeld, J. A., and J. S. Wettlaufer (2008a), An experimental study of shear-enhanced convection in a mushy layer, *Journal of Fluid Mechanics*, *612*, 363-385.

Neufeld, J. A., and J. S. Wettlaufer (2008b), Shear-enhanced convection in a mushy layer, *Journal of Fluid Mechanics*, *612*, 339-361.

Nguyen, D., and R. Maranger (2011), Respiration and bacterial carbon dynamics in Arctic sea ice, *Polar Biology*, *34*(12), 1843-1855.

Nicolaus, M., C. Haas, and J. Bareiss (2003), Observations of superimposed ice formation at melt-onset on fast ice on Kongsfjorden, Svalbard, *Physics and Chemistry of the Earth, Parts A/B/C*, *28*(28), 1241-1248.

Niedrauer, T. M., and S. Martin (1979), An Experimental Study of Brine Drainage and Convection in Young Sea Ice, *Journal of Geophysical Research*, *84*(C3), 1176-1186.

Nisbet, E. G. (2002), Have sudden large releases of methane from geological reservoirs occurred since the Last Glacial Maximum, and could such releases occur again?, *Philosophical Transactions of the Royal Society of London Series a-Mathematical Physical and Engineering Sciences*, *360*(1793), 581-607.

Nomura, D., H. Yoshikawa-Inoue, and T. Toyota (2006), The effect of sea-ice growth on air-sea CO_2 flux in a tank experiment, *Tellus Series B Chemical and Physical Meteorology*, *58*(5), 418-426.

Nomura, D., H. Eicken, R. Gradinger, and K. Shirasawa (2010), Rapid physically driven inversion of the air-sea ice CO(2) flux in the seasonal landfast ice off Barrow, Alaska after onset of surface melt, *Continental Shelf Research*, *30*(19), 1998-2004.

Nomura, D., S. Koga, N. Kasamatsu, H. Shinagawa, D. Simizu, M. Wada, and M. Fukuchi (2012), Direct measurements of DMS flux from Antarctic fast sea ice to the atmosphere by a chamber technique, *Journal of Geophysical Research: Oceans*, *117*(C4), C04011.

Norman, L., D. N. Thomas, C. A. Stedmon, M. A. Granskog, S. Papadimitriou, R. H. Krapp, K. M. Meiners, D. Lannuzel, P. van der Merwe, and G. S. Dieckmann (2011), The characteristics of dissolved organic matter (DOM) and chromophoric dissolved organic matter (CDOM) in Antarctic sea ice, *Deep Sea Research Part II: Topical Studies in Oceanography*, *58*(9–10), 1075-1091.

Notz, D., and M. G. Worster (2008), In situ measurements of the evolution of young sea ice, *Journal of Geophysical Research : Oceans*, *113*(C3), C03001.

Notz, D., and M. G. Worster (2009), Desalination processes of sea ice revisited, *Journal of Geophysical Research: Oceans*, *114*(C5), C05006.

Notz, D., J. S. Wettlaufer, and M. G. Worster (2005), A non-destructive method for measuring the salinity and solid fraction of growing sea ice in situ, *Journal of Glaciology*, *51*(172), 159-166.

O'Connor, F. M., et al. (2010), Possible role of wetlands, permafrost, and methane hydrates in the methane cycle under future climate change: A review, *Reviews of Geophysics*, *48*(4), RG4005.

Ono, N., and T. Kasai (1985), Surface layer salinity of young sea ice, *Ann. Glaciol*, *6*(298-299), 57.

Papadimitriou, S., D. N. Thomas, H. Kennedy, C. Haas, H. Kuosa, A. Krell, and G. S. Dieckmann (2007), Biogeochemical composition of natural sea ice brines from the Weddell Sea during early austral summer, *Limnology and Oceanography*, *52*(5), 1809-1823.

Papakyriakou, T. N., and L. A. Miller (2011), Springtime CO2 exchange over seasonal sea ice in the Canadian Arctic Archipelago, *Annals of Glaciology*, *52*, 215-224.

Passow, U. (2002), Production of transparent exopolymer particles (TEP) by phyto- and bacterioplankton, *Marine Ecology-Progress Series*, *236*, 1-12.

Pelegri, S. P., J. Dolan, and F. Rassoulzadegan (1999), Use of high temperature catalytic oxidation (HTCO) to measure carbon content of microorganisms, *Aquatic Microbial Ecology*, *16*(3), 273-280.

Perovich, D. K., and A. J. Gow (1996), A quantitative description of sea ice inclusions, *Journal of Geophysical Research: Oceans*, *101*(C8), 18327-18343.

Petrich, C., and H. Eicken (2010), Growth, Structure and Properties of Sea Ice, in *Sea ice*, edited by D. N. Thomas and G. S. Dieckmann, pp. 23-77, Blackwell Publishing Ltd, UK.

Petrich, C., P. J. Langhorne, and Z. F. Sun (2006), Modelling the interrelationships between permeability, effective porosity and total porosity in sea ice, *Cold Regions Science and Technology*, *44*(2), 131-144.

Pratt, K. A., et al. (2013), Photochemical production of molecular bromine in Arctic surface snowpacks, *Nature Geosci*, *6*(5), 351-356.

Pringle, D. J., and M. Ingham (2009), Thermal, Electrical, and hydraulic Properties of Sea Ice, in *Field Techniques for Sea Ice Research*, edited by H. Eicken, R. Gradinger, M. Salganek, K. Shirasawa, D. Perovich and M. Lepparanta, pp. 141-180, University of Alaska Press, Alaska.

Pringle, D. J., H. Eicken, H. J. Trodahl, and L. G. E. Backstrom (2007), Thermal conductivity of landfast Antarctic and Arctic sea ice, *Journal of Geophysical Research*, *112*(C04017).

Pringle, D. J., J. E. Miner, H. Eicken, and K. M. Golden (2009), Pore space percolation in sea ice single crystals, *Journal of Geophysical Research*, *114*(C12017).

Priscu, J. C., M. T. Downes, L. R. Priscu, A. C. Palmisano, and C. W. Siullivan (1990), Dynamics of ammonium oxidizer activity and nitrous oxide (N20) within and beneath Antarctic sea ice *Marine Ecology Progress Series*, *62*, 37-46.

Randall, K., M. Scarratt, M. Levasseur, S. Michaud, H. Xie, and M. Gosselin (2012), First measurements of nitrous oxide in Arctic sea ice, *Journal of Geophysical Research*, *117*, C00G15.

Raynaud, D., R. Delmas, J. M. Ascencio, and M. Legrand (1982), Gas extraction from polar ice cores: a critical issue for studying the evolution of atmospheric CO_2 and ice-sheet surface elevation, *Annals of Glaciology*, *3*, 265-268.

Reagan, M. T., and G. T. Moridis (2008), Dynamic response of oceanic hydrate deposits to ocean temperature change, *Journal of Geophysical Research*, *113*(C12023).

Reeburgh, W. S., and M. Springer-Young (1983), New measurements of sulfate and chlorinity in natural sea ice, *Journal of Geophysical Research: Oceans*, *88*(C5), 2959-2966.

Reuer, M. K., B. A. Barnett, M. L. Bender, P. G. Falkowski, and M. B. Hendricks (2007), New estimates of Southern Ocean biological production rates from O2/Ar ratios and the triple isotope composition of O2, *Deep Sea Research Part I: Oceanographic Research Papers*, *54*(6), 951-974.

Riedel, A., C. Michel, and M. Gosselin (2006), Seasonal study of sea-ice exopolymeric substances on the Mackenzie shelf: implications for transport of sea-ice bacteria and algae, *Aquatic microbial ecology*, *45*(2), 195-206.

Riedel, A., C. Michel, G. M., and B. Leblanc (2007), Enrichment of nutrients, exopolymeric substances and microorganisms in newly formed sea ice on the Makenzie shelf, *Marine Ecology Progress Series*, *342*, 55-67.

Riedel, A., C. Michel, M. Gosselin, and B. LeBlanc (2008), Winter–spring dynamics in sea-ice carbon cycling in the coastal Arctic Ocean, *Journal of Marine Systems*, *74*(3), 918-932.

Rijkenberg, M. J. A., L. J. A. Gerringa, K. R. Timmermans, A. C. Fischer, K. J. Kroon, A. G. J. Buma, B. T. Wolterbeek, and H. J. W. de Baar (2008), Enhancement of the reactive iron pool by marine diatoms, *Marine Chemistry*, *109*(1–2), 29-44.

Romanovskii, N. N., H. W. Hubberten, A. V. Gavrilov, V. E. Tumskoy, G. S. Tipenko, M. N. Grigoriev, and C. Siegert (2000), Thermokarst and land-ocean interactions, Laptev Sea Region, Russia, *Permafrost and Periglacial Processes*, *11*(2), 137-152.

Rysgaard, S., and R. N. Glud (2004), Anaerobic N2 production in Arctic sea ice, *Limnology Oceanography 49*(1), 86-94.

Rysgaard, S., R. N. Glud, M. K. Sejr, J. Bendtsen, and P. B. Christensen (2007), Inorganic carbon transport during sea ice growth and decay: A carbon pump in polar seas, *Journal of Geophysical Research-Oceans*, *112*(C3).

Rysgaard, S., R. N. Glud, M. K. Sejr, M. E. Blicher, and H. J. Stahl (2008), Denitrification activity and oxygen dynamics in Arctic sea ice, *Polar Biology*, *31*(5), 527-537.

Rysgaard, S., J. Bendtsen, B. Delille, G. S. Dieckmann, R. Glud, H. Kennedy, J. Mortensen, S. Papadimitriou, D. N. Thomas, and J. L. Tison (2011), Sea ice contribution to the air–sea CO2 exchange in the Arctic and Southern Oceans, *Tellus B*.

Rysgaard, S., et al. (2013), Ikaite crystal distribution in winter sea ice and implications for CO2 system dynamics, *The Cryosphere*, *7*(2), 707-718.

Saeki, H., T. Takeuchi, M. Sakai, and E. Suenaga (1986), Experimental study on permeability coefficient of sea ice, paper presented at Ice technology, Proceedings of the 1st International Conference, Springer-Verlag, Cambridge, Mass. USA.

Saito, T., and N. Ono (1978), Percolation of sea ice. I - Measuremetns of kerosene permeability of NaCl ice, *Low Temp. Sci. Ser. A*, *37*, 55-62.

Savvichev, A. S., I. I. Rusanov, S. K. Yusupov, N. V. Pimenov, A. Y. Lein, and M. V. Ivanov (2004), The biogeochemical cycle of methane in the coastal zone and littoral of the Kandalaksha Bay of the White Sea, *Microbiology*, *73*(4), 457-468.

Schubert, C. J., F. Vazquez, T. Lösekann-Behrens, K. Knittel, M. Tonolla, and A. Boetius (2011), Evidence for anaerobic oxidation of methane in sediments of a freshwater system (Lago di Cadagno), *FEMS Microbiology Ecology*, *76*(1), 26-38.

Schwerdtfeger, P. (1963), The thermal properties of sea ice, *Journal of Glaciology*, *4*, 789-807.

Shadwick, E. H., B. Tilbrook, N. Cassar, T. W. Trull, and S. R. Rintoul (in press.), Summertime physical and biological controls on O2 and CO2 in the Australian Sector of the Southern Ocean, *Journal of Marine Systems*.

Shakhova, N., I. Semiletov, and G. Panteleev (2005), The distribution of methane on the Siberian Arctic shelves: Implications for the marine methane cycle, *Geophys. Res. Lett.*, *32*(L09601).

Shakhova, N., I. Semiletov, and O. Gustafsson (2010a), Methane from the East Siberian Arctic Shelf Response, *Science*, *329*(5996), 1147-1148.

Shakhova, N., I. Semiletov, A. Salyuk, V. Yusupov, D. Kosmach, and O. Gustafsson (2010b), Extensive Methane Venting to the Atmosphere from Sediments of the East Siberian Arctic Shelf, *Science*, *327*(5970), 1246-1250.

Simpson, W. R., R. von Glasow, K. Riedel, P. Anderson, P. Ariya, J. Bottenheim, J. Burrows, L. J. Carpenter, U. Frieß, and M. E. Goodsite (2007), Halogens and their role in polar boundary-layer ozone depletion, *Atmospheric Chemistry and Physics*, *7*(16), 4375-4418.

Skoog, D. A., D. M. West, and F. J. Holler (1997), *Chimie analytique*, De Boeck Université, Paris, Bruxelles.

Smedsrud, L. H., T. M. Saloranta, P. M. Haugan, and T. Kangas (2003), Sea ice formation on a very cold surface, *Geophysical Research Letters*, *30*(6), 1284.

Smith, I. J., P. J. Langhorne, R. D. Frew, R. Vennell, and T. G. Haskell (2012), Sea ice growth rates near ice shelves, *Cold Regions Science and Technology*, *83–84*(0), 57-70.

Smith, R. H., and P. Clement (1990), Heterotrophic activity and bacterial productivity in assemblages of microbes from sea ice in the high Arctic, *Polar Biology*, *10*(5), 351-357.

Smith, W. O., and D. M. Nelson (1986), Importance of ice edge phytoplankton production, *BioScience*, *36*, 251-257.

Souchez, R., and J. Jouzel (1984), On the isotopic composition in δD and $\delta^{18}O$ of water and ice during freezing, *Journal of Glaciology*, *30*(106), 369-372.

Souchez, R., J. L. Tison, and J. Jouzel (1987), Freezing Rate Determination by the Isotopic Composition of the Ice, *Geophysical Research Letters*, *14*(6), 599-602.

Souchez, R., J. Jouzel, A. Landais, J. Chappellaz, R. Lorrain, and J. L. Tison (2006), Gas isotopes in ice reveal a vegetated central Greenland during ice sheet invasion, *Geophysical Research Letters*, *33*(24), -.

Stander, E., and B. Michel (1989), The development of aligned columnar sea ice: a field investigation, *Journal of Glaciology*, *35*(120), 217-223.

Stedmon, C. A., D. N. Thomas, S. Papadimitriou, M. A. Granskog, and G. S. Dieckmann (2011), Using fluorescence to characterize dissolved organic matter in Antarctic sea ice brines, *Journal of Geophysical Research: Biogeosciences*, *116*(G3), G03027.

Stedmon, C. A., D. N. Thomas, M. Granskog, H. Kaartokallio, S. Papadimitriou, and H. Kuosa (2007), Characteristics of dissolved organic matter in Baltic coastal sea ice: Allochthonous or autochthonous origins?, *Environmental Science & Technology*, *41*(21), 7273-7279.

Stefels, J., M. Steinke, S. Turner, G. Malin, and S. Belviso (2007), Environmental Constraints on the Production and Removal of the Climatically Active Gas Dimethylsulphide (DMS) and Implications for Ecosystem Modelling, *Biogeochemistry*, *83*(1/3), 245-275.

Stefels, J., G. Carnat, J. W. H. Dacey, T. Goossens, J. T. M. Elzenga, and J. L. Tison (2012), The analysis of dimethylsulfide and dimethylsulfoniopropionate in sea ice: Dry-crushing and melting using stable isotope additions, *Marine Chemistry*, *128-129*, 34-43.

Sturges, W., G. Cota, and P. Buckley (1992), Bromoform emission from Arctic ice algae.

Sturges, W., C. Sullivan, R. Schnell, L. Heidt, and W. Pollock (1993), Bromoalkane production by Antarctic ice algae, *Tellus B*, *45*(2), 120-126.

Thomas, D. N., and G. S. Dieckmann (2002), Antarctic Sea Ice--a Habitat for Extremophiles, *Science*, *295*(5555), 641-644.

Thomas, D. N., S. Papadimitriou, and C. Michel (2010), Biogeochemistry of Sea Ice, in *Sea ice*, edited by D. N. Thomas and G. S. Dieckmann, pp. 425-467, Blackwell Publishing Ltd, UK.

Thomas, D. N., R. J. Lara, H. Eicken, G. Kattner, and A. Skoog (1995), Dissolved organic matter in Arctic multi-year sea ice in winter: major components and relationships to ice characteristics, *Polar Biology*, *15*, 477–483.

Thomas, D. N., G. Kattner, R. Engbrodt, V. Giannelli, H. Kennedy, C. Haas, and G. S. Dieckmann (2001), Dissolved organic matter in Antarctic sea ice, *Annals of Glaciology*, *33*, 297-303.

Timco, G. W., and R. M. W. Frederking (1996), A review of sea ice density, *Cold Regions Science and Technology*, *24*, 1-6.

Tison, J.-L., F. Brabant, I. Dumont, and J. Stefels (2010), High resolution DMS and DMSP time series profiles in decaying summer first-year sea ice at ISPOL (Western Weddell Sea, Antarctica). Submitted to, *Journal of Geophysical Research*.

Tison, J.-L., C. Haas, M. M. Gowing, S. Sleewagen, and A. Bernard (2002), Tank study of physico-chemical controls on gas content and composition during growth of young sea-ice, *Journal of Glaciology*, *48*, 267-278.

Tison, J.-L., R. D. Lorrain, A. Bouzette, M. Dini, A. Bondesan, and M. Stiévenard (1998), *Linking landfast sea ice variability to marine ice accretion at Hells Gate Ice Shelf, Ross Sea*, American Geophysical Union, Washington, D. C.

Tison, J.-L., A. Worby, B. Delille, F. Brabant, S. Papadimitriou, D. Thomas, J. de Jong, D. Lannuzel, and C. Haas (2008), Temporal evolution of decaying summer first-year sea ice in the Western Weddell Sea, Antarctica, *Deep Sea Research Part II: Topical Studies in Oceanography*, *55*(8-9), 975-987.

Trevena, A., and G. Jones (2012), DMS flux over the Antarctic sea ice zone, *Marine Chemistry*, *134–135*(0), 47-58.

Tsurikov, V. (1979), The formation and composition of the gas content of sea ice, *J Glaciol*, *22*(86), 67-81.

Tucker, W. B., A. J. Gow, and J. A. Richter (1984), On small-scale horizontal variations of salinity in first-year sea ice, *Journal of Geophysical Research: Oceans*, *89*(C4), 6505-6514.

Underwood, G. J. C., S. Fietz, S. Papadimitriou, D. N. Thomas, and G. S. Dieckmann (2010), Distribution and composition of dissolved extracellular polymeric substances (EPS) in Antarctic sea ice, *Marine Ecology Progress Series*, *404*, 1-19.

Untersteiner, N. (1968), Natural desalinisation and equilibrium salinity profile of perennial sea ice, *Journal of Geophysical Research*, *73*, 1251-1257.

Upstill-Goddard, R. C., J. Barnes, T. Frost, S. Punshon, and N. J. P. Owens (2000), Methane in the southern North Sea: Low-salinity inputs, estuarine removal, and atmospheric flux, *Global Biogeochem. Cycles*, *14*(4), 1205-1217.

Valentine, D. L., D. C. Blanton, W. S. Reeburgh, and M. Kastner (2001), Water column methane oxidation adjacent to an area of active hydrate dissociation, Eel River Basin, *Geochimica Et Cosmochimica Acta*, *65*(16), 2633-2640.

Vancoppenolle, M., C. M. Bitz, and T. Fichefet (2007), Summer landfast sea ice desalination at Point Barrow, Alaska: Modeling and observations, *Journal of Geophysical Research-Oceans*, *112*(C4), -.

Vancoppenolle, M., H. Goosse, A. de Montety, T. Fichefet, B. Tremblay, and J. L. Tison (2010), Modeling brine and nutrient dynamics in Antarctic sea ice: The case of dissolved silica, *Journal of Geophysical Research: Oceans*, *115*, C02005.

Vancoppenolle, M., et al. (2013a), Technical Note: On the use of the mushy-layer Rayleigh number for the interpretation of sea-ice-core data, *The Cryosphere Discuss.*, *7*(4), 3209-3230.

Vancoppenolle, M., et al. (2013b), Role of sea ice in global biogeochemical cycles: emerging views and challenges, *Quaternary Science Reviews*, *79*(0), 207-230.

Vaughan, D. G., et al. (2013), Observations: Cryosphere*Rep.*, Cambridge University Press, Cambridge, United Kingdom and New York, NY, USA.

Verdugo, P., A. L. Alldredge, F. Azam, D. L. Kirchman, U. Passow, and P. H. Santschi (2004), The oceanic gel phase: a bridge in the DOM-POM continuum, *Marine Chemistry*, *92*(1-4), 67-85.

Wanninkhof, R. (1992), Relationship between wind speed and gas exchange over the ocean, *Journal of Geophysical Research*, *97*(C5), 7373-7382.

Weeks, W. F. (2010), *On sea ice*, 664 pp., University of Alaska Press, Fairbanks, Alaska.

Weeks, W. F., and A. J. Gow (1978), Preferred crystal orientations in the fast ice along the margins of the Arctic Ocean, *Journal of Geophysical Research: Oceans*, *83*(C10), 5105-5121.

Weeks, W. F., and S. F. Ackley (1986), The growth, structure and properties of sea ice, in *The geophysics of sea ice*, edited by N. Untersteiner, pp. 9-164, Plenum Press, New York.

Weiss, R. F. (1970), The solubility of nitrogen, oxygen and argon in water and seawater, *Deep Sea Research and Oceanographic Abstracts*, *17*(4), 721-735.

Weissenberger, J., and S. Grossmann (1998), Experimental formation of sea ice: importance of water circulation and wave action for incorporation of phytoplankton and bacteria, *Polar Biology*, *20*(3), 178-188.

Westbrook, G. K., et al. (2009), Escape of methane gas from the seabed along the West Spitsbergen continental margin, *Geophysical Research Letters*, *36*(15), L15608.

Weston, R. E. (1955), Hydrogen isotope fractionation between ice and water, *Geochimica Et Cosmochimica Acta*, *8*, 281-284.

Wettlaufer, J. S., M. G. Worster, and H. E. Huppert (1997), Natural convection during solidification of an alloy from above with application to the evolution of sea ice, *Journal of Fluid Mechanics*, *344*, 291-316.

Wheeler, P. A., J. M. Watkins, and R. L. Hansing (1997), Nutrients, organic carbon and organic nitrogen in the upper water column of the Arctic Ocean: implications for the sources of dissolved organic carbon, *Deep Sea Research Part II: Topical Studies in Oceanography*, *44*(8), 1571-1592.

Whitman, W. G. (1926), Elimination of salt from sea-water ice, *American Journal of Science*, *Series 5 Vol. 11*(62), 126-132.

Wiesenburg, D. A., and N. L. Guinasso (1979), Equilibrium solubilities of methane, carbon monoxide and hydrogen in water and sea water, *J. Chem. Eng. Data*, *24*, 356-360.

WMO (1970), WMO Sea-ice Nomenclature: Terminology, Codes, Illustrated Glossary and Symbols, edited by W. M. Organization, p. 145, WMO/OMM/BMO, Geneva.

Worster, M. G. (2000), Solidification of fluids, *Perspectives in fluid dynamics*, *742*, 393-446.

Worster, M. G., and J. S. Wettlaufer (1997), Natural convection, solute trapping, and channel formation during solidifi cation of saltwater, *Journal of Physical Chemistry B*, *101*, 6132-6136.

Yamamoto-Kawai, M., E. C. Carmack, F. A. McLaughlin, and K. K. Falkner (2010), Oxygen isotope ratio, barium and salinity in waters around the North American coast from the Pacific to the Atlantic: Implications for freshwater sources to the Arctic throughflow, *Journal of Marine Research*, *68*, 97-117.

Zeebe, R. E., and D. A. Wolf-Gladrow (2001), *CO2 in Seawater: Equilibrium, Kinetics, Isotopes*, Elsevier Oceanography Series, Amsterdam.

Zeikus, J. G., and M. R. Winfrey (1976), Temperature limitation of methanogenesis in aquatic sediments, *Applied and Environmental Microbiology*, *31*, 99-107.

Zemmelink, H. J., J. W. H. Dacey, L. Houghton, E. J. Hintsa, and P. S. Liss (2008), Dimethylsulfide emissions over the multi-year ice of the western Weddell Sea, *Geophys. Res. Lett.*, *35*(L06603).

Zermatten, E., M. Schneebeli, H. Arakawa, and A. Steinfeld (2014), Tomography-based determination of porosity, specific area and permeability of snow and comparison with measurements, *Cold Regions Science and Technology*, *97*(0), 33-40.

Zhou, J., B. Delille, F. Brabant, and J. L. Tison (2014a), Insights into oxygen transport and net community production in sea ice from oxygen, nitrogen and argon concentrations, *Biogeosciences*, *11*(18), 5007-5020.

Zhou, J., J. L. Tison, G. Carnat, N. X. Geilfus, and B. Delille (2014b), Physical controls on the storage of methane in landfast sea ice, *The Cryosphere*, *8*(3), 1019-1029.

Zhou, J., B. Delille, H. Eicken, M. Vancoppenolle, F. Brabant, G. Carnat, N.-X. Geilfus, T. Papakyriakou, B. Heinesch, and J.-L. Tison (2013), Physical and biogeochemical properties in landfast sea ice (Barrow, Alaska): Insights on brine and gas dynamics across seasons, *Journal of Geophysical Research: Oceans*, *118*(6), 3172-3189.

Zhu, J., A. Jabini, K. M. Golden, H. Eicken, and M. Morris (2006), A network model for fluid transport through sea ice, *Annals of Glaciology*, *44*(1), 129-133.

Zindler, C., A. Bracher, C. A. Marandino, B. Taylor, E. Torrecilla, A. Kock, and H. W. Bange (2012), Sulphur compounds, methane, and phytoplankton: interactions along a north-south transit in the western Pacific Ocean, *Biogeosciences Discuss.*, *9*, 15011-15049.

THE PHYSICAL AND BIOLOGICAL CONTROLS ON THE DISTRIBUTION OF GASES AND SOLUTES IN SEA ICE FROM ICE GROWTH TO ICE DECAY

The ongoing changes in the extent and the properties of sea ice, associated with the warming climate, are affecting the polar ecosystem and the interactions between the atmosphere, sea ice and the underlying waters. How sea ice biogeochemistry will change in the foreseeable future is currently uncertain, but is a crucial problem to tackle.

To better understand how sea ice biogeochemistry could change, we investigated the factors regulating the distribution of some dissolved compounds (e.g., nutrients, dissolved organic matter (DOM)) and gaseous compounds (e.g., Ar, O_2, N_2, CH_4) in sea ice, from ice growth to ice decay. The results were obtained from a 19-day indoor experiment in Hamburg (Germany) and a five-month-long field survey in Barrow (Alaska). They were then compared to the physical properties of the ice (temperature, salinity, and other derived parameters such as brine volume fraction) and different biological parameters (bacterial activity, bacterial abundance, chlorophyll-a and phaeopigments).

Our work indicates that the physical properties of sea ice exert a strong influence on the distribution of the biogeochemical compounds in the ice, through their impact on brine dynamics, gas bubble formation and ice permeability. We have described 4 stages of brine dynamics, which affect the distribution of the dissolved compounds (e.g., silicate and DOM) in sea ice. However, inert gas (Ar) shows a different dynamic in comparison to the dissolved compounds, indicating a different transport pathway. We suggest that the formation of gas bubbles in sea ice is responsible for that different transport pathway, because gas bubbles should move upward owing to their buoyancy in comparison to brine, while dissolved compounds are drained downward due to gravity. Our observations further indicate that the critical permeability threshold for the upward gas bubble transport should range between 7.5 and 10 % of brine volume fraction, which is higher than the 5 % suggested for the downward brine transport. Increasing ice permeability and prolonged gas exchange tend to draw gas concentrations toward their solubility values, except when the under-ice water is supersaturated relative to the atmosphere (e.g., CH_4) or when there is in-situ production (e.g., O_2).

Because ammonium and O_2 obviously accumulate in the ice layers where convection is limited, we suggest that the changes of these biogeochemical compounds in sea ice depend on the competing effect between the physical transport and the biological activity; the biological impact on these biogeochemical compounds in sea ice is obvious when the biological production rate exceeds largely the physical transport rate. We further discussed on the potential of using Ar and N_2 as inert tracers to correct the physical controls on O_2 and to determine the net community production in sea ice.

In addition to the physical and biological controls, the chemical properties of some biogeochemical compounds (e.g., nitrate, ammonium, DOM) may further influence their distribution in sea ice; further investigations are however needed to confirm this.

Finally, based on our findings, we present an update of the processes regulating the distribution of gases in sea ice, with references to recent observations supporting each of the process. We also provide some insights on how sea ice biogeochemistry could change in the future and the research priorities for an accurate quantification of these changes.